



2013 | Faculteit Wetenschappen

DOCTORAATSPROEFSCHRIFT

Valorization of agricultural waste cake by pyrolysis: Characterization of pyrolysis products and adsorption study on produced activated carbons

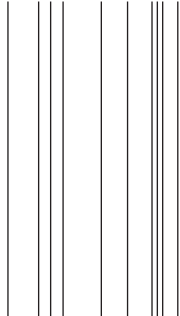
*Proefschrift voorgelegd tot het behalen van de graad van
doctor in de wetenschappen, chemie, te verdedigen door:*

Koen Smets

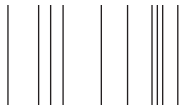
Promotor: prof. dr. Jan Yperman

Copromotoren: prof. dr. Robert Carleer

dr. Sonja Schreurs (UH-XIOS)



D/2013/2451/34



met medewerking van:



Dankwoord

Zes jaar geleden begon ik aan een nieuwe uitdaging: een doctoraat in de scheikunde met als onderwerp: "Pyrolyse van biomassa-afvalstromen". Is een doctoraat niet vier jaar? hoor ik u al denken. Inderdaad, maar als assistent krijg je twee jaar "extra" omdat je een aanzienlijk gedeelte van je tijd aan onderwijsopdrachten spendeert, iets wat ik als een echte meerwaarde ervaren heb. Nu, na een periode van ups en soms ook wel eens downs is het schrijven van het "doctoraatsproefschrift" voltooid. Tijd om heel wat mensen te bedanken zonder wie dit proefschrift nooit gerealiseerd zou kunnen zijn.

Vooreerst richt ik mijn oprechte dank aan mijn promotor en co-promotoren Prof. dr. Jan Yperman, Prof. dr. Robert Carleer en dr. Sonja Schreurs. Zij hebben mij de kans gegeven om mij te verdiepen in een onderwerp dat mijn twee grote interesses, scheikunde en milieu, met elkaar combineert. Hun enthousiasme, kennis, tips en het veelvuldig nalezen en becommentariëren van mijn schrijfsels waren onmisbaar om dit doctoraatsproefschrift te maken tot wat het is geworden. Een welgemeend dank u wel!

I would also like to thank prof. Grazyna Gryglewicz and dr. Iwona Lupul for performing the N₂-adsorption analyses of the AC samples. The data were very important for gaining a better understanding of the performance of the ACs and provide an added-value to this thesis.

Graag wil ik ook Prof. dr. Peter Adriaensens en Prof. dr. Jan D'Haen bedanken voor de hulp en de uitleg bij respectievelijk de ¹H-NMR en SEM metingen.

Ook wil ik de mensen bedanken die mij de nodige biomassa-afvalstromen ter beschikking hebben gesteld. Want zonder biomassa viel er niet veel te pyrolyseren. De koolzaadperskoek werd mij bezorgd door ing. Eric Claesen (ACRO, KHLim - Dep. IWT). Ing. Sven Boedrij en ing. Roel Conings lieten mij kennis maken met hun geautomatiseerde persinstallatie voor koolzaad en gaven heel wat randinformatie over het persproces. Ir. Kris Schatteman van Eco Treasures (Lokeren) wil ik bedanken voor het aanleveren van de framboospittenkoek. De afvalkoek van olijven werd ter beschikking gesteld door Prof.

Hikmat Hilal en Prof. Amer El-Hamouz van de An-Najah National University (Palestina).

Zonder reactoren viel er uiteraard ook niet veel te pyrolyseren. Bedankt Tom en Caroline voor het ontwerpen en op punt stellen van respectievelijk de "flash" en "slow" pyrolysereactoren. Jos was de man die de theoretische ontwerpen heeft omgetoverd in "real life" goed werkende pyrolyseopstellingen. Ook Tim (glaswerk), Johan (werkplaats) en Koen V. (elektronica) verdienen een dank je wel voor hun bijstand, het opkrikken van mijn technische kennis en zo hun bijdrage aan deze doctoraatsthesis.

Mijn collega's van TANC (het vroegere TOES) wil ik ten eerste bedanken voor hun hulp bij de vele analyses en het mij wegwijs maken in de wereld van de chemische analysetechnieken, maar zeker ook voor de leuke babbels en de zeer aangename werksfeer. Bedankt Martine, Elsy, Greet, Jenny, Linda, Jan C., Guy en Yvo. De vele "after-lunch" wandelingen, de leuke kerstfeestjes met bijhorende bowling, de leuke terrasjes (af en toe) en vele andere leuke momenten zullen mij altijd bijblijven.

Gelukkig stond ik er niet alleen voor in het labo. Collega doctoraatstudenten/pyrolyseerders die ik wil bedanken zijn vooreerst Tom, Mark, Niels en Eva. Zij waren er toen ik aan mijn doctoraat begon en hebben mij de kneepjes van het pyrolyseren geleerd. Later hebben Inge en Kenny zich bij het pyrolyse team gevoegd. Palina, Iwona en Lenia hebben reeds hun PhD behaald terwijl Jens, Marco, Elena en Shaahin "in progress" zijn. Ook wil ik jullie allemaal bedanken voor de aangename werksfeer, de leuke compagnie op congressen en de vele gespreken over pyrolyse en koetjes en kalfjes. Ook buiten het werk werden er allerlei activiteiten georganiseerd zoals af en toe een bezoek aan de schaakclub op woensdag, een bezoek aan een andere (onlangs gesloten) club op donderdag, een bezoek aan de zwemclub bij mooi weer, een bezoek aan de minivoetbal club,...

De collega-doctoraatstudenten van organische en anorganische chemie verdienen eveneens een dank je wel voor de leuke momenten waarbij onder andere al eens "touwtje moest gesprongen worden" of pizza's werden gegeten.

Tijdens de zes jaar van het doctoraat heb ik een aantal studenten begeleid tijdens hun bachelor- of masterproef. Omdat hun inzet en toewijding een grote bedrage heeft geleverd tot een aantal wetenschappelijke publicaties en hoofdstukken in dit proefschrift, wil ik hen dan ook nog eens langs deze weg uitvoerig bedanken. Bedankt Wouter, Arnout, Jens, Mats en Ruben.

Naast onderzoek heb ik ook heel wat tijd doorgebracht met lesgeven. Hoewel het soms moeilijk was om dit met het doctoraatsonderzoek te combineren, heb ik hier heel wat uit geleerd en heb ik het ervaren als een enorme meerwaarde. Daarom wil ik ook de vele studenten van vnl. Biomedische wetenschappen, Chemie, Geneeskunde en Handelsingenieur bedanken voor de aangename momenten tijdens het lesgeven, een soms welgekomen afwisseling voor het onderzoek. Ook de mensen van Didactiek die steeds zorgen dat al het nodige wordt gedaan opdat de labo's vlot verlopen verdienen een pluim. Bedankt Hilde, Eugène en Rita.

De mensen van het secretariaat die alle administratie regelden voor congressen en bestellingen wil ik langs deze weg ook bedanken voor het in orde brengen van de (toch wel zeer) vele papieren.

Mijn vrienden, met een speciale vermelding voor Nick S., Tom B. en Stijn S., hebben gezorgd voor welgekomen ontspanningsmomenten tijdens mijn doctoraat in de vorm van game- en filmavonden, fitness en après-fitness, fietstochten, terrasjes, allerlei uitstapjes en af en toe ook stapjes in de wereld. Ook mijn familie wil ik bedanken voor hun steun en interesse in mijn onderzoek, en voor het gezelschap tijdens de winterse trein- en busreizen. En ja, het doctoraat is nu eindelijk af ☺.

Last but not least, wil ik mijn ouders, mijn zus Ine en haar vriend Raf bedanken voor hun steun tijdens mijn studies, mijn doctoraat en zoveel meer...

Aan iedereen een welgemeend DANK JE WEL

Koen

Table of content

Research objectives and outline	1
1 Introduction	3
1.1 Biomass as renewable energy source.....	3
1.2 Biomass and agricultural waste cake	5
1.2.1 Definition and classification of biomass	5
1.2.2 Agricultural waste cake	5
1.2.2.1 Rapeseed cake	6
1.2.2.2 Raspberry seed cake	7
1.2.2.3 Olive waste cake.....	7
1.2.3 Composition of biomass	7
1.2.3.1 Cellulose.....	8
1.2.3.2 Hemicellulose	9
1.2.3.3 Lignin.....	9
1.2.3.4 Bulk extractives: triglycerides and proteins	11
1.2.3.5 Inorganic matter.....	12
1.3 Biomass conversion techniques.....	13
1.3.1 Mechanical conversion	13
1.3.2 Biochemical conversion	14
1.3.2.1 Anaerobic digestion.....	14
1.3.2.2 Fermentation.....	14
1.3.3 Thermochemical conversion.....	15
1.3.3.1 Combustion.....	15
1.3.3.2 Gasification	16
1.3.3.3 Pyrolysis.....	16

1.3.3.4	<i>Liquefaction</i>	16
1.3.4	Selection of the appropriate biomass conversion process	17
1.4	Pyrolysis	18
1.4.1	Pyrolysis of biomass	18
1.4.1.1	<i>Pyrolysis characteristics of biomass constituents</i>	19
1.4.1.2	<i>Thermal zones in biomass pyrolysis</i>	20
1.4.2	Pyrolysis process parameters	21
1.4.2.1	<i>Pyrolysis temperature</i>	21
1.4.2.2	<i>Heating rate</i>	21
1.4.2.3	<i>Vapor residence time</i>	22
1.4.2.4	<i>Biomass particle size</i>	22
1.4.2.5	<i>Effect of sweeping gas</i>	23
1.4.3	Types of pyrolysis	23
1.4.3.1	<i>Slow pyrolysis</i>	23
1.4.3.2	<i>Fast pyrolysis</i>	24
1.4.3.3	<i>Flash pyrolysis</i>	24
1.4.3.4	<i>Catalytic pyrolysis</i>	24
1.4.4	Pyrolysis reactor types	24
1.4.4.1	<i>Fixed bed pyrolysis reactor</i>	24
1.4.4.2	<i>Bubbling fluidized bed reactor</i>	25
1.4.4.3	<i>Circulating fluidized bed (CFB) reactor</i>	25
1.4.4.4	<i>Rotating cone reactor</i>	25
1.4.4.5	<i>Ablative pyrolysis reactor</i>	26
1.4.4.6	<i>Screw and Auger reactor</i>	26
1.5	Properties and applications of pyrolysis products	28
1.5.1	Pyrolysis liquid	28

1.5.1.1	<i>Chemical composition</i>	28
1.5.1.2	<i>Physicochemical properties</i>	29
1.5.1.3	<i>Upgrading of pyrolysis liquids to (transportation) fuels</i>	33
1.5.1.4	<i>Applications of pyrolysis liquids</i>	35
1.5.2	Solid residue.....	38
1.5.2.1	<i>Solid residue as energy source</i>	39
1.5.2.2	<i>Solid residue as fertilizer (biochar)</i>	39
1.5.2.3	<i>Solid residue as precursor of activated carbon</i>	39
1.5.3	Pyrolysis gas.....	43
1.6	Conclusion	44
1.7	References.....	45
2	Material and methods	59
2.1	Agricultural waste cakes	61
2.1.1	Rapeseed cake	61
2.1.2	Olive waste cake	61
2.1.3	Raspberry seed cake.....	61
2.2	Lab-scale pyrolysis experiments.....	62
2.2.1	Semi-continuous flash pyrolysis experiments	62
2.2.2	Batch slow pyrolysis with separated liquid collection	64
2.2.3	Batch slow pyrolysis experiments without sand	65
2.2.4	Batch slow catalytic pyrolysis experiments.....	65
2.3	Characterization of agricultural waste cake.....	68
2.3.1	Moisture content	68
2.3.2	Component analysis.....	68
2.3.3	Thermogravimetric analysis (TGA) and proximate analysis	70
2.3.4	Elemental analysis.....	71

2.3.5	Energy content.....	72
2.3.6	Minor elements	72
2.4	Characterization of pyrolysis liquid	74
2.4.1	Gas Chromatography/Mass Spectrometry (GC/MS).....	74
2.4.2	Water content.....	74
2.4.3	Elemental analysis.....	75
2.4.4	Energy content.....	75
2.4.5	Gel Permeation Chromatography (GPC).....	75
2.4.6	High Performance Liquid Chromatography (HPLC)	76
2.4.7	Fourier Transform Infrared spectroscopy (FTIR)	76
2.4.8	Proton Nuclear Magnetic Resonance spectroscopy ($^1\text{H-NMR}$)	77
2.4.9	pH-value	77
2.4.10	Total Acid Number (TAN).....	77
2.4.11	Density	77
2.4.12	Viscosity.....	77
2.5	Characterization of solid residue	78
2.5.1	Thermogravimetric analysis (TGA).....	78
2.5.2	Elemental analysis.....	78
2.5.3	Energy content.....	78
2.6	Production of activated carbon.....	79
2.7	Characterization of activated carbon.....	81
2.7.1	Nitrogen adsorption study	81
2.7.1.1	<i>Nitrogen adsorption isotherms.....</i>	<i>81</i>
2.7.1.2	<i>Pore size distribution by the QSDFT method</i>	<i>82</i>
2.7.1.3	<i>Specific surface area by the BET method (s_{BET}).....</i>	<i>83</i>
2.7.1.4	<i>Micropore characterization by the Dubinin-Radushkevich (DR) method</i>	<i>85</i>

2.7.1.5	Mesopore and total pore volume	87
2.7.2	Elemental analysis.....	87
2.7.3	Attenuated Total Reflectance-FTIR spectroscopy.....	87
2.7.4	Scanning Electron Microscopy (SEM).....	88
2.8	Batch phenol adsorption study.....	89
2.8.1	Phenol adsorption isotherms	89
2.8.2	Adsorption isotherm models	89
2.8.3	Effect of the initial pH of the phenol solution	92
2.8.4	Batch adsorption kinetic studies	92
2.9	References	94
3	Valorization of agricultural waste cake: Feedstock characterization and preliminary flash pyrolysis experiments.....	99
3.1	Characterization of the agricultural waste cakes.....	99
3.1.1	Component analysis.....	100
3.1.2	Thermogravimetric analysis	102
3.1.3	Proximate analysis, energy content and elemental analysis	105
3.2	Preliminary flash pyrolysis experiments	108
3.2.1	Product distribution	108
3.2.2	Pyrolysis liquid: screening parameters for fuel use.....	109
3.3	Conclusion and outlook.....	112
3.4	References	113
4	Valorization of rapeseed cake	115
4.1	Flash pyrolysis of rapeseed cake: Influence of pyrolysis temperature on the product yield and the characteristics of the pyrolysis liquid	116
4.1.1	Product yield and energy recovery.....	116
4.1.2	Characterization of the organic oil fraction.....	120

4.1.2.1	<i>Physicochemical properties</i>	120
4.1.2.2	<i>Chemical composition</i>	122
4.1.2.3	<i>GPC and HPLC analysis</i>	126
4.1.2.4	<i>FTIR analysis</i>	128
4.1.2.5	<i>¹H-NMR analysis</i>	130
4.1.3	Characterization of the aqueous fraction.....	132
4.1.3.1	<i>Physical properties</i>	132
4.1.3.2	<i>Chemical composition</i>	132
4.1.4	Characterization of the solid residue	136
4.2	Flash pyrolysis of rapeseed cake: Reduction of the water content of the pyrolysis liquid – a preliminary study	138
4.2.1	Flash pyrolysis of rapeseed cake with fractionated condensation of the pyrolysis liquid	138
4.2.2	Co-pyrolysis of rapeseed cake with PEG10k polymer.....	140
4.3	Slow pyrolysis of rapeseed cake: Collection of the pyrolysis liquid in fractions as a function of pyrolysis temperature	143
4.3.1	Experimental setup and observations.....	143
4.3.2	Product yield and properties of the liquid fractions.....	144
4.3.3	Chemical composition of the liquid fractions.....	145
4.4	Slow catalytic pyrolysis of rapeseed cake: Product yield and characterization of the pyrolysis liquid	152
4.4.1	Experimental setup and catalyst characteristics.....	153
4.4.2	Product yield and energy recovery.....	154
4.4.3	Characterization of the organic oil fraction.....	157
4.4.3.1	<i>Physicochemical properties</i>	157
4.4.3.2	<i>Chemical composition</i>	160
4.4.3.3	<i>GPC analysis</i>	168

4.4.3.4	<i>FTIR analysis</i>	169
4.4.4	Characterization of the aqueous fraction.....	170
4.4.4.1	<i>Chemical composition</i>	170
4.4.4.2	<i>Physical properties</i>	176
4.4.5	Characterization of the solid residue	179
4.5	Conclusion	180
4.6	References	183
5	Valorization of raspberry seed cake	187
5.1	Flash pyrolysis of raspberry seed cake: Influence of pyrolysis temperature on the product yield and the characteristics of the pyrolysis liquid.....	187
5.1.1	Product yield and energy recovery.....	187
5.1.2	Characterization of the pyrolysis liquid	188
5.1.2.1	<i>Physical properties</i>	188
5.1.2.2	<i>Chemical composition</i>	190
5.1.3	Characterization of the solid residue	194
5.2	Slow pyrolysis of raspberry seed cake: Collection of the pyrolysis liquid in fractions as a function of pyrolysis temperature	196
5.2.1	Product yield and properties of the liquid fractions.....	196
5.2.2	Chemical composition of the liquid fraction	197
5.2.3	Solid residue.....	202
5.3	Conclusion	203
5.4	References	204
6	Production and characterization of AC from agricultural waste cake.....	205
6.1	Introduction	205
6.2	Production of activated carbon.....	206
6.2.1	Production of solid residue – AC precursor	206

6.2.2	Production of activated carbon by physical activation	206
6.2.2.1	<i>Yield of activated carbon</i>	206
6.2.2.2	<i>Ash content of activated carbon and HCl-washing</i>	208
6.3	Characterization of activated carbon.....	211
6.3.1	Nitrogen adsorption isotherms and pore size distributions	211
6.3.1.1	<i>Rapeseed cake</i>	211
6.3.1.2	<i>Raspberry seed cake</i>	212
6.3.2	Textural characteristics of ACs	217
6.3.2.1	<i>Rapeseed cake</i>	217
6.3.2.2	<i>Raspberry seed cake</i>	221
6.3.3	Elemental composition of activated carbons	224
6.3.4	Functional groups of activated carbons.....	226
6.3.5	Surface morphology of activated carbons	227
6.4	Phenol adsorption study.....	229
6.4.1	Phenol adsorption isotherms	229
6.4.1.1	<i>Rapeseed cake</i>	229
6.4.1.2	<i>Raspberry seed cake</i>	232
6.4.2	Adsorption models of Freundlich and Langmuir.....	232
6.4.2.1	<i>Rapeseed cake</i>	233
6.4.2.2	<i>Raspberry seed cake</i>	234
6.4.3	Phenol adsorption vs textural characteristics of ACs	235
6.4.4	AC from agricultural waste cake vs commercial grade AC	237
6.4.5	Effect of solution's initial pH on phenol removal.....	238
6.4.6	Phenol adsorption: kinetic study.....	239
6.4.7	Intraparticle diffusion model	241
6.5	Conclusion	245

6.6 References	247
7 Water content of pyrolysis liquids: Comparison between Karl Fischer titration, GC/MS-corrected azeotropic distillation and ¹H-NMR spectroscopy	251
7.1 Introduction	251
7.2 Experimental setup	253
7.2.1 Pyrolysis liquids.....	253
7.2.2 Water determination of pyrolysis liquids	253
7.2.2.1 Volumetric Karl Fischer titration.....	253
7.2.2.2 Azeotropic distillation by the Dean-Stark method	254
7.2.2.3 GC/MS-correction for azeotropic distillation by the Dean-Stark method	255
7.2.2.4 ¹ H-NMR spectroscopy	256
7.3 Results and discussion.....	258
7.3.1 Karl Fischer titration: sensitivity for interferences.....	258
7.3.2 Water content of pyrolysis liquids	259
7.3.2.1 Pyrolysis liquids with a low water content	259
7.3.2.2 Pyrolysis liquids with a high water content	262
7.3.2.3 Pyrolysis liquids originating from different types of biomass ..	263
7.3.2.4 Overview of the different water determination methods.....	263
7.4 Conclusion	265
7.5 References.....	266
Summary and general conclusion	269
Samenvatting en algemeen besluit	279

List of abbreviations

°C	degree Celsius
µL	microliter
¹ H-NMR	proton Nuclear Magnetic Resonance
A	ash
AC	activated carbon
AD	azeotropic distillation
AD	acid detergent
ADF	acid detergent fibre
ASTM	American Society for Testing and Materials
ATR-FTIR	Attenuated Total Reflectance Fourier Transform Infrared
BBOT	2,5-bis(5-tert-butyl-benzoxazol-2-yl)thiophene (C ₂₆ H ₂₆ N ₂ O ₂ S)
BET	Brunauer, Emmett and Teller
BHT	butylated hydroxytoluene
C	carbon
C ₀	initial concentration
C _e	equilibrium concentration
CFB	circulating fluidized bed
cST	centistokes (1 mm ² /s)
Da	Dalton
daf	dry ash-free
d _f	film thickness
DR	Dubinín-Radushkevich
DTG	differential thermogravimetric
DW	dry weight
e.g.	for example ("exempli gratia")
Eq.	equation
et al.	and others ("et alii")
eV	electron volt
FAO/STAT	Food and Agriculture Organization of the United Nations
FTIR	Fourier Transform Infrared
g	gram
GC/MS	Gas Chromatography/Mass Spectrometry
GHG	greenhouse gases
GPC	Gel Permeation Chromatography

H	hydrogen
h	hour
HC	hydrocarbons
HHV	higher heating value
HPLC	High Performance Liquid Chromatography
i.e.	that is ("id est")
IC	Ion Chromatography
ICP-AES	Inductively Coupled Plasma - Atom Emission Spectrometry
IEA	International Energy Agency
IPD	intraparticle diffusion
IUPAC	International Union of Pure and Applied Chemistry
J	Joule
K	Kelvin ($^{\circ}\text{C} + 273.15$)
k_1	rate constant of the pseudo-first-order model
k_2	rate constant of the pseudo-second-order model
K_F	Freundlich constant
KF	Karl Fischer
K_L	Langmuir constant
L_0	average micropore width
M	molar concentration
m	meter
m/V%	mass-volume percentage (g solute per 100 mL solvent)
min	minutes
mL	milliliter
mm	millimeter
Mt	million metric tons
Mtoe	million tons of oil equivalent (10^{13} kcal)
mV	millivolt
Mw	molecular weight
Mwe	megawatts of electric output
N	nitrogen
N_A	Avogadro constant ($6.022 \cdot 10^{23} \text{ mole}^{-1}$)
ND	neutral detergent
NDF	neutral detergent fibre
n_F	Freundlich constant
NIST	National Institute of Standards and Technology

List of abbreviations

nm	nanometer (1 nm = 10 ⁻⁹ meter)
no.	number ("numero")
nos.	numbers
NO _x	nitrogen oxides (i.e. NO and NO ₂)
NREL	National Renewable Energy Laboratory
O	oxygen
Pa	Pascal
PEG10k	polyethylene glycol (molecular weight: 10 000 Da)
PFO	pseudo-first-order
PP	pyrolysis product
ppm	parts per million
PSD	pore size distribution
PSO	pseudo-second-order
PTFE	polytetrafluoroethylene
q	adsorption capacity
q _e	equilibrium adsorption capacity
q _m	monolayer adsorption capacity
QSDFT	Quenched Solid Density Functional Theory
R _L	separation factor
rpm	rotations per minute
RSD	relative standard deviation
RT	retention time
s	seconds
S	sulfur
S _{BET}	BET specific surface area
SD	standard deviation
SEM	Scanning Electron Microscopy
SO _x	SO ₂ and SO ₃
SR	solid residue
STP	Standard Temperature (273.15 K) and Pressure (101325 Pa)
T	temperature
T _{act}	activation temperature
t _{act}	activation time
TAN	Total Acid Number
TG	triglycerides
TG	thermogravimetric

TGA	thermogravimetric analysis
THF	tetrahydrofuran
UNFCCC	United Nations Framework Convention on Climate Change
USDA	United States Department of Agriculture
V/V%	volume-volume percentage (mL solute per 100 mL solvent)
V_{DR}	micropore volume by the Dubinin-Radushkevich method
V_m	monolayer adsorption capacity
V_{me}	mesopore volume
VOCs	volatile organic compounds
V_t	total pore volume
wt%	weight percentage

Research objectives and outline

Nowadays, the largest part of world's energy demand is still fulfilled by fossil fuels, although their use has led to serious environmental problems. However, growing environmental concern, predictions of scarcity, supply oscillations and rising prices of fossil fuels strongly stimulate the search for sustainable and renewable sources of energy.

Renewable energy includes solar, water, tidal, wind and geothermal power as well as biomass. Moreover, biomass is considered as the renewable energy source with the highest potential to contribute to the energy needs of modern society. However, conversion of the (solid) biomass into a more useful and valuable form is usually required. In general, a liquid or solid energy carrier that is easily transportable and storable is preferred. Depending on the biomass characteristics and the desired energy form, a suitable conversion process has to be selected. Pyrolysis is very promising since it is the only thermochemical conversion technique that converts biomass into three fractions: solid, liquid and gas. Pyrolysis can be defined as the thermochemical decomposition of material, including biomass waste, at moderate temperatures (350 - 700 °C) and in the absence of oxygen (or oxygen deficient). The yield of each fraction depends on the applied pyrolysis conditions (temperature, heating rate, vapor residence time, etc.) and the properties of the biomass feedstock. In general, the production of solid residue is favored by relatively low pyrolysis temperatures and long vapor residence times, while high liquid yields require moderate temperatures and short vapor residence times. The pyrolysis liquid has potential as renewable (transportation) fuel (after upgrading) or as source of added-value chemicals. The solid residue (or char) can be valorized as precursor in the production of activated carbon, as fertilizer or as improved solid energy carrier. Frequently, the gaseous fraction still has a moderate energy content that can be used to provide process heat by combustion.

In this study, the valorization of three agricultural waste cakes by pyrolysis is the main objective. Hereby, the focus is mainly on two pathways: valorization of the pyrolysis liquid as renewable (transportation) fuel and/or valorization of the solid residue as fuel or as precursor in the production of activated carbon. Most of the work is performed on rapeseed cake and in a lesser extent on raspberry seed cake, while olive waste cake is only evaluated in a preliminary study.

In Chapter 1, a general introduction on biomass (waste) as renewable source of energy and chemicals is provided. Additionally, this chapter introduces pyrolysis as a promising thermochemical conversion technique and gives a general overview of the properties and applications of the pyrolysis products.

Chapter 2 describes the experimental approach and the methodology used for production and characterization of the pyrolysis products obtained in this study.

A profound characterization of the agricultural waste cakes together with preliminary flash pyrolysis experiments are discussed in Chapter 3. Based on these preliminary results, a well-founded choice can be made in selecting the most promising valorization pathway for each agricultural waste cake.

Chapter 4 focusses on the valorization of **rapeseed cake**. In §4.1, the influence of the pyrolysis temperature on the product yield and the characteristics of the pyrolysis liquid in flash pyrolysis is investigated. The potential of fractionated condensation and the use of a polymer to reduce the water content of pyrolysis liquids produced by flash pyrolysis are briefly discussed in §4.2. Slow pyrolysis of rapeseed cake with collection of the pyrolysis liquid as a function of pyrolysis temperature is the topic of §4.3. The potential of three catalysts (γ -Al₂O₃, HZSM-5 and Na₂CO₃) to improve the quality of pyrolysis liquids in slow catalytic pyrolysis are discussed in §4.4.

Chapter 5 describes the valorization of **raspberry seed cake**. In §5.1, the influence of the pyrolysis temperature on the product yield and characteristics of the pyrolysis liquid is investigated, while slow pyrolysis with collection of the pyrolysis liquid in fractions as a function of temperature is the topic of §5.2.

Chapter 6 is dedicated to the valorization of the **solid residue** produced from **rapeseed cake** and **raspberry seed cake** as precursor in the production of activated carbon. The influence of the temperature, time and activation agent (steam or CO₂) in physical activation of the solid residue is investigated. The activated carbons are characterized by N₂-adsorption (BET specific surface area and pore size distribution) and their performance is evaluated by batch adsorption experiments using phenol as target compound.

In Chapter 7, Karl Fischer titration, GC/MS-corrected azeotropic distillation and ¹H-NMR spectroscopy are evaluated and compared as analytical techniques to determine the water content of pyrolysis liquids.

1 Introduction

1.1 Biomass as renewable energy source

The demand for energy and its sources is increasing every day due to the rapid growth of world's population and developing technologies (Figure 1-1) [1, 2]. According to the most recent figures of the International Energy Agency (IEA), this energy demand is still mainly fulfilled from conventional fossil fuels (oil: 41.2 %, natural gas: 15.2 % and coal: 9.8 %), while biofuels and waste only have minor contributions (12.7 %) [2].

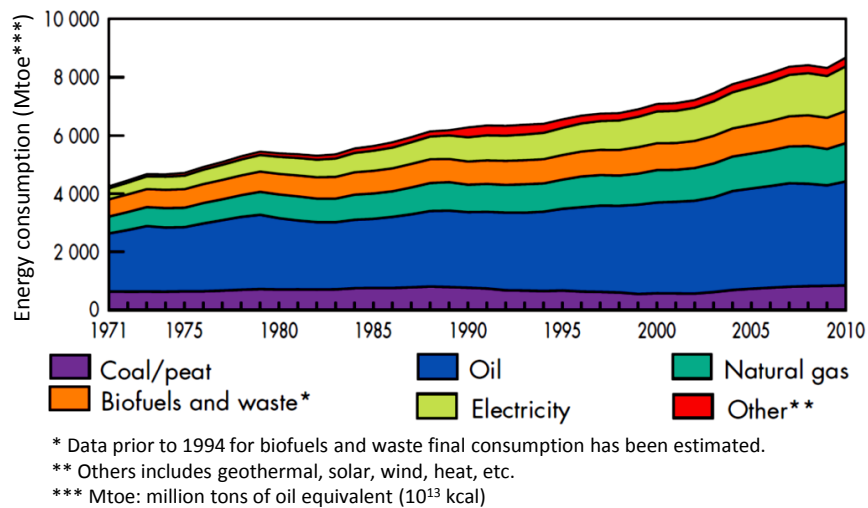


Figure 1-1: World total final consumption from 1971 to 2010 by fuel [2].

Obtaining energy from fossil fuels is accompanied by major drawbacks. Firstly, sources of fossil fuels are at the verge of getting exhausted and are not renewable within a time scale mankind can use [3]. Oil sources, for instance, are estimated to be depleted around 2050 [1]. Secondly, obtaining energy from fossil fuels has led to serious environmental problems such as atmospheric pollution, acid rain and global warming due to the production of greenhouse gases (GHG). Thirdly, supply oscillations and the contradiction between the global energy demand and the limited number of energy supplying countries may lead to sociopolitical tensions in the near future. As a result, a shift to alternative and renewable energy sources seems to be inevitable [1]. However,

conventional energy sources remain important to bridge the period until renewable energy carriers are in common use.

Renewable energy sources include solar, water, tidal, wind and geothermal power as well as biomass [4]. The latter is considered as the renewable energy source with the highest potential to contribute to the energy needs of modern society for both developed and developing economies worldwide [2, 5]. Moreover, biomass energy is destined to play an important role in the future energy systems of the world [6, 7].

Biomass is available on a renewable basis either through natural processes or as by-product of human activities (e.g. agricultural residues). Hence, plant biomass is continuously formed by photosynthesis i.e. the reaction of atmospheric carbon dioxide and water in presence of sunlight and chlorophyll. In this way, solar energy is stored in the chemical bonds of the structural components of biomass [3]. Biomass is considered as a source of "carbon-neutral" fuels because the CO₂ released during biomass fuel combustion was already absorbed from the atmosphere during plant growth in the recent past [8]. In contrast, burning fossil fuels releases "new" CO₂ that contributes to the greenhouse effect and depletes non-renewable sources [3]. Besides being CO₂ neutral, biomass based fuels are reported to have lower emissions of NO_x, SO_x and particulate matter compared to fossil fuels [9]. However, one should be aware that biomass fuel is still an incomplete renewable energy source at present when considering the complete life cycle due to the energy consumption (and so CO₂ production) during harvesting and processing of biomass [10].

Besides environmental advantages, biomass as renewable energy source has sociopolitical benefits as well. Hence, biomass is a locally grown resource that is quite easily accessible for many countries, resulting in a more secure and diversified energy supply [3, 10]. As a result, many countries can decrease their reliance on foreign fossil fuels in terms of less reliable supply and price fluctuations [8]. Additionally, the biomass industry will have a positive impact on the local economy (employment) [10].

1.2 Biomass and agricultural waste cake

1.2.1 Definition and classification of biomass

Biomass can be defined as non-fossilized and biodegradable organic material originating from plants, animals and micro-organisms. This shall also include by-products, residues and waste from agriculture, forestry and related industries as well as the non-fossilized and biodegradable organic fractions of industrial and municipal wastes [8, 11]. Hence, biomass covers a wide spectrum of organic materials. Therefore, a general classification of biomass varieties as fuel resources might be convenient. Based on biological diversity and similarity in source and origin, the following biomass groups can be distinguished [3, 10, 12]:

- (1) wood and woody biomass (including forestry residues and wastes)
- (2) herbaceous and agricultural biomass (including residues and wastes)
- (3) aquatic biomass (e.g. algae)
- (4) animal and human biomass wastes
- (5) contaminated biomass and industrial biomass wastes
- (6) biomass mixtures

Concerning the production of renewable fuels and chemicals, it is important to choose a biomass that does not threaten the world's food supply. One of the biggest problems for large-scale renewable energy production from biomass is the availability of sustainable biomass resources. In this view, groups 1 and 2 are of particular interest. The first group is composed of relatively quick growing trees and ligneous plants that are not easily accessible for food production. Within the second group, agricultural biomass is composed of all kinds of crops, even those that can be used for food purposes. However, agricultural crops also result in residues and wastes that are not suitable for food consumption and therefore are considered as agricultural wastes.

1.2.2 Agricultural waste cake

In this work, the valorization of three agricultural waste cakes, representatives of the second group in the general biomass classification above, is the main objective. Hereby, the focus lies mainly on rapeseed cake and in a lesser extent

on raspberry seed cake, while the opportunities of olive waste cake are assessed in a preliminary study.

1.2.2.1 Rapeseed cake

Rapeseed (*Brassica napus* L.) is one of world's most important oilseed crops and is nowadays mainly cultivated for the production of vegetable oil. Rapeseed includes several varieties such as high erucic acid rapeseed, low erucic acid (< 2 %) rapeseed and "double low" rapeseed (or Canola) which has a low content of both erucic acid and glucosinolates¹ [13]. The worldwide annual production of rapeseed in 2012 was estimated at about 60 million metric tons (Mt) by the United States Department of Agriculture (USDA). Most of the rapeseed is mechanically pressed to produce vegetable oil (about 23.9 Mt), resulting in a considerable amount (about 35.5 Mt) of solid residue, known as rapeseed cake [14]. Typically, cold pressing reduces the oil content from 40 – 45 % in the whole seeds to 14 – 15 % in rapeseed cake [15]. The oil remaining in rapeseed cake can eventually be further recovered by solvent extraction using hexane, but then it is not suitable anymore for food consumption. Rapeseed oil has various applications. Oil originating from low erucic rapeseed can be valorized as human food (e.g. margarines, cooking oil or sauces) or in animal feed. Additionally, rapeseed oil is used in a range of technical purposes such as biodegradable lubricating oils (high erucic acid), surfactants, paints, inks, polymers, personal care products and pharmaceuticals or in the production of biodiesel via transesterification with light alcohols such methanol and ethanol [16, 17]. The "double low" rapeseed cake, formed as by-product in vegetable oil production, is currently valorized as substitute for soybean meal in animal feeding (cattle, pigs and poultry) because of its high content of proteins and triglycerides [7, 18]. However, since animal feed can only contain a limited amount of rapeseed cake (< 20 % [17]) and not all types of rapeseed cake are suitable for animal feed due to a high content of erucic acid and glucosinolates, other valorization pathways for rapeseed cake are desirable as well [7].

¹ Glucosinolates in rapeseed result in palatability and nutritional problems when fed to animals due to their decomposition into toxic compounds including nitriles and thiocyanates. Erucic acid is also known as *cis*-13-docosenoic acid (C22:1,n-9).

1.2.2.2 *Raspberry seed cake*

The total global production of raspberries (*Rubus Idaeus* L.) in 2011 was estimated at 0.54 Mt by the Food and Agriculture Organization of the United Nations (FAOSTAT) [19]. In the production of raspberry juice, raspberry seeds are obtained as by-product. These seeds (about 10 wt% of fresh berries) are a source of high quality oil (10 - 23 wt%) and polyphenolic compounds that are effective antioxidants [20, 21]. Oil produced from raspberry seeds can be valorized in food, cosmetic and pharmaceutical industries. For the solid residue obtained after processing of raspberry seeds, i.e. raspberry seed cake, a suitable valorization pathway still has to be found [21].

1.2.2.3 *Olive waste cake*

The cultivation of olives (*Olea Europaea* L.) is a typical activity in Mediterranean countries. The total global olive production in 2011 was estimated at 19 Mt [19]. About 15 - 22 wt% of the olives can be recovered as olive oil and about 35 - 45 wt% as olive waste cake, the solid residue in the oil production process [22]. Olive oil is mainly used in food, cosmetic and pharmaceutical industries, while olive waste cake can be valorized as renewable energy source by combustion or as precursor in the production of activated carbon [23, 24].

1.2.3 Composition of biomass

Biomass can be regarded as a complex heterogeneous mixture of major structural organic components, bulk extractives and minor amounts of inorganic matter [12]. The structural components consist of three organic polymers, namely cellulose, hemicellulose and lignin. Bulk extractives are defined as those compounds that are not an integral part of the biomass structure [25]. They are composed of various types of compounds including lipids, waxes, resins, proteins, tannins, simple sugars, alkaloids, pectins, gums and pigments [9, 12, 26]. The proportions of structural components and bulk extractives in biomass are highly variable. Lignocellulosic biomass, for instance, typically has a high content of cellulose (40 - 50 wt%), hemicellulose (20 - 30 wt%) and lignin (20 - 30 wt%), while bulk extractives are only present in minor amounts [3]. In contrast, agricultural and herbaceous biomass usually contains relatively high

proportions of bulk extractives [12]. The variability in composition between different biomass species is illustrated in Table 1-1.

Table 1-1: Major components present in different biomass species.

Component (wt%)	Willow (stems) [27]	Rapeseed cake [28]	Olive husk [23]
Hemicellulose	18	41	22
Cellulose	41	29	24
Lignin	25	5	45
Extractives	8	19	9

1.2.3.1 Cellulose

Cellulose is the primary structural component of cell walls and can be represented by the general formula $(C_6H_{10}O_5)_n$ [8, 29]. This linear polymer has a high molecular weight ($\geq 10^6$ Da) and consists of D-glucopyranose units (up to 10000) that are connected by $\beta(1\rightarrow4)$ glycosidic bonds [9]. Parallel cellulose chains are stabilized by intra- and intermolecular hydrogen bonds, leading to a fibrous structure (Figure 1-2). This well-ordered (semi-crystalline) structure explains the relatively high thermal stability of cellulose [9, 30]. Thermal degradation typically occurs in the temperature range from 315 to 400 °C [31].

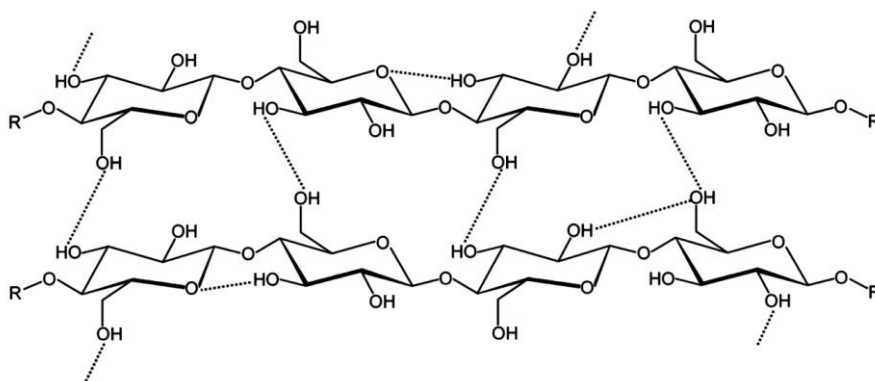


Figure 1-2: A segment of two cellulose chains showing some of the intra- and intermolecular hydrogen bonds (dotted lines) [30].

1.2.3.2 Hemicellulose

Hemicellulose (also known as xylan, pentosan or polyose) is a carbohydrate polymer that is composed of various C5 and C6 monosaccharides such as xylose, glucose, galactose, mannose, arabinose and some acids including glucuronic and galacturonic acid (Figure 1-3) [9]. The average molecular weight is usually below 30000 Da, which is considerably lower than that of cellulose. In contrast to cellulose, hemicellulose is a hetero-polysaccharide with a random and amorphous structure that is highly branched. These side-chain branches can be quite easily removed from the main chain by heating, explaining the lower thermal stability of hemicellulose compared to cellulose (no branches). Thermal degradation of hemicellulose typically occurs in the temperature range from 220 to 315 °C [31].

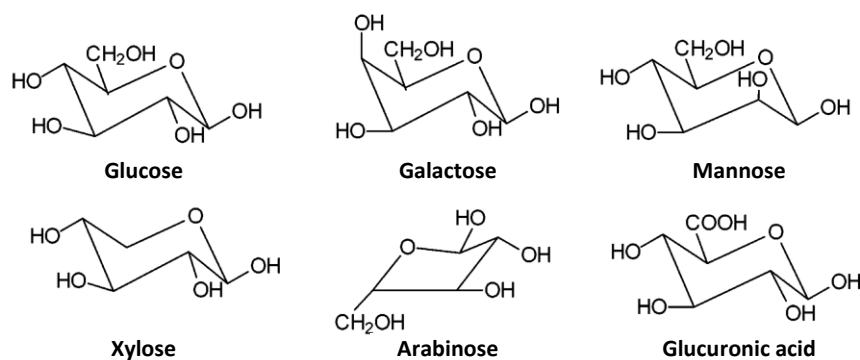


Figure 1-3: Chemical structures of the main monosaccharides present in hemicellulose [9].

1.2.3.3 Lignin

Lignin is a complex, highly branched and highly substituted aromatic polymer with a high molecular weight. It is the main binder for fibrous components (such as cellulose) in plants [12]. This biopolymer can be considered as a random three-dimensional network of three basic building blocks. These building blocks consist of phenylpropane units containing zero, one or two methoxyl groups and are named structure I, II and III, respectively (Figure 1-4). The proportion of each structure depends on the source of lignin, i.e. structure I is mainly found in plants such as grasses, structure II in the woods of conifers, while structure III is predominant in deciduous woods [3]. The building blocks are randomly linked together by non-selective radical reactions, leading to an amorphous lignin

structure (Figure 1-5). Ether bonds dominate, but C-C and other covalent bonds also occur between the phenylpropane units. The wide variability in strength of these chemical bonds explains why thermal degradation of lignin typically occurs in a wide temperature range (100 – 900 °C) [31]. Compared to cellulose and hemicellulose, lignin has a lower oxygen and a higher carbon content, resulting in a considerably higher calorific value (about 30 %) [12].

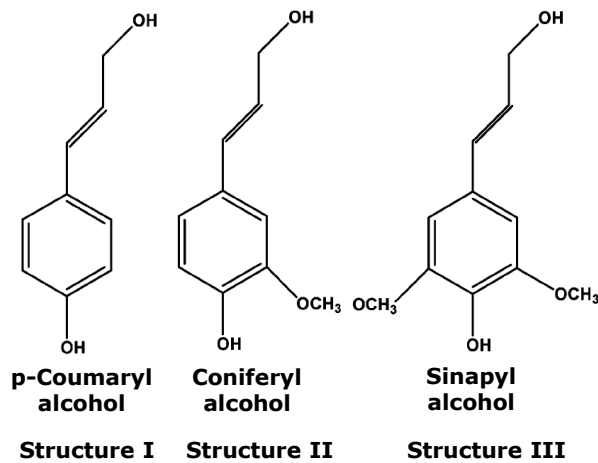


Figure 1-4: The three building blocks of lignin: p-coumaryl alcohol, coniferyl alcohol and sinapyl alcohol [9].

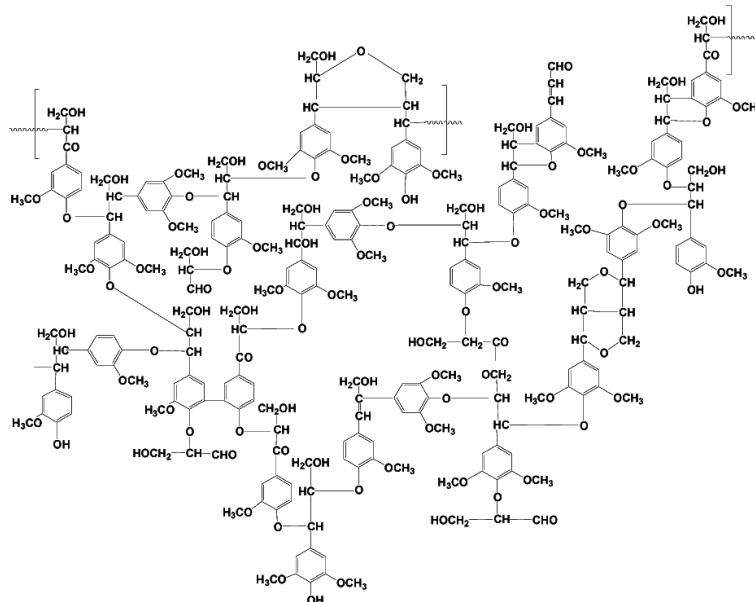


Figure 1-5: Partial structure of lignin from European Beech [9].

1.2.3.4 Bulk extractives: triglycerides and proteins

Besides three structural components, biomass also contains compounds that are not an integral part of the biomass structure. Since these compounds can be easily extracted from biomass with solvents, they are named bulk extractives. The composition and the quantity of these extractives depend on the biomass variety as well as on the solvent used and the extraction time. The water-ethanol extraction, for instance, is reported to remove approximately 90 % of all biomass extractives [12].

In contrast to lignocellulosic biomass, herbaceous and agricultural biomass generally contains relatively high amounts of bulk extractives [12]. Rapeseed, for instance, is reported to have a high content of vegetable oil (about 40 wt%) and proteins (about 22 wt%) [32]. Chemically, vegetable oils consist of triglycerides that are made up of three fatty acids connected to glycerol by ester bonds (Figure 1-6). An overview of the fatty acid composition of vegetable oils originating from different biomass species is shown in Table 1-2. The thermal behavior of both saturated and unsaturated triglycerides is extensively studied. A good review is published by Maher and Bressler [33].

Proteins, on the other hand, consist of a variety of amino acids arranged in a linear chain and linked together by peptide bonds between the carboxyl and amino groups of adjacent amino acid residues. These compounds are considered as the main source of nitrogenated compounds (including amines, nitriles, pyridine and indole) found in thermal conversion of biomass [34].

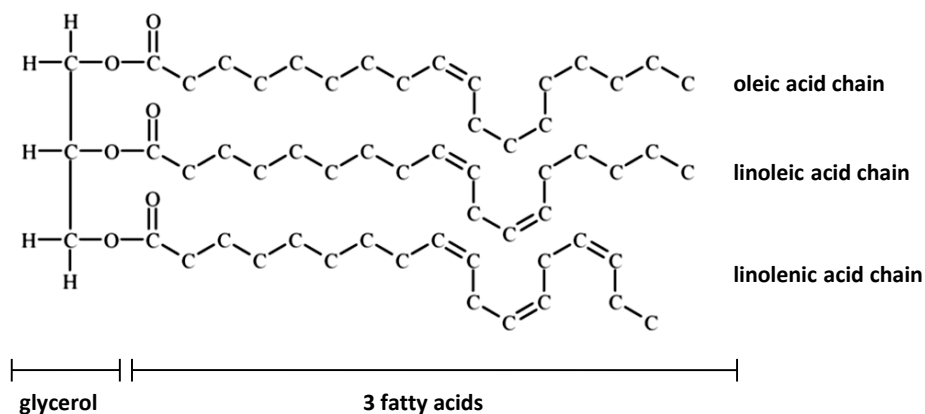


Figure 1-6: Chemical structure of a triglyceride present in rapeseed oil (adapted from [16]).

Table 1-2: Fatty acid composition (free and esterified) in different vegetable oils (%).

Fatty acid	Structure	Rapeseed oil [16]	Olive oil [35]	Raspberry seed oil [21]
Palmitic acid	C16:0	4.8	11.9	2.7
Stearic acid	C18:0	1.5	2.9	1.0
Oleic acid	C18:1	60.7	81.3	12.0
Linoleic acid	C18:2	21.2	0.3	54.5
Linolenic acid	C18:3	11.8	-	29.1
Miscellaneous		-	3.6	0.7

1.2.3.5 Inorganic matter

Besides organic compounds, biomass also contains inorganic matter including the following elements: Ca, K, Si, Mg, Al, Fe, Cl, Na, Mn and Ti [12]. The concentration of ash arising from these inorganics can range from less than 1 wt% in softwoods to 15 wt% in herbaceous biomass and agricultural residues [29].

1.3 Biomass conversion techniques

Biomass is a very promising resource for renewable fuels and/or added-value chemicals. However, solid biomass cannot be handled, stored and transported as easily as liquid fuels due to its low bulk density and inconvenient form [3, 29]. Additionally, liquid fuels have advantages in retrofitting and flexibility in production and marketing [36]. Therefore, conversion of biomass into a more valuable and useful (mostly liquid) energy form is generally preferred [37]. Although the potential energy amount of a given biomass is irrespective of the conversion method selected, the actual amount of energy recovered from biomass and the form of that energy are strongly dependent on the conversion process [3].

In general, biomass conversion can be achieved by three main routes: a mechanical, a biochemical and a thermochemical route [1, 8, 37, 38]. An overview is shown in Figure 1-7.

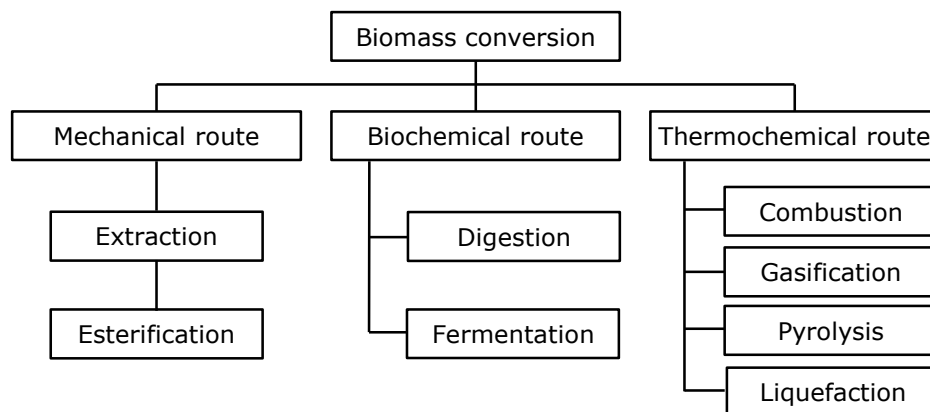


Figure 1-7: Three main routes of biomass conversion into renewable fuels and/or added-value chemicals (adapted from [8]).

1.3.1 Mechanical conversion

Mechanical or physical conversion of biomass is usually applied for energy production from various oil crops such as rapeseed, soybean, sunflower and safflower [4, 39]. Oil extraction from these crops, both for food and fuel purposes, using a mechanical screw press is a well-known process [15]. The extracted vegetable oil can be used as such or further converted into biodiesel

by reaction with light alcohols such as methanol or ethanol (transesterification) [39]. The solid residue (or waste cake) of the extraction process can often be valorized as animal feed [38]. Recently, the use of bio-fuels produced from edible oils has been widely countered as unethical due to competition with the basic food supply chain [40]. However, biodiesel production from non-edible vegetative oils is considered as an effective way to overcome all associated problems with edible oils and could make a substantial contribution to the world's future energy demands [41].

1.3.2 Biochemical conversion

Biochemical conversion involves the decomposition of biomass components into smaller molecules with the aid of micro-organisms or enzymes (biological catalysts). This process is usually very selective and produces a small number of discrete products in high yield [37]. In general, biochemical conversion encompasses two process options: anaerobic digestion and fermentation [38].

1.3.2.1 Anaerobic digestion

Anaerobic digestion is the conversion of the biodegradable part of biomass into biogas (mainly CH₄ and CO₂) by bacteria in an anaerobic environment. It is a commercially proven technology that is widely used for treating organic wastes with a high moisture content (> 80 wt%). The biogas can be used directly in gas turbines to produce electricity or upgraded to natural gas by the removal of CO₂ [8, 38].

1.3.2.2 Fermentation

In fermentation, small (fermentable) sugars are converted into ethanol, CO₂, CH₄, H₂ and other organic chemicals, depending on the selected yeasts and/or bacteria. Fermentation of starch crops (e.g. maize and wheat) and sugar crops (e.g. sugar cane and sugar beet) to produce ethanol is commercially used on a large scale in various countries. In contrast, conversion of lignocellulosic biomass (such as wood and grasses) is more complex due to the presence of disturbing components such as lignin. Therefore, a pretreatment using acid or enzymatic hydrolysis is required to make the sugar monomers from the biomass available to the micro-organisms for conversion into ethanol [8, 38]. After

fermentation, the purification of ethanol involves a very energy-intensive distillation process. This ethanol can be used directly as a renewable fuel or as a supplement in petrol fuel, while the solid residue can be valorized as cattle feed or as fuel to provide process heat [4, 38].

1.3.3 Thermochemical conversion

Thermochemical conversion of biomass frequently results in multiple and often complex products, whether or not in presence of inorganic catalysts to improve the product quality. The main driver for these processes is the production of thermal energy, although the production of chemicals is also possible [37]. Compared with biochemical conversion, thermochemical conversion involves much shorter reaction times, but generally requires much higher amounts of external energy [8]. Generally, four process options are available within thermochemical conversion: combustion, gasification, pyrolysis and liquefaction [38].

1.3.3.1 Combustion

Combustion, i.e. the burning of biomass in excess air, converts the chemical energy stored in biomass into heat, mechanical power or electricity using various items of process equipment such as stoves, furnaces, boilers and gas turbines. Combustion of biomass produces hot gases (mainly CO₂ and steam) at temperatures around 800 to 1000 °C [38]. Net electrical efficiencies for biomass combustion power plants range from 20 to 40 %. The higher efficiencies are obtained with systems over 100 MWe or when the biomass is co-combusted in coal-fired power plants [4, 38]. Combustion is a well-established proven technology and development is mainly concentrated on resolving environmental problems [37, 42]. However, in most cases, biomass combustion requires pretreatment steps, including drying, chopping and grinding, that are associated with an energy expenditure and financial costs [1, 38]. The low calorific value, the relatively high ash content, the low bulk density and associated high transportation costs make biomass combustion less economic favorable than combustion of fossil fuels.

1.3.3.2 Gasification

Gasification converts biomass into a combustible gas mixture by partial oxidation in oxygen deficient conditions at high temperatures (500 – 1300 °C) [1, 8]. Gas (air, oxygen, subcritical steam or a mixture of these) or supercritical water are used as reaction medium [8]. Typical products are CO₂, CH₄ and syngas (a mixture of CO and H₂) [4]. These gases can be used directly as fuel (CH₄) or be converted into added-value chemicals by further processing. For instance, syngas can be converted into liquid transport fuels by Fischer-Tropsch synthesis, while CO can be indirectly hydrogenated by steam to produce methanol, an important precursor for a large number of chemicals [8].

1.3.3.3 Pyrolysis

Pyrolysis is the thermal decomposition of biomass into solid, liquid and gaseous fractions in absence of oxygen and at moderate temperatures (350 – 700 °C) [9]. The yield of each fraction can be optimized by choosing appropriate process conditions. For instance, moderate temperatures, high heating rates and short vapor residence times favor the production of pyrolysis liquid [37]. In contrast to combustion and gasification, which produce energy in a form that is best used at the point of production (heat, steam or gas), (fast) pyrolysis converts biomass mainly into a liquid form that is easily storable and can be used when and where needed [37, 38]. As a result, pyrolysis offers the possibility of decoupling (time, place and scale), easy handling of liquids and more-consistent quality compared to solid biomass [9]. However, most applications require upgrading of the pyrolysis liquid due to the poor stability, the complex composition and the low calorific value.

1.3.3.4 Liquefaction

Liquefaction of solid biomass into a liquid fuel can be performed by pyrolysis, gasification as well as by hydrothermal upgrading (HTU) [8]. The latter is performed in a wet environment at relatively low temperatures (250 – 330 °C), at high pressures (12 - 20 MPa) and in presence of a catalyst to produce partly oxygenated hydrocarbons [4, 8, 38].

1.3.4 Selection of the appropriate biomass conversion process

Factors that influence the choice of the biomass conversion process are [38]:

- ⇒ the type and quantity of the biomass feedstock
- ⇒ the desired energy form (solid, liquid or gas)
- ⇒ environmental standards
- ⇒ economic conditions

Important biomass properties include moisture content, bulk density, thermal conductivity and ash content [3]. Among these parameters, moisture content is considered as the most important preliminary parameter due to the high economic cost of biomass drying. As a result, high-moisture biomass is preferably converted by (aqueous) biochemical techniques, while low-moisture biomass is more suitable for thermochemical conversion [4]. The bulk density of biomass strongly affects transport and storage costs, while the thermal conductivity is an important factor concerning thermochemical conversion. A high ash content (especially alkali metals) can complicate further biomass processing (e.g. blockage of airways in furnaces or boiler plants) [3]. The environmental impact of a particular biomass species will vary from one region to another, depending on socioeconomic and political factors [38]. However, some biomass feedstocks are amenable to more than one conversion technology. Rapeseed, for instance, can be processed by combustion, gasification, pyrolysis or mechanical extraction, while others such as wood and cereal crops are suitable for combustion, gasification, pyrolysis and fermentation [3].

1.4 Pyrolysis

Pyrolysis is the thermochemical decomposition of (biomass) material at a moderate temperature (350 - 700 °C) and in the absence of oxygen or significantly less oxygen than required for complete combustion [9]. This biomass degradation involves the dissociation of chemical bonds and the production of free radicals [29, 43]. The primary pyrolysis products consist of gas, condensable vapors (tar) and char (Figure 1-8). The condensable vapors may be further degraded to form non-condensable gases (e.g. CO, CO₂, H₂, CH₄ and small organic compounds such as C₂H₆, C₂H₄ and C₂H₂), pyrolysis liquid and char in secondary reactions. This decomposition occurs partly through gas-phase homogeneous reactions and partly through gas-solid phase heterogeneous thermal reactions [8]. In case of the former, condensable vapors are cracked into smaller molecules or permanent gases, while the latter involves the continuous interaction between primary vapors and char [9].

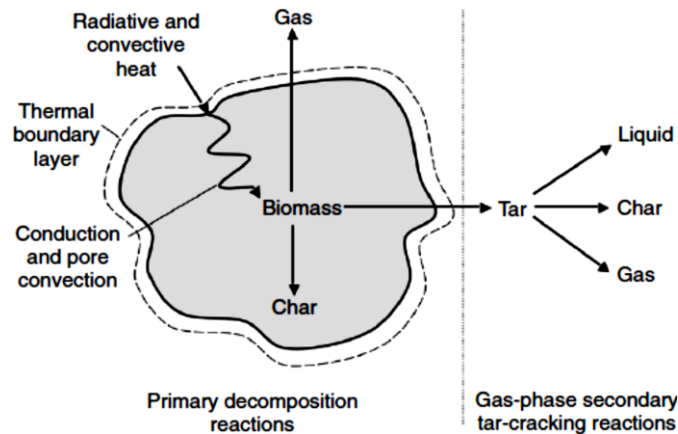


Figure 1-8: Pyrolysis of a biomass particle [8].

1.4.1 Pyrolysis of biomass

Virtually any kind of biomass can be considered for pyrolysis. While most work has been carried out on wood and wood wastes [9, 40, 44, 45], over 100 different biomass types have been tested, ranging from energy crops such as rapeseed [32, 46-50] over agricultural residues like rapeseed cake [7, 28, 51-55], rapeseed plant [56-58] and olive wastes [23, 59-65], to solid wastes such as sewage sludge [66] and municipal solid waste [67].

1.4.1.1 *Pyrolysis characteristics of biomass constituents*

Each kind of biomass has a characteristic pyrolysis behavior that can be mainly explained based on the characteristics of its individual constituents. Important biomass constituents include the initial moisture, the major components, the bulk extractives and the inorganic ashes [6].

Initial moisture

The initial moisture content affects both the behavior of biomass during pyrolysis and the physicochemical properties of the obtained pyrolysis liquid [68]. Low initial moisture contents (typically < 30 wt%) are usually preferable since they result in lower heat energy requirements during pyrolysis and a better quality of the pyrolysis liquid. However, completely dry biomass suffers from heat transfer limitations due to the low thermal conductivity of biomass [69].

Biomass components and extractives

The proportions of individual biomass constituents and their chemical structure considerably affect the pyrolysis characteristics of biomass [70]. Pyrolysis of individual components is well described in literature and often comparison with pyrolysis of biomass is made [31, 70-73]. However, pyrolysis of biomass is a superposition of the kinetic mechanisms of individual constituents [31]. Hence, each constituent reacts at a different rate and by a different mechanism or pathway [74].

- ⇒ *Hemicellulose* is thermally the most unstable component and is usually degraded between 220 and 315 °C [31]. Typically, more gas and less tar and char are produced from hemicellulose compared with cellulose [8]. More information on pyrolysis of hemicellulose can be found in [75].
- ⇒ *Cellulose* decomposes in the temperature range from 315 to 400 °C and shows the highest rate of decomposition [31]. Thermal decomposition of cellulose can be considered as a complex multistage process. After an intermediate pre-reaction (formation of short-lived active cellulose), two competing first-order reactions are reported to occur. The first reaction path includes dehydration, decarboxylation and carbonization reactions to produce mainly gases (H₂O, CO₂ and CO) and char. These reactions are favored at

lower temperatures (< 300 °C) and at low heating rates. The second path involves depolymerization and scission reactions, resulting in vapors and condensable gases with levoglucosan as an important intermediate product. These reactions are favored at higher temperatures (> 300 °C) and fast heating rates (Broido-Shafizadeh model) [8]. More information on the mechanism of thermal decomposition of cellulose can be found in [76].

- ⇒ *Lignin* decomposition occurs in a broad temperature range (100 – 900 °C), producing aromatics and solid residue (40 - 50 %) [31, 70]. It also contributes to the liquid yield by forming phenolic compounds via cleavage of ether and carbon-carbon bonds. For further information on the mechanism of lignin pyrolysis is referred to [77].
- ⇒ *Extractives* generally decompose in a similar way to lignin but at slightly higher rates and at slightly lower temperatures [70]. Proteins are reported to decompose simultaneously with carbohydrates (around 320 °C [78]), while thermal decomposition of triglycerides occurs at higher temperatures (395 – 500 °C) [72, 79]. An extensive overview of the thermal decomposition of saturated and unsaturated triglycerides can be found in literature [16, 33].

Inorganic matter

Biomass can contain varying amounts of inorganic matter (< 1 – 25 wt%) [29]. In general, inorganic matter decreases the yield of pyrolysis liquid and tends to increase the formation of char and gas because it favors charring and dehydration reactions during both primary and secondary pyrolysis [69]. Alkaline metals, for instance, are reported to catalyze biomass decomposition and char forming reactions [9, 29]. However, most of the alkali and alkaline earth metals present in the biomass feedstock are concentrated in the char, which enables an easy separation of these metals from the product stream [9, 80].

1.4.1.2 Thermal zones in biomass pyrolysis

From a thermal point of view, pyrolysis of biomass can be divided into four stages. Although divided by temperature, the boundaries between these stages are not sharp and some overlap is possible [8]:

- ⇒ *Drying step* (< 100 °C): free moisture and loosely bound water is released. When free moisture is evaporated, heat is conducted to the biomass interior.
- ⇒ *Initial stage* (100 – 300 °C): exothermic biomass dehydration with release of water and gases of low molecular weight (e.g. CO and CO₂).
- ⇒ *Intermediate stage* (> 200 °C): primary pyrolysis takes place between 200 and 600 °C. Large biomass components decompose into (primary) char, condensable gases (precursors of pyrolysis liquid) and non-condensable gases.
- ⇒ *Final stage* (300 – 900 °C): secondary cracking of volatiles into char and non-condensable gases. In case of long residence times, condensable gases of higher molecular weight can crack yielding additional gases and (secondary) char [8].

1.4.2 Pyrolysis process parameters

Pyrolysis of biomass produces three fractions: solid, liquid and gas. The proportion of each fraction can be varied over a relatively wide range by adjustment of several process parameters [69]. The most important parameters are briefly discussed below.

1.4.2.1 Pyrolysis temperature

The pyrolysis temperature is considered as the most important process parameter because it affects the degree of biomass devolatilization and thus both composition and yield of the pyrolysis products [69]. In general, low temperatures (300 – 400 °C) result in a high solid yield, while intermediate temperatures (450 – 550 °C) are required to maximize the yield of pyrolysis liquid. At high pyrolysis temperatures (> 550 °C), secondary decomposition of pyrolysis vapors is predominant, resulting in a higher gas yield at the expense of the solid and liquid yield [29, 32, 48, 69, 81-83].

1.4.2.2 Heating rate

The heating rate is another important factor that affects the pyrolysis product distribution. Low heating rates favor carbonization and promote secondary reactions increasing the yield of solid residue and non-condensable gases [29]. High heating rates (> 300 °C/min in case of rapeseed) are reported to break

biomass heat and mass transfer limitations, resulting in a considerable increase in liquid yield [49, 81]. In general, higher heating rates result in higher liquid yields [84]. However, once heat and mass transfer limitations are overcome, a further increase in heating rate usually does not result in a higher liquid yield [69]. Some authors report that higher heating rates reduce the water content of pyrolysis liquids [84, 85]. Probably, rapid heating inhibits secondary condensation and dehydration reactions [69].

1.4.2.3 Vapor residence time

The vapor residence time describes the time that condensable and non-condensable vapors remain in the hot reactor zone. Short vapor residence times minimize secondary reactions such as secondary cracking or repolymerization, leading to higher liquid yields. In case of fast pyrolysis, vapor residence times are typically less than 2 s [37]. In contrast, long vapor residence times permit secondary reactions between the char particles and volatiles, leading to secondary char formation and thus a higher char yield [8].

Although very short vapor residence times are required to maximize the liquid yield, relatively long vapor residence times enhance deoxygenation reactions. Therefore, optimization of the vapor residence time has to take into account both yield and quality of the pyrolysis liquid [69].

1.4.2.4 Biomass particle size

The size of biomass particles considerably affects the heating rate and heat transfer in pyrolysis due to the low thermal conductivity of biomass [9]. Small particles allow higher heat transfer rates and offer less resistance to primary condensable vapors escaping to the surroundings than large particles. Therefore, small particles result in less secondary cracking and thus in higher liquid yields [6, 37]. The appropriate particle size may vary depending on the biomass type and the pyrolysis reactor setup [69]. Typically, particles sizes smaller than 2 mm are recommended when the purpose is to obtain high liquid yields [9, 86]. Further size reduction is reported to hardly affect the solid and liquid yield [15], while it is associated with a relatively high economic cost (about 1.4 €/ton) [6, 87].

1.4.2.5 Effect of sweeping gas

The reaction environment can affect the distribution and composition of pyrolysis products. The interaction of escaping pyrolysis vapors with the surrounding solid environment can lead to secondary exothermic reactions and the formation of char. These reactions can be minimized by rapid mass transfer using an inert sweeping gas (usually N₂) or vacuum pyrolysis [69, 84]. High sweeping gas velocities generally increase the liquid yield, but too high velocities can be counterproductive since they prevent good condensation and possible reactions with non-condensable vapors to form condensable vapors [69]. However, the effect of the sweeping gas velocity was found to be rather limited in slow pyrolysis (7 °C/min) of rapeseed cake at 500 °C [7].

In general, it can be concluded that:

- ⇒ production of **solid residue** is favored by lower process temperatures and longer vapor residence times
- ⇒ high yields of **pyrolysis liquid** require moderate temperatures and short vapor residence times
- ⇒ conversion of biomass to **pyrolysis gas** is increased by high temperatures and longer vapor residence times [8, 37].

1.4.3 Types of pyrolysis

In literature, three types of pyrolysis are usually distinguished: slow (conventional), fast and flash pyrolysis [36]. However, the terms “slow” and “fast” pyrolysis are arbitrary and have no precise definition of the time or heating rate involved [9]. Other types include catalytic pyrolysis, vacuum pyrolysis and microwave pyrolysis [8]. Below, the main types of pyrolysis used in this study are briefly discussed.

1.4.3.1 Slow pyrolysis

Slow pyrolysis of biomass is performed at relatively low temperatures (about 400 °C) using low heating rates (5 – 7 °C/min). The vapor residence time is very long (hours to days), allowing the condensable vapors to be converted into char and non-condensable gases [8]. This type of pyrolysis is primarily applied for the production of char (solid residue) [1, 6, 29].

1.4.3.2 Fast pyrolysis

Fast pyrolysis is characterized by high heating rates, very high heat transfer rates, short vapor residence times (typically less than 2 s) to minimize secondary reactions, moderate temperatures (400 - 500 °C) to maximize the liquid yield and rapid quenching of the pyrolysis vapors [29, 37, 88]. Typically, the biomass is heated so rapidly (≥ 300 °C/min [1]) that it reaches pyrolysis temperature before decomposition [8]. Fast pyrolysis results in higher liquid yields compared with slow pyrolysis of the same biomass feedstock [49, 89].

1.4.3.3 Flash pyrolysis

Flash pyrolysis is performed by heating the biomass to moderate temperatures (450 - 600 °C) in a very short time [8]. The very high heating rate (> 100 °C/min [40, 90]) requires a special reactor design that also allows very short vapors residence times (30 - 1500 ms) [74]. Additionally, an efficient condensation system is required for rapid cooling (quenching) of the pyrolysis vapors and aerosols to pyrolysis liquid.

1.4.3.4 Catalytic pyrolysis

Catalytic pyrolysis is used to improve the quality of pyrolysis liquids, concerning their use as (transportation) fuel. This process is mainly focused on reducing the oxygen and water content of the pyrolysis liquids by means of catalysts [1].

1.4.4 Pyrolysis reactor types

Several reactor configurations are developed to meet the conditions required for pyrolysis of biomass. A brief overview of the most commonly used reactor types is discussed below.

1.4.4.1 Fixed bed pyrolysis reactor

The fixed bed pyrolysis reactor, operating in batch mode, is the oldest type of pyrolyzer. Heat required for thermal decomposition of biomass is provided by an external source or by limited combustion of the biomass itself [8]. Pyrolysis vapors are removed from the hot reactor zone by an inert sweeping gas or by volume expansion of the biomass itself. Because of the low heating rate and the long vapor residence time, this reactor type is mainly used for the production of

char [8]. Hence, the basic requirements of fast or flash pyrolysis are difficult to satisfy for fixed bed reactors above laboratory or bench scale [37].

1.4.4.2 Bubbling fluidized bed reactor

The biomass is mixed with a bed of solids (usually sand) and fluidized by an inert gas (Figure 1-9a). This results in an intensive mixing of the solids, a high heat transfer from the hot solids to the biomass particles and a uniform bed temperature, all being necessary for fast pyrolysis [6]. Heat for thermal decomposition is usually provided either by partial burning of product gas inside the fluidized bed or by burning the char in a separate chamber and transferring that heat to the bed of solids [8]. The solid and vapor residence time is controlled by the flow rate of the fluidizing gas [9, 37]. Typically, solids have longer residence times than the fluidizing gas. Rapid and effective char removal from the reactor is required to avoid secondary vapor cracking and to maximize the liquid yield. Hence, char is known as an effective vapor cracking catalyst. Once removed from the reactor, char can be used within the process to provide process heat by combustion or it can be separated from the sand using cyclones and valorized as precursor in the production of activated carbon [37].

1.4.4.3 Circulating fluidized bed (CFB) reactor

The CFB reactor is based on the same principles as the bubbling fluidized bed reactor, except that the bed of solids is more expanded and continuously recycled in an external loop containing a cyclone and a loop seal (Figure 1-9b). As a result, similar residence times for both char and pyrolysis vapors are achieved (about 0.5 – 1.0 s) [6, 9]. The solids (sand and char) are separated from the pyrolysis vapors using a cyclone and sent to the secondary char combustor. Here, the char is burned to re-heat the circulating solids providing heat to the primary pyrolysis reactor [8]. Despite the complex hydrodynamics, the CFB reactor is widely used because it allows high biomass throughputs [37].

1.4.4.4 Rotating cone reactor

In this reactor type, biomass and hot solids are fed into a rotating cone pyrolyzer, pushed against the hot wall by centrifugal forces and transported spirally upward along the rotating heated cone (Figure 1-9c). The pyrolysis

vapors leave the reactor, while char and sand spill over the rotating cone into a fluidized bed combustor. Here, the char is burned to re-heat the solids (sand) before being dropped back into the rotating cone together with fresh biomass [6, 37]. Very short solid residence times and no need for high amounts of inert carrier gas are the main advantages of this setup. However, scale-up may be difficult due to the complex geometry of the system [8].

1.4.4.5 Ablative pyrolysis reactor

In ablative pyrolysis, heat is transferred to biomass by moving it over a hot reactor wall while pressing it down by mechanical or centrifugal forces (Figure 1-9d) [9]. In this way, the pyrolysis front moves unidirectionally through the biomass particle and reactions are no longer limited by the rate of heat transfer through the biomass particle [37]. As moved away, the biomass particles leave a liquid film that provides lubrication for successive particles. However, this film rapidly evaporates from the pyrolysis zone and is converted into pyrolysis vapors that can be collected in a similar way to other processes [8, 9]. Because of the high heat transfer and short vapor residence times, high liquid yields are obtained. The main process parameters are the applied pressure, the reactor surface temperature and the relative velocity of the biomass particle over the hot surface [37]. This reactor design does not require an inert carrier gas and allows a more efficient collection of condensable vapors (because of the high vapor partial pressure). However, it is very costly at industrial scale due to the high surface area required for reaction.

1.4.4.6 Screw and Auger reactor

In the Auger reactor, the biomass is moved mechanically through the hot reactor zone (Figure 1-9e) rather than by using a fluidizing gas. The vapor residence time can be controlled by adjusting the length of the heated zone that vapors have to pass through before being condensed. The liquid yield typically is lower than that of a fluidized bed reactor due to longer residence times and longer contact times with the char, while the solid yield is higher. Therefore, this reactor type can also be used for slow pyrolysis. The strength of this design is the continuous operation mode in a compact reactor without the need of an inert

carrier gas, making it appealing for its potential to reduce operating costs [6]. However, heat transfer may be a problem at larger scales [9].

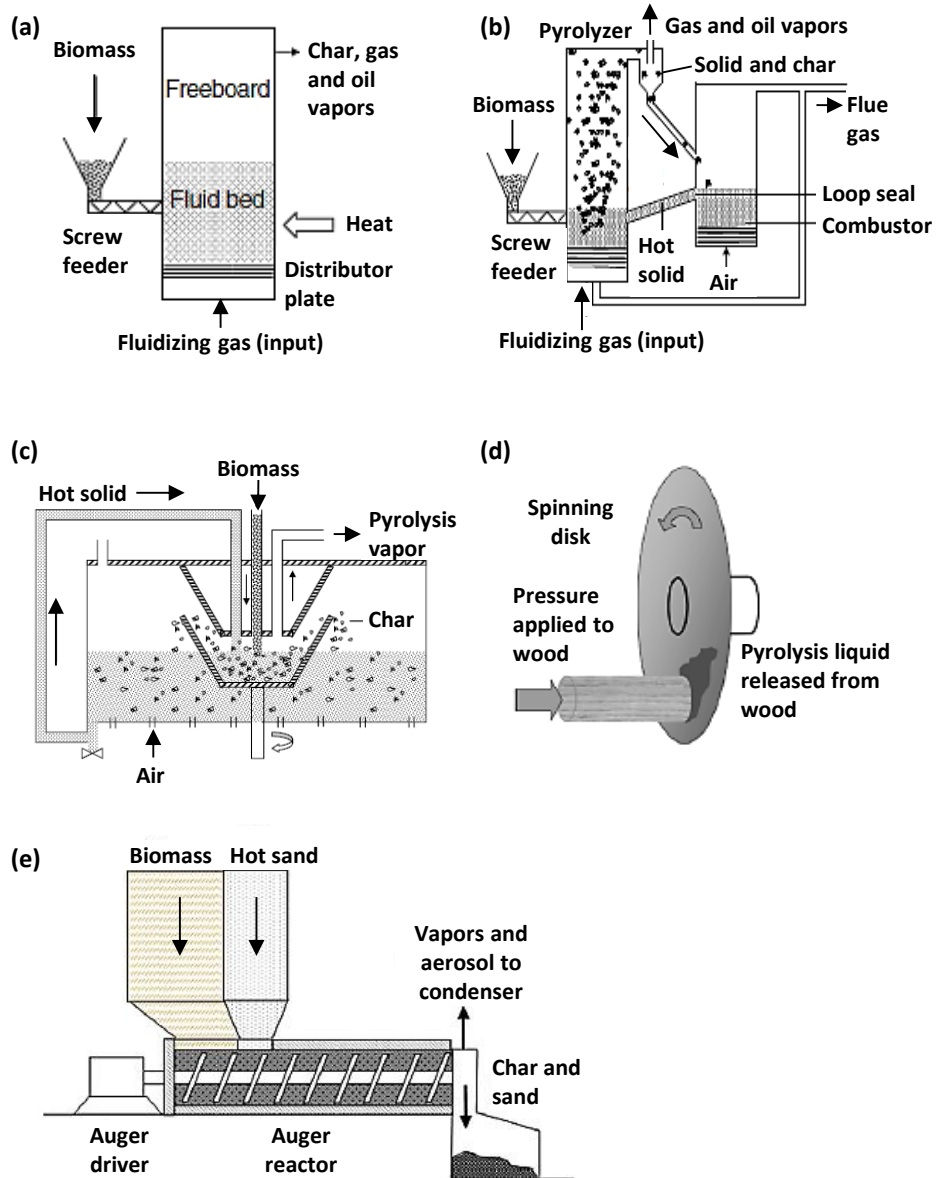


Figure 1-9: Schematic overview of several pyrolysis reactor designs: (a) bubbling fluidized bed, (b) circulating fluidized bed, (c) rotating cone, (d) ablative pyrolysis reactor and (e) Auger reactor (adapted from [6, 8]).

1.5 Properties and applications of pyrolysis products

Pyrolysis of biomass yields three fractions: solid, liquid and gas. An overview of the main properties and applications of each fraction is discussed in this section.

1.5.1 Pyrolysis liquid

Pyrolysis liquid (also known as pyrolysis oil, bio-oil, biocrude oil or bio-fuel oil) is a highly oxygenated, dark brown free-flowing organic liquid with a distinctive odor [8, 37, 91, 92]. The yield and properties of pyrolysis liquids depend on the biomass feedstock as well as on the pyrolysis process parameters [69, 92]. Pyrolysis liquids can be valorized as renewable fuel to substitute or to supplement fossil fuels or as feedstock in the production of chemicals.

1.5.1.1 Chemical composition

Pyrolysis liquid can be considered as a complex mixture of (oxygenated) primary products from pyrolysis of individual biomass components and of secondary products formed by cross-reactions between the primary products, together with an appreciable proportion of water [9, 37]. Pyrolysis liquid derived from lignocellulosic biomass is described as a micro-emulsion in which the continuous phase is an aqueous solution of cellulose, hemicellulose and monomeric lignin decomposition products that stabilize the discontinuous phase of pyrolytic lignin macromolecules through mechanisms such as hydrogen bonding [43].

The major classes of organic compounds present in pyrolysis liquids include carboxylic acids, esters, alcohols, ketones, aldehydes, phenols, alkenes, nitrogenated compounds, furans, sugars, etc. [1]. The chemical composition of a (fast) pyrolysis liquid is illustrated in Table 1-3. However, complete chemical characterization of pyrolysis liquids is difficult (or even impossible) and requires a combination of several complementary analytical techniques: GC/MS (volatile compounds), HPLC (non-volatile compounds), FTIR (functional groups), GPC (molecular weight distribution) and NMR spectroscopy (types of hydrogens or carbons in specific structural groups) [9]. Usually, 25 – 40 wt% of the wet pyrolysis liquid is eluted from the GC, while about 70 – 90 % of the eluted fraction can be identified [43, 93].

Table 1-3: Chemical composition of a typical fast pyrolysis liquid produced from wood [8, 94].

Major group	Compounds	wt%
Water		20 - 30
Lignin fragments	Insoluble pyrolytic lignin	15 - 30
Aldehydes	Formaldehyde, acetaldehyde, hydroxyl-acetaldehyde, glyoxal, methylglyoxal	10 - 15
Carboxylic acids	Formic, acetic, propanoic, butanoic, pentanoic, hexanoic, glycolic	10 - 15
Carbohydrates	Cellobiosan, α -D-levoglucosan, oligo-saccharides, 1,6-anhydroglucofuranose	5 - 10
Phenols	Phenol, cresol, guaiacols, syringols, vanillins	2 - 5
Furfurals		1 - 4
Alcohols	Methanol, ethanol	2 - 5
Ketones	Acetol, cyclopentanone	1 - 5

1.5.1.2 Physicochemical properties

The physicochemical properties of pyrolysis liquids are strongly dependent on the nature of the biomass feedstock and on the pyrolysis process parameters. Generally, their elemental composition is still very similar to that of the original biomass feedstock and differs considerably from that of petroleum-derived fuels [9, 36, 92]. Table 1-4 shows the physicochemical properties of pyrolysis liquids derived from wood and rapeseed cake compared to the properties of heavy fuel oil. An excellent guide to physical property characterization of biomass-derived pyrolysis liquids is published by Oasmaa and Peacocke [95]. In this section, only a brief overview of the most important physicochemical properties of pyrolysis liquids derived from biomass is discussed.

Table 1-4: Physicochemical properties of pyrolysis liquids derived from wood and rapeseed cake compared to heavy fuel oil (adapted from [92]).

Physical property	Pyrolysis liquid		Heavy fuel oil [92, 96]
	Wood [92]	Rapeseed cake [51]	
Water content (wt%)	15 – 30	16.2	0.1
pH	2.5	-	-
Density (kg/L)	1.2	0.97	0.94
Elemental composition (wt%)			
C	54 – 58	63.9	85
H	5.5 – 7.0	10.3	11
O	35 – 40	21.6	1.0
N	0 – 0.2	3.7	0.3
S	-	0.4	< 4
Ash	0 – 0.2	0.2	0.1
HHV (MJ/kg)	16 – 19	29.8	40
Viscosity at 50 °C (cP)	40 – 100	20.2	180
Solids (wt%)	0.2 – 1.0	-	1
Distillation residue (wt%)	Up to 50	-	1

Water content

Pyrolysis liquids contain varying quantities of water (usually 15 – 30 wt%) depending on the biomass feedstock, how it was produced and subsequently collected [37]. This water originates from the initial moisture in the biomass feedstock (typically less than 10 wt%) and from dehydration reactions occurring during pyrolysis (pyrolytic water) [69, 92, 97]. The presence of water has both positive and negative effects on the properties of pyrolysis liquids concerning their use as renewable fuel (additive). It improves the flow characteristics (lower viscosity) which is beneficial for combustion (pumping and atomization). It also leads to a more uniform temperature profile in the cylinder of a diesel engine, to lower NO_x emissions and a less acidic pH of the pyrolysis liquid [92]. However, the beneficial effects of the aqueous phase in pyrolysis liquids are usually outbalanced by the negative ones [98]. Hence, increased water contents lower

the heating value, density and stability of pyrolysis liquids [36, 37]. In general, water contents below 28 wt% are considered as being acceptable for valorization of pyrolysis liquids as fuel in static applications [99].

Removal of water from pyrolysis liquids is difficult by conventional methods [69]. Distillation, for instance, is not an option because the pyrolysis liquid cannot be completely vaporized once it is recovered from the vapor phase. Hence, when heated to 100 °C or more, the pyrolysis liquid rapidly reacts and a solid residue up to 50 wt% of the original liquid can be produced [37]. Another option to reduce the water content is co-pyrolysis of biomass in presence of bio-polymers. Cornelissen et al. report a significant reduction of the water content in flash co-pyrolysis of willow and polylactic acid (PLA) or polyhydroxybutyrate (PHB) because of synergistic effects between the biomass and the bio-polymers [40, 100, 101].

Elemental composition

The elemental composition of pyrolysis liquids approximates that of the biomass feedstock and is considerably different from that of fossil fuels. The high proportion of oxygen is the primary reason for this difference and explains the high polarity and hydrophilic nature of pyrolysis liquids [9]. As a result, pyrolysis liquids are totally immiscible with petroleum-derived fuels [37, 92]. Removal of oxygen can be achieved by upgrading, but requires complex catalytic processes (see section 1.5.1.3).

Higher heating value (HHV)

The HHV of pyrolysis liquids is considerably lower than that of fossil fuels (about 40 MJ/kg and more) due to the large number of oxygenated compounds and the relatively high water content [36].

Density

The density of (oxygenated) pyrolysis liquids is usually much higher (about 1.2 kg/L) than that of petroleum-derived fuels (about 0.85 kg/L) [36, 37]. Pyrolysis liquids with relatively higher densities typically have lower water contents [36, 102].

Viscosity

The viscosity of pyrolysis liquids is an indication of their resistance to flow. It is an important property for many fuel applications because it affects the pumping, injection and atomization characteristics of the liquid. The viscosity is dependent on the biomass feedstock, the water content of the pyrolysis liquid, the production and storage conditions, the age and especially the efficiency of collection of low boiling vapors during condensation [37, 92]. In general, the viscosity of pyrolysis liquids decreases rapidly at higher temperatures. As a result, even very viscous pyrolysis liquids can be pumped after moderate preheating [92].

pH and corrosiveness

Pyrolysis liquids usually have low pH-values (2 – 3) caused by the relatively high amount of organic acids (mainly acetic and formic acid) originating from the degradation of biomass components [92]. As a result, pyrolysis liquids are corrosive to common construction materials such as carbon steel and aluminum and can affect some sealing materials [36]. Therefore, appropriate materials such as PTFE (polytetrafluoroethylene), PP (polypropylene) or HDPE (high density polyethylene) have to be used for storing, transporting and sampling of pyrolysis liquids [95].

Stability and aging

Pyrolysis liquids are usually produced using high heating rates and subsequent rapid quenching of the pyrolysis vapors. As a result, these liquids are not at thermodynamic equilibrium, even at ambient temperature, and slow secondary reactions continue after production [43]. This phenomenon is known as aging and leads to a gradual increase in viscosity, average molecular weight and water content. In extreme cases phase separation can occur. Aging is accelerated by higher storage temperatures, the presence of char, exposure to oxygen or ultra-violet light [37, 102]. Additionally, alkali and alkaline earth metallic species are also associated with accelerated aging of pyrolysis liquids during storage [6, 103]. For a detailed review on the storage stability of pyrolysis liquids is referred to Diebold [102]. Solvents including methanol, ethanol, acetone and methyl

isobutyl ketone can be used to reduce the aging rate of pyrolysis liquids and to increase their stability [9].

1.5.1.3 Upgrading of pyrolysis liquids to (transportation) fuels

Pyrolysis liquids are known to be viscous, acidic and thermally unstable liquids that contain high proportions of oxygenated compounds and water, both leading to low calorific values. One way to improve their quality and to make them suitable to replace or to supplement the current fossil fuel usage is upgrading [36, 92].

Pyrolysis liquids can be upgraded into liquid transportation fuels by physical, chemical or catalytic processes. Physical upgrading includes hot-vapor filtration (reduction of char and alkali content), solvent addition or emulsification with diesel fuel using surfactants. Chemical upgrading includes aqueous phase processing/reforming, esterification, mild cracking and gasification for synfuels [37]. In case of the latter, the pyrolysis liquid is gasified into CO and H₂ (synthesis gas), which can be further converted into liquid fuels by Fischer-Tropsch synthesis [9]. In this work the main focus lies on catalytic upgrading, which can be considered as a special form of chemical upgrading.

Catalytic upgrading of pyrolysis liquids to renewable (transportation) fuels essentially requires (full) deoxygenation, which can be accomplished by two main routes: catalytic hydrotreating (hydrodeoxygenation) or catalytic vapor cracking [92, 104-106]. **Catalytic hydrotreating** of pyrolysis liquids is carried out at moderate temperatures (up to 400 °C), high hydrogen pressures (up to 20 MPa) and in the presence of heterogeneous catalysts (e.g. sulfided NiMo or CoMo supported on alumina [36, 92]). This process involves hydrogenation and hydrocracking of the oxygenated compounds, while oxygen is eliminated as water [36, 37]. **Catalytic vapor cracking** is performed at atmospheric pressure without hydrogen and at temperatures similar to those of pyrolysis liquid production, reducing the operating costs [36]. In general, catalytic upgrading is performed as *post-treatment* or as *in situ* catalytic pyrolysis. Post-treatment upgrading is carried out after the production of pyrolysis liquid, making costly condensation and re-evaporation steps necessary. During *in situ* catalytic pyrolysis, both production and upgrading of pyrolysis liquid simultaneously occur in a special designed reactor. The catalyst can be mixed with the biomass (in-

bed mode) or placed separately from the biomass as a fixed bed (ex-bed mode) [107]. Catalytic deoxygenation enhances the physical properties of pyrolysis liquids (higher calorific value, lower oxygen and water content, and a higher stability). However, the use of a catalyst frequently reduces the liquid yield due to coke formation and more severe cracking of pyrolysis vapors into non-condensable gases [108].

Upgrading catalysts are usually categorized into four main classes: activated alumina, molecular sieve catalysts, sodium carbonate and transition metal catalysts [33]. Both acidity and shape selectivity are important catalyst characteristics that strongly affect yield and composition of the pyrolysis products [109, 110]. For instance, the HZSM-5 zeolite is a crystalline and shape selective catalyst that shows mild secondary cracking activity, whereas the amorphous γ -Al₂O₃ catalyst is not shape selective and enhances secondary cracking reactions. Typically, highly oxygenated compounds are converted by these catalysts into hydrocarbons and/or aromatics while oxygen is eliminated as H₂O, CO and CO₂ [111-113]. The influence of zeolites during catalytic pyrolysis of several lignocellulosic biomass samples was studied by Mihalcik et al. The HZSM-5 zeolite was found to be most effective in producing aromatics from oxygen-rich vapors [114]. The effects of zeolites on the conversion of rapeseed cake were investigated by Giannakopoulou et al. [51]. These authors concluded that the quality of pyrolysis liquid was improved the most by HZSM-5. Dupain et al. reported that triglyceride degradation occurs in two successive steps under fluid catalytic cracking (FCC) conditions [16]. First, triglycerides decompose into fatty acids by a fast thermal radical cracking process. Then, secondary catalytic reactions (including dehydration, decarboxylation and aromatization) further convert the fatty acids into smaller and less oxygenated compounds. Saturated fatty acids are preferably converted into aliphatic hydrocarbons, while highly unsaturated fatty acids enhance the formation of aromatics. Babich et al. studied slow catalytic pyrolysis of microalgae in presence of Na₂CO₃ [78]. Higher calorific values, increased aromatic contents and lower acidities were reported for the catalytically produced pyrolysis liquids.

1.5.1.4 Applications of pyrolysis liquids

A schematic overview of the applications of pyrolysis liquids is shown in Figure 1-10. In general, three main options are possible: valorization as renewable fuel, as effective energy carrier or as source of added-value chemicals.

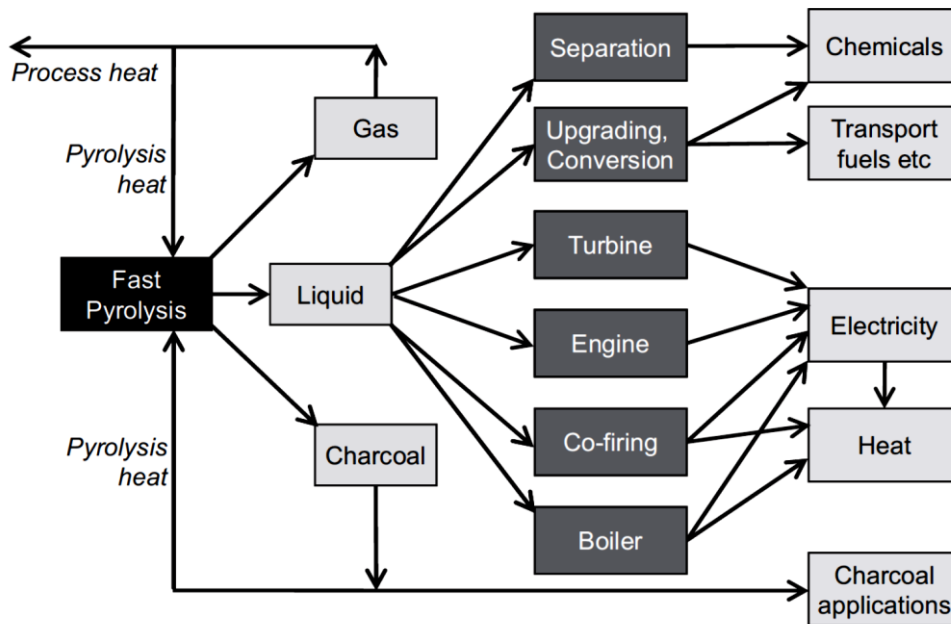


Figure 1-10: Applications of (fast) pyrolysis liquids [37].

Pyrolysis liquid as renewable fuel

Pyrolysis liquid can substitute fuel oil or diesel in many static applications including boilers, furnaces, engines and gas turbines for heat, power and electricity generation [29, 36, 37, 92]. However, poor volatility, high viscosity, coking and corrosiveness are some of the drawbacks of pyrolysis liquids concerning their use as fuel [36, 92]. Therefore, direct use of pyrolysis liquids in standard equipment constructed for petroleum-derived fuels is often problematic and (slight) changes (e.g. fuel pump or injection system of a diesel engine) are usually required [9]. A profound discussion of these issues and possible solutions is published by Oasmaa et al. [115]. The quality of pyrolysis liquids can also be improved by upgrading (see section 1.5.1.3). However, although significant differences in ignition, viscosity, energy content, stability, pH and emission

levels, flame combustion tests show that pyrolysis liquids can replace heavy and light fuels in industrial boiler applications [9].

Co-firing of biomass fuels with conventional fuels is potentially a very attractive option that enables full economies of scale to be realized as well as reducing the problems of product quality and clean up. Co-firing of pyrolysis liquid with coal, for instance, is reported to be clean and efficient without adverse effects on the boiler operation or on the emission levels [37].

Despite the drawbacks (low stability, high viscosity, low calorific value and corrosiveness), pyrolysis liquids as renewable fuel have some major advantages as well [97]:

- ⇒ Bio-fuel with the lowest cost and a clearly positive CO₂ balance
- ⇒ Possibility of utilization in existing small-scale power generation systems as well as use in large power stations (co-firing)
- ⇒ Possibility to decouple solid bio-fuel handling from utilization (reduced capital and operation costs in utilization)
- ⇒ Storability and transportability of liquid fuels
- ⇒ High-energy density compared to atmospheric biomass gasification fuel gases
- ⇒ Intermittent operation feasible
- ⇒ If light fuel oil is replaced, middle distillates are released to be used for transportation

Pyrolysis liquid as effective energy carrier

Biomass has a low bulk density which means that transport costs are high and a large number of vehicle movements are required for transportation to a large scale processing facility. Therefore, conversion of biomass into a liquid form by pyrolysis at or near the biomass source will reduce transport costs and environmental concerns as pyrolysis liquids have a considerably higher density than biomass materials (about 10 times higher than low density crops). This leads to the concept of a small decentralized pyrolysis plant for the production of liquids to be transported to a central processing (gasification) plant [37].

Pyrolysis liquid as source of added-value chemicals

Valorization of pyrolysis liquids as source of added-value chemicals is of major interest from an economic point of view since chemicals typically have a higher economic value than fuel products. More than 300 organic compounds have been identified in pyrolysis liquids including various types of functional groups: carboxyls, alcohols, ketones, aldehydes, phenols, furans and other oxygenates [9]. However, their proportions are small and isolation of a specific single compounds is seldom practical or economical as it usually requires complex separation techniques. Therefore, the whole pyrolysis liquid or relatively easily separable fractions are currently believed to have more potential than pyrolysis liquids as source of specific chemicals. However, economic valorization of chemicals derived from pyrolysis liquids remains difficult due to low-cost alternatives that are readily available [92].

The **whole pyrolysis liquid** can be converted into useful chemicals by taking advantage of its most abundant functional groups (carboxyl, carbonyl and phenolic groups) and react them in such a way that the non-reacting part would not have to be separated from the final product. For instance, carboxylic acids and phenols can easily react with lime to form calcium salts and phenates (alkyl phenate sulfides). This process was commercialized by Dynamotive Corp. in the production of BioLime™, an agent used for control of SO_x and NO_x emissions in coal combustors [92, 116, 117]. By reacting pyrolysis liquids with ammonia, urea or other -NH₂ containing materials, various imide and amide bonds are formed between carbonyl carbons and nitrogen. As a result, about 10 % of nitrogen can be incorporated in an organic matrix that proved to have properties of an efficient biodegradable slow-release nitrogen fertilizer [92, 116, 118].

The **aqueous extract** of pyrolysis liquids can be used as source of smoke flavors (phenolic compounds), browning agents (low molecular weight aldehydes) or environmentally friendly road deicers. The latter have potential to replace calcium chloride, which is known to have deleterious effects on plants [92, 116, 119]. The **water-insoluble fraction** of pyrolysis liquids has a high content of pyrolytic lignin, which can be used as phenol replacement in phenol-formaldehyde resins. These phenolic resins, in turn, can be used as adhesives in plywood and particleboard manufacturing [4, 9, 92] or as construction materials in the automobile industry [120]. Additionally, several of the monomeric lignin

derived products are of significant economic value as synthetic raw materials, flavor chemicals (e.g. vanillin), plant grow inhibitors, plant pathogen control agents and pharmaceutical precursors [116, 121, 122].

Production of **specific chemicals** from pyrolysis liquid is possible but has not been developed in larger scale due to the complexity of separation techniques. Generally, individual compounds present in greatest abundance are of major interest. These compounds include hydroxyacetaldehyde (the most active meat-browning agent in "liquid smoke") and low molecular weight acids such as acetic and formic acid [9]. However, their recovery as pure compounds turns out to be rather problematic [116]. Another promising compounds is levoglucosan (1,6-anhydro- β -D-glucopyranose), which is obtained in relatively high amounts by pyrolysis of (demineralized) cellulose or lignocellulosic biomass. Levoglucosan has potential for manufacturing of pharmaceuticals, pesticides, surfactants and biodegradable polymers. However, the high production price (mostly due to costly purification procedures) makes its extensive use in the near future unlikely [92, 116, 123]. For more information on the production and potential applications for levoglucosan is referred to Radlein [123], while Bennett et al. describe the extraction of levoglucosan from pyrolysis liquids [124]. More information on several fractionation procedures for pyrolysis liquids can be found in Mohan et al. [9].

1.5.2 Solid residue

The solid residue is composed of the solid carbonaceous residue (char) and inorganic ashes remaining after the pyrolysis process. The properties and yield of solid residue depend on the biomass feedstock and on the pyrolysis conditions. In general, the production of solid residue is favored by low heating rates and long vapor residence times as well as by using a biomass feedstock with a large amount of coke-forming components such as lignin [12]. In contrast, rapid and effective separation of solid residue from the pyrolysis vapors (e.g. by cyclones or hot vapor filtration) is essential to maximize the liquid yield, since the solid residue is known to act as a vapor cracking catalyst [37]. Commonly, the solid residue is valorized by three main routes: as energy source, as fertilizer or as precursor in the production of activated carbon.

1.5.2.1 Solid residue as energy source

The solid residue generally has a higher calorific value than the initial biomass feedstock or the pyrolysis liquid, especially in case of lignocellulosic biomass [8]. Therefore, the solid residue can be valorized as solid fuel in boilers to produce electricity [1]. In commercial pyrolysis at industrial scale, the solid residue is often valorized by combustion in a secondary reactor (combustor) to provide heat to the pyrolysis process. Typically, the solid residue contains about 25 % of the energy of the biomass feedstock and about 75 % of this energy is typically required to drive the pyrolysis process [37].

1.5.2.2 Solid residue as fertilizer (biochar)

The solid residue (also called biochar) has potential as fertilizer and soil conditioner leading to an improved soil fertility, increased carbon storage and decreasing GHG emissions (e.g. CH₄ and N₂O). The long-term benefits of biochar application include an increased adsorption ability of the soil and thus a reduced loss of nutrients via leaching, together with an increased soil organic carbon content. Important properties of the solid residue concerning its use as biochar are the surface acidity/alkalinity, the cation exchange capacity (CEC) and the content of nutrients (e.g. N and available P) and extractible cations (e.g. K⁺, Ca²⁺, Na⁺ and Mg²⁺). These properties are mainly affected by the pyrolysis temperature (optimum around 400 °C) rather than by the residence time during slow pyrolysis [125]. In addition, biochars have potential for the reduction of a variety of organic and inorganic contaminants present in soils by both immobilization of the pollutant and by improving some physicochemical properties of the soil (e.g. pH, CEC and surface area) [126].

1.5.2.3 Solid residue as precursor of activated carbon

Activated carbon (AC) is a porous carbonaceous material with a high internal surface area and a large number of micropores (pore width < 2 nm) [127]. AC is widely used as adsorbent to remove pollutants from liquid (wastewater treatment) or gaseous (air pollution control) phases, but it can also serve as catalyst or as catalyst support [128]. Removal of phenols, acid dyes, pesticides and heavy metals are examples of AC applications in wastewater treatment, while adsorption of volatile organic compounds (VOCs), NO_x and SO_x illustrate

the possibilities of AC in air pollution control. As a result, ACs are used in many industries including food and beverage processing, pharmaceuticals, chemical, petroleum, mining, nuclear and automobile industry [129].

Frequently, ACs are produced from organic precursors with a relatively high carbon content such as coal, lignite or wood [129]. However, the usage of these non-renewable and/or relatively expensive precursors is detrimental for the use of ACs due to economic reasons [130]. Therefore, renewable and low cost precursors such as agricultural wastes are getting more and more attention [131, 132]. Numerous agricultural wastes have already been evaluated as precursor for AC production, including fruit stones [133-135], nut shells [131, 136-138], waste cakes of oil crops [129, 130, 139, 140] and olive stones [141, 142]. However, AC production on industrial scale requires precursors with a high carbon and a low ash content, a high bulk availability and with minimal seasonal variations in quality of the biomass precursor [143, 144].

Generally, AC production involves a carbonization step followed by a physical or chemical activation. A schematic overview is presented in Figure 1-11.

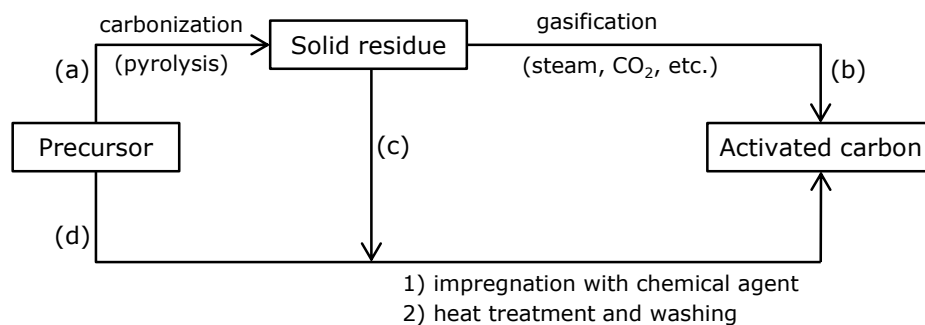


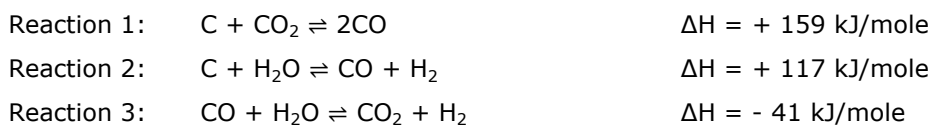
Figure 1-11: AC production by physical activation (route a-b) or by chemical activation (route a-c or route d) [27, 143].

Physical activation involves a two-step process: carbonization of the precursor followed by gasification of the solid residue at elevated temperatures using an oxidizing agent such as steam or CO_2 (route a-b) [129]. Although chemical activation can also be carried out as a two-step process (route a-c), one-step chemical activation in which the precursor (instead of solid residue) is impregnated with chemical agent is more commonly used (route d). Chemical

activation has the advantage that it is performed in a single-step and usually at lower temperatures, but environmental concerns can be formulated due to the use of chemical agents [128].

Carbonization in an inert atmosphere (pyrolysis) is performed to remove considerable amounts of tars and volatile matter from the precursor, resulting in a solid residue with a preliminary raw porosity and a relatively high carbon content [141]. Typically, carbonization temperatures range between 400 and 850 °C, but sometimes even temperatures up to 1000 °C are reported [128]. In case of two-stage AC production, the carbonization conditions (temperature, time and atmosphere) are found to significantly affect the pore development during the subsequent activation stage [128]. Hence, the tars and volatile matter formed by carbonization can cause pore blocking and so prevent the activation agent from entering the pore structure during physical activation [143]. Commonly, the raw porosity created by carbonization is not enough for most AC applications and additional activation is required to create new pores or to unclog and widen existing ones.

Physical activation involves the removal of carbon atoms from the solid residue by gasification using mild oxidizing agents such as steam or CO₂ (or a mixture of both) at temperatures between 700 and 950 °C. The following reactions can be distinguished [131, 144]:



CO₂ activation is described by the Boudouard reaction (reaction 1), while steam activation involves reactions 1 to 3. Hence, steam reacts with carbon to produce CO (reaction 2), which can be further oxidized to CO₂ according to the water-shift reaction (reaction 3). This CO₂, in turn, can gasify carbon as described by reaction 1. The reactions of steam and CO₂ with carbon (reactions 1 and 2) are endothermic, making pore development quite easy to control [141, 145]. In contrast, the reaction of oxygen with carbon is strongly exothermic and

therefore requires low partial pressures of oxygen during activation to prevent sample combustion. Additionally, pore development involves reaction anisotropy since carbon atoms with equal reactivity would be rather "etched" from the solid residue without pore development [144]. Different mechanisms are reported in literature for steam and CO₂ activation. Steam is believed to attack the active sites at the pore center and on the pore walls simultaneously. In contrast, CO₂ primarily reacts with active sites located at the pore center (creating microporosity) and only attacks the pore walls when activation times become larger (broadening of micropores) [131, 141, 145]. As a result, CO₂ needs more time to develop new and to widen existing micropores. Therefore, steam is considered to be more reactive than CO₂ under analogous experimental conditions [131, 141]. The higher reactivity of steam is assigned to its more advantageous kinetics. Hence, steam has a lower molecular size than CO₂ and therefore can diffuse faster through the pore network and gain easier access to (existing) micropores [131, 146]. As a result, steam generally produces ACs with broader pore size distributions and larger specific surface areas, whereas CO₂ is more selective towards the creation of microporosity.

To obtain an optimum physical activation, it is important that gasification occurs uniformly through the carbon particles. In this view, the resistance to diffusion of the activation agent through the carbon particle has to be small compared to the chemical resistance to gasification. Hence, if the resistance to diffusion is very large compared to resistance to gasification, carbon removal occurs solely at the exterior of the particles and almost no activation occurs [141, 147].

Chemical activation is usually performed by impregnation of the precursor with a chemical agent such as ZnCl₂, H₃PO₄, KOH, K₂CO₃, NaOH, Na₂CO₃ or H₂SO₄ prior to activation [139]. These chemical agents do not selectively remove carbon atoms as is the case for physical activation, but rather interact with the lignocellulosic structure of the precursor according to mechanisms depending on the activation agent [144]. For instance, impregnation with ZnCl₂ causes degradation and, on carbonization (at about 500 °C), dehydration of the precursors' lignocellulosic structure. This results in charring and aromatization of the carbon skeleton and the creation of a porous structure [135, 148]. Recently, ZnCl₂ is more and more abandoned in favor of H₃PO₄ because of environmental

concerns [129]. H_3PO_4 is reported to combine chemically within lignocellulosic structures below 250 °C, while pore development reaches a maximum at about 350 – 450 °C [27, 149]. KOH activation involves intercalation of potassium atoms between the graphene layers during carbonization followed by destruction of the carbon structure by an almost explosive desorption at higher temperatures (850 – 900 °C) [144]. Additionally, carbon atoms can be oxidized by the oxygen originating from the hydroxide. For more details on the mechanisms of several activation agents is referred to Marsh et al. [144].

Depending on the precursor and the production process, the appropriate AC application can be selected. Important AC properties are the surface area, the pore size distribution, the ash content, the hydrophobicity and the surface chemistry [150]. The latter is associated with the presence of heteroatoms (e.g. oxygen or nitrogen) occurring in organic functional groups at the edge of carbon crystallites. Typical functional groups are carbonyls, carboxyls, phenols, ethers, lactones, amines and nitro groups. Besides the AC properties, properties of the adsorbate (polarity, hydrophobicity, size and acidity or basicity) and adsorption conditions (temperature, solvent polarity and presence of other species competing for the adsorption sites) are important in choosing the appropriate AC application [150].

1.5.3 Pyrolysis gas

Pyrolysis gas is mainly composed of CO_2 , H_2O , CO , CH_4 , H_2 , together with small organic compounds such as ethane, ethylene, ethyne, propane, propylene, butane and butene [1, 88]. The proportions of these gases depend on several factors including heating rate and pyrolysis temperature.

Pyrolysis gas containing significant amounts of CO_2 along with CH_4 can be used as a fuel for industrial combustion purposes [1]. At industrial scale, pyrolysis gas can also be valorized by combustion to provide heat to maintain the process temperature. However, in contrast to the solid residue, pyrolysis gas typically contains only about 5 % of the biomass energy, which is not sufficient to drive the pyrolysis process. As a result, supplementation with other energy sources will be required [37].

1.6 Conclusion

There is a strong need for renewable sources of energy and chemicals due to environmental and sociopolitical issues associated with the use of conventional fossil fuels. Among various renewable energy sources, biomass is considered as the source with the highest potential to contribute to the energy needs of modern society. Hereby, it is important to select a biomass (waste) that is readily available and does not interfere with the world's food supply. In this view, agricultural by-products and wastes are interesting candidates.

Solid biomass needs conversion into a more useful and valuable form. In general, a liquid form that is easily storable and transportable is preferred. Pyrolysis is a very promising thermochemical conversion technique since it converts biomass into three fractions (solid, liquid and gas) in oxygen deficient conditions and at moderate temperatures. The proportion of each fraction can be varied over a relatively wide range by adjustment of several process parameters including pyrolysis temperature, heating rate and vapor residence time. In general, the production of solid residue is favored by relatively low pyrolysis temperatures and long vapor residence times, while high liquid yields require moderate temperatures and short vapor residence times.

The pyrolysis liquid has potential as renewable fuel or as source of added-value chemicals. Further improvement (upgrading) of the pyrolysis liquid is required to obtain the properties and quality of conventional petroleum-derived fuels. Reduction of the water and oxygen content turns out to be the biggest challenge. The solid residue (or char) can be valorized as improved solid energy carrier, as fertilizer or as precursor in the production of activated carbon. Hereby, an in-depth study of the activation conditions (temperature, time and activation agent) is necessary to obtain an optimized production of high grade activated carbon. The gaseous fraction still has a moderate energy content that can be used to provide a part of the process heat by combustion.

In this study, the valorization of agricultural waste cake is focused on the production of pyrolysis liquid with opportunities as renewable (transportation) fuel and on the valorization of the solid residue as precursor in the production of activated carbon.

1.7 References

- [1] Goyal, H.B., Seal, D. and Saxena, R.C. Bio-fuels from thermochemical conversion of renewable resources: A review. *Renewable & Sustainable Energy Reviews*, 2008. **12**(2): 504-517.
- [2] International Energy Agency, Key world energy statistics. IEA, 2012: 1 - 82.
- [3] McKendry, P. Energy production from biomass (part 1): overview of biomass. *Bioresource Technology*, 2002. **83**(1): 37-46.
- [4] Demirbas, A. Biomass resource facilities and biomass conversion processing for fuels and chemicals. *Energy Conversion And Management*, 2001. **42**(11): 1357-1378.
- [5] Bridgwater, A.V. Renewable fuels and chemicals by thermal processing of biomass. *Chemical Engineering Journal*, 2003. **91**(2-3): 87-102.
- [6] Isahak, W.N.R.W., Hisham, M.W.M., Yarmo, M.A. and Yun Hin, T. A review on bio-oil production from biomass by using pyrolysis method. *Renewable and Sustainable Energy Reviews*, 2012. **16**(8): 5910-5923.
- [7] Özçimen, D. and Karaosmanoglu, F. Production and characterization of bio-oil and biochar from rapeseed cake. *Renewable Energy*, 2004. **29**(5): 779-787.
- [8] Basu, P. Biomass gasification and pyrolysis - Practical design and theory. 2010: Elsevier Inc.
- [9] Mohan, D., Pittman, C.U. and Steele, P.H. Pyrolysis of wood/biomass for bio-oil: A critical review. *Energy & Fuels*, 2006. **20**(3): 848-889.
- [10] Vassilev, S.V., Baxter, D., Andersen, L.K. and Vassileva, C.G. An overview of the chemical composition of biomass. *Fuel*, 2010. **89**(5): 913-933.
- [11] UNFCCC. Clarifications of definition of biomass and consideration of changes in carbon pools due to a CHD project activity. EB-20. Annex 8. 2005.
- [12] Vassilev, S.V., Baxter, D., Andersen, L.K., Vassileva, C.G. and Morgan, T.J. An overview of the organic and inorganic phase composition of biomass. *Fuel*, 2012. **94**(0): 1-33.
- [13] Canola council of Canada.
<http://www.canolacouncil.org/crop-production/canola-grower's-manual-contents/chapter-2-canola-varieties/canola-varieties>
(Accessed on 07.05.2013).

- [14] USDA - Oilseeds: World markets and trade.
<http://www.fas.usda.gov/psdonline/circulars/oilseeds.pdf>
(Accessed on 02.05.2013).
- [15] Sensoz, S., Angin, D. and Yorgun, S. Influence of particle size on the pyrolysis of rapeseed (*Brassica napus* L.): fuel properties of bio-oil. *Biomass and Bioenergy*, 2000. **19**(4): 271-279.
- [16] Dupain, X., Costa, D.J., Schaverien, C.J., Makkee, M. and Moulijn, J.A. Cracking of a rapeseed vegetable oil under realistic FCC conditions. *Applied Catalysis B: Environmental*, 2007. **72**(1-2): 44-61.
- [17] EU Oil and Proteinmeal Industry (also known as FEDIOL).
<http://www.fediol.eu/web/rapeseed/1011306087/list1187970106/f1.html>
(Accessed on 07.05.2013).
- [18] Brzoska, F. Milk production and composition as influenced by soybean meal, rapeseed meal or rapeseed cake in concentrates for dairy cows. *Annals Of Animal Science*, 2008. **8**(2): 133-143.
- [19] FAOSTAT.
<http://faostat.fao.org/site/567/DesktopDefault.aspx?PageID=567#ancor>
(Accessed 02.05.2013).
- [20] Johansson, A., Laakso, P. and Kallio, H. Characterization of seed oils of wild, edible Finnish berries. *Zeitschrift Fur Lebensmittel-Untersuchung Und -Forschung. A, Food Research and Technology*, 1997. **204**(4): 300-307.
- [21] Oomah, B.D., Ladet, S., Godfrey, D.V., Liang, J. and Girard, B. Characteristics of raspberry (*Rubus idaeus* L.) seed oil. *Food Chemistry*, 2000. **69**(2): 187-193.
- [22] Pütün, A.E., Uzun, B.B., Apaydin, E. and Pütün, E. Bio-oil from olive oil industry wastes: Pyrolysis of olive residue under different conditions. *Fuel Processing Technology*, 2005. **87**(1): 25-32.
- [23] Demirbas, A. Producing bio-oil from olive cake by fast pyrolysis. *Energy Sources Part A: Recovery Utilization and Environmental Effects*, 2008. **30**(1): 38-44.
- [24] Zabaniotou, A., Stavropoulos, G. and Skoulou, V. Activated carbon from olive kernels in a two-stage process: Industrial improvement. *Bioresource Technology*, 2008. **99**(2): 320-326.
- [25] Huber, G.W., Iborra, S. and Corma, A. Synthesis of transportation fuels from biomass: chemistry, catalysts and engineering. *Chemical Reviews*, 2006. **106**(9): 4044 - 4098.

-
- [26] Rabou, L.P.L.M. and Lips, S.J.J. Phyllis database uitbreiding met biochemische samenstellingen ten behoeve van de productie van vloeibare en gasvormige brandstoffen. 2003: ECN.
- [27] Stals, M. Pyrolysis of heavy metal contaminated biomass: characterization of obtained pyrolysis oils and study of derived activated carbon, in PhD thesis - Research Group: Analytical and Applied Chemistry 2011, Hasselt University: Diepenbeek. 201.
- [28] Ucar, S. and Ozkan, A.R. Characterization of products from the pyrolysis of rapeseed oil cake. *Bioresource Technology*, 2008. **99**(18): 8771-8776.
- [29] Yaman, S. Pyrolysis of biomass to produce fuels and chemical feedstocks, *Energy Conversion and Management*, 2004. **45**(5): 651-671.
- [30] Sullivan, A.L. and Ball, R. Thermal decomposition and combustion chemistry of cellulosic biomass. *Atmospheric Environment*, 2012. **47**(0): 133-141.
- [31] Yang, H., Yan, R., Chen, H., Lee, D.H. and Zheng, C. Characteristics of hemicellulose, cellulose and lignin pyrolysis. *Fuel*, 2007. **86**(12-13): 1781-1788.
- [32] Onay, O. and Kockar, O.M. Fixed-bed pyrolysis of rapeseed (*Brassica napus* L.), *Biomass & Bioenergy*, 2004. **26**(3): 289-299.
- [33] Maher, K.D. and Bressler, D.C. Pyrolysis of triglyceride materials for the production of renewable fuels and chemicals. *Bioresource Technology*, 2007. **98**(12): 2351-2368.
- [34] Du, Z.Y., Hu, B., Ma, X.C., Cheng, Y.L., Liu, Y.H., Lin, X.Y., Wan, Y.Q., Lei, H.W., Chen, P. and Ruan, R. Catalytic pyrolysis of microalgae and their three major components: Carbohydrates, proteins, and lipids. *Bioresource Technology*, 2013. **130**: 777-782.
- [35] Lappi, H. and Alén, R. Pyrolysis of vegetable oil soaps - Palm, olive, rapeseed and castor oils. *Journal of Analytical and Applied Pyrolysis*, 2011. **91**(1): 154-158.
- [36] Balat, M., Balat, M., Kirtay, E. and Balat, H. Main routes for the thermo-conversion of biomass into fuels and chemicals. Part 1: Pyrolysis systems. *Energy Conversion and Management*, 2009. **50**(12): 3147-3157.
- [37] Bridgwater, A.V. Review of fast pyrolysis of biomass and product upgrading. *Biomass and Bioenergy*, 2012. **38**(0): 68-94.
- [38] McKendry, P. Energy production from biomass (part 2): conversion technologies. *Bioresource Technology*, 2002. **83**(1): 47-54.

- [39] Atabani, A.E., Silitonga, A.S., Badruddin, I.A., Mahlia, T.M.I., Masjuki, H.H. and Mekhilef, S. A comprehensive review on biodiesel as an alternative energy resource and its characteristics. *Renewable and Sustainable Energy Reviews*, 2012. **16**(4): 2070-2093.
- [40] Cornelissen, T. Flash pyrolysis of biomass and co-pyrolysis with biopolymers, in PhD thesis - Research Group: Applied and Analytical Chemistry 2009, Hasselt University: Diepenbeek. 202.
- [41] Atabani, A.E., Silitonga, A.S., Ong, H.C., Mahlia, T.M.I., Masjuki, H.H., Badruddin, I.A. and Fayaz, H. Non-edible vegetable oils: A critical evaluation of oil extraction, fatty acid compositions, biodiesel production, characteristics, engine performance and emissions production. *Renewable and Sustainable Energy Reviews*, 2013. **18**(0): 211-245.
- [42] Koppejan, J. and van Loo, S. Biomass combustion: an overview, in *Thermal biomass conversion*, Bridgwater, A.V., Hofbauer, H. and van Loo, S., Editors. 2009, CPL Press.
- [43] Fahmi, R., Bridgwater, A., Donnison, I., Yates, N. and Jones, J.M. The effect of lignin and inorganic species in biomass on pyrolysis oil yields, quality and stability. *Fuel*, 2008. **87**(7): 1230-1240.
- [44] Stals, M., Carleer, R., Reggers, G., Schreurs, S. and Yperman, J. Flash pyrolysis of heavy metal contaminated hardwoods from phytoremediation: Characterisation of biomass, pyrolysis oil and char/ash fraction. *Journal of Analytical and Applied Pyrolysis*, 2010. **89**(1): 22-29.
- [45] Lievens, C., Carleer, R., Cornelissen, T. and Yperman, J. Fast pyrolysis of heavy metal contaminated willow: Influence of the plant part. *Fuel*, 2009. **88**(8): 1417-1425.
- [46] Haykiri-Acma, H. and Yaman, S. Thermal reactivity of rapeseed (*Brassica napus* L.) under different gas atmospheres. *Bioresource Technology*, 2008. **99**(2): 237-242.
- [47] Haykiri-Acma, H., Yaman, S. and Kucukbayrak, S. Effect of heating rate on the pyrolysis yields of rapeseed. *Renewable Energy*, 2006. **31**(6): 803-810.
- [48] Onay, O. and Kockar, O.M. Pyrolysis of rapeseed in a free fall reactor for production of bio-oil. *Fuel*, 2006. **85**(12-13): 1921-1928.
- [49] Onay, O. and Kockar, O.M. Slow, fast and flash pyrolysis of rapeseed. *Renewable Energy*, 2003. **28**(15): 2417-2433.
- [50] Sensoz, S., Angin, D., Yorgun, S. and Kockar, O.M. Biooil production from an oilseed crop: Fixed-bed pyrolysis of rapeseed (*Brassica napus* L.). *Energy Sources*, 2000. **22**(10): 891-899.

- [51] Giannakopoulou, K., Lukas, M., Vasiliev, A., Brunner, C. and Schnitzer, H. Conversion of rapeseed cake into bio-fuel in a batch reactor: Effect of catalytic vapor upgrading. *Microporous and Mesoporous Materials*, 2010. **128**(1-3): 126-135.
- [52] Culcuoglu, E., Unay, E., Karaosmanoglu, F., Angin, D. and Sensoz, S. Characterization of the bio-oil of rapeseed cake. *Energy Sources*, 2005. **27**(13): 1217-1223.
- [53] Karaosmanoglu, F. and Culcuoglu, E. Pyrolysis of rapeseed cake. *Energy Sources*, 2001. **23**(4): 377-382.
- [54] Sensoz, S., Yorgun, S., Angin, D., Culcuoglu, E., Ozcimen, D. and Karaosmanoglu, F. Fixed bed pyrolysis of the rapeseed cake. *Energy Sources*, 2001. **23**(10): 873-876.
- [55] Smets, K., Adriaensens, P., Reggers, G., Schreurs, S., Carleer, R. and Yperman, J. Flash pyrolysis of rapeseed cake: Influence of temperature on the yield and the characteristics of the pyrolysis liquid. *Journal of Analytical and Applied Pyrolysis*, 2011. **90**(2): 118-125.
- [56] Karaosmanoglu, F., Isigigur-Ergundenler, A., and Sever, A. Biochar from the straw-stalk of rapeseed plant. *Energy & Fuels*, 2000. **14**(2): 336-339.
- [57] Karaosmanoglu, F. and Tetik, E. Charcoal from the pyrolysis of rapeseed plant straw-stalk. *Energy Sources*, 1999. **21**(6): 503-510.
- [58] Karaosmanoglu, F., Tetik, E. and Gollu, E. Biofuel production using slow pyrolysis of the straw and stalk of the rapeseed plant. *Fuel Processing Technology*, 1999. **59**(1): 1-12.
- [59] Encinar, J.M., González, J.F., Martínez, G. and Román, S. Catalytic pyrolysis of exhausted olive oil waste. *Journal of Analytical and Applied Pyrolysis*, 2009. **85**(1-2): 197-203.
- [60] Petrov, N., Budinova, T., Razuigorova, M., Parra, J. and Galiatsatou, P. Conversion of olive wastes to volatiles and carbon adsorbents. *Biomass & Bioenergy*, 2008. **32**(12): 1303-1310.
- [61] Encinar, J.M., González, J.F., Martínez, G. and González, J.M. Two stages catalytic pyrolysis of olive oil waste. *Fuel Processing Technology*, 2008. **89**(12): 1448-1455.
- [62] Sensöz, S., Demiral, I. and Ferdi Gerçel, H. Olive bagasse (*Olea europea* L.) pyrolysis. *Bioresource Technology*, 2006. **97**(3): 429-436.
- [63] Zanzi, R., Sjostrom, K., and Bjornbom, E. Rapid pyrolysis of agricultural residues at high temperature. *Biomass & Bioenergy*, 2002. **23**(5): 357-366.

- [64] Zabaniotou, A.A., Kalogiannis, G., Kappas, E. and Karabelas, A.J. Olive residues (cuttings and kernels) rapid pyrolysis product yields and kinetics. *Biomass & Bioenergy*, 2000. **18**(5): 411-420.
- [65] Encinar, J.M., Beltrán, F.J., Bernalte, A., Ramiro, A. and González, J.F. Pyrolysis of two agricultural residues: Olive and grape bagasse. Influence of particle size and temperature. *Biomass and Bioenergy*, 1996. **11**(5): 397-409.
- [66] Pokorna, E., Postelmans, N., Jenicek, P., Schreurs, S., Carleer, R. and Yperman, J. Study of bio-oils and solids from flash pyrolysis of sewage sludges. *Fuel*, 2009. **88**(8): 1344-1350.
- [67] Velghe, I., Carleer, R., Yperman, J. and Schreurs, S. Study of the pyrolysis of municipal solid waste for the production of valuable products. *Journal of Analytical and Applied Pyrolysis*, 2011. **92**(2): 366-375.
- [68] Demirbas, A. Effect of initial moisture content on the yields of oily products from pyrolysis of biomass. *Journal of Analytical and Applied Pyrolysis*, 2004. **71**(2): 803-815.
- [69] Akhtar, J. and Amin, N.S. A review on operating parameters for optimum liquid oil yield in biomass pyrolysis. *Renewable & Sustainable Energy Reviews*, 2012. **16**(7): 5101-5109.
- [70] Raveendran, K., Ganesh, A. and Khilar, K.C. Pyrolysis characteristics of biomass and biomass components. *Fuel*, 1996. **75**(8): 987-998.
- [71] Wang, S., Guo, X., Wang, K. and Luo, Z. Influence of the interaction of components on the pyrolysis behavior of biomass. *Journal of Analytical and Applied Pyrolysis*, 2011. **91**(1): 183-189.
- [72] Agrawal, A. and Chakraborty, S. A kinetic study of pyrolysis and combustion of microalgae *Chlorella vulgaris* using thermo-gravimetric analysis. *Bioresource Technology*, 2013. **128**(0): 72-80.
- [73] Shen, D.K., Gu, S. and Bridgwater, A.V. The thermal performance of the polysaccharides extracted from hardwood: Cellulose and hemicellulose. *Carbohydrate Polymers*, 2010. **82**(1): 39-45.
- [74] Bridgwater, A.V. Principles and practice of biomass fast pyrolysis processes for liquids. *Journal of Analytical and Applied Pyrolysis*, 1999. **51**(1-2): 3-22.
- [75] Shen, D.K., Gu, S. and Bridgwater, A.V. Study on the pyrolytic behaviour of xylan-based hemicellulose using TG-FTIR and Py-GC-FTIR. *Journal of Analytical and Applied Pyrolysis*, 2010. **87**(2): 199-206.

- [76] Shen, D.K. and Gu, S. The mechanism for thermal decomposition of cellulose and its main products. *Bioresource Technology*, 2009. **100**(24): 6496-6504.
- [77] Shen, D.K., Gu, S., Luo, K.H., Wang, S.R. and Fang, M.X. The pyrolytic degradation of wood-derived lignin from pulping process. *Bioresource Technology*, 2010. **101**(15): 6136-6146.
- [78] Babich, I.V., van der Hulst, M., Lefferts, L., Moulijn, J.A., O'Connor, P. and Seshan, K. Catalytic pyrolysis of microalgae to high-quality liquid bio-fuels. *Biomass and Bioenergy*, 2011. **35**(7): 3199-3207.
- [79] Peng, W.M., Wu, Q.Y. and Tu, P.G. Pyrolytic characteristics of heterotrophic *Chlorella protothecoides* for renewable bio-fuel production. *Journal of Applied Phycology*, 2001. **13**(1): 5-12.
- [80] Kang, B.-S., Lee, K.H., Park, H.J., Park, Y.-K. and Kim, J.-S. Fast pyrolysis of radiata pine in a bench scale plant with a fluidized bed: Influence of a char separation system and reaction conditions on the production of bio-oil. *Journal of Analytical and Applied Pyrolysis*, 2006. **76**(1-2): 32-37.
- [81] Onay, Ö., Beis, S.H. and Koçkar, Ö.M. Fast pyrolysis of rape seed in a well-swept fixed-bed reactor. *Journal of Analytical and Applied Pyrolysis*, 2001. **58-59**(0): 995-1007.
- [82] Yorgun, S., Sensoz, S. and Kockar, O.M. Flash pyrolysis of sunflower oil cake for production of liquid fuels. *Journal of Analytical and Applied Pyrolysis*, 2001. **60**(1): 1-12.
- [83] Özbay, N., Pütün, A.E., Uzun, B.B. and Pütün, E. Biocrude from biomass: pyrolysis of cottonseed cake. *Renewable Energy*, 2001. **24**(3-4): 615-625.
- [84] Uzun, B.B., Pütün, A.E. and Pütün, E. Fast pyrolysis of soybean cake: Product yields and compositions. *Bioresource Technology*, 2006. **97**(4): 569-576.
- [85] Ozbay, N., Putun, A.E. and Putun, E. Bio-oil production from rapid pyrolysis of cottonseed cake: product yields and compositions. *International Journal of Energy Research*, 2006. **30**(7): 501-510.
- [86] Bridgwater, A.V., Czernik, S. and Piskorz, J. *Progress in thermochemical biomass conversion*. 2001, Oxford: Blackwell Science.
- [87] Himmel, M.E., Tucker, M.P., Baker, J.O., Rivard, C.J., Oh, K.K. and Grohmann, K. Comminution of biomass: hammer and knife mills. In *Seventh symposium on biotechnology for fuels and chemicals*. 1986. Gatlinburg, Tennessee: John Wiley and Sons Inc.

- [88] Klass, D.L. Biomass for renewable energy, fuels and chemicals. 1998, San Diego, CA: Academic Press. 688.
- [89] Duman, G., Okutucu, C., Ucar, S., Stahl, R. and Yanik, J. The slow and fast pyrolysis of cherry seed. *Bioresource Technology*, 2011. **102**(2): 1869-1878.
- [90] Demirbas, A. and Arin, G. An overview of biomass pyrolysis. *Energy Sources*, 2002. **24**(5): 471-482.
- [91] Bridgwater, A., Czernik, S., Diebold, U., Meier, D., Oasmaa, A., Pajares, C., Piskorz, J. and Radlein, D. *Fast pyrolysis of biomass: a handbook*. 1999, Newbury, UK: CPL Press.
- [92] Czernik, S. and Bridgwater, A.V. Overview of applications of biomass fast pyrolysis oil. *Energy & Fuels*, 2004. **18**(2): 590-598.
- [93] Scholze, B. and Meier, D. Characterization of the water-insoluble fraction from pyrolysis oil (pyrolytic lignin). Part I. PY-GC/MS, FTIR, and functional groups. *Journal of Analytical and Applied Pyrolysis*, 2001. **60**(1): 41-54.
- [94] Bridgwater, A.V., Czernik, S. and Piskorz, J. An overview of fast pyrolysis, in *Progress in thermochemical biomass conversion*, Bridgwater, A.V., Editor. 2001, Blackwell Science. 977 - 997.
- [95] Oasmaa, A. and Peacocke, C. A guide to physical property characterisation of biomass-derived fast pyrolysis liquids, ed. Finland, T.r.c.o. Vol. 450. 2001, Technical research centre of Finland, Espoo, Finland: VTT Publications.
- [96] Mortensen, P.M., Grunwaldt, J.D., Jensen, P.A., Knudsen, K.G. and Jensen, A.D. A review of catalytic upgrading of bio-oil to engine fuels. *Applied Catalysis A: General*, 2011. **407**(1-2): 1-19.
- [97] Chiaramonti, D., Oasmaa, A. and Solantausta, Y. Power generation using fast pyrolysis liquids from biomass. *Renewable and Sustainable Energy Reviews*, 2007. **11**(6): 1056-1086.
- [98] Boucher, M.E., Chaala, A., Pakdel, H. and Roy, C. Bio-oils obtained by vacuum pyrolysis of softwood bark as a liquid fuel for gas turbines. Part II: Stability and ageing of bio-oil and its blends with methanol and a pyrolytic aqueous phase. *Biomass & Bioenergy*, 2000. **19**(5): 351-361.
- [99] Oasmaa, A. and Meier, D. Characterisation, analysis, norms and standards, in *Fast pyrolysis of biomass: a handbook*, vol. 3, Bridgwater, A.V., Editor. 2005, CPL Press: Newbury, UK. 19 - 59.
- [100] Cornelissen, T., Yperman, J., Reggers, G., Schreurs, S. and Carleer, R. Flash co-pyrolysis of biomass with polylactic acid. Part 1: Influence on bio-oil yield and heating value. *Fuel*, 2008. **87**(7): 1031-1041.

-
- [101] Cornelissen, T., Jans, M., Yperman, J., Reggers, G., Schreurs, S. and Carleer, R. Flash co-pyrolysis of biomass with polyhydroxybutyrate: Part 1. Influence on bio-oil yield, water content, heating value and the production of chemicals. *Fuel*, 2008. **87**(12): 2523-2532.
- [102] Diebold, J.P. A review of the chemical and physical mechanisms of the storage stability of fast pyrolysis bio-oils, 2000, NREL. 1-59.
- [103] Hoekstra, E., Hogendoorn, K.J.A., Wang, X.Q., Westerhof, R.J.M., Kersten, S.R.A., van Swaaij, W.P.M. and Groeneveld, M.J. Fast Pyrolysis of Biomass in a Fluidized Bed Reactor: In Situ Filtering of the Vapors. *Industrial & Engineering Chemistry Research*, 2009. **48**(10): 4744-4756.
- [104] Bridgwater, A.V. Catalysis in thermal biomass conversion. *Applied Catalysis A: General*, 1994. **116**(1-2): 5-47.
- [105] Vitolo, S., Seggiani, M., Frediani, P., Ambrosini, G. and Politi, L. Catalytic upgrading of pyrolytic oils to fuel over different zeolites. *Fuel*, 1999. **78**(10): 1147-1159.
- [106] Elliott, D.C. Historical developments in hydroprocessing bio-oils. *Energy & Fuels*, 2007. **21**(3): 1792-1815.
- [107] Samolada, M.C., Papafotica, A. and Vasalos, I.A. Catalyst evaluation for catalytic biomass pyrolysis. *Energy & Fuels*, 2000. **14**: 1161 - 1167.
- [108] Pütün, E., Uzun, B.B. and Pütün, A.E. Fixed-bed catalytic pyrolysis of cotton-seed cake: Effects of pyrolysis temperature, natural zeolite content and sweeping gas flow rate. *Bioresource Technology*, 2006. **97**(5): 701-710.
- [109] Idem, R.O., Katikaneni, S.P.R. and Bakhshi, N.N. Catalytic conversion of canola oil to fuels and chemicals: Roles of catalyst acidity, basicity and shape selectivity on product distribution. *Fuel Processing Technology*, 1997. **51**(1-2): 101-125.
- [110] Katikaneni, S.P.R., Adjaye, J.D. and Bakhshi, N.N. Catalytic conversion of canola oil to fuels and chemicals over various cracking catalysts. *The Canadian Journal of Chemical Engineering*, 1995. **73**: 484-497.
- [111] Prasad, Y.S., Bakhshi, N.N., Mathews, J.F. and Eager, R.L. Catalytic conversion of canola oil to fuels and chemical feedstocks part 1. Effect of process conditions on the performance of HZSM-5 catalyst. *The Canadian Journal Of Chemical Engineering*, 1986. **64**(2): 278-284.
- [112] Williams, P.T. and Horne, P.A. The influence of catalyst type on the composition of upgraded biomass pyrolysis oils. *Journal of Analytical and Applied Pyrolysis*, 1995. **31**(0): 39-61.

- [113] Horne, P.A. and Williams, P.T. Upgrading of biomass-derived pyrolytic vapours over zeolite ZSM-5 catalyst: effect of catalyst dilution on product yields. *Fuel*, 1996. **75**(9): 1043-1050.
- [114] Mihalcik, D.J., Mullen, C.A. and Boateng, A.A. Screening acidic zeolites for catalytic fast pyrolysis of biomass and its components. *Journal of Analytical and Applied Pyrolysis*, 2011. **92**(1): 224-232.
- [115] Oasmaa, A., Peacocke, C., Gust, S., Meier, D. and McLellan, R. Norms and standards for pyrolysis liquids. End-user requirements and specifications. *Energy & Fuels*, 2005. **19**(5): 2155-2163.
- [116] Radlein, D. The production of chemicals from fast pyrolysis bio-oils, in *Fast pyrolysis of biomass: a handbook*, Bridgwater, A.V., et al., Editors. 1999, CPL Press: Newbury, UK. 164 - 188.
- [117] Zhou, J., Oehr, K.H., Simons, G. and Barrass, G. Simultaneous NO_x and SO_x control using BioLime™, in *Biomass gasification and pyrolysis, State of the art and future prospects*, Kaltschmitt, M. and Bridgwater, A.V., Editors. 1997, CPL Press: Newbury, UK. 490 - 494.
- [118] Radlein, D., Piskorz, J. and Majerski, P. Method of producing slow-release nitrogenous organic fertilizer from biomass, US Patent 5,676,727, 1997.
- [119] Oehr, K.H., Scott, D.S. and Czernik, S. Method of producing calcium salts from biomass, US Patent 5,264,623, 1993.
- [120] Hameed, B.H. and Rahman, A.A. Removal of phenol from aqueous solutions by adsorption onto activated carbon prepared from biomass material. *Journal of Hazardous Materials*, 2008. **160**(2-3): 576-581.
- [121] Vaughn, S.V. and Spencer, G.F. Aromatic aldehydes and alcohols as potato sprout inhibitors, US Patent 5,129,951, 1992.
- [122] Emerson, R.W. and Crandall, B.G. Use of saponin in methods and compositions for pathogen control, US Patent 5,639,794, 1996.
- [123] Radlein, D. Study of levoglucosan production - a review, in *Fast pyrolysis of biomass: a handbook*, Vol. 2, Bridgwater, A.V., Editor. 2002, CPL Press: Newbury, UK. 205 - 241.
- [124] Bennett, N.M., Helle, S.S. and Duff, S.J.B. Extraction and hydrolysis of levoglucosan from pyrolysis oil. *Bioresource Technology*, 2009. **100**(23): 6059-6063.
- [125] Wu, W., Yang, M., Feng, Q., McGrouther, K., Wang, H., Lu, H. and Chen, Y. Chemical characterization of rice straw-derived biochar for soil amendment. *Biomass and Bioenergy*, 2012. **47**(0): 268-276.

- [126] Beesley, L., Moreno-Jiménez, E., Gomez-Eyles, J.L., Harris, E., Robinson, B. and Sizmur, T. A review of biochars' potential role in the remediation, revegetation and restoration of contaminated soils. *Environmental Pollution*, 2011. **159**(12): 3269-3282.
- [127] Sing, K.S.W., Everett, D.H., Haul, R.A.W., Moscou, L., Pierotti, R.A., Rouquerol, J. and Siemieniowska, T. Reporting physisorption data for gas solid systems with special reference to the determination of surface-area and porosity (recommendations 1984). *Pure and Applied Chemistry*, 1985. **57**(4): 603-619.
- [128] Ioannidou, O. and Zabaniotou, A. Agricultural residues as precursors for activated carbon production - A review. *Renewable and Sustainable Energy Reviews*, 2007. **11**(9): 1966-2005.
- [129] Stavropoulos, G.G. and Zabaniotou, A.A. Production and characterization of activated carbons from olive-seed waste residue. *Microporous and Mesoporous Materials*, 2005. **82**(1-2): 79-85.
- [130] Tan, I.A.W., Ahmad, A.L. and Hameed, B.H. Adsorption isotherms, kinetics, thermodynamics and desorption studies of 2,4,6-trichlorophenol on oil palm empty fruit bunch-based activated carbon. *Journal of Hazardous Materials*, 2009. **164**(2-3): 473-482.
- [131] Gonzalez, J.F., Roman, S., Gonzalez-Garcia, C.M., Nabais, J.M.V. and Ortiz, A.L. Porosity Development in Activated Carbons Prepared from Walnut Shells by Carbon Dioxide or Steam Activation. *Industrial & Engineering Chemistry Research*, 2009. **48**(16): 7474-7481.
- [132] Dias, J.M., Alvim-Ferraz, M.C.M., Almeida, M.F., Rivera-Utrilla, J. and Sanchez-Polo, M. Waste materials for activated carbon preparation and its use in aqueous-phase treatment: A review. *Journal of Environmental Management*, 2007. **85**(4): 833-846.
- [133] Durán-Valle, C.J., Gómez-Corzo, M., Pastor-Villegas, J. and Gómez-Serrano, V. Study of cherry stones as raw material in preparation of carbonaceous adsorbents. *Journal of Analytical and Applied Pyrolysis*, 2005. **73**(1): 59-67.
- [134] Hameed, B.H., Salman, J.M. and Ahmad, A.L. Adsorption isotherm and kinetic modeling of 2,4-D pesticide on activated carbon derived from date stones. *Journal of Hazardous Materials*, 2009. **163**(1): 121-126.
- [135] Olivares-Marín, M., Fernández-González, C., Macías-García, A. and Gómez-Serrano, V. Preparation of activated carbon from cherry stones by chemical activation with ZnCl₂. *Applied Surface Science*, 2006. **252**(17): 5967-5971.

- [136] Izquierdo, M.T., Martínez de Yuso, A., Rubio, B. and Pino, M.R. Conversion of almond shell to activated carbons: Methodical study of the chemical activation based on an experimental design and relationship with their characteristics. *Biomass and Bioenergy*, 2011. **35**(3): 1235-1244.
- [137] Singh, K.P., Malik, A., Sinha, S., and Ojha, P. Liquid-phase adsorption of phenols using activated carbons derived from agricultural waste material. *Journal of Hazardous Materials*, 2008. **150**(3): 626-641.
- [138] Shawabkeh, R.A. and Abu-Nameh, E.S.M. Absorption of Phenol and Methylene Blue by Activated Carbon from Pecan Shells. *Colloid Journal*, 2007. **69**(3): 355-359.
- [139] Tay, T., Ucar, S. and Karagöz, S. Preparation and characterization of activated carbon from waste biomass. *Journal of Hazardous Materials*, 2009. **165**(1-3): 481-485.
- [140] Bacaoui, A., Yaacoubi, A., Dahbi, A., Bennouna, C., Luu, R.P.T., Maldonado-Hodar, F.J., Rivera-Utrilla, J. and Moreno-Castilla, C. Optimization of conditions for the preparation of activated carbons from olive-waste cakes. *Carbon*, 2001. **39**(3): 425-432.
- [141] Román, S., González, J.F., González-García, C.M. and Zamora, F. Control of pore development during CO₂ and steam activation of olive stones. *Fuel Processing Technology*, 2008. **89**(8): 715-720.
- [142] Martínez, M.L., Torres, M.M., Guzmán, C.A. and Maestri, D.M. Preparation and characteristics of activated carbon from olive stones and walnut shells. *Industrial Crops And Products*, 2006. **23**(1): 23-28.
- [143] Jia, Q. and Lua, A.C. Effects of pyrolysis conditions on the physical characteristics of oil-palm-shell activated carbons used in aqueous phase phenol adsorption. *Journal of Analytical and Applied Pyrolysis*, 2008. **83**(2): 175-179.
- [144] Marsh, H. and Rodríguez-Reinoso, F. *Activated carbon*. 2006: Elsevier Science & Technology Books. 536.
- [145] Rodríguez-Reinoso, F., Molina-Sabio, M. and González, M.T. The use of steam and CO₂ as activating agents in the preparation of activated carbons. *Carbon*, 1995. **33**(1): 15-23.
- [146] Wigmans, T. Industrial aspects of production and use of activated carbons. *Carbon*, 1989. **27**(1): 13-22.
- [147] Walker, P.L., Rusinko, F. and Austin, L.G. Gas Reactions of Carbon, in *Advances in Catalysis*, D.D. Eley, P.W.S. and Paul, B.W., Editors. 1959, Academic Press. 133-221.

- [148] Smíšek, M. and Černý, S. Active carbon: Manufacture, properties and applications. 1970, Amsterdam: Elsevier. 479.
- [149] Solum, M.S., Pugmire, R.J., Jagtoyen, M. and Derbyshire, F. Evolution of carbon structure in chemically activated wood. Carbon, 1995. **33**(9): 1247-1254.
- [150] Salame, I.I. and Bandosz, T.J. Role of surface chemistry in adsorption of phenol on activated carbons. Journal of Colloid and Interface Science, 2003. **264**(2): 307-312.

2 Material and methods

This chapter summarizes the experimental approach of this thesis. In section 2.1, some background information on the three agricultural waste cakes (rapeseed cake, raspberry seed cake and olive waste cake) is provided. The setups used for the lab-scale pyrolysis experiments are presented in section 2.2. In the next three sections, the analytical techniques used for characterization of the agricultural waste cakes (section 2.3), the pyrolysis liquid (section 2.4) and the solid residue (section 2.5) are discussed in detail. The next two sections describe the production (section 2.6) and the characterization of activated carbon (section 2.7), while the methodology of the batch phenol adsorption study is discussed in section 2.8.

A schematic overview of the experimental approach is presented in Figure 2-1. Below the header "Pyrolysis process" is indicated which type of pyrolysis process is performed on a certain type of biomass. For each pyrolysis experiment, the product yield and the energy recovery are determined. The obtained solid and liquid pyrolysis products are characterized into further detail using a set of complementary analytical techniques. Pyrolysis liquids that spontaneously separate into two fractions (an aqueous and an organic fraction) are characterized after this phase separation. The characterized products are shown below the header "Characterized pyrolysis products". The analyses that are performed on a certain pyrolysis product (solid or liquid) are indicated by a marker in the same color as the corresponding pyrolysis process below the header "Characterization". The pyrolysis gas is not further characterized in this study. The solid residue produced by slow pyrolysis of rapeseed cake (light green color) and raspberry seed cake (light blue color) is converted into activated carbon by physical activation using steam or CO₂ and further characterized as indicated below "Characterization".

2.1 Agricultural waste cakes

This thesis investigates the potential of pyrolysis to convert three agricultural waste cakes into renewable fuels and/or added-value chemicals. Prior to analysis or pyrolysis, the waste cakes are ground to a particle size smaller than 2 mm and stored in a sealed container at room temperature.

2.1.1 Rapeseed cake

The rapeseed cake was obtained as the solid waste formed by cold-pressing of “double low” winter rapeseed² (*Brassica napus* L.). The rapeseed was delivered and pressed with a small mechanical screw press by ACRO (KHLim, Diepenbeek, Belgium). During the cold-pressing, the temperature was always kept below 60 °C. Since the aim of the supplier was to produce high quality oil, not all oil could be removed from the seeds, leaving a substantial amount of oil in the rapeseed cake. In this manner, the investigated cake differs from solvent-extracted rapeseed cake that is pressed in presence of a solvent (usually n-hexane) to maximize the oil recovery from the seeds.

2.1.2 Olive waste cake

The opportunities of pyrolysis to valorize waste cake produced from olives (*Olea Europaea* L.) were investigated in cooperation with the An-Najah National University of Palestine. The samples were obtained as the solid residue after vegetable oil production and delivered by olive mills located in the Nablus area of Palestine.

2.1.3 Raspberry seed cake

The raspberry seed cake was delivered by Eco Treasures (Lokeren, Belgium). It was obtained as the solid waste product after supercritical CO₂-extraction of raspberry seeds (*Rubus Idaeus* L.) to produce high value chemicals (such as antioxidants and high quality oil). The raspberry seeds were collected after separation from the fruit flesh during the production of raspberry fruit juice.

² “double low” or (00)-kind rapeseed has a low content of both erucic acid and glucosinolates.

2.2 Lab-scale pyrolysis experiments

2.2.1 Semi-continuous flash pyrolysis experiments

Flash pyrolysis experiments were performed in a home-built semi-continuous lab-scale reactor that has been used in view of fundamental research within the research group of Analytical and Applied Chemistry [1-5]. An overview of the reactor setup is given in Figure 2-2.

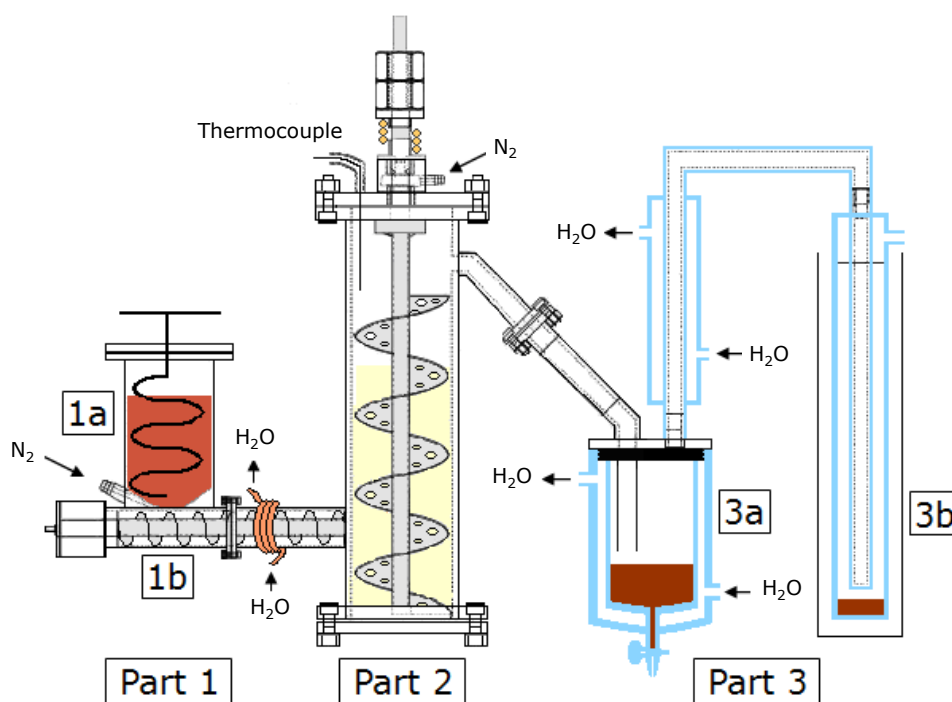


Figure 2-2: Flash pyrolysis reactor setup: (1) biomass injection system, (2) pyrolysis reactor and (3) pyrolysis liquid condensation system.

The reactor setup consisted of three main parts: the biomass injection system (part 1), the pyrolysis reactor (part 2) and the pyrolysis liquid condensation system (part 3). The injection system was composed of a storage vessel (height: 165 mm; diameter: 69 mm) (1a) and an injector pipe with water cooled copper windings (1b). The pyrolysis reactor was manufactured in stainless steel (AISI 304) and had a height of 360 mm and a diameter of 88 mm [6]. The condensation system consisted of two units (part 3a and 3b), both made of glass. The water cooled condensation vessel (part 3a) was equipped with a valve

at the bottom, allowing to remove the pyrolysis liquid from the vessel during the pyrolysis experiment when needed. To ensure pyrolysis atmosphere, nitrogen gas was injected into the reactor via two ways: one via the storage vessel of the injection system (70 mL/min) and one via the hollow shaft of the Archimedical screw inside the reactor (70 mL/min).

Before each experiment, the agricultural waste cake (about 100 g) was placed in the storage vessel of the injection system, while the reactor was filled with white sand (about 700 g) used as a heat transfer medium. Preliminary, this sand (particle size: 125 – 500 μm) had been pre-treated in an oven at 650 °C for 6 h to remove all organic contamination and stored in enclosed containers. Sand and reactor were externally heated using an electric heating jacket equipped with a temperature controller (Horst, GmbH, Germany). Monitoring of the pyrolysis temperature occurred by measuring the temperature at the top of the sand bed, using a thermocouple type K and an ATAL Smart Reader Plus data logger that was connected to a PC. The perforated Archimedical screw, placed inside the reactor, was rotated by an engine at 850 rpm to ensure a homogenous temperature of the sand and to create a “fluidized bed effect” for intimate mixing and heat transfer between sand and biomass. At the desired pyrolysis temperature, the agricultural waste cake was injected from the storage vessel (at room temperature) into the reactor (at pyrolysis temperature) by the Archimedical screw inside the injector at about 1.5 g sample/s (depending on density of the waste cake). To avoid heating up of the waste cake before injection, the injector pipe was cooled by water-circulated copper windings. By injecting the waste cake sample into the hot sand, it was heated from room temperature to pyrolysis temperature in a very short period of time (reaction and vapor residence time less than 5 s) and flash pyrolysis conditions were accomplished. As a result, the waste cake was volatilized and/or decomposed into vapors that left the hot reactor and entered into the condensation system. A considerable amount of vapors was already condensed into pyrolysis liquid by the water cooled condensation vessel (3a). Uncondensed vapors were led through a second condensation unit cooled by ice (3b) to collect as much condensable vapors as possible. The non-condensable vapors left the condensation system as permanent gases into the fume hood. Optionally, an aerosol filter could be mounted to the outlet of the condensation system to

calculate the amount of aerosols that was leaving the condensation system together with the pyrolysis gas.

Prior to each experiment, the agricultural waste cake and the sand were dried overnight at 110 °C to remove moisture. After the pyrolysis experiment, the yield of the pyrolysis products was calculated as follows:

- ⇒ The pyrolysis liquid was collected from the condensation system, decanted into a storage vessel and weighed afterwards.
- ⇒ The yield of solid residue (char and ash) was obtained by subtraction of the amount of sand before pyrolysis from the amount of sand and solid residue obtained after pyrolysis. Although the collection of the sand/solid residue mixture was performed with greatest care, this procedure was sensitive to small unavoidable errors due to residues that stuck to the reactor walls. Afterwards, the solid residue was separated from the sand by sieving and the aid of an electrostatic device.
- ⇒ The gas yield was calculated by difference.

2.2.2 Batch slow pyrolysis with separated liquid collection

The slow pyrolysis experiments with liquid collection in fractions as a function of pyrolysis temperature were performed with the reactor setup described in section 2.2.1. In case of slow pyrolysis, the waste cake sample (about 140 g) was placed, together with sand (about 700 g), inside the reactor at the beginning of the experiment. The following heating profile was applied. First, the reactor was heated from room temperature to 100 °C at 3 °C/min and kept isothermal for 30 min. Then, heating was continued to 195 °C followed by an isothermal period of 30 min. This temperature was chosen since preliminary experiments indicated that the degradation of the investigated samples started at this temperature. Finally, the reactor was heated to 550 °C at 5 °C/min and kept isothermal for 30 min. During the last heating segment, the actual pyrolysis of the waste cake sample occurred and the pyrolysis liquid was collected as a function of temperature using the condensation vessel equipped with a valve at the bottom (Figure 2-2; part 3a).

2.2.3 Batch slow pyrolysis experiments without sand

The reactor setup described in section 2.2.1 was used for the slow pyrolysis experiments without sand as a heat transfer medium. In this case, the waste cake sample was placed inside the reactor at the beginning of the experiment and heated at 10 °C/min to 150 °C and kept isothermal for 10 min to remove remaining moisture. Then, the agricultural waste cake was further heated at 10 °C/min to the final pyrolysis temperature (450 °C) and kept isothermal for 1 h. The pyrolysis temperature was monitored as the temperature of the reactor wall by means of a thermocouple type K. Product collection occurred analogously as described in section 2.2.1 (but without the need of separation of the solid residue from the sand).

2.2.4 Batch slow catalytic pyrolysis experiments

The slow catalytic pyrolysis experiments were carried out using a horizontal tubular quartz reactor at atmospheric pressure. A schematic diagram of the setup is shown in Figure 2-3.

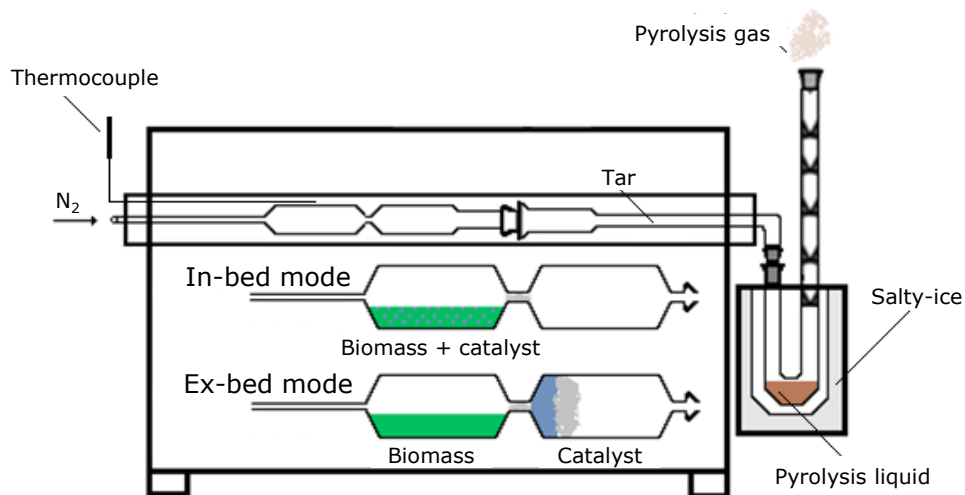


Figure 2-3: Experimental setup for the slow (catalytic) pyrolysis experiments. Two configurations were used: in-bed and ex-bed mode.

The home-built reactor tube consisted of two compartments (38 mm i.d. x 70 mm long) separated by a constriction (10 mm i.d. x 10 mm long). Two configurations were used in this thesis. In the mixed configuration (in-bed

mode), biomass and catalyst were premixed and loaded in the same compartment. In the separated configuration (ex-bed mode), the biomass was loaded in the first compartment while the catalyst was placed as a fixed-bed (between two quartz wool plugs of about 0.3 g) in the second compartment. Hence, there was no direct contact between biomass and catalyst. To ensure pyrolysis conditions (oxygen deficient), the reactor was continuously flushed with nitrogen (50 mL/min).

Typically, the tests were performed with 7.5 g of waste cake and a certain quantity of catalyst (see Table 2-1). In case of ex-bed mode, the amount of catalyst was chosen to obtain a fixed-bed height of 1.5 cm. The average vapor residence time³ was estimated as the total volume of catalyst divided by the gas flow rate and was found to be less than 20 s for catalysts tested in ex-bed mode. The waste cake sample and catalyst were heated by an electric tube furnace (Nabertherm) using a fixed heating program. Pyrolysis temperature was monitored by a thermocouple placed near the reactor wall of the biomass compartment. Firstly, the reactor was heated at 10 °C/min to 150 °C and kept isothermal for 10 min to remove remaining moisture from the waste cake sample. Then, the heating was continued at 30 °C/min to 450 °C. Finally, the sample was heated at 10 °C/min to 550 °C and kept at that temperature for 30 min as no further release of vapors was observed after this period of time. The final temperature of 550 °C was chosen based on TGA of the waste cake and literature data [7, 8]. During heating, the waste cake was degraded and volatilized. After catalyst interaction, small part of the vapors was condensed at the end of the reactor tube, forming the tar fraction. The more volatile part of the vapors only started condensing in the cold trap (cooled by salty-ice), resulting in the pyrolysis liquid. The non-condensable vapors left the setup as gaseous fraction. The yield of solid residue was determined by the weight difference of the reactor tube before and after pyrolysis. The yield of pyrolysis liquid was obtained from the weight difference of the condensation unit before and after the experiment. The gas yield was calculated by difference. In this study, pyrolysis experiments were carried out in duplicate.

³ average vapor residence time $\approx \left(\frac{\pi d^2 h}{4}\right)/Q = \left(\frac{\pi \cdot 3.8^2}{4} \cdot 1.5\right)/50 = 0.34 \text{ min} = 20 \text{ s}$ with d the inner diameter of the reactor tube (cm), h the bed height (cm) and Q the nitrogen flow rate (cm³/min).

Catalyst characteristics and preparation

Three types of catalysts were tested in two configurations during slow catalytic pyrolysis of rapeseed cake (Table 2-1). Activated alumina ($\gamma\text{-Al}_2\text{O}_3$) and sodium carbonate (Na_2CO_3) were used as purchased. The HZSM-5 zeolite was prepared from ZSM-5 zeolite by ion-exchange, based on a method of Song et al. [9]. Firstly, the ZSM-5 zeolite (20 g) was heated at 550 °C for 2 h in nitrogen atmosphere to remove moisture. Secondly, it was converted into the NH_4^+ -form by ion-exchange in three consecutive steps. Therefore, the ZSM-5 zeolite was added three times to a 1 M ammonium nitrate solution (750 mL) and heated at 90 °C for 3 h. The excess of nitrate ions was removed by thoroughly washing of the exchanged sample with deionized water. Finally, the $\text{NH}_4\text{ZSM-5}$ was converted into HZSM-5 by calcination at 550 °C in dry air (50 mL/min) for 4 h.

Table 2-1: Characteristics of catalysts used in slow catalytic pyrolysis.

Catalyst	Producer	Form	Type	Configuration	wt%^a
$\gamma\text{-Al}_2\text{O}_3$	Alfa Aesar	Pellets	Acidic-neutral	Ex-bed	68
				In-bed	44
HZSM-5	Acros	Pellets	Strong acidic	Ex-bed	47
				In-bed	34
Na_2CO_3	Merck	Powder	Alkaline	In-bed	10

^a wt% = (mass catalyst/mass biomass) x 100%

2.3 Characterization of agricultural waste cake

2.3.1 Moisture content

The moisture content of the agricultural waste cakes (as received) was determined by drying them in an oven at 110 °C to constant weight. Since high moisture contents are undesirable for pyrolysis feedstocks [10], the waste cakes were oven-dried prior to all analyses and pyrolysis experiments. The moisture that could not be removed by drying will be indicated in this study as residual moisture.

2.3.2 Component analysis

In literature, several indirect chemical methods (e.g. ASTM, Van Soest and Wine, Browning, Klason, NREL and Scott) and their modifications are described to determine the biomass composition. Concerning the analysis of agricultural waste cakes, the method of Van Soest and Wine is most commonly used [11]. However, since indirect chemical methods are time consuming and expensive, more and more attention is given to faster and less expensive techniques based on Near Infrared Reflectance spectroscopy [12-14] and TGA [15] to determine the biomass composition.

In this thesis, the composition of the agricultural waste cakes was determined by an adapted version of the wet chemical method of Van Soest and Wine [16]. In this gravimetric method, the neutral detergent fibre (NDF) and acid detergent fibre (ADF) were determined after removal of interfering compounds by two consecutive extractions. Separate analyses were used to determine the content of ash, crude proteins and triglycerides. A flowchart of the method used in this study is given in Figure 2-4. Each analysis was performed at least in duplicate. Prior to analysis, the waste cakes were ground to a particle size smaller than 0.7 mm and dried overnight at 110 °C to remove moisture. Then, two consecutive Soxhlet extractions (24 h) with respectively 95 % ethanol (160 mL; VWR) and hot distilled water (160 mL) were performed to remove interfering compounds as extractives. The ethanol extraction was used to remove lipids, waxes and resins, while free sugars, tannins, gums and pigments were removed by the hot water extraction [17]. Both extractions were carried out according to the ASTM E1690 method [18] and were reported in literature to remove approximately 90 % of the extractives [19].

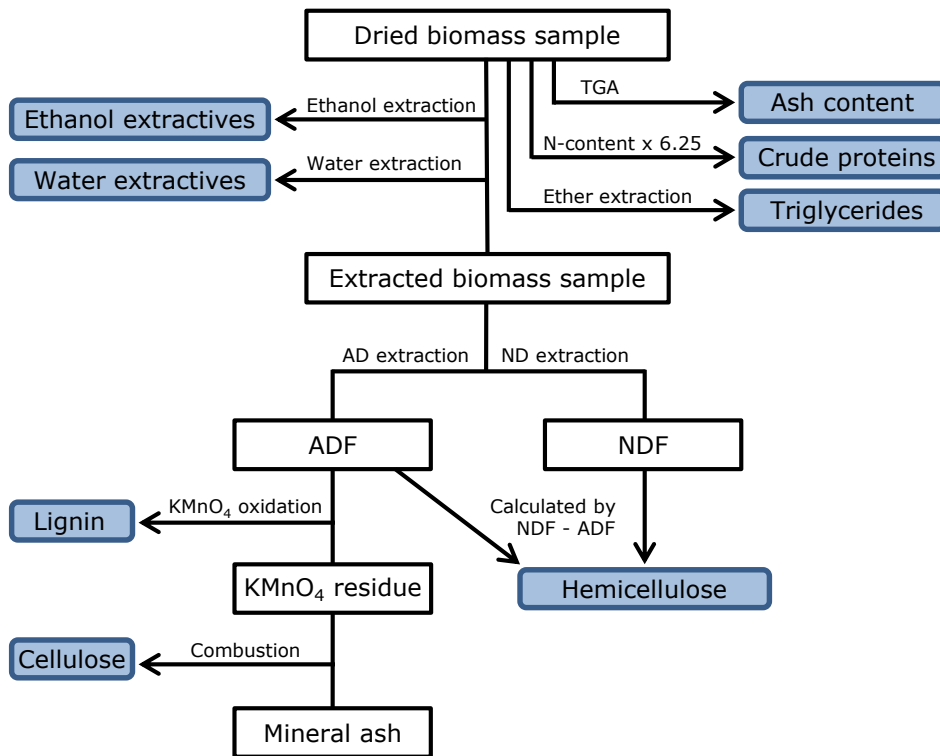


Figure 2-4: Flowchart of the component analysis performed on the agricultural waste cakes.

After the consecutive ethanol and water extractions, the actual component analysis was performed by four wet-chemical treatments (Figure 2-4). Firstly, the extracted biomass sample was subjected to an acid detergent (AD) extraction, resulting in the ADF. The AD solution contained H_2SO_4 (0.5 M) and cetyl trimethylammonium bromide (20 g/L) as detergent. Secondly, the lignin content was calculated from the weight loss on oxidation of the ADF by a saturated KMnO_4 – acetate buffer solution. The residue from this oxidation step was composed of (mainly) cellulose and mineral ash. Thirdly, the cellulose content was obtained from the weight loss on combustion of the KMnO_4 -residue. Fourthly, the extracted biomass sample was further extracted with neutral detergent (ND) solution to obtain the NDF. The ND solution contained sodium dodecyl sulfate (30 g/L) as detergent and Na_2SO_3 (20 g/L) was added to remove interfering proteins that otherwise would be falsely identified as hemicellulose [11]. The pH was set at 7 using HCl (0.1 M). The hemicellulose content was

calculated by subtraction of the ADF from the NDF content. More information on the preparation of the reactant solutions can be found in [16].

The content of ash, crude proteins and triglycerides was determined by separate analyses starting from the oven-dried agricultural waste cake. Ash was obtained by TGA at 850 °C under oxygen atmosphere, while the content of crude proteins was estimated by multiplying the N-content (determined by elemental analysis) by a nitrogen-to-protein conversion factor of 6.25⁴ [16, 20]. The triglyceride content was found by a separate Soxhlet extraction (24 h) with diethyl ether [16].

Remarks on the component analysis

During component analysis, proteins turned out to interfere with several extraction/reaction steps. Therefore, the combustion method (see section 2.3.4: elemental analysis) was used to determine the protein content of each residue (as N% x 6.25) [16, 21]. This allowed to explain the high amount of not identified components found after component analysis. However, care should be taken when interpreting the results because rather the total N-content (including non-protein nitrogenous compounds) than the N-content of proteins and amino acids was measured by the combustion method. Moreover, the conversion factor is also dependent on the biomass material since different proteins can have different N-contents [20].

2.3.3 Thermogravimetric analysis (TGA) and proximate analysis

Thermogravimetric analysis (TGA) is a quick thermal analysis technique that records the weight loss of a biomass sample as a function of temperature (time) under a controlled temperature program and atmosphere. This weight loss, caused by volatilization and/or decomposition reactions, provides useful information on the thermal conversion characteristics of agricultural waste cakes. However, one should keep in mind that due to the low sample size, secondary reactions and other heat and mass transfer effects are much less prominent than in case of lab-scale or industrial-scale experiments [22]. From

⁴ The nitrogen-to-protein conversion factor assumes that 100 g of plant or animal protein contains 16 g of nitrogen ($100/16 = 6.25$) [20].

the TG curves, differential thermogravimetric analysis (DTG) curves can be derived and plotted as a function of temperature (time).

In this study, TGA was performed using a DuPont Instruments 951 Thermogravimetric Analyzer. The samples (about 20 mg) were loaded on a quartz crucible and heated at 20 °C/min from room temperature to 600 °C under flowing nitrogen (80 mL/min). This carrier gas provided an inert atmosphere for pyrolysis and removed the gaseous and condensable products from the heating zone, thus minimizing secondary reactions in the vapor phase. Then, an isothermal period of 10 min was applied and the gas stream was switched to oxygen. After the isothermal period, heating was continued at 20 °C/min to 850 °C under flowing oxygen (80 mL/min). After the experiment, TA Universal Analysis was used to interpret the results.

Proximate analysis (i.e. the content of residual moisture, volatile matter, fixed carbon and ash) was obtained from TGA as proposed by Klass [23]. Although this method is not an industrial standard, it can quickly provide information about the thermochemical conversion of biomass [24]. The residual moisture content of the oven-dried waste cakes was calculated from the weight loss between room temperature and 165 °C. The volatile matter, calculated from the weight loss between 165 and 600 °C, was indicative for the amount of biomass that would be "available" for conversion under pyrolysis conditions. The fixed carbon content, an indication of the char yield, was determined from the weight loss under oxygen atmosphere between 600 and 850 °C, while the ash content was calculated from the residual weight at 850 °C.

2.3.4 Elemental analysis

The content of carbon (C), hydrogen (H), nitrogen (N) and sulfur (S) was determined by elemental analysis using a FlashEA 1112 Elemental Analyzer (Thermo Electron Corporation). The samples (2 – 4 mg) were weighed into a small container made of tin. Vanadium pentoxide (5 - 10 mg) was added as combustion catalyst to obtain sulfur contents as accurate as possible. The apparatus was calibrated using six samples (0.5 – 4.0 mg) of the 2,5-bis(5-tert-butyl-benzoxazol-2-yl)thiophene (BBOT – $C_{26}H_{26}N_2O_2S$) standard. Unknown samples were measured in triplicate, while control (BBOT) and blank samples were measured periodically to ensure proper functioning of the apparatus. The

content of oxygen (O) was calculated by difference as: $O\% = 100\% - (C\% + H\% + N\% + S\%)$. In case of biomass samples, the results of the elemental analysis were expressed on dry ash-free (daf) basis to allow easy comparison with other biomass samples, regardless their different ash and moisture content [19].

2.3.5 Energy content

Calorimetric values were measured to determine the gross energy content of a sample, expressed as higher heating value (HHV). The HHV is the total energy content released when the sample is burned in air, including the latent heat of water vaporization. Therefore, it represents the maximum amount of energy potentially recoverable from a given sample [24].

Measurements were performed with an IKA C5003 calorimeter equipped with an IKA KV 600 Digital water cooler and a Sartorius CP224S analytical balance. The waste cake samples (0.5 – 1 g) were weighed in a gelatin capsule, then placed in a quartz crucible and charged into the decomposition vessel (bomb). Before the sample was ignited, the bomb was filled with pure oxygen (99.95%) to a pressure of 30 bar to ensure complete sample combustion. The experiments were executed in dynamic measurement mode. The HHV of the sample was obtained from the temperature increase of the calorimeter system. The gelatin capsules were used for operating safety and as combustion aid to ensure complete combustion of the agricultural waste cakes. All samples were measured in triplicate. Prior to analysis, calibration of the system was performed using benzoic acid (tablet form, 0.5 g, IKA) with a known HHV of 26.46 MJ/kg (RSD = 0.01 %).

2.3.6 Minor elements

The minor elements in the agricultural waste cakes were determined by a method adapted from the standard method "Microwave digestion of plant tissue in a closed vessel" [21]. The waste cakes (250 mg) were digested by the aid of microwaves in a solution of HCl - HNO₃ (3:1) for the determination of the alkali metals (Na and K), the alkaline earth metals (Ca and Mg) and some trace elements (Al, Fe and Mn). For Si and P determination, a mixture of HF - HNO₃ (3:2) was used as digestion solution. After digestion, the samples were filtered

and diluted with purified water (18 M Ω) to 50 mL and analyzed by Inductively Coupled Plasma Atomic Emission Spectrometry (ICP-AES). Merck ICP Multi Standard IV was used to calibrate the Perkin Elmer Optima 3000 DV apparatus. The amount of chlorides, phosphates and sulfates was determined after complete combustion of the agricultural waste cake (250 mg) using the Parr bomb at an oxygen pressure of 30 bar. Pure mineral oil (400 mg) was added to ensure complete sample combustion. After combustion, the samples were filtered and diluted with purified water (18 M Ω) to 100 mL and analyzed by ion chromatography (IC). A Dionex DX120 ion chromatograph equipped with an IonPac AS14A column (250 mm x 4 mm) was used to separate the inorganic anions using a carbonate/bicarbonate eluent (0.72 mL/min) and a conductivity detector. A combined seven anion standard was used for calibration. All analyses were performed at least in twofold.

2.4 Characterization of pyrolysis liquid

In this study, most of the pyrolysis liquids were two-phased liquids. If this was the case, the liquid was separated into two fractions before being analyzed. Typically, a light brown water rich fraction (named *aqueous fraction*) and a dark brown, more viscous fraction with an oily appearance (named *organic oil fraction*) were obtained after phase separation of the pyrolysis liquid.

2.4.1 Gas Chromatography/Mass Spectrometry (GC/MS)

The chemical composition of the pyrolysis liquid was analyzed by gas chromatography/mass spectrometry (GC/MS). A Varian 3400 gas chromatograph, equipped with a DB-WAX capillary fused silica column (30 m x 0.25 mm; $d_f = 0.25 \mu\text{m}$; Agilent Technologies), was used and coupled to a Finnigan TSQ 700 mass selective quadrupole detector. Samples were prepared by dissolving the pyrolysis liquid (about 10 – 20 mg per mL solution) in a mixture of dichloromethane - methanol (3:2) (Suprasolv, Merck). After filtration over a PTFE-filter (0.45 μm), 1 μL of the sample solution was injected in splitless mode (injector temperature: 250 °C). The following heating program was used: after an initial isothermal period of 1 min, the column was heated at 12 °C/min from 35 to 260 °C and kept isothermal for 11 min. The transfer line between column and mass spectrometer had a temperature of 260 °C. The quadrupole mass spectrometer was set at the ionizing voltage of 70 eV (EI+ mode) with a mass range m/z of 35 – 500 and a scan rate of 2 scans/s. Chromatograms were analyzed with Xcalibur Qual Browser, using a commercial database (NIST 2001 mass spectral library) for compound identification.

In some cases, the peak area of each identified compound was normalized to the peak area of an internal standard (butylated hydroxytoluene, BHT; 50 ppm) to allow better comparison of the samples.

2.4.2 Water content

In literature, two major methods are reported to determine the water content of pyrolysis liquids, namely Karl Fischer titration and azeotropic distillation by the Dean Stark method. In Chapter 7 of this thesis, a profound discussion and comparison of both methods is presented. Moreover, an additional technique based on $^1\text{H-NMR}$ is proposed and tested. Since Karl Fischer titration turned out

to be the most suitable method for the pyrolysis liquids investigated in this study [5], only this method was further used in Chapters 3 to 5.

The water content of the pyrolysis liquids was determined by the volumetric Karl Fischer titration method. Analyses were performed using a Schott Geräte titrator (TR85) and an one-component solution (Combititrant 5, Merck). The Karl Fischer apparatus was calibrated by titrating six amounts of distilled water (1 – 20 μL) in triplicate. Pyrolysis liquid samples were loaded on a plastic container and weighed with an analytical balance (Mettler Toledo AG245). Sample size (20 - 100 mg) was dependent on the water content of the sample and was chosen to produce results within the calibration curve. After weighing, the sample was brought into the titration vessel of the Karl Fischer apparatus. Once the sample was completely dissolved in the methanol (Normapur AR1, VWR) working solution, the titration was started. The endpoint of the titration (+ 100 mV) was detected with a double platinum electrode (type Pt1400). Each pyrolysis liquid sample was measured at least in triplicate.

2.4.3 Elemental analysis

The elemental composition of the pyrolysis liquids was determined with the same instrument setup as described in section 2.3.4 for biomass samples. To prevent sample evaporation, the pyrolysis liquids were adsorbed on about 5 to 10 mg of Chromosorb W AW Media (1 m^2/g ; acid washed) during sample preparation.

2.4.4 Energy content

The gross energy content of the pyrolysis liquids was determined by the same apparatus as described for the agricultural waste cakes (see section 2.3.5). In contrast to the biomass samples, about 0.5 – 1 g of liquid sample was loaded directly into the quartz crucible, together with two paraffin strips (instead of gelatin capsules) as combustion aid.

2.4.5 Gel Permeation Chromatography (GPC)

The molecular weight distribution of the organic oil fraction of pyrolysis liquids was obtained by Gel Permeation Chromatography (GPC) using a SpectraSERIES P100 pump of Spectra-Physics, equipped with a Shodex RI-71 refractometer and

a PLgel Mixed BLS 10 μm column at 35 $^{\circ}\text{C}$. A flow of 1 mL/min of tetrahydrofuran (THF; LiChrosolv, Merck) was maintained. Calibration was performed with polyethylene glycol standards (Polymer Laboratories; molecular weight range: 106 – 3930 Da). A 1mV% solution of the samples was made in THF. Before injection, the sample solution was dried with Na_2SO_4 and filtered over a PTFE-filter (0.45 μm).

2.4.6 High Performance Liquid Chromatography (HPLC)

HPLC analysis was performed with an Agilent 1100 liquid chromatograph using a Phenomenex C8(2) column (Luna 3 μm ; 150 x 4.60 mm) operated at 25 $^{\circ}\text{C}$ and connected to a photodiode array detector. Detection was performed at 210 nm. A 1 mV% solution of the sample was made in a mixture of 50 % THF (LiChrosolv, Merck) and 50 % acetonitrile (ACN; HiPerSolv Chromanorm, VWR) that contained 1 % acetic acid (HAc; pro analysis, Merck) to protonate the (fatty) acids. Before injection (20 μL), the solution was filtered over a 0.45 μm PTFE-filter. The composition of the eluent as a function of time is given in Table 2-2.

Table 2-2: Eluent gradient program of the HPLC mobile phase.

Time (min)	ACN (+1% HAc)	THF (+1% HAc)	Flow (mL/min)
0 - 10	80	20	0.5
10 - 15	60	40	0.5
15 - 20	40	60	0.5
20- 30	30	70	0.5

2.4.7 Fourier Transform Infrared spectroscopy (FTIR)

The FTIR spectra were recorded with a Brüker Vertex 70 FTIR spectrometer. A sample of the pyrolysis liquid was placed as a thin film between KBr windows. Typically, 32 scans/min were taken with a resolution of 4 cm^{-1} and a background correction was performed.

2.4.8 Proton Nuclear Magnetic Resonance spectroscopy

(¹H-NMR)

A Varian Inova 300 spectrometer with a 5 mm four-nucleus PFG probe was used to record the ¹H-NMR spectra of the organic oil fraction of the pyrolysis liquid. The samples were prepared as a 1 mV% solution in CDCl₃ (Cambridge Isotope Laboratories, Inc). During the measurements, a spectral width of 5 kHz, a 90° pulse of 4 μs, an acquisition time of 7.5 s and a preparation delay of 20 s were used.

2.4.9 pH-value

The pH of the pyrolysis liquid was measured at 20 °C using a Hamilton Polilyte Lab electrode. Calibration was performed with two buffer solutions (pH 4.0 and 7.0).

2.4.10 Total Acid Number (TAN)

The Total Acid Number (TAN) of the organic oil fraction of the pyrolysis liquid was determined by the ASTM D664-04 method [25]. The end-point of the titration was detected by a Mettler Toledo InLab 412 electrode (electrolyte solution: 3 M LiCl in ethanol) and set at pH 11.0 as prescribed by the ASTM method.

2.4.11 Density

The density of the pyrolysis liquid was estimated by weighing about 5 mL of pyrolysis liquid that was poured into a 10 mL graduated cylinder.

2.4.12 Viscosity

The dynamic viscosity of the pyrolysis liquid (organic oil fraction) was measured with a TA Instruments AR-G2 rheometer at 40 °C. The kinematic viscosity was calculated from the dynamic viscosity divided by the density of the organic oil fraction.

2.5 Characterization of solid residue

2.5.1 Thermogravimetric analysis (TGA)

TGA of the solid residue was performed with the same instrument setup as described for the biomass samples (see section 2.3.3). However, the applied temperature profile was adjusted: the solid residue (about 20 mg) was loaded on a quartz crucible and heated at 20 °C/min from room temperature to 850 °C under flowing nitrogen (80 mL/min). Then, an isothermal period of 15 min was applied and the gas stream was switched from nitrogen to oxygen (80 mL/min). In this way, the amount of vapors that were not released during the pyrolysis process and the ash content could be determined.

2.5.2 Elemental analysis

Elemental analysis of the solid residue was performed in a similar way as described for the biomass samples (see section 2.3.4). Only the oxygen injection time was increased (from 5 to 10 s) to obtain complete sample combustion.

2.5.3 Energy content

The energy content of the solid residue was determined as described in section 2.3.5. In some cases, complete separation of the solid residue from the sand (used as heat transfer medium) was impossible. If this was the case, the energy content of the solid residue with sand included was determined. Afterwards, this energy content was corrected for the amount of sand and ash that were found after combustion of the solid residue in the calorimetric bomb. This amount was obtained as the weight difference between the quartz crucible after and before the experiment. Hence, rather the energy content of the char (without ash; HHV_{char}) than the energy content of the solid residue (HHV_{SR}) was measured. The latter was obtained by correcting HHV_{char} for the ash content of the solid residue, which in turn was calculated from the ash content of the agricultural waste cake and the yield of solid residue after the pyrolysis experiment.

2.6 Production of activated carbon

The solid residue, produced by slow pyrolysis up to 450 °C as described in section 2.2.3 (without sand as heat transfer medium), was converted into activated carbon (AC) by physical activation using steam or carbon dioxide as activation agent. Prior to activation, the solid residue was sieved (particle size: 125 - 700 μm), washed with hot distilled water and dried at 110 °C to constant weight. Then, the solid residue (about 7 g) was placed as a fixed bed between quartz wool plugs inside the horizontal tubular quartz reactor. The sample was heated by an electric furnace (Nabertherm) using a FGH 1000 controller connected to a thermocouple (placed against the outer reactor wall) for temperature control. An overview of the activation setup is shown in Figure 2-5.

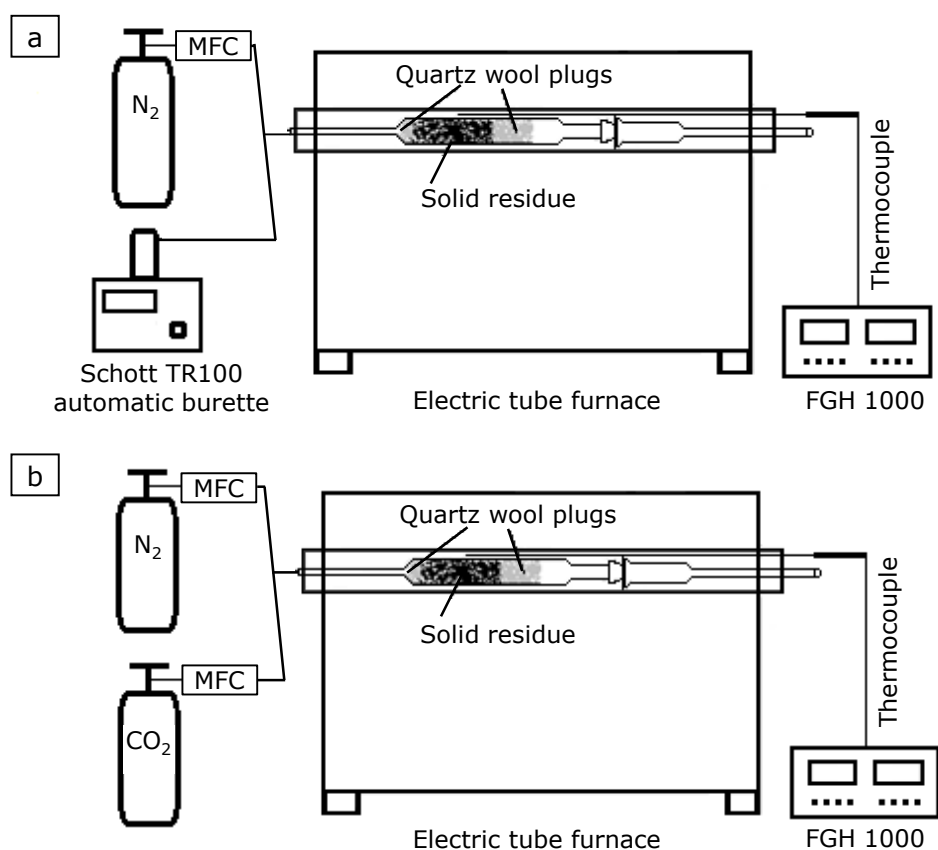


Figure 2-5: Schematic overview of the horizontal tubular reactor setup for AC production using steam (a) or CO₂ (b) as activation agent. (MFC = mass flow controller).

The sample was heated at 10 °C/min to the final activation temperature (850, 900 or 950 °C) under flowing nitrogen (70 mL/min). Once the activation temperature was reached, steam (Figure 2-5a) or carbon dioxide (Figure 2-5b) was applied to the sample. Steam was obtained by injecting 0.1 mL/min of liquid water by a Schott TR 100 automatic burette into the nitrogen flow just before the entrance of the reactor tube. Inside the hot reactor, the liquid water was converted into steam (about 534 mL/min at 900 °C)⁵ before reaching the sample. In case of activation by carbon dioxide, the nitrogen flow was replaced by pure CO₂ gas (70 mL/min) once the activation temperature was reached. Activation agents were applied for an activation time of 30, 60, 90 or 120 min. The effect of the activation temperature was studied by maintaining a fixed activation time of 30 min, while the influence of the activation time was tested at a fixed temperature of 900 °C. After activation, the sample was cooled down in the reactor under flowing nitrogen (70 mL/min), washed with hot (about 85 °C) distilled water, dried at 110 °C and stored in a desiccator.

⁵ Calculated by the ideal gas law: $V_{\text{steam}} = \frac{m(\text{H}_2\text{O})RT}{M_w P} = \frac{0.1}{18.02} \frac{8.314 \cdot 1173.15}{101325} = 5.34 \cdot 10^{-4} \text{ m}^3$

2.7 Characterization of activated carbon

2.7.1 Nitrogen adsorption study

The nitrogen adsorption studies were performed with a NOVA 2200 gas sorption analyzer (Quantachrome Instruments) at 77.4 K in the relative pressure (p/p_0) range from 0.008 to 0.98 by the Department of Polymer and Carbon Materials of the Wrocław University of Technology (Poland). Prior to analysis, the AC samples were outgassed overnight at 300 °C. From the adsorption isotherms, qualitative information on the nature of the adsorption process (section 2.7.1.1) and several important textural characteristics (BET specific surface area and pore size distribution) of the ACs could be inferred (sections 2.7.1.2 to 2.7.1.5).

2.7.1.1 Nitrogen adsorption isotherms

The first step in interpreting N_2 adsorption isotherms is to identify the isotherm type and hence the nature of the adsorption process [26]. According to the IUPAC classification, six types of isotherms can be distinguished. Additionally, adsorption isotherms can show hysteresis loops which can be classified into four types based on their shape [26]. An overview of the adsorption isotherms and hysteresis loops according to the IUPAC classification is shown in Figure 2-6.

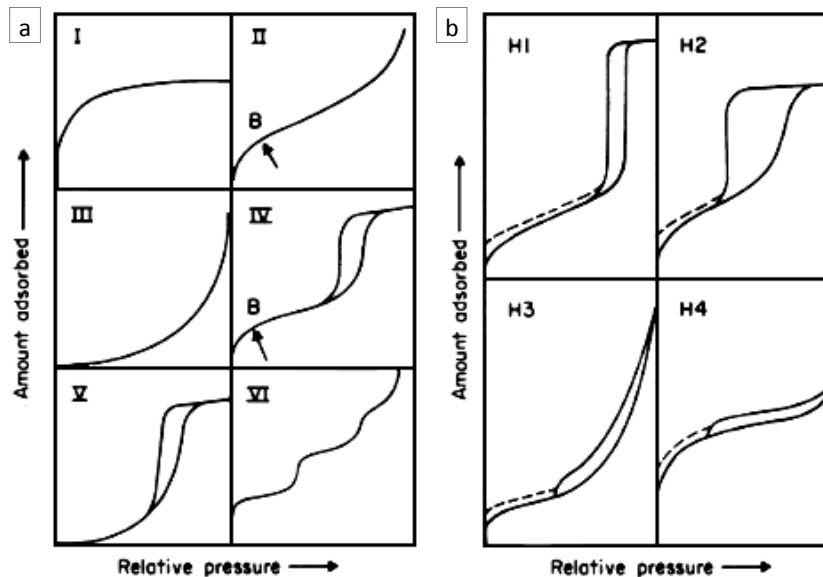


Figure 2-6: IUPAC classification of adsorption isotherms (a) and hysteresis loops (b) [26].

Type I isotherms are typical of (solely) microporous solids with a relatively small external surface. Type II isotherms are obtained for non-porous or macroporous adsorbents with unrestricted monolayer-multilayer adsorption, but that can also contain a certain degree of microporosity [27]. Adsorbents with low affinity for the adsorbate molecules are represented by type III isotherms. This type is not very common and adsorbate-adsorbate interactions play an important role in the adsorption process. Type IV isotherms show a characteristic hysteresis loop that is associated with capillary condensation in the mesopores of the adsorbent. Type V isotherms are a combination of type III isotherms and the hysteresis loop of type IV isotherms. Type VI isotherms represent stepwise multilayer adsorption on an uniform non-porous surface. Point B in type II and IV isotherms indicates the stage at which monolayer coverage is complete and multilayer adsorption is about to begin [26].

Hysteresis loops appear in type IV and type V adsorption isotherms. Although the influence of various factors on hysteresis is not fully understood, the shape of a hysteresis loop has often been identified with specific pore structures [26]. Types H1 and H2 hysteresis are characteristic for solids consisting of particles crossed by nearly cylindrical channels or formed by aggregates/agglomerates of spheroidal particles. In both cases, the pores can have an uniform size and shape (type H1 hysteresis) or have a nonuniform size or shape (type H2 hysteresis). Near cylindrical through pores and ink-bottle pores are typical pore shapes resulting in type H2 hysteresis. Types H3 and H4 hysteresis usually occur in solids consisting of aggregates/agglomerates of particles forming slit-shaped pores (plates or edged particles like cubes) with uniform (type H4) or nonuniform (type H3) size and/or shape. Typical examples of these types are activated carbons and zeolites [28].

2.7.1.2 Pore size distribution by the QSDFT method

Typically, pores are classified according to their width into micropores (< 2 nm), mesopores (between 2 and 50 nm) and macropores (> 50 nm) [26]. A description of the pore volume as a function of the pore size is called the pore size distribution (PSD) of an adsorbent. In this study, the PSD of the ACs was inferred from the N₂ adsorption data by applying the Quenched Solid Density Functional Theory (QSDFT) method using Quantachrome ASiQWin software

(Quantachrome Instruments) [29]. This method represents the experimental adsorption isotherm as the convolution of a set of theoretical isotherms (the QSDFT kernel) in a series of pores with a given range of pore sizes [30]. In this way, the PSD calculations of various micro-mesoporous carbons can be carried out for pores with widths between 0.4 and 35 nm [29]. Originally, the QSDFT method for carbons was developed assuming slit-shaped pores, but recently it has been extended to cage-like and channel-like pore geometries by the development of additional QSDFT kernels [30]. The selection of the appropriate kernel is based on the type of hysteresis loop observed in the adsorption isotherm. In contrast to standard Non-Local Density Functional Theory (NLDFT) models, which treat the pore walls as smooth homogeneous graphite-like plane surfaces, the QSDFT model is devised for adsorption in heterogeneous materials with corrugated amorphous pore walls. This surface heterogeneity is characterized by a single roughness parameter that represents the characteristic scale of surface corrugation on a molecular level [29]. For further details on this method is referred to literature [29, 30].

2.7.1.3 Specific surface area by the BET method (s_{BET})

The specific surface area of the ACs was estimated by the Brunauer, Emmett and Teller (BET) gas adsorption method [31]. Originally, this method was considered only applicable to type II or type IV adsorption isotherms (non-porous solids or macro- and mesoporous solids), but recently the method has been extended to microporous adsorbents as well [32].

The BET method involves the determination of the amount of adsorbate gas (N_2) required to cover the external and accessible internal pore surface of an adsorbent with a complete monolayer of adsorbate. This monolayer adsorption capacity (V_m) can be calculated from the adsorption isotherm using the BET equation (equation 2-1) [31]:

$$\text{Eq. 2-1: } \frac{p}{V_{ads}(p_0 - p)} = \frac{1}{V_m C} + \left(\frac{C-1}{V_m C}\right) \frac{p}{p_0}$$

with p the equilibrium pressure, p_0 the saturation pressure, V_m the monolayer adsorption capacity, V_{ads} the adsorbed volume of gas at pressure p and C the BET constant. The latter is an indication of the adsorbent-adsorbate interaction

energy [26]. Commonly, equation 2-1 is expressed in terms of the equilibrium relative pressure (p/p_0), which is more easily accessible from adsorption isotherms, as shown in equation 2-2.

$$\text{Eq. 2-2:} \quad \frac{p/p_0}{V_{\text{ads}}(1-p/p_0)} = \frac{1}{V_m C} + \left(\frac{C-1}{V_m C}\right) \frac{p}{p_0}$$

A plot of $(p/p_0)/(V_{\text{ads}}(1-p/p_0))$ against p/p_0 should give a straight line with slope $(C-1)/(V_m C)$ and intercept $1/(V_m C)$. From this BET plot, V_m and C can be evaluated by linear regression as follows: $V_m = 1/(\text{slope} + \text{intercept})$ and $C = (\text{slope}/\text{intercept}) + 1$.

The second stage in the BET method is the calculation of the specific surface area (S_{BET}) from V_m using equation 2-3:

$$\text{Eq. 2-3:} \quad S_{\text{BET}} = \frac{V_m}{22414} \times N_A \times a_m \quad (\text{m}^2/\text{g})$$

with V_m the monolayer adsorption capacity ($\text{cm}^3/\text{g STP}$)⁶, N_A the Avogadro constant ($6.022 \times 10^{23} \text{ mol}^{-1}$), a_m the average area occupied per adsorbate molecule in the completed monolayer (0.162 nm^2 per N_2 molecule at 77 K [26]) and assuming that one mole of N_2 gas equals 22414 cm^3 under STP conditions.

Remarks

To obtain true values of V_m , it is important to select the appropriate p/p_0 range in which equation 2-2 yields a straight line (i.e. the BET range). Typically, a BET range from 0.05 to 0.30 is used for mesoporous materials [26]. However, for microporous materials, this BET range does not give a straight line in the BET plot and negative values for the BET constant C are obtained, which is physically impossible [32]. Therefore, the following criteria are recommended to find the appropriate BET range for microporous materials [32, 33]:

- (1) The selected relative pressure range has to be chosen so that $V_m(1-p/p_0)$ continuously increases with p/p_0 .

⁶ STP: Standard Temperature (273.15 K) and Pressure (101325 Pa)

- (2) In this pressure range, the BET plot must result in a straight line with a positive intercept to yield a meaningful positive value of the BET constant C .
- (3) The relative pressure corresponding to the calculated value of V_m must lie within the selected pressure range.

The AC samples, analyzed in this work, did not show a straight line in the BET range from 0.05 to 0.30. Therefore, the criteria for microporous materials mentioned above were used, resulting in a BET range of $0.01 \leq p/p_0 \leq 0.05$ for all samples. In this range, at least six experimental data points were used for linear regression and all R^2 values were above 0.99. The obtained BET constant C had positive values (between 141 and 1502 for ACs produced from rapeseed cake; between 423 and 3834 for ACs derived from raspberry seed cake). It should be noted that this procedure does not result in the true specific surface area, but should be considered as a kind of characteristic or equivalent surface area [32].

2.7.1.4 Micropore characterization by the Dubinin-Radushkevich (DR) method

Micropores are defined as pores with an internal width less than 2 nm [26]. The mechanism of adsorption in very fine pores differs from that in wider pores or at the external surface. Hence, the close proximity of the pore wall in case of micropores increases the strength of adsorbent-adsorbate interactions and so the adsorption energy. As a consequence, micropores are rather filled at very low p/p_0 values (micropore filling) instead of covered with a layer of adsorbate (surface covering) [34]. Therefore, reporting of the micropore volume instead of the micropore surface is preferred.

Adsorption isotherms of pure gases on microporous sorbents can be described by means of the Polanyi's potential theory of adsorption [35]. In this theory, each gas/sorbent system is characterized by an adsorption potential which is influenced by the chemical properties of the sorbent [34]. The volume V_{ads} at a relative pressure p/p_0 is a function of this adsorption potential. According to Dubinin, the adsorption potential equals the work required to bring an adsorbed molecule into the gas phase. The Dubinin-Radushkevich (DR) equation, widely used for the description of adsorption in microporous materials (especially those

of carbonaceous origin), is based on assumptions of a change in the potential energy between the gas and adsorbed phases and the characteristic energy of the sorbent.

The physical adsorption of vapors by microporous ACs is well described by the (semi-empirical) Dubinin-Radushkevich equation [36], which can be expressed as shown in equation 2-4:

$$\text{Eq. 2-4: } V_{\text{ads}} = V_{\text{micro}} \exp \left[- \left\{ \left(\frac{RT}{\beta E_0} \right) \ln \frac{p}{p_0} \right\}^2 \right]$$

with p the equilibrium pressure, p_0 the saturation pressure, V_{ads} the adsorbed volume of gas at pressure p , V_{micro} the micropore volume (also indicated as V_{DR}), R the universal gas constant, T absolute temperature, β the affinity coefficient relative to benzene⁷ and E_0 the "characteristic" energy of a standard adsorbate (benzene) with respect to the adsorbent. Writing the Dubinin-Radushkevich equation in logarithmic form yields equation 2-5:

$$\text{Eq. 2-5: } \log_{10} V_{\text{ads}} = \log_{10} V_{\text{micro}} - D \left[\log_{10} \frac{p}{p_0} \right]^2 \quad \text{with } D = \frac{1}{\log_{10}(e)} \left[\frac{RT}{\beta E_0} \right]^2$$

A plot of $\log_{10} V_{\text{ads}}$ against $[\log_{10}(p/p_0)]^2$ results in a straight line from which the micropore volume (V_{micro}) can be calculated in a limited range of p/p_0 , usually $10^{-4} < p/p_0 < 0.1$ [34]. After regression, V_{micro} can be calculated from the intercept, while the absolute value of the slope equals the D parameter. Parameter D can be used to calculate the characteristic adsorption energy (E_0) as shown by equation 2-6:

$$\text{Eq. 2-6: } E_0 = \frac{RT}{\beta} \sqrt{\frac{1}{D \log_{10}(e)}} \quad (\text{J/mole})$$

with $\beta = 0.33$ for N_2 [37]. E_0 (in kJ/mole) can be used to estimate the average micropore width L_0 (nm) of ACs when ideal slit-shaped micropores are assumed,

⁷ Benzene is considered as a "reference substance" ($\beta = 1$). The value of β for other substances is determined relatively to benzene.

as shown by equation 2-7 [38]. This empirical correlation (Stoeckli formula) is valid for L_0 values between 0.5 and 2.0 nm.

$$\text{Eq. 2-7: } L_0 = \frac{10.8}{(E_0 - 11.4)} \text{ (nm)}$$

In this thesis, the DR equation was used in the p/p_0 range from 0.008 to 0.05 to calculate the (apparent) micropore volume (V_{micro} or V_{DR}) and L_0 . At least six data points were used for linear regression, resulting in R^2 values always higher than 0.99.

2.7.1.5 Mesopore and total pore volume

The total pore volume (V_t) was estimated by converting the adsorbed volume of N_2 at a relative pressure of 0.96 into the equivalent liquid volume at 77 K, as shown by equation 2-8:

$$\text{Eq. 2-8: } V_t = \frac{Mw}{\rho V_{\text{molar}}} V_{\text{ads}}$$

with V_t the total pore volume (cm^3/g), ρ the density of liquid N_2 at 77 K (0.8086 g/cm^3), V_{molar} the molar gas volume at STP ($22414 \text{ cm}^3/\text{mole}$), Mw the molecular weight of N_2 (28.02 g/mole) and V_{ads} ($\text{cm}^3/\text{g STP}$) the adsorbed volume of N_2 gas at $p/p_0 = 0.96$. Hereby, it is assumed that only macropore filling and coverage of flat surfaces occur at p/p_0 values above 0.96.

The mesopore volume (V_{me}) could then be estimated by subtracting the micropore volume (V_{DR}) from the total pore volume (V_t) [39, 40].

2.7.2 Elemental analysis

Elemental analysis of the ACs was carried out in a similar way as described for the solid residue (section 2.5.2).

2.7.3 Attenuated Total Reflectance-FTIR spectroscopy

The functional groups of the ACs were analyzed using Attenuated Total Reflectance Fourier Transform Infrared (ATR-FTIR) spectroscopy. Spectra were recorded with a Brüker Vertex 70 FTIR spectrometer equipped with a HYPERION

1000 microscope and a MCT (mercury cadmium telluride) detector. Typically, 32 scans/min were taken with a resolution of 4 cm^{-1} and a background correction was performed.

2.7.4 Scanning Electron Microscopy (SEM)

The surface morphology of the ACs was examined by Scanning Electron Microscopy (SEM) using a FEI Quanta 200 FEG-SEM apparatus at IMO (Instituut voor Materiaalonderzoek, Diepenbeek, Belgium). Imaging was performed in high vacuum mode at an accelerating voltage of 15.0 kV using an ET (Everhart-Thornley) detector.

2.8 Batch phenol adsorption study

2.8.1 Phenol adsorption isotherms

The batch adsorption tests were carried out in a set of 100 mL glass Erlenmeyer flasks using about 25.0 mg of AC and 25.0 mL of aqueous phenol solution. At least six different initial concentrations (C_0) between 5 and 400 mg/L were selected. The phenol solutions were prepared in distilled water without any pH adjustment. After being placed in an isothermal shaking water bath (GFL mbH) at 25 °C for 48 h, the AC was removed from the phenol solution by filtration (Whatmann 40). The phenol concentration at equilibrium (C_e), remaining in the aqueous solution after the adsorption process, was determined by the direct photometric method at 510 nm according to ASTM D1783 [41]. In this method, phenol reacts with 4-aminoantipyrine in presence of $K_3Fe(CN)_6$ to produce a colored derivate at a pH-value of about 10 (NH_4^+/NH_3 buffer). Since this reaction is specific for phenolic compounds, interference of other organic compounds (e.g. compounds desorbed from the AC) is avoided. The Pharmacia Biotech Ultrospec 2000 UV/VIS spectrophotometer was calibrated using six phenol solutions with known concentrations between 1.0 and 10.0 mg/L. Unknown samples were diluted to a concentration within the calibration range. Distilled water, subjected to a similar procedure as the unknown samples, was used as blank sample. Once C_e was determined, the amount of phenol adsorbed on the AC at equilibrium could be calculated using equation 2-9:

$$\text{Eq. 2-9: } q_e = \frac{(C_0 - C_e)V}{m_{AC}}$$

with q_e the mass of phenol adsorbed per mass unit of AC (mg/g), C_0 the initial concentration of phenol (mg/L), C_e the concentration of phenol at equilibrium (mg/L), V the volume of the phenol solution (L) and m_{AC} the mass of AC (g). In this way, six experimental data points (C_e , q_e) were obtained to construct the phenol adsorption isotherm (i.e. q_e as a function of C_e).

2.8.2 Adsorption isotherm models

In literature, several adsorption isotherm models are reported for analyzing experimental adsorption data at equilibrium [42-45]. The obtained model

parameters provide important information on the sorption mechanisms and the surface properties and affinities of the adsorbent.

In this thesis, the Langmuir and Freundlich models were used to fit the adsorption equilibrium data (C_e , q_e) since they are widely the most accepted adsorption models for single solute systems [42].

The **Langmuir model** is valid for monolayer adsorption on a homogeneous surface containing a finite number of sites that have an equal adsorption energy and that are equally available for adsorption. The model assumes uniform adsorption on the surface and no transmigration of adsorbate on the plane of the surface [42, 46]. The Langmuir model is described by equation 2-10 [47]:

$$\text{Eq. 2-10:} \quad q_e = \frac{q_m K_L C_e}{(1 + K_L C_e)} \quad \text{Langmuir model}$$

with q_m and K_L the Langmuir model parameters. The former represents the Langmuir monolayer adsorption capacity (mg/g), while the latter (called Langmuir constant; L/mg) is related to the free energy of adsorption. The essential characteristics of the Langmuir isotherm can be expressed by a dimensionless constant, called separation factor (R_L), which is calculated by equation 2-11 [48]. This factor indicates if the adsorption process is unfavorable ($R_L > 1$), linear ($R_L = 1$), favorable ($0 < R_L < 1$) or irreversible ($R_L = 0$).

$$\text{Eq. 2-11:} \quad R_L = \frac{1}{1 + K_L C_0}$$

The **Freundlich model** is an empirical equation based on sorption on a heterogeneous surface or surfaces supporting sites of varied affinities and with interaction between the molecules adsorbed [42]. It is assumed that stronger binding sites are occupied first and that the binding strength decreases with increasing degree of surface coverage [46, 49]. The Freundlich model can be described by equation 2-12 [49]:

$$\text{Eq. 2-12:} \quad q_e = K_F C_e^{1/n_F} \quad \text{Freundlich model}$$

with K_F ((mg/g)(L/mg)^{1/n}) and $1/n_F$ (dimensionless number) the Freundlich constants. The K_F constant (also called unity-capacity factor) is indicative of the relative adsorption capacity of the adsorbent as it represents the quantity of adsorbate adsorbed at an equilibrium concentration of 1 mg/L. The $1/n_F$ parameter is a measurement of the adsorption intensity or surface heterogeneity [43, 46]. Hence, a $1/n_F$ value closer to zero represents a more heterogeneous surface [50]. Moreover, the n_F parameter can be used to indicate whether the adsorption is linear ($n_F = 1$), whether it is a chemical process ($n_F < 1$) or whether a physical process is favorable ($n_F > 1$) [42]. Since the Freundlich model does not impose any requirement that the coverage must approach a constant value corresponding to a complete monolayer at high equilibrium concentrations of the adsorbate, failure of this model might be expected at high concentrations [51].

Unknown parameters of two-parameter adsorption models can be obtained by linear regression from a linearized form of the adsorption model equation⁸. However, the model parameters can also be calculated without linearization by applying non-linear regression to the original model equation. In this thesis, the unknown parameters of both models were calculated using **non-linear regression** according to the method of the least squares. Hereby, the unknown model parameters (Langmuir model: q_m and K_L ; Freundlich model: K_F and n_F) were calculated iteratively using the Excel Solver function (GRG non-linear engine) with the aim to minimize the "sum of squares error" (SSE). The SSE represented the square of the difference (error) between each q_e determined experimentally ($(q_e)_{i,exp}$) and each q_e calculated by the model ($(q_e)_{i,cal}$), summed over all experimental data points (n) and was calculated as shown in equation 2-13:

$$\text{Eq. 2-13:} \quad \text{SSE} = \sum_{i=1}^n [(q_e)_{i,exp} - (q_e)_{i,cal}]^2$$

⁸ For instance, the Langmuir equation linearized after Weber or after Stumm and Morgan are widely used to calculate the Langmuir model parameters by linear regression.

The correlation coefficient (R^2 value) of the fitted model was then obtained by equation 2-14, with SSTO the 'total sum of squares' and n the total number of experimental data points.

$$\text{Eq. 2-14: } R^2 = 1 - \frac{\text{SSE}}{\text{SSTO}} \quad \text{with} \quad \text{SSTO} = \sum_{i=1}^n \left[(q_e)_{i,\text{exp}} - \frac{1}{n} \sum_{i=1}^n (q_e)_{i,\text{exp}} \right]^2$$

2.8.3 Effect of the initial pH of the phenol solution

The effect of the initial solution pH on the phenol removal was studied in a pH range from 3 to 13. The pH of the initial phenol solutions (about 6) was adjusted by adding a few drops of diluted 0.1 M HCl or 0.1 M NaOH. The pH was measured using a Hamilton Polilyte Lab electrode. The initial concentration of the phenol solution was fixed at 150 mg/L for ACs produced from rapeseed cake and 200 mg/L for ACs produced from raspberry seed cake. About 25 mg AC was loaded in 25 mL of phenol solution and adsorption experiments were performed in a shaking water bath at 25 °C for 48 h.

2.8.4 Batch adsorption kinetic studies

Kinetic studies were performed by loading the AC (about 25 mg) into nine 100 mL glass Erlenmeyer flasks containing a phenol solution (25.0 mL) with an initial concentration of 100 mg/L without pH adjustment. After shaking in a water bath at 25 °C for a given period of time (5, 15, 30, 60, 90, 120, 240, 1440 and 2880 min), the adsorption was stopped by filtration (Whatmann 40). The phenol concentration after a certain time interval (C_t) was measured by the direct photometric method as described in section 2.8.1. Finally, the amount of phenol adsorbed on the AC in the corresponding time interval (q_t) could be calculated by equation 2-15:

$$\text{Eq. 2-15: } q_t = \frac{(C_0 - C_t)V}{m_{\text{AC}}}$$

In literature, numerous empirical models are reported to describe the kinetics of adsorption processes [42, 43, 52, 53]. In this work, the kinetics of phenol

adsorption on the ACs was evaluated by two commonly used models, i.e. the pseudo-first-order (PFO) and the pseudo-second-order (PSO) kinetic model. The PFO model (equation 2-16) was suggested by Lagergren [54], while the PSO model (equation 2-17) was introduced by Blanchard et al. [55].

Eq. 2-16: $q_t = q_e(1 - \exp(-k_1 t))$ PFO model

Eq. 2-17: $q_t = \frac{k_2 q_e^2 t}{(1 + k_2 q_e t)}$ PSO model

with q_t and q_e the adsorbed amount of phenol per mass unit of AC after a contact time t (min) and at equilibrium respectively, k_1 (1/min) the PFO rate constant and k_2 (g/mg min) the PSO rate constant. The unknown model parameters (q_e and k_1 or k_2) were calculated by non-linear regression according to the method of the least squares, analogously as described in section 2.8.2.

2.9 References

- [1] Cornelissen, T., Jans, M., Yperman, J., Reggers, G., Schreurs, S. and Carleer, R. Flash co-pyrolysis of biomass with polyhydroxybutyrate: Part 1. Influence on bio-oil yield, water content, heating value and the production of chemicals. *Fuel*, 2008. **87**(12): 2523-2532.
- [2] Cornelissen, T., Yperman, J., Reggers, G., Schreurs, S. and Carleer, R. Flash co-pyrolysis of biomass with polylactic acid. Part 1: Influence on bio-oil yield and heating value. *Fuel*, 2008. **87**(7): 1031-1041.
- [3] Cornelissen, T., Jans, M., Stals, M., Kuppens, T., Thewys, T., Janssens, G.K., Pastijn, H., Yperman, J., Reggers, G., Schreurs, S. and Carleer, R. Flash co-pyrolysis of biomass: The influence of biopolymers. *Journal of Analytical and Applied Pyrolysis*, 2009. **85**(1-2): 87-97.
- [4] Stals, M., Thijssen, E., Vangronsveld, J., Carleer, R., Schreurs, S. and Yperman, J. Flash pyrolysis of heavy metal contaminated biomass from phytoremediation: Influence of temperature, entrained flow and wood/leaves blended pyrolysis on the behaviour of heavy metals. *Journal of Analytical and Applied Pyrolysis*, 2010. **87**(1): 1-7.
- [5] Smets, K., Adriaensens, P., Vandewijngaarden, J., Stals, M., Cornelissen, T., Schreurs, S., Carleer, R. and Yperman, J. Water content of pyrolysis oil: Comparison between Karl Fischer titration, GC/MS-corrected azeotropic distillation and ¹H NMR spectroscopy. *Journal of Analytical and Applied Pyrolysis*, 2011. **90**(2): 100-105.
- [6] Cornelissen, T. Flash pyrolysis of biomass and co-pyrolysis with biopolymers, in PhD thesis - Research Group: Applied and Analytical Chemistry 2009, Hasselt University: Diepenbeek. 202.
- [7] Vitolo, S., Seggiani, M., Frediani, P., Ambrosini, G. and Politi, L. Catalytic upgrading of pyrolytic oils to fuel over different zeolites. *Fuel*, 1999. **78**(10): 1147-1159.
- [8] Pütün, E., Uzun, B.B. and Pütün, A.E. Fixed-bed catalytic pyrolysis of cotton-seed cake: Effects of pyrolysis temperature, natural zeolite content and sweeping gas flow rate. *Bioresource Technology*, 2006. **97**(5): 701-710.
- [9] Song, Y., Zhu, X., Xie, S., Wang, Q. and Xu, L. The effect of acidity on olefin aromatization over potassium modified ZSM-5 catalysts. *Catalysis Letters*, 2004. **97**: 31-36.
- [10] Akhtar, J. and Amin, N.S. A review on operating parameters for optimum liquid oil yield in biomass pyrolysis. *Renewable & Sustainable Energy Reviews*, 2012. **16**(7): 5101-5109.

- [11] Van Soest, P.J., Robertson, J.B. and Lewis, B.A. Methods for dietary fiber, neutral detergent fiber and nonstarch polysaccharides in relation to animal nutrition. *Journal of Dairy Science*, 1991. **74**(10): 3583-3597.
- [12] McLellan, T.M., Aber, J.D., Martin, M.E., Melillo, J.M. and Nadelhoffer, K.J. Determination of nitrogen, lignin and cellulose content of decomposing leaf material by near-infrared reflectance spectroscopy. *Canadian Journal of Forest Research-Revue Canadienne De Recherche Forestiere*, 1991. **21**(11): 1684-1688.
- [13] Hayes, D.J.M. Development of near infrared spectroscopy models for the quantitative prediction of the lignocellulosic components of wet *Miscanthus* samples. *Bioresource Technology*, 2012. **119**: 393-405.
- [14] Huang, C., Han, L., Liu, X. and Ma, L. The Rapid Estimation of Cellulose, Hemicellulose, and Lignin Contents in Rice Straw by Near Infrared Spectroscopy. *Energy Sources Part A: Recovery Utilization and Environmental Effects*, 2011. **33**(2): 114-120.
- [15] Carrier, M., Loppinet-Serani, A., Denux, D., Lasnier, J.-M., Ham-Pichavant, F., Cansell, F. and Aymonier, C. Thermogravimetric analysis as a new method to determine the lignocellulosic composition of biomass. *Biomass and Bioenergy*, 2011. **35**(1): 298-307.
- [16] Faithfull, N.T. *Methods in agricultural chemical analysis: a practical handbook*. 2002, Wallingford UK: CABI Publishing.
- [17] Rabou, L.P.L.M. and Lips, S.J.J. Phyllis database uitbreiding met biochemische samenstellingen ten behoeve van de productie van vloeibare en gasvormige brandstoffen. 2003: ECN.
- [18] ASTM E1690 "Standard Test Method for Determination of Ethanol Extractives in Biomass" 2004. *Annual Book of ASTM Standards*. Vol.11.06.
- [19] Vassilev, S.V., Baxter, D., Andersen, L.K., Vassileva, C.G. and Morgan, T.J. An overview of the organic and inorganic phase composition of biomass. *Fuel*, 2012. **94**(0): 1-33.
- [20] Sriperum, N., Pesti, G.M. and Tillman, P.B. Evaluation of the fixed nitrogen-to-protein (N:P) conversion factor (6.25) versus ingredient specific N:P conversion factors in feedstuffs. *Journal of the Science of Food and Agriculture*, 2011. **91**(7): 1182-1186.
- [21] Soil and Plant Analysis Council, I. *Handbook of reference methods for plant analysis*, ed. Karla, Y.P. 1998: CRC Press.
- [22] Raveendran, K., Ganesh, A. and Khilar, K.C. Pyrolysis characteristics of biomass and biomass components. *Fuel*, 1996. **75**(8): 987-998.

- [23] Klass, D.L. Biomass for renewable energy, fuels and chemicals. 1998, San Diego, CA: Academic Press. 688.
- [24] Basu, P. Biomass gasification and pyrolysis - Practical design and theory. 2010: Elsevier Inc.
- [25] ASTM D664 "Standard Test Method for Acid Number of Petroleum Products by Potentiometric Titration" 2004. Annual Book of ASTM Standards.
- [26] Sing, K.S.W., Everett, D.H., Haul, R.A.W., Moscou, L., Pierotti, R.A., Rouquerol, J. and Siemieniewska, T. Reporting physisorption data for gas solid systems with special reference to the determination of surface-area and porosity (recommendations 1984). Pure and Applied Chemistry, 1985. **57**(4): 603-619.
- [27] Marsh, H. and Rodríguez-Reinoso, F. Activated carbon. 2006: Elsevier Science & Technology Books. 536.
- [28] Leofanti, G., Padovan, M., Tozzola, G. and Venturelli, B. Surface area and pore texture of catalysts. Catalysis Today, 1998. **41**(1-3): 207-219.
- [29] Neimark, A.V., Lin, Y.Z., Ravikovitch, P.I. and Thommes, M. Quenched solid density functional theory and pore size analysis of micro-mesoporous carbons. Carbon, 2009. **47**(7): 1617-1628.
- [30] Gor, G.Y., Thommes, M., Cychosz, K.A. and Neimark, A.V. Quenched solid density functional theory method for characterization of mesoporous carbons by nitrogen adsorption. Carbon, 2012. **50**: 2012.
- [31] Brunauer, S., Emmett, P.H. and Teller, E. Adsorption of gases in multimolecular layers. Journal of the American Chemical Society, 1938. **60**(2): 309 - 319.
- [32] ISO 9277:2010 "Determination of the specific surface area of solids by gas adsorption - BET method" Second Edition of ISO 9277, ISO, Geneva, 2010.
- [33] Rouquerol, J., Llewellyn, P. and Rouquerol, F. Is the BET equation applicable to microporous adsorbents?, in Characterization of Porous Solids VII - Proceedings of the 7th International Symposium on the Characterization of Porous Solids, Llewellyn, P.L., et al., Editors. 2006. 49-56.
- [34] Klobes, P., Meyer, K. and Munro, R.G. Porosity and specific surface area measurements for solid materials. Washington: National Institute for Standards and Technology, 2006.
- [35] Polanyi, M. Theories of the adsorption of gases. A general survey and some additional remarks. Transactions of the Faraday Society, 1932. **28**: 316-333.

- [36] Dubinin, M.M. The potential theory of adsorption of gases and vapors for adsorbents with energetically nonuniform surfaces. *Chemical Reviews*, 1960. **60**(2): 235-241.
- [37] Dubinin, M.M. and Zhukovskaia, E.G. Adsorption properties of carbon adsorbents Communications 2. Adsorption properties of active carbons with respect to benzene and nitrogen vapors. *Russian Chemical Bulletin*, 1958. **7**(5): 519-528.
- [38] Stoeckli, F. and Centeno, T.A. On the characterization of microporous carbons by immersion calorimetry alone. *Carbon*, 1997. **35**(8): 1097-1100.
- [39] Gonzalez, J.F., Roman, S., Gonzalez-Garcia, C.M., Nabais, J.M.V. and Ortiz, A.L. Porosity Development in Activated Carbons Prepared from Walnut Shells by Carbon Dioxide or Steam Activation. *Industrial & Engineering Chemistry Research*, 2009. **48**(16): 7474-7481.
- [40] Stavropoulos, G.G. and Zabaniotou, A.A. Production and characterization of activated carbons from olive-seed waste residue. *Microporous and Mesoporous Materials*, 2005. **82**(1-2): 79-85.
- [41] ASTM D1783 "Standard Test Method for Phenolic compounds in water". 2004. Annual Book of ASTM Standards.
- [42] Vargas, A.M.M., Cazetta, A.L., Kunita, M.H., Silva, T.L. and Almeida, V.C. Adsorption of methylene blue on activated carbon produced from flamboyant pods (*Delonix regia*): Study of adsorption isotherms and kinetic models. *Chemical Engineering Journal*, 2011. **168**(2): 722-730.
- [43] Tan, I.A.W., Ahmad, A.L. and Hameed, B.H. Adsorption isotherms, kinetics, thermodynamics and desorption studies of 2,4,6-trichlorophenol on oil palm empty fruit bunch-based activated carbon. *Journal of Hazardous Materials*, 2009. **164**(2-3): 473-482.
- [44] Hameed, B.H. and Rahman, A.A. Removal of phenol from aqueous solutions by adsorption onto activated carbon prepared from biomass material. *Journal of Hazardous Materials*, 2008. **160**(2-3): 576-581.
- [45] Özkaya, B. Adsorption and desorption of phenol on activated carbon and a comparison of isotherm models. *Journal of Hazardous Materials*, 2006. **129**(1-3): 158-163.
- [46] Singh, K.P., Malik, A., Sinha, S. and Ojha, P. Liquid-phase adsorption of phenols using activated carbons derived from agricultural waste material. *Journal of Hazardous Materials*, 2008. **150**(3): 626-641.
- [47] Langmuir, I. The constitution and fundamental properties of solids and liquids. Part I: Solids. *Journal of the American Chemical Society*, 1916. **38**(11): 2221-2295.

- [48] Weber, T.W. and Chakkravorti, R.K. Pore and solid diffusion models for fixed-bed adsorbers. *AIChE Journal*, 1974. **20**(2): 228-238.
- [49] Freundlich, H.M.F. Over the adsorption in solution. *Journal of Physical Chemistry*, 1906. **57**(A): 385-470.
- [50] Haghseresht, F. and Lu, G.Q. Adsorption characteristics of phenolic compounds onto coal-reject-derived adsorbents. *Energy & Fuels*, 1998. **12**(6): 1100-1107.
- [51] Salame, I.I. and Bandosz, T.J. Role of surface chemistry in adsorption of phenol on activated carbons. *Journal of Colloid and Interface Science*, 2003. **264**(2): 307-312.
- [52] Azizian, S. Kinetic models of sorption: a theoretical analysis. *Journal of Colloid and Interface Science*, 2004. **276**(1): 47-52.
- [53] Azizian, S. and Fallah, R.N. A new empirical rate equation for adsorption kinetics at solid/solution interface. *Applied Surface Science*, 2010. **256**(17): 5153-5156.
- [54] Lagergren, S. Zur theorie der sogenannten adsorption gelöster stoffe. *Kungliga Svenska Vetenskapsakademiens. Handlingar*, 1898. **24**(4): 1-39.
- [55] Blanchard, G., Maunaye, M. and Martin, G. Removal of heavy metals from water by means of natural zeolites. *Water Research*, 1984. **18**(12): 1501-1507.

3 Valorization of agricultural waste cake: Feedstock characterization and preliminary flash pyrolysis experiments

An in-depth characterization of the agricultural waste cakes is absolutely necessary to assess their opportunities for valorization by pyrolysis as a source of renewable fuels and/or added-value chemicals. Therefore, the agricultural waste cakes are investigated using complementary analytical techniques to determine their major constituents, their thermochemical behavior under pyrolysis conditions and their physicochemical characteristics. Moreover, preliminary flash pyrolysis experiments are carried out to evaluate the product yield and the quality of the pyrolysis liquid, both important factors in identifying the most suitable valorization pathway for the waste cakes. Based on these preliminary results, the appropriate pyrolysis conditions are selected and the research can be focused on the most promising valorization pathway, i.e. production of renewable fuels and/or added-value chemicals (including activated carbon).

3.1 Characterization of the agricultural waste cakes

The characteristics of the three agricultural waste cakes were investigated using complementary analytical techniques as described in Chapter 2 (section 2.3). First, the major biomass components were determined by a method adapted from that of Van Soest and Wine [1]. Then, TGA was performed to study their thermal behavior under pyrolysis conditions. Finally, important physicochemical properties such as the elemental composition (major and minor elements) and the energy content were determined. These parameters are not only important to evaluate the potential of the waste cakes as sources of renewable fuels and/or chemicals, but also provide important information about the thermal design of a pyrolysis reactor on industrial scale.

3.1.1 Component analysis

Biomass can be regarded as a complex heterogeneous mixture of major structural components and bulk extractives. The former consist of three organic biopolymers, namely cellulose, hemicellulose and lignin, while the latter are compounds that are not an integral part of the biomass structure [2]. The proportion of these components has a considerable effect on the properties and the pyrolytic behavior of the waste cakes. Therefore, the three agricultural waste cakes were investigated by a comprehensive component analysis prior to performing the preliminary flash pyrolysis experiments.

Moisture (water) was a major constituent of the fresh agricultural waste cakes (as received). Typically, a moisture content of 8.3 wt%, 11.1 wt% and 6.4 wt% (all SDs \leq 0.2 wt%) was found for rapeseed cake, olive waste cake and raspberry seed cake, respectively. Since a high moisture content is undesirable for pyrolysis feedstocks [3], the waste cakes were oven-dried at 110 °C prior to all analyses and pyrolysis experiments.

A flowchart of the component analysis is shown in Figure 2-4 (section 2.3.2). The dried agricultural waste cakes were subjected to two consecutive extractions to prevent interference from nonstructural constituents during component analysis. Ethanol was used to extract lipids, waxes and resins, while free sugars, gums, pigments and tannins were removed by the consecutive hot water extraction [4]. Then, component analysis was performed to determine the content of hemicellulose, cellulose and lignin present in the waste cakes. The ash content was obtained by combustion of the samples at 850 °C under pure oxygen atmosphere (TGA). The content of triglycerides and crude proteins was determined by separate analyses starting from the initial oven-dried waste cakes. Results are shown in Table 3-1.

Table 3-1: Component analysis of the three agricultural waste cakes. (SD between brackets)

Component (dry, wt%)	Rapeseed cake		Olive waste cake		Raspberry seed cake	
EtOH extractives	35.3	(0.1)	11.5	(1.5)	10.5	(0.1)
H ₂ O extractives	8.4	(0.2)	6.2	(2.0)	5.2	(0.2)
Hemicellulose	10.0	(0.6)	23.3	(2.6)	16.9	(2.9)
Cellulose	10.6	(1.8)	40.8	(2.0)	42.1	(1.6)
Lignin	6.3	(1.2)	13.7	(0.3)	19.3	(1.2)
Ash ^a	4.9	(0.1)	2.5	(0.1)	2.6	(0.1)
Not identified	24.5		2.0		3.4	
Crude proteins	30.7	(1.4)	5.1	(0.4)	11.6	(1.2)
Triglycerides	20.7	(0.5)	9.7	(1.8)	5.2	(0.1)

^a determined by TGA

The amount of ethanol extractives was found to be much higher for rapeseed cake than for both other waste cakes. Analysis of these extractives identified triglycerides and fatty acids as major constituents. A separate extraction with diethyl ether revealed a triglyceride content of 20.7 wt% for rapeseed cake⁹. This triglyceride content was significantly higher than that of both other waste cakes, explaining the results of the ethanol extraction and thus that not all triglycerides have been removed from the rape seeds by cold-pressing oil production. However, complete removal of the oil was not possible without compromising its quality or using a solvent (e.g. hexane). In case of raspberry seed cake, the low triglyceride content (5.2 wt%) was the result of extractions performed by the supplier to recover high-value chemicals such as antioxidants. The water extraction, performed consecutively after the ethanol extraction, could only remove lower amounts of nonstructural components in case of all waste cakes.

The actual component analysis revealed cellulose as principal component for all waste cakes. However, the cellulose content (both absolute and relative) was

⁹ FTIR and GPC analysis confirmed that the diethyl ether extract (after rotary evaporation) was almost completely composed of triglycerides (instead of free fatty acids).

significantly higher for olive waste cake and raspberry seed cake than for rapeseed cake. Hemicellulose was found as second most abundant component, except for raspberry seed cake. In case of the latter, lignin was much more prominent. Since lignin is reported as an important precursor in the char formation process [5], the highest char yield is expected from pyrolysis of raspberry seed cake. The crude protein content of rapeseed cake (30.7 wt%) was significantly higher than that of both other waste cakes.

Remarks on the component analysis

A considerable part of the waste cakes could not be characterized by the method used in this thesis and is indicated as “not identified” in Table 3-1. The hypothesis was made that the largest part of the not identified compounds consisted of biomass proteins. Since the crude protein content (determined as N-content $\times 6.25$)¹⁰ was higher than the amount of not identified compounds, it was assumed that the biomass proteins were also interfering with other extraction/reaction steps during the component analysis. Further research by elemental analysis of the residues from each extraction/reaction step revealed that most proteins (about 70 wt%) were removed during the ND extraction (with Na₂SO₃) and therefore were indeed classified as “not identified” by the analysis method used in this study. However, part of the proteins (about 30 wt%) was only removed by other extraction/reaction steps, and therefore was interfering with other components.

3.1.2 Thermogravimetric analysis

Thermogravimetric analysis (TGA) was performed to gain a better understanding of the pyrolytic behavior of the agricultural waste cakes. Hence, the TG and DTG curves provide useful information on the pyrolysis product yield (volatiles and non-volatiles). Moreover, the content of the major structural components (hemicellulose, cellulose and lignin) can be estimated since their decomposition is reported to proceed in specific temperature zones [5-8] as a result of their chemical structures [7, 9]. Typically, hemicellulose is thermally the most

¹⁰ The nitrogen-to-protein conversion factor of 6.25 assumes that 100 g of plant or animal protein contains 16 g nitrogen ($100/16 = 6.25$) (see also section 2.3.2).

unstable component and decomposes between 220 and 315 °C, while cellulose decomposition is focused at higher temperatures (315 – 400 °C) [7]. In contrast, lignin decomposition occurs in a wide temperature range (200 - 900 °C) due to its complex chemical structure. Therefore, the corresponding DTG peak is not commonly distinguishable [5-7]. The results of the TGA are shown in Figure 3-1.

The initial weight loss (25 - 165 °C) in the TG profile (green line) was indicative of the residual moisture content of the oven-dried waste cakes. The largest weight loss occurred between 165 and 600 °C for all waste cakes. In this temperature interval, the DTG profile (blue line) showed a prominent peak that could be considered as a superposition of decomposition peaks of several biomass components. In case of **rapeseed cake** (Figure 3-1a), a prominent peak with three shoulders was observed. The first (241 °C) and second (281 °C) shoulder were assigned to hemicellulose decomposition, while the third shoulder at 362 °C represented the decomposition of cellulose. The main peak at 425 °C was identified as the volatilization of triglycerides and their partial thermal decomposition into free fatty acids. The absence of this peak in the thermogram of rapeseed cake extracted with diethyl ether (removal of triglycerides) supported this assignment (Figure 3-1b). The DTG profile of **olive waste cake** was similar to that of rapeseed cake, except for the absence of the triglyceride peak at 425 °C (Figure 3-1c). In case of **raspberry seed cake**, the prominent peak at 358 °C (assigned to cellulose decomposition) only had one shoulder at 295 °C that represented the decomposition of hemicellulose (Figure 3-1d).

Halfway the isothermal period at 600 °C, the reaction atmosphere was changed from nitrogen to oxygen. As a result, the remaining biomass sample was combusted resulting in a prominent peak in the DTG profile. From this weight loss, the amount of fixed carbon (an estimation for char yield) could be calculated (see also section 3.1.3). The small temperature increase (red line) during the isothermal period was caused by the exothermal nature of the combustion reactions. The small peak at the end of the DTG profile represented the decomposition of carbonates with release of CO₂.

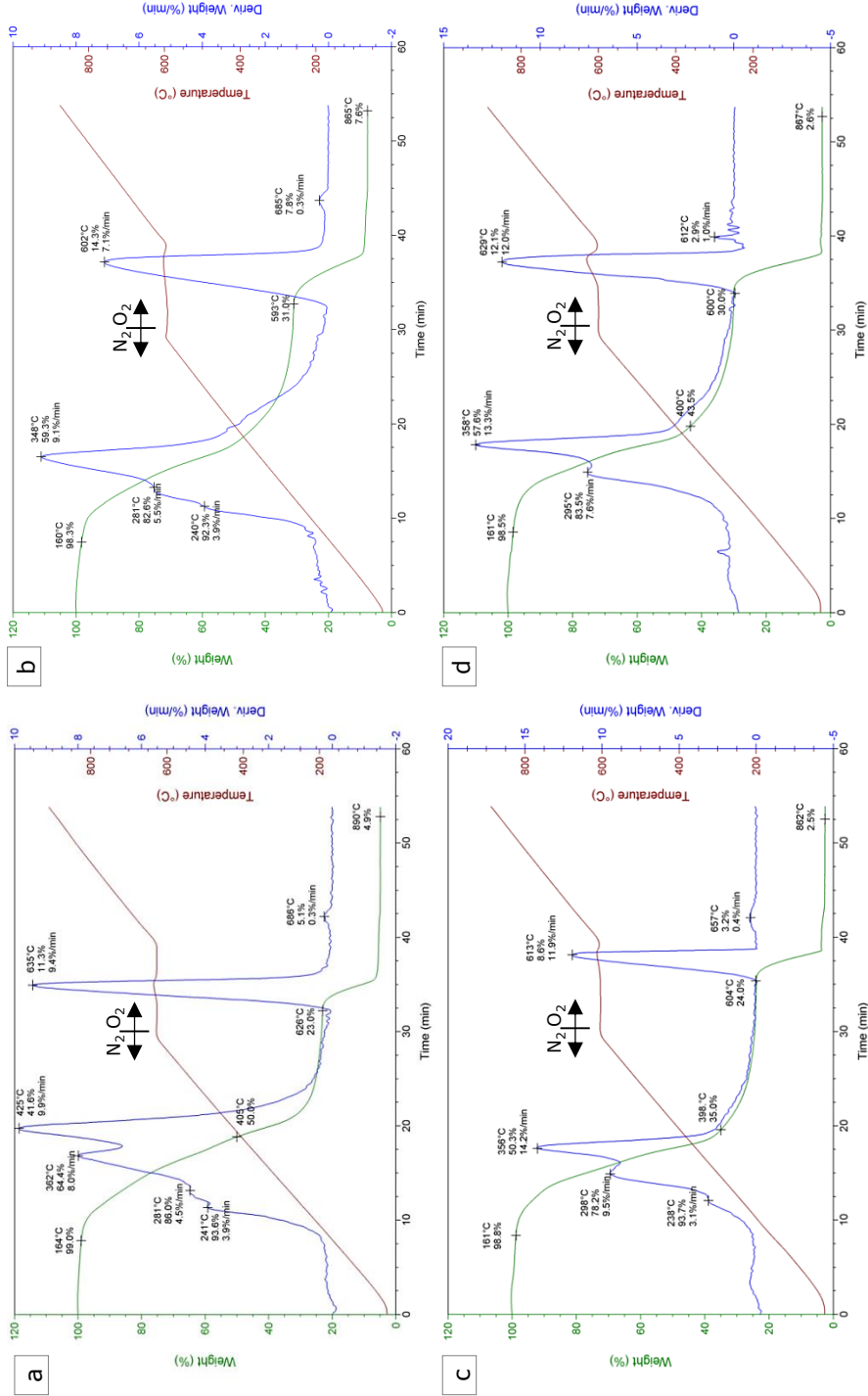


Figure 3-1: TG and DTG curves of rapeseed cake (a), rapeseed cake after extraction with diethyl ether (b), olive waste cake (c) and raspberry seed cake (d).

The thermograms (Figure 3-1) indicate that the decomposition of the agricultural waste cakes is almost complete at 450 °C. Therefore, this temperature is selected as pyrolysis temperature for the preliminary flash pyrolysis experiments discussed in section 3.2.

3.1.3 Proximate analysis, energy content and elemental analysis

Proximate analysis of the agricultural waste cakes was inferred from the TGA curves (Figure 3-1) as described in section 2.3.3. The major elements (C, H, N, S and O) were determined by elemental analysis, while the minor elements (alkali metals, alkaline earth metals and some trace elements) were measured by ICP-AES after microwave digestion of the biomass samples. The content of chlorides, phosphates and sulfates was determined by IC after complete biomass combustion using the Parr-bomb. The energy content of the waste cakes was measured as higher heating value (HHV) using bomb calorimetry. Results are shown in Table 3-2.

Proximate analysis revealed a residual moisture content below 1.6 wt% for all oven-dried waste cakes. The content of volatile matter, indicative of the amount of waste cake that is “available” for pyrolysis, was significantly lower for raspberry seed cake than for both other waste cakes. As a result, the fixed carbon content, an estimation of the char yield, was more pronounced for raspberry seed cake. The higher lignin content of the latter (see Table 3-1) can explain this result since lignin is the biomass component with the highest contribution to char production during pyrolysis [2, 5, 6]. The ash content provides information about the amount of bulk inorganic matter [10] and can significantly affect the pyrolytic behavior of the biomass components [5]. The highest ash content (4.9 wt%) was found for rapeseed cake.

Elemental analysis identified carbon (C), oxygen (O) and hydrogen (H) as principal elements of the waste cakes. The C- and H-content of rapeseed cake was slightly higher than that of both other waste cakes, while the O-content was significantly lower. The high O-content of the waste cakes was the result of the chemical structure of their major components (cellulose, hemicellulose and lignin). The lower O-content of rapeseed cake could be explained by the high content of triglycerides, which contain less oxygen in their chemical structure than the major biomass components [2]. The highest content of nitrogen (N)

and sulfur (S) was also observed for rapeseed cake. These values were quite high and were assigned to the high protein content of this waste cake. As a result, care should be taken when using rapeseed cake as a precursor in the production of renewable fuels due to environmental problems related to NO_x and SO_x production.

The calorific value of rapeseed cake (24.2 MJ/kg) was significantly higher than that of both other waste cakes. These observations are in accordance with the results of the elemental analysis. Hence, there is a strong relation between the elemental composition and the energy content of biomass samples, as is illustrated by equation 3-1 reported by Channiwala and Parikh:

$$\text{Eq. 3-1: HHV} = 0.3491\text{C} + 1.1783\text{H} + 0.1005\text{S} - 0.1034\text{O} - 0.0151\text{N} - 0.0211\text{A}$$

with HHV in MJ/kg and the content of C, H, S, O, N and ash (A) expressed in wt% on dry basis [11]. Equation 3-1 indicates that a high content of carbon and hydrogen are beneficial, while a high oxygen and ash content are detrimental for the energy content of biomass materials.

Besides major elements, minor elements are determined as well since they can influence the pyrolysis process or cause environmental and/or technological problems during biomass processing [2]. For instance, alkali metals catalyze cracking reactions during pyrolysis [12] or cause slagging and/or the formation of deposits during biomass processing [13]. The amount of phosphorus is an indication of the content of phospholipids, which are undesirable compounds concerning the storage and processing of crude vegetable oil [14]. A high chloride content is undesirable due to the risk of HCl formation and corresponding corrosion problems [2]. The sulfate content can be seen as an indication of total sulfur (organic, inorganic, oxidized and reduced S) and provides information on sulfur emissions when using the biomass or its pyrolysis products for energy purposes [15]. Significant differences in the content of the minor elements were observed for the three agricultural waste cakes. However, all contents were within the expected range for biomass materials [15].

Table 3-2: Thermochemical properties and elemental analysis of the agricultural waste cakes (SD between brackets).

Properties	Rapeseed cake	Olive waste cake	Raspberry seed cake
Proximate analysis (wt%)			
Residual moisture	1.0	1.2	1.5
Volatile matter	76.0	74.8	68.5
Fixed carbon	18.1	21.5	27.4
Ash	4.9	2.5	2.6
Elemental analysis (daf) ^a			
Carbon (C)	55.0 (0.3)	52.4 (0.7)	53.4 (0.5)
Hydrogen (H)	7.8 (0.1)	4.1 (0.5)	6.5 (0.1)
Nitrogen (N)	4.9 (0.2)	0.8 (0.1)	1.9 (0.2)
Sulfur (S)	1.4 (0.6)	0.7 (0.2)	0.3 (0.1)
Oxygen (O) ^b	30.9 (0.7)	42.0 (0.9)	37.9 (0.5)
O/C ratio	0.42	0.60	0.53
H/C ratio	1.69	0.94	1.44
Calorific value (MJ/kg)	24.2 (0.1)	20.2 (0.6)	20.3 (0.1)
Minor elements (mg/kg DW) ^c			
Calcium (Ca)	8372 (694)	10122 (1749)	2386 (128)
Potassium (K)	8531 (737)	2469 (253)	2264 (53)
Magnesium (Mg)	3702 (325)	379 (62)	1729 (5)
Sodium (Na)	94 (1)	188 (66)	61 (6)
Aluminum (Al)	21 (0.3)	367 (102)	13 (0.4)
Iron (Fe)	105 (7)	454 (161)	75 (0.1)
Manganese (Mn)	43 (3)	13 (1)	128 (2)
Silicon (Si)	294 (7)	5022 (131)	302 (21)
Phosphorus (P)	10766 (23)	390 (52)	2371 (57)
Chlorides	370 (51)	784 (107)	235 (50)
Phosphates	9071 (459)	103 (9)	3193 (577)
Sulfates	16485 (1555)	1215 (152)	3600 (37)

^a dry ash-free base; ^b determined by difference; ^c dry weight

3.2 Preliminary flash pyrolysis experiments

The opportunities of flash pyrolysis to valorize the three agricultural waste cakes were investigated in a preliminary study at lab-scale. In contrast to TGA, pyrolysis in a lab-scale setup enhances secondary reactions since the volatiles remain in longer contact with the biomass particles due to higher bed-heights. Moreover, heat and mass transfer effects are more pronounced at lab-scale, making this kind of experiments more suitable to do predictions for processes at industrial scale [5].

The main focus of this preliminary study lies on the product yield and the characterization of the pyrolysis liquids concerning their use as renewable fuels. Therefore, three important screening parameters (water content, calorific value and energy recovery) were determined. Based on these parameters, a well-founded choice could be made in selecting the most promising valorization pathway for each waste cake.

3.2.1 Product distribution

Flash pyrolysis experiments of the three waste cakes were performed in a home-built lab-scale semi-continuous reactor (see section 2.2.1). Based on TGA, a pyrolysis temperature of 450 °C was chosen since the biomass conversion was found to be almost complete at this temperature (see section 3.1.2). The product yields are shown in Table 3-3.

Table 3-3: Product yield obtained by flash pyrolysis of three agricultural waste cakes at 450 °C.

Product yield (wt%)	Rapeseed cake	Olive waste cake	Raspberry seed cake
Solid residue	21.7	21.7	25.6
<i>Char</i>	16.8	19.2	23.0
<i>Ash^a</i>	4.9	2.5	2.6
Pyrolysis liquid	53.4	50.4	53.7
<i>Organic fraction</i>	36.3	13.1	-
<i>Aqueous fraction</i>	17.1	37.3	-
Gas ^b	24.9	27.9	20.7

^a Determined by TGA of the biomass; ^b Calculated by difference

The highest yield of solid residue (char and ash) was found for raspberry seed cake (25.6 wt%). This yield was 3.9 wt% higher than that of the solid residues of both other waste cakes. These observations are in accordance with the results of the proximate analysis and the higher lignin content found for raspberry seed cake [2]. As a result, raspberry seed cake is a promising precursor for activated carbon production in terms of char yield.

The yield of pyrolysis liquid was significantly higher for rapeseed cake and raspberry seed cake than for olive waste cake. Moreover, pronounced differences in appearance and viscosity were observed. The pyrolysis liquid of rapeseed cake and olive waste cake could be separated into two fractions, while for raspberry seed cake a single-phased liquid with low viscosity was found. In case of rapeseed cake, the pyrolysis liquid spontaneously separated into a more organic like fraction (68 wt%) with an oily dark brown appearance and into a more aqueous like fraction (32%) with a light brown color. In contrast, a membrane filter (Sartorius, cellulose nitrate, pore size: 0.45 μm) was used to separate the pyrolysis liquid from olive waste cake into a very viscous organic tar fraction (26%) and an aqueous fraction (74%).

The lowest gas yield was observed for raspberry seed cake, while rapeseed cake and especially olive waste cake resulted in a considerably higher gas production.

3.2.2 Pyrolysis liquid: screening parameters for fuel use

The physicochemical properties of pyrolysis liquids are important to evaluate their potential for use as renewable fuels. In this preliminary study, the water content and the calorific value of the pyrolysis liquids, together with the energy recovery from the initial biomass feedstock into the pyrolysis liquid were used as primary criteria to select the most promising agricultural waste cake for a more in-depth investigation. The energy recovery was calculated by equation 3-2. Results are shown in Table 3-4. The pyrolysis liquid of rapeseed cake and olive waste cake was analyzed after phase separation, while that of raspberry seed cake was investigated as a single-phased liquid.

$$\text{Eq. 3-2: Energy recovery (liquid)} = \frac{\text{mass(liquid)} \times \text{HHV (liquid)}}{\text{mass(biomass)} \times \text{HHV (biomass)}} \times 100$$

Table 3-4: Screening parameters of the pyrolysis liquids concerning their use as renewable fuels.

Pyrolysis liquid	Water content (wt%)	HHV (MJ/kg)	Energy recovery (%)
Rapeseed cake:			
- Organic fraction	8.4 (0.4)	31.7 (0.1)	47.6
- Aqueous fraction	54.6 (0.4)	-	-
Olive waste cake:			
- Organic fraction	10.0 (0.2)	27.6 (0.3)	17.9
- Aqueous fraction	31.4 (0.4)	-	-
Raspberry seed cake:			
- Pyrolysis liquid	26.2 (1.2)	18.6 (0.2)	49.2

In case of **rapeseed cake**, the organic fraction of the pyrolysis liquid had a low water content (8.4 wt%) and a high calorific value (31.7 MJ/kg). The latter was significantly higher than that of the initial waste cake (24.2 MJ/kg), but still not as high as that of diesel fuel (44.8 MJ/kg) [16]. The energy recovery showed that about half of the biomass energy was converted into the organic fraction. The aqueous fraction contained, next to a high amount of water (54.6 wt%), also a considerable amount of water soluble organic compounds of low molecular weight and with a high polar character. These preliminary results reveal that the organic fraction produced from rapeseed cake has potential as renewable fuel (after upgrading), while the aqueous fraction can be a source of added-value chemicals. However, the latter requires an efficient and economic viable extraction and/or separation of the chemicals from the pyrolysis liquid.

Flash pyrolysis of **olive waste cake** resulted in an organic fraction with a water content (10.0 wt%), a calorific value (27.6 wt%) and an energy recovery that were less favorable for fuel purposes compared to the organic fraction produced from rapeseed cake. The aqueous fraction of olive waste cake had a water content of 31.4 wt%, indicating that some interesting water soluble organic compounds could be present.

In case of **raspberry seed cake**, a single-phased pyrolysis liquid was obtained. As a result, a relatively high water content (26.2 wt%) and a relatively low calorific value (18.6 wt%) were found, as most of the water did not separate

spontaneously from the organic compounds. These results are similar to those reported for pyrolysis liquids derived from lignocellulosic biomass such as wood [17]. The energy recovery from the initial biomass into pyrolysis liquid was slightly higher than in case of rapeseed cake, but the energy density was significantly lower due to the considerably higher water content. As a result, this pyrolysis liquid is believed to have a lower potential as renewable fuel than that from rapeseed cake. However, the pyrolysis liquid from raspberry seed cake still contained a considerable amount of energy and could also have potential as source of added-value chemicals.

3.3 Conclusion and outlook

Among the tested agricultural waste cakes, rapeseed cake is found to have the highest potential as source of renewable fuels. Hence, flash pyrolysis at 450 °C results, after spontaneous phase separation of the pyrolysis liquid, in an organic fraction with the highest calorific value (31.7 MJ/kg), the lowest water content (8.4 wt%) and an energy recovery from the initial biomass of 47.6 wt%. The organic tar fraction of olive waste cake is less promising due to its low yield and very viscous appearance. Flash pyrolysis of raspberry seed cake yields a single-phased pyrolysis liquid with properties comparable to those of pyrolysis liquids from lignocellulosic biomass. Additionally, raspberry seed cake is a promising precursor in the production of activated carbon because of the high solid yield. However, further characterization of the solid residue is required since the quality of the precursor also is an important factor concerning the production of activated carbon.

Based on this preliminary study, it is decided to investigate the potential of rapeseed cake as a source of renewable fuels. In Chapter 4, the influence of pyrolysis temperature, fractionated condensation and the presence of a catalyst on the product yield, the composition and the properties of the pyrolysis liquid are investigated. In case of raspberry seed cake, the main focus lies on the valorization of the pyrolysis liquid as source of added-value chemicals (Chapter 5). The potential of the solid residue of both rapeseed cake and raspberry seed cake as precursor in the production of activated carbon is the topic of Chapter 6. Olive waste cake is not further investigated in this thesis because the properties of its pyrolysis liquid are less favorable than that of rapeseed cake. The solid residue of olive waste cake has potential as precursor in the production of activated carbon. However, since this has already been studied extensively in literature [18-25], it is decided to focus on the production of activated carbon from both other agricultural waste cakes.

3.4 References

- [1] Faithfull, N.T. *Methods in agricultural chemical analysis: a practical handbook*. 2002, Wallingford UK: CABI Publishing.
- [2] Vassilev, S.V., Baxter, D., Andersen, L.K., Vassileva, C.G. and Morgan, T.J. An overview of the organic and inorganic phase composition of biomass. *Fuel*, 2012. **94**(0): 1-33.
- [3] Demirbas, A. Effect of initial moisture content on the yields of oily products from pyrolysis of biomass. *Journal of Analytical and Applied Pyrolysis*, 2004. **71**(2): 803-815.
- [4] Rabou, L.P.L.M. and Lips, S.J.J. *Phyllis database uitbreiding met biochemische samenstellingen ten behoeve van de productie van vloeibare en gasvormige brandstoffen*. 2003: ECN.
- [5] Raveendran, K., Ganesh, A. and Khilar, K.C. Pyrolysis characteristics of biomass and biomass components. *Fuel*, 1996. **75**(8): 987-998.
- [6] Wang, S., Guo, X., Wang, K. and Luo, Z. Influence of the interaction of components on the pyrolysis behavior of biomass. *Journal of Analytical and Applied Pyrolysis*, 2011. **91**(1): 183-189.
- [7] Yang, H., Yan, R., Chen, H., Lee, D.H. and Zheng, C. Characteristics of hemicellulose, cellulose and lignin pyrolysis. *Fuel*, 2007. **86**(12-13): 1781-1788.
- [8] Carrier, M., Loppinet-Serani, A., Denux, D., Lasnier, J.-M., Ham-Pichavant, F., Cansell, F. and Aymonier, C. Thermogravimetric analysis as a new method to determine the lignocellulosic composition of biomass. *Biomass and Bioenergy*, 2011. **35**(1): 298-307.
- [9] McKendry, P. Energy production from biomass (part 1): overview of biomass. *Bioresource Technology*, 2002. **83**(1): 37-46.
- [10] Vassilev, S.V., Baxter, D., Andersen, L.K. and Vassileva, C.G. An overview of the chemical composition of biomass. *Fuel*, 2010. **89**(5): 913-933.
- [11] Channiwala, S.A. and Parikh, P.P. A unified correlation for estimating HHV of solid, liquid and gaseous fuels. *Fuel*, 2002. **81**(8): 1051-1063.
- [12] Fahmi, R., Bridgwater, A., Donnison, I., Yates, N. and Jones, J.M. The effect of lignin and inorganic species in biomass on pyrolysis oil yields, quality and stability. *Fuel*, 2008. **87**(7): 1230-1240.
- [13] Mohan, D., Pittman, C.U. and Steele, P.H. Pyrolysis of wood/biomass for bio-oil: A critical review. *Energy & Fuels*, 2006. **20**(3): 848-889.

- [14] Zufarov, O., Schmidt, S. and Sekretar, S. Degumming of rapeseed and sunflower oils. *Acta Chimica Slovaca*, 2008. **1**(1): 321 - 328.
- [15] Soil and Plant Analysis Council, I. Handbook of reference methods for plant analysis, ed. Karla, Y.P. 1998: CRC Press.
- [16] Özçimen, D. and Karaosmanoglu, F. Production and characterization of bio-oil and biochar from rapeseed cake. *Renewable Energy*, 2004. **29**(5): 779-787.
- [17] Czernik, S. and Bridgwater, A.V. Overview of applications of biomass fast pyrolysis oil. *Energy & Fuels*, 2004. **18**(2): 590-598.
- [18] Román, S., González, J.F., González-García, C.M. and Zamora, F. Control of pore development during CO₂ and steam activation of olive stones. *Fuel Processing Technology*, 2008. **89**(8): 715-720.
- [19] Petrov, N., Budinova, T., Razuigorova, M., Parra, J. and Galiatsatou, P. Conversion of olive wastes to volatiles and carbon adsorbents. *Biomass & Bioenergy*, 2008. **32**(12): 1303-1310.
- [20] El-Hamouz, A., Hilal, H.S., Nassar, N. and Mardawi, Z. Solid olive waste in environmental cleanup: Oil recovery and carbon production for water purification. *Journal of Environmental Management*, 2007. **84**(1): 83-92.
- [21] Martínez, M.L., Torres, M.M., Guzmán, C.A. and Maestri, D.M. Preparation and characteristics of activated carbon from olive stones and walnut shells. *Industrial Crops and Products*, 2006. **23**(1): 23-28.
- [22] Stavropoulos, G.G. and Zabaniotou, A.A. Production and characterization of activated carbons from olive-seed waste residue. *Microporous and Mesoporous Materials*, 2005. **82**(1-2): 79-85.
- [23] Rodríguez-Valero, M.A., Martínez-Escandell, M., Molina-Sabio, M. and Rodríguez-Reinoso, F. CO₂ activation of olive stones carbonized under pressure. *Carbon*, 2001. **39**(2): 320-323.
- [24] Bacaoui, A., Yaacoubi, A., Dahbi, A., Bennouna, C., Luu, R.P.T., Maldonado-Hodar, F.J., Rivera-Utrilla, J. and Moreno-Castilla, C. Optimization of conditions for the preparation of activated carbons from olive-waste cakes. *Carbon*, 2001. **39**(3): 425-432.
- [25] Zabaniotou, A.A., Kalogiannis, G., Kappas, E. and Karabelas, A.J. Olive residues (cuttings and kernels) rapid pyrolysis product yields and kinetics. *Biomass & Bioenergy*, 2000. **18**(5): 411-420.

4 Valorization of rapeseed cake

The results of the preliminary study (Chapter 3) reveal that rapeseed cake has potential to be valorized by pyrolysis as source of renewable fuels. In this chapter, the effects of several pyrolysis conditions on the product yield and the physicochemical characteristics of the pyrolysis products are discussed. Hereby, the main focus lies on the valorization of the pyrolysis liquid as renewable fuel.

Firstly, the effect of the pyrolysis temperature on the yield and the properties of the pyrolysis products obtained by flash pyrolysis of rapeseed cake will be discussed (section 4.1). Moreover, the chemical composition of the pyrolysis liquids is determined by complementary analytical techniques in order to explain their physicochemical properties and to screen for added-value chemicals [1].

Secondly, flash pyrolysis with fractionated condensation of the pyrolysis liquid and flash co-pyrolysis with polyethylene glycol (PEG10k) are assessed on their abilities to reduce the water content of the pyrolysis liquid in a preliminary study (section 4.2).

Thirdly, slow pyrolysis with collection of the pyrolysis liquid in fractions as a function of pyrolysis temperature is studied to gain a better understanding of the pyrolytic behavior of rapeseed cake under (slow) pyrolysis conditions (section 4.3).

Fourthly, upgrading of the pyrolysis liquid by slow catalytic pyrolysis of rapeseed cake at 550 °C is the topic in section 4.4. Hereby, the main focus lies on the effect of the catalyst type (γ -Al₂O₃, HZSM-5 or Na₂CO₃) and configuration (ex-bed or in-bed mode) on the quality of the pyrolysis liquids concerning their use as renewable fuel. Moreover, the chemical composition of the pyrolysis liquids is characterized in detail for better understanding of the catalyst activity and the (improved) physicochemical properties of the pyrolysis liquids.

4.1 Flash pyrolysis of rapeseed cake: Influence of pyrolysis temperature on the product yield and the characteristics of the pyrolysis liquid

The observations and conclusions of this section have already been published:
Flash pyrolysis of rapeseed cake: Influence of temperature on the yield and the characteristics of the pyrolysis liquid
K. Smets, P. Adriaensens, G. Reggers, S. Schreurs, R. Carleer, J. Yperman
Journal of Analytical and Applied Pyrolysis, 2011. 90(2): 118 - 125

4.1.1 Product yield and energy recovery

Flash pyrolysis of rapeseed cake was performed in the semi-continuous lab-scale reactor setup (section 2.2.1) at four pyrolysis temperatures: 350, 400, 450 and 550 °C. These temperatures were selected respectively before, at the middle, at the end and at the very end of the peak assigned to the volatilization of the biomass triglycerides ($T_{\max} = 425$ °C) during TGA (see section 3.1.2). The effect of the pyrolysis temperature on the product yield and the energy recovery is shown in Table 4-1.

Table 4-1: Product yield and energy recovery from flash pyrolysis of rapeseed cake at different pyrolysis temperatures.

Product yield (wt%)	Pyrolysis temperature			
	350 °C	400 °C	450 °C	550 °C
Solid residue	40.6	39.6	21.7	17.0
<i>Char</i>	35.7	34.7	16.8	12.1
<i>Ash^a</i>	4.9	4.9	4.9	4.9
Pyrolysis liquid	28.3	34.3	53.4	58.2
<i>Organic fraction</i>	10.4	16.3	36.3	42.1
<i>Aqueous fraction</i>	17.9	18.0	17.1	16.1
Gas ^b	31.1	26.1	24.9	24.8
Energy recovery (%)				
Solid residue	45.1	46.1	17.5	11.7
Organic fraction	11.0	19.3	47.6	57.0

^a Determined by TGA of the biomass; ^b Calculated by difference

A temperature increase from 350 to 550 °C resulted in a larger liquid yield because more rapeseed cake components (especially triglycerides) were decomposed and/or volatilized at higher temperatures. The largest increase in pyrolysis liquid yield (+ 19.1 wt% in absolute terms) was found between 400 and 450 °C, while a further temperature increase to 550 °C only added 4.8 wt% in absolute terms. On the other hand, the yield of the solid residue was reduced to less than half between 350 and 550 °C, indicating that the larger liquid yield at higher temperatures was mainly obtained at the expense of solid residue. The gas yield showed a slightly negative tendency as a function of pyrolysis temperature with the largest decrease (- 4.0 wt%) between 350 and 400 °C. This negative tendency was not in agreement with expectations of larger gas yields at higher temperatures, as reported in literature [2-4]. The occurrence of secondary reactions inside the hot reactor might explain this negative tendency. Hence, these secondary reactions could involve reactions of non-condensable gases with each other or with condensable vapors, leading to an increased yield of condensable vapors. As a result, smaller gas yields and larger liquid yields would be obtained at higher pyrolysis temperatures.

Each pyrolysis liquid spontaneously separated into two fractions: an organic oil fraction and a water-rich aqueous fraction. This is in accordance with most of the pyrolysis liquids produced from press cakes of oil crops [3, 5-7]. Table 4-1 shows that the larger liquid yield at higher temperatures was almost completely caused by an increase in organic oil fraction, while the yield of the aqueous fraction was hardly dependent on the pyrolysis temperature. Since the rapeseed cake was dried prior to each pyrolysis experiment, most of the water in the pyrolysis liquid (apart from residual moisture) had to be pyrolytic water that was originating from the degradation (pyrolysis) of biomass components such as hemicellulose, cellulose and lignin. On the other hand, the increased yield of the organic oil fraction was assumed to be mainly caused by elevated volatilization and/or decomposition of the rapeseed cake triglycerides. Hence, TGA of the rapeseed cake (section 3.1.2) indicated that the degradation of hemicellulose, cellulose and lignin mainly occurred before 370 °C, while triglyceride volatilization was observed between 350 and 550 °C with a maximum at 425 °C. Therefore, it is stated that hemicellulose, cellulose and lignin are mainly decomposed below 350 °C under flash pyrolysis conditions, while the increased

yield of the organic oil fraction is mainly caused by flash distillation of the biomass triglycerides with only limited decomposition into free fatty acids. Moreover, this flash distillation is more prominent at higher pyrolysis temperatures. In this context, the large yield of solid residue at 350 and 400 °C can be explained by the fact that it still contains incompletely pyrolyzed rapeseed cake. To confirm the hypothesis made, the organic oil and the aqueous fractions of all pyrolysis liquids were further investigated with complementary analytical techniques (sections 4.1.2 and 4.1.3).

The energy recovery from the initial rapeseed cake (RSC) into the pyrolysis products (PP) was calculated using equation 4-1:

$$\text{Eq. 4-1: Energy recovery(PP)} = \frac{\text{mass(PP)} \times \text{HHV(PP)}}{\text{mass(RSC)} \times \text{HHV(RSC)}} \times 100$$

Most of the biomass energy was recovered in the solid residue at lower pyrolysis temperatures (350 and 400 °C), while the organic oil fraction showed the highest energy recovery at higher temperatures (450 and 550 °C). The highest energy recovery (57 %) was found for the organic oil fraction of the pyrolysis liquid produced at 550 °C.

It can be concluded that the product yield from flash pyrolysis of rapeseed cake is significantly affected by the pyrolysis temperature. If the production of renewable liquid fuels is the objective, relatively high pyrolysis temperatures (≥ 450 °C) turn out to be favorable in terms of both liquid yield and energy recovery.

Remarks on reproducibility, aerosol condensation and energy recovery

- ⇒ Flash pyrolysis at 450 °C was carried out in triplicate to assess the reproducibility of the experiments. The standard deviation was found to be less than 1.8 wt% for the yield of each pyrolysis product. The largest standard deviation (2.0 wt%) was found for the yield of organic oil fraction after *phase separation* of the pyrolysis liquid.
- ⇒ Incomplete condensation/collection of aerosols is a common problem for (flash) pyrolysis experiments [8]. To quantify the loss of aerosols via the gaseous fraction, an additional experiment was performed at the highest

pyrolysis temperature (550 °C) using an aerosol filter mounted at the exhaust of the condensation unit. It was found that less than 1.5 wt% of the initial rapeseed cake left the condensation unit as aerosol in the gaseous fraction. This implicates that the liquid yield could be increased by maximum 1.5 wt% if a better performing condensation unit was available.

- ⇒ The high water content of the aqueous fractions made the determination of their HHVs impossible. As a result, the energy recovery in the aqueous fractions and in the gaseous fractions (by difference) could not be calculated.

4.1.2 Characterization of the organic oil fraction

The organic oil fractions of the pyrolysis liquids were investigated by several complementary analytical techniques. Firstly, the effect of pyrolysis temperature on the physicochemical properties important for renewable fuel use were studied. Secondly, their chemical composition was determined by several techniques to explain the physicochemical properties and to gain a better understanding of the pyrolytic behavior of rapeseed cake as a function of temperature under flash pyrolysis conditions.

4.1.2.1 Physicochemical properties

The properties of the organic oil fractions produced by flash pyrolysis of rapeseed cake are shown in Table 4-2.

Table 4-2: Physicochemical properties of the organic oil fractions produced by flash pyrolysis of rapeseed cake at different temperatures (SD between brackets).

Properties	Pyrolysis temperature			
	350 °C	400 °C	450 °C	550 °C
Elemental analysis (wt%)				
C	53.6 (1.9)	58.7 (1.7)	64.4 (0.7)	70.8 (0.5)
H	7.8 (0.2)	8.9 (0.3)	9.3 (0.3)	9.7 (0.1)
N	5.5 (0.1)	5.6 (0.1)	4.7 (0.2)	5.2 (0.1)
S	1.0 (0.1)	0.3 (0.1)	0.9 (0.3)	1.1 (0.4)
O ^a	32.1	26.5	20.7	13.2
H/C molar ratio	1.73	1.80	1.72	1.63
O/C molar ratio	0.45	0.34	0.24	0.14
Water content (wt%)	17.9 (0.4)	15.4 (0.1)	8.4 (0.4)	6.7 (0.4)
HHV (MJ/kg)	25.6 (0.8)	28.7 (0.2)	31.7 (0.1)	32.8 (0.5)
TAN (mg KOH/g)	84 (2.1)	81 (0.6)	83 (6.3)	72 (1.9)
pH (20 °C)	7.0	7.8	6.8	6.9

^a Calculated by difference

The carbon and hydrogen content of the organic oil fractions considerably increased by a temperature shift from 350 to 550 °C, while the oxygen content strongly decreased from 32.1 to 13.2 wt%. As a result, the O/C molar ratio

tended to the theoretical value of 0.11 found for triglycerides consisting of glycerol esterified with three oleic acid (C18:1) fatty acids. This observation supports the hypothesis of an increasing organic oil yield as a result of a more pronounced volatilization and/or decomposition of the biomass triglycerides at higher pyrolysis temperatures. Additionally, low oxygen contents are favorable for the polarity, HHV, viscosity and acidity of pyrolysis liquids in general [9]. No systematic effect of the pyrolysis temperature on the nitrogen and sulfur contents was observed. However, both contents were rather high for direct use of the organic oil fraction as renewable fuel.

The water content of the organic oil fraction significantly decreased from 17.9 to 6.7 wt% between 350 and 550 °C. This was in accordance with the tendency observed for the oxygen content. Compared to pyrolysis liquids in general [9], the water content of the organic oil fractions obtained in this study was very low. However, a further reduction still would be more advantageous concerning their use as renewable fuels. Therefore, the opportunities of fractionated condensation of the pyrolysis liquid and co-pyrolysis with PEG10k were assessed in a preliminary study on their ability to further reduce the water content (see section 4.2).

The calorific values, measured as HHVs, were positively affected by an increase in pyrolysis temperature and were in line with the decreased water content of the organic oil fractions. The highest HHV (32.8 MJ/kg) was found for the organic oil fraction produced at 550 °C. This value was considerably higher than that of the initial rapeseed cake (24.2 MJ/kg).

The Total Acid Number (TAN) turned out to be rather independent of the pyrolysis temperature. Only the organic oil fraction produced at 550 °C showed a slightly lower TAN (72 mg KOH/g) than the samples produced at lower pyrolysis temperatures. Since the TAN of pure free fatty acids was found to be much higher than that of pure rapeseed press oil (217 mg KOH/g for palmitic acid vs < 1 mg KOH/g for rapeseed oil), the lower TAN of the organic oil fraction produced at 550 °C supported the hypothesis of elevated flash distillation of the biomass triglycerides at higher pyrolysis temperatures.

The pH-values of the organic oil fractions were rather independent of the pyrolysis temperature and varied between neutral to slightly alkaline values. Since most pyrolysis liquids (especially these produced from woods) are much

more acidic (pH-values of about 2 [10]), the obtained pH-values are favorable for the organic oil fractions to be used as renewable fuels.

4.1.2.2 Chemical composition

The chemical composition of the organic oil fractions was investigated using GC/MS. An overview of the chromatograms as a function of pyrolysis temperature is shown in Figure 4-1.

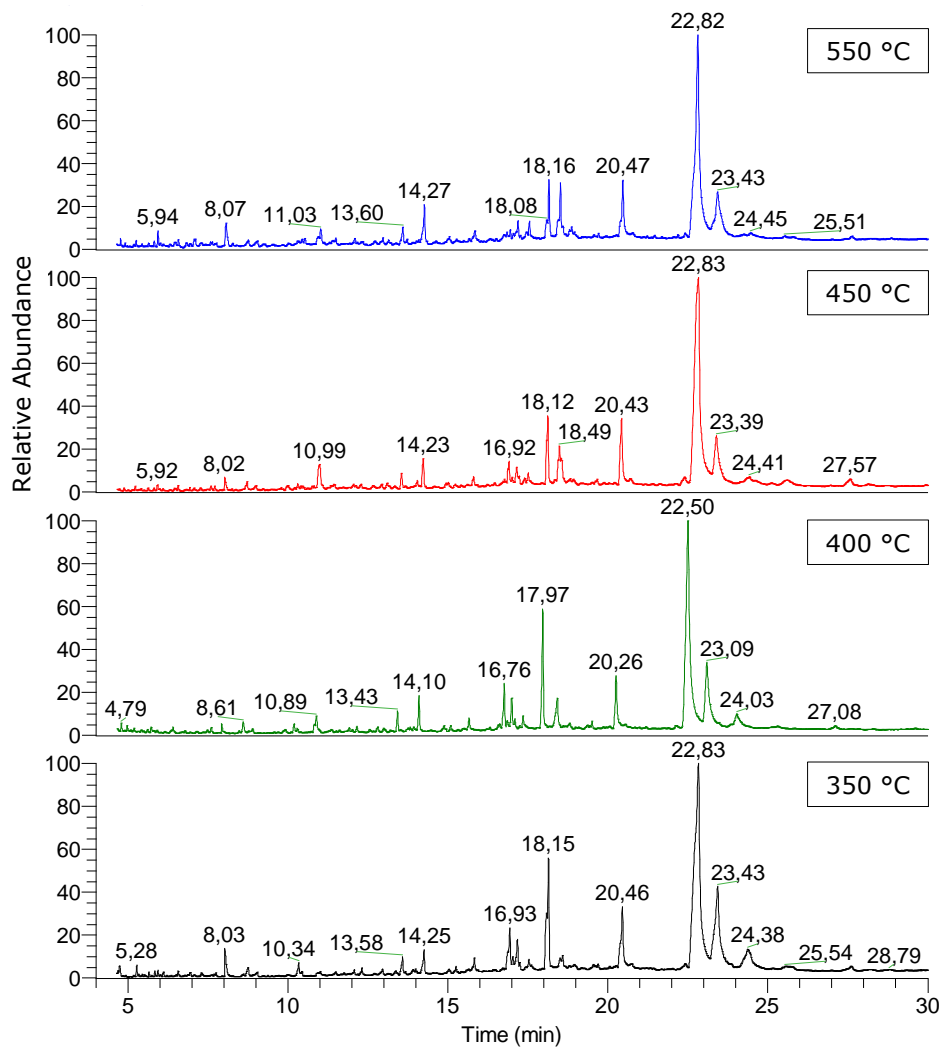


Figure 4-1: GC/MS chromatograms of the organic oil fractions produced by flash pyrolysis of rapeseed cake at different temperatures.

The major compounds, based on peak area, are listed in Table 4-3. The cumulative peak area is included as an indication of the percentage of the total area of the chromatogram that is represented by the listed compounds. Moreover, it should be noted that two compounds with a similar peak area are not necessarily present in the same amount. Hence, not all compounds have a similar response factor [11].

Table 4-3: Major compounds of the organic oil fractions as a function of pyrolysis temperature. Compound abundance is given as peak area (%) in the chromatogram. RT: retention time (min).

RT	Compound	Pyrolysis temperature			
		350 °C	400 °C	450 °C	550 °C
5.23	Pyridine	0.28	0.33	0.16	0.21
5.41	Propylbenzene	0.20	0.21	0.07	0.20
5.64	4-methylpyridine	0.12	0.12	0.14	0.35
6.56	Butylbenzene	0.21	0.34	0.19	-
7.26	2-methyl-2-cyclopenten-1-one	-	0.19	0.26	0.42
7.72	Pentylbenzene	0.17	0.37	0.21	0.32
8.02	Acetic acid	1.28	0.58	0.64	1.60
8.76	2-methyl-4-hexyne-3-one	0.58	0.82	-	0.66
10.31	3-furanmethanol	0.67	0.56	0.33	-
10.41	3-methylbutanoic acid	0.23	0.22	0.19	0.46
10.99	8-heptadecene	0.27	1.58	2.43	0.98
11.73	4-methylpentanoic acid	0.25	0.18	0.23	-
12.05	2-hydroxy-3-methyl-2-cyclopenten-1-one	0.42	0.39	0.22	0.44
12.29	4-methoxyphenol	0.43	0.45	0.49	0.22
12.94	1-isocyano-2-methylbenzene	0.47	0.42	0.40	0.63
13.10	Heptanoic acid	-	0.40	0.52	0.42
13.12	1-(1H-pyrrol-2-yl)-ethanone	0.31	0.22	-	0.17
13.55	Phenol	0.88	1.25	0.79	1.16
13.97	Benzenepropanenitrile	0.27	0.67	0.18	-
14.05	Octanoic acid	-	0.40	0.46	0.43
14.23	4-methylphenol	1.55	2.03	1.68	2.72
15.01	2-ethylphenol	-	0.61	0.35	0.69

Table 4-3: Continued.

RT	Compound	350 °C	400 °C	450 °C	550 °C
15.23	4-hydroxy-2-methylacetophenone	0.39	0.37	0.27	-
15.81	2,6-dimethoxyphenol	1.20	1.06	0.84	1.23
16.77	Hexadecanenitrile	-	0.69	0.69	-
16.88	1,2,3-trimethoxy-5-methylbenzene	2.81	2.55	1.14	0.69
17.00	3-pyridinol	0.58	-	0.46	0.30
17.15	Indole	1.87	2.52	1.17	1.51
17.23	Methyl-9-octadecanoate	-	0.55	0.27	-
17.44	2,5-pyrrolidinedione	-	0.24	-	0.67
17.51	2-methyl-1H-indole	0.95	1.16	0.96	1.16
18.12	3,4-dimethoxyacetophenone	7.70	7.20	4.09	4.12
18.49	1,3,12-nonadecatriene-5,14-diol	-	-	2.24	4.97
18.54	Octadecenitrile	0.87	3.51	1.45	-
19.51	2,6-dimethylphenylisocyanate	-	0.33	0.22	0.35
20.43	Hexadecanoic acid	5.31	4.56	5.29	5.19
20.69	9-hexadecenoic acid	0.93	0.82	0.87	-
21.40	Hydroquinone	-	0.21	0.16	0.23
22.39	Octadecanoic acid	0.45	-	0.82	-
22.83	9-octadecenoic acid	34.97	33.10	39.32	32.20
23.39	9,12-octadecadienoic acid	13.24	10.49	9.77	9.45
24.41	Methyl-9,12,15-octadecatrienoate	4.38	3.39	1.56	-
27.57	9-octadecenamide	0.88	0.77	1.49	0.56
Cumulative peak area (%):		85.1	85.9	83.0	74.7
Number of compounds:		33	40	40	32

A wide range of compounds was found in the organic oil fractions of the pyrolysis liquids. Based on peak area, 9-octadecenoic acid (RT: 22.83 min) was found as the most abundant compound in all organic oil fractions. Other important compounds were 9,12-octadecadienoic acid (RT: 23.39 min), hexadecanoic acid (RT: 20.43 min), methyl-9,12,15-octadecatrienoate (RT: 24.41 min), 9-hexadecenoic acid (RT: 20.69 min) and octadecanoic acid (RT: 22.39 min). All these compounds were degradation products of biomass triglycerides. However, it should be noted that biomass triglycerides themselves could not be detected by the used GC/MS setup. Therefore, additional analytical

techniques were performed on the organic oil fractions (sections 4.1.2.3 to 4.1.2.5). Besides compounds derived from triglycerides, a wide range of compounds originating from other biomass components such as hemicellulose, cellulose, lignin and proteins was also detected. Among them, 3,4-dimethoxyacetophenone (RT: 18.12 min) and 1,2,3-trimethoxy-5-methylbenzene (RT: 16.88 min) were the most abundant ones, based on their peak area.

The organic oil fractions turned out to be complex mixtures of compounds with a wide variety of chemical functionalities. To make the results more manageable, all identified compounds (about 165 in total) were classified into 10 categories based on their functional groups (Figure 4-2). If a compound had more than one functional group, the functional group with the highest number of bonds with a hetero-atom was given priority. For instance, a compound with an alcohol and a ketone functionality was classified as ketone. The hydrocarbons included saturated, unsaturated as well as cyclic hydrocarbons, while aromatic hydrocarbons were classified in a separate class. Compounds with a phenol structure or a N-containing cyclic structure were classified as phenols or N-heterocyclic compounds respectively, no matter what other functional group was present in their chemical structure. Finally, the sum of the peak areas of all classes was normalized to 100% because not all compounds of the organic oil fraction could be identified. A graphical overview of the chemical classes of compounds present in the organic oil fractions produced by flash pyrolysis of rapeseed cake is presented in Figure 4-2.

Figure 4-2 shows carboxylic acids as the most abundant class of compounds for all organic oil fractions. Most of these acids were originating from (partial) degradation of biomass triglycerides. Phenols were found as a second important class. These compounds were formed by degradation of lignin components. The amount of alcohols slightly increased as a function of pyrolysis temperature, while an opposite tendency was observed for the amount of esters. In case of the other classes of compounds, no systematic tendency was observed as a function of pyrolysis temperature.

Since biomass triglycerides could not be detected with the GC/MS setup used in this study due to their high molecular weight, additional analytical techniques such as GPC, HPLC, FTIR and ¹H-NMR were performed to characterize the organic oil fractions in more detail.

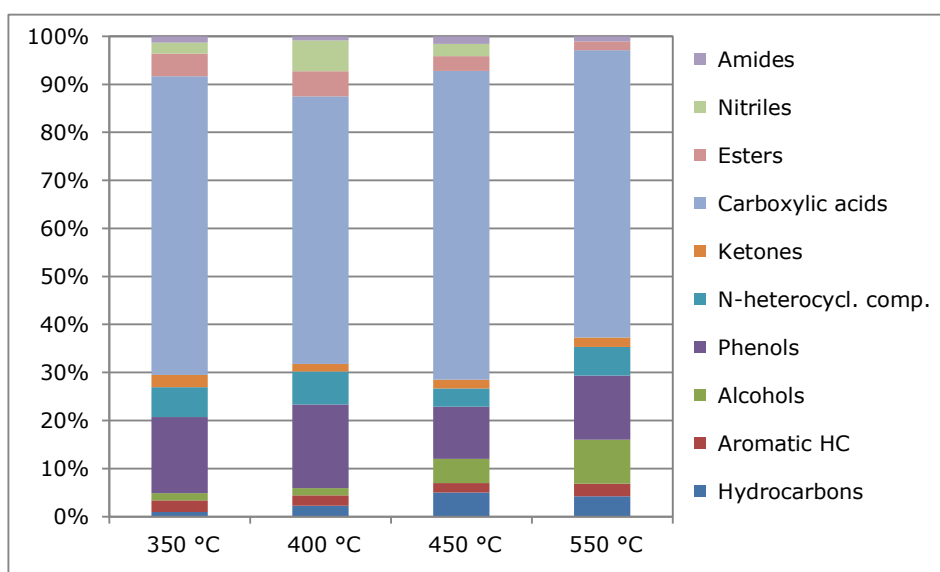


Figure 4-2: Classes of compounds present in the organic oil fractions produced by flash pyrolysis of rapeseed cake at different temperatures.

4.1.2.3 GPC and HPLC analysis

GPC analysis provides information on the molecular weight distribution of the organic oil fractions (Figure 4-3). Two major peaks were observed in the chromatograms. The first peak was assigned to free fatty acids (around 330 Da) and the second one to triglycerides (around 860 Da) present in the organic oil fractions. These assignments were confirmed by GPC analysis of a pure free fatty acid (oleic acid) and pure rapeseed oil, respectively. The triglyceride peak strongly increased when rapeseed cake was pyrolyzed at higher temperatures, while the peak of the free fatty acids did not significantly change. Similar conclusions were made from the HPLC analysis of the organic oil fractions. Figure 4-4 shows the absorbance (210 nm) of the organic oil fraction as a function of retention time in the time interval of triglyceride elution (12 - 18 min). Again, the yield of triglycerides increased with pyrolysis temperature, explaining the higher yield of the organic oil fraction at higher pyrolysis temperatures (Table 4-1). Hence, both techniques strongly support the hypothesis that the increased yield in organic oil fraction is mainly caused by elevated flash distillation of biomass triglycerides at higher pyrolysis temperatures, with only limited decomposition into free fatty acids.

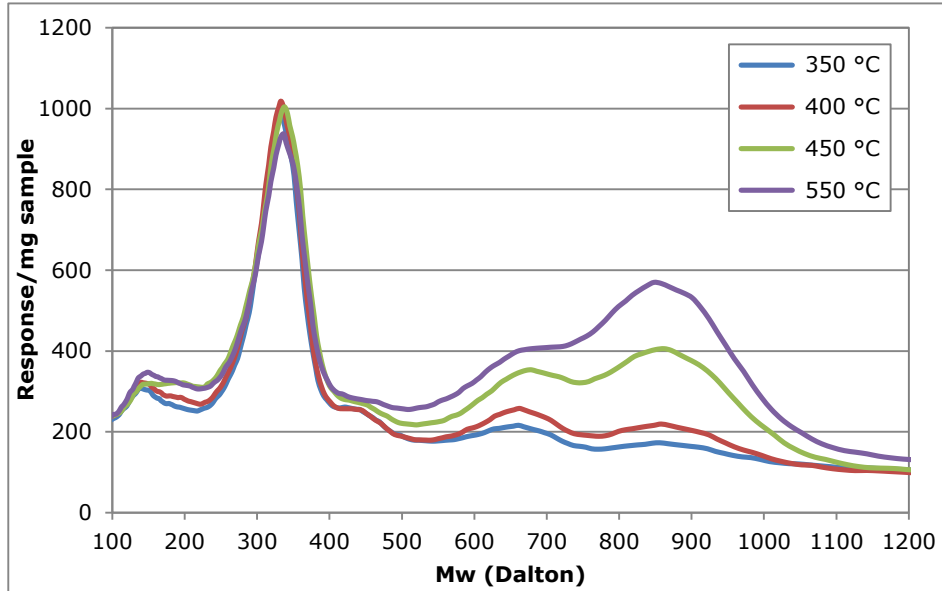


Figure 4-3: GPC chromatograms of the organic oil fractions produced by flash pyrolysis of rapeseed cake at different temperatures.

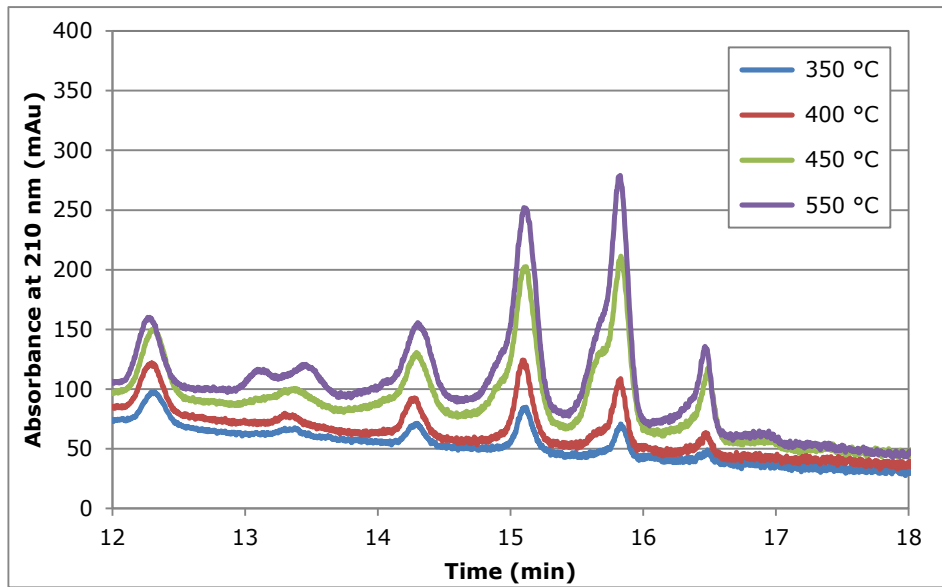


Figure 4-4: HPLC chromatograms of the organic oil fractions produced by flash pyrolysis of rapeseed cake at different temperatures.

4.1.2.4 FTIR analysis

The functional groups of the organic oil fractions were identified by FTIR analysis. An overview of the spectra is shown in Figure 4-5. Table 4-4 summarizes the most important functional groups present in the organic oil fractions and their corresponding IR absorption bands.

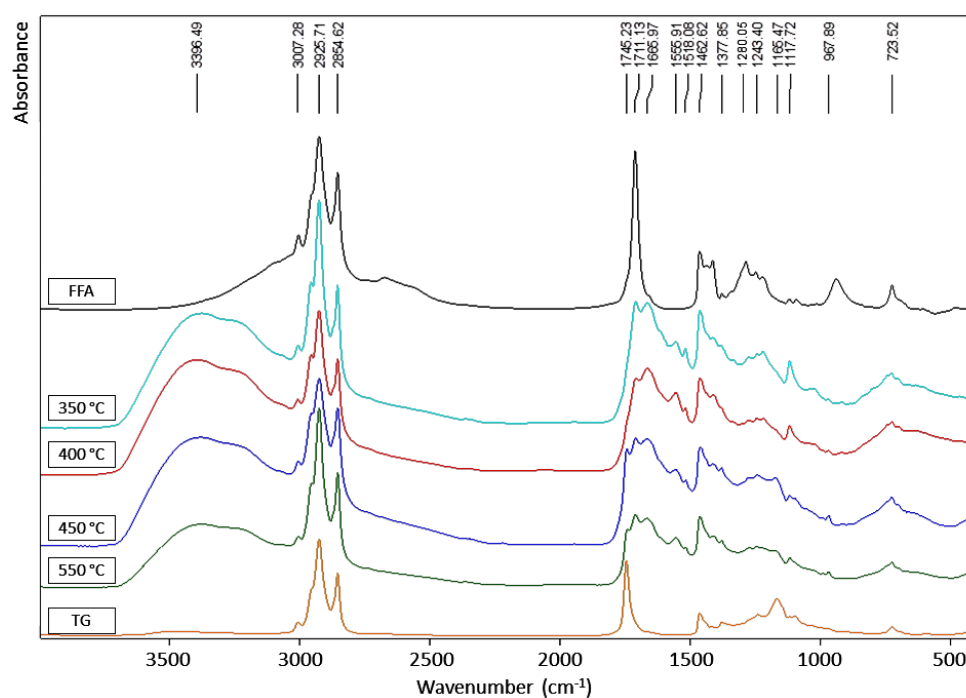


Figure 4-5: FTIR spectra of the organic oil fractions as a function of pyrolysis temperature (350 - 550 °C). The spectra of a pure free fatty acid (FFA; oleic acid) and pure triglycerides (TG; rapeseed oil) are included for comparison.

The functional groups of the organic oil fractions were very similar regardless the pyrolysis temperature. The intense broad absorption band between 3600 and 2300 cm^{-1} was assigned to the O-H stretching vibration of residual water in the samples, next to that of carboxylic acid and alcohol functionalities. The asymmetric and symmetric C-H stretching vibrations between 2970 and 2855 cm^{-1} , the C-H deformation vibrations between 1465 and 1375 cm^{-1} and the CH_2 -rocking vibrations around 724 cm^{-1} were indicative of the long aliphatic chains of mainly triglycerides and free fatty acids. An important difference between the

spectra was found for the carbonyl (C=O) stretching vibration in the spectral region of 1800 to 1600 cm^{-1} . Here, the spectra of the organic oil fractions produced at 450 and 550 °C showed a band at 1745 cm^{-1} , while this band was absent in the spectra of 350 and 400 °C. This band is typical for the carbonyl stretching vibration of ester bonds [12, 13]. In contrast, the band at 1711 cm^{-1} , which is typical for the carbonyl stretching vibration of aliphatic carboxylic acids, was found in all of the samples. The C-O stretching region showed a similar result: the C-O stretching vibration of esters was situated at about 1166 cm^{-1} and was only found in the spectra of the samples obtained at 450 and 550 °C, while the C-O stretching vibration of carboxylic acids (1280 cm^{-1}) was observed for all of the samples. Comparison with the FTIR spectra of pure rapeseed oil and a pure free fatty acid (oleic acid), representing respectively triglycerides and carboxylic acids, supported these assignments (Figure 4-5). Hence, the FTIR results support the hypothesis of flash distillation of the biomass triglycerides (esters) at higher pyrolysis temperatures (> 400 °C) with only limited degradation into free fatty acids (carboxylic acids). The absorption bands between 1675 and 1575 cm^{-1} and the weak band at 3007 cm^{-1} , representing the C=C and the C=C-H stretching vibrations respectively, were indicative of internal alkenes and aromatic compounds.

Table 4-4: Overview of the major functional groups present in the organic oil fractions identified by FTIR analysis [12, 13].

Wavenumber	Functional group	Class of compounds
3600 – 2300 cm^{-1}	O-H stretching	Acids, alcohols, water
3100 – 3000 cm^{-1}	C-H stretching	Aromatic and olefinic compounds
2970 – 2855 cm^{-1}	C-H stretching	Alkyl, aliphatic compounds
1800 – 1600 cm^{-1}	C=O stretching	Carbonyls (ester, acid, ketone, etc.)
1675 – 1575 cm^{-1}	C=C stretching	Aromatic compounds, unsaturated aliphatic C=C stretching
1470 – 1430 cm^{-1}	O-H bending	Acids
1465 – 1375 cm^{-1}	C-H bending	Alkanes
1280 – 1000 cm^{-1}	C-O stretching	Esters, acids
900 – 700 cm^{-1}	C-H bending	Aromatic and olefinic compounds
724 cm^{-1}	CH ₂ rocking	Long aliphatic chains

4.1.2.5 $^1\text{H-NMR}$ analysis

The organic oil fractions were investigated with $^1\text{H-NMR}$ spectroscopy. A typical spectrum is shown in Figure 4-6.

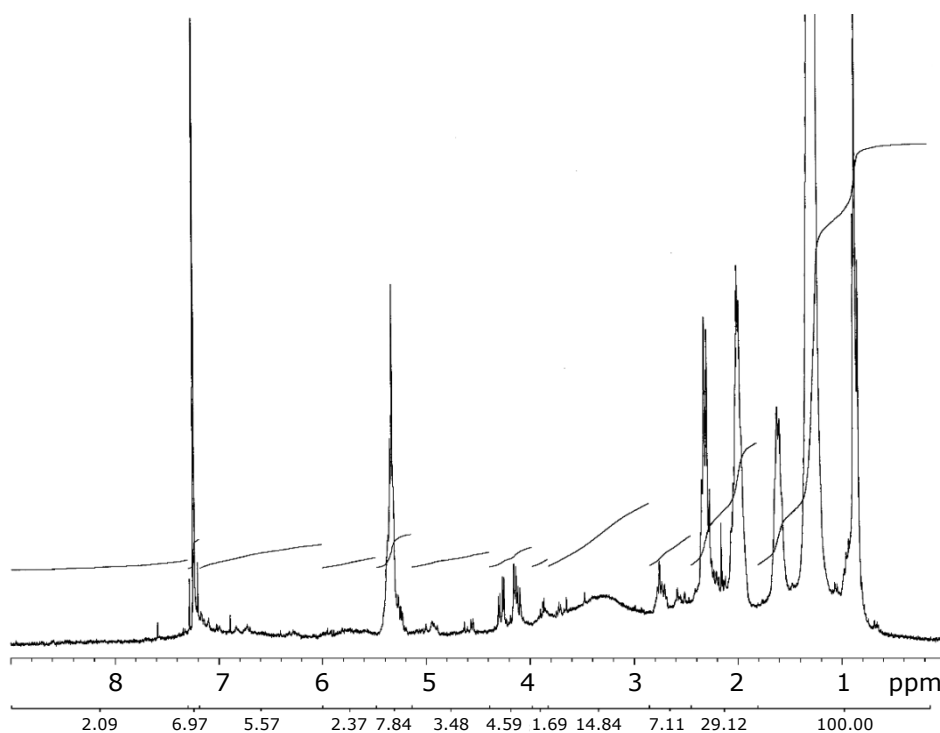


Figure 4-6: A typical $^1\text{H-NMR}$ spectrum of the organic oil fraction produced by flash pyrolysis of rapeseed cake at 550 °C. Peak areas are shown at the bottom line.

The signals between 0.6 and 1.8 ppm were assigned to protons attached to the methyl, methylene and methine carbons of saturated carbon-hydrogen chain fragments. The signals between 1.8 and 2.4 ppm represented protons attached to carbons next to sp^2 -hybridized carbons. The broad signal between 3.0 and 3.8 ppm was caused by water present in the organic oil fraction. Another set of important signals was located at chemical shifts between 4.0 and 4.4 ppm. These signals were associated with α - and α' -protons of the glycerol part of the triglycerides. The signal at 5.4 ppm represented protons attached to carbon atoms of double bonds, mainly present in the long chains of unsaturated free

fatty acids and triglycerides. The signal at 7.2 ppm was assigned to small amounts of CHCl_3 present in the CDCl_3 solvent.

The integrated areas of the diagnostic spectral regions mentioned above were normalized against the integrated area of the region between 0.6 and 1.8 ppm to present an overview of tendencies as a function of pyrolysis temperature (Figure 4-7). The area between 4.0 and 4.4 ppm, associated with α - and α' -protons of glycerol, was found to increase as a function of pyrolysis temperature. This observation supports the hypothesis of an increased organic oil yield because of elevated flash distillation of the biomass triglycerides at higher pyrolysis temperatures. The area between 3.0 and 3.8 ppm was indicative of the water content of the organic oil fractions and was in accordance with the water content determined by Karl Fischer titration (Table 4-2).

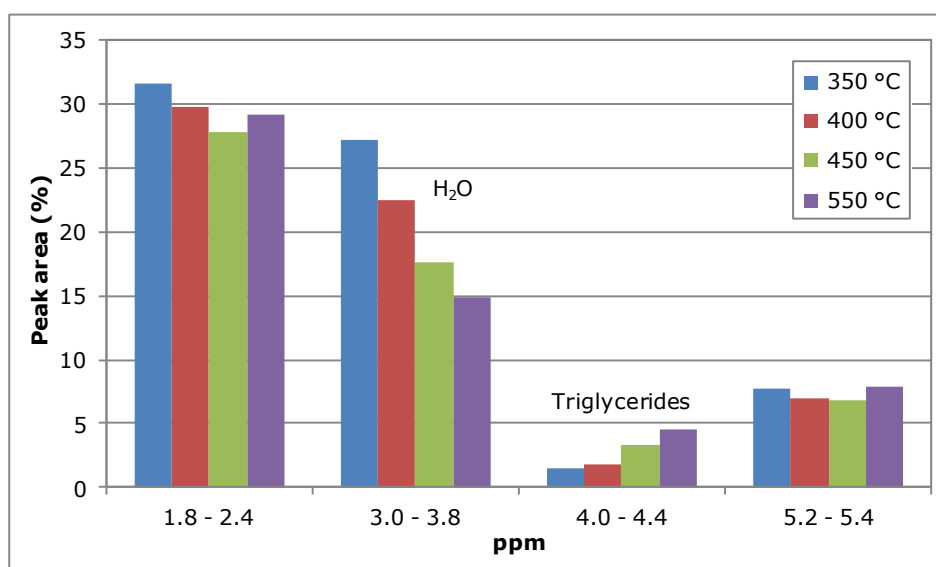


Figure 4-7: Overview of the ^1H -NMR analysis of the organic oil fractions as a function of pyrolysis temperature.

4.1.3 Characterization of the aqueous fraction

4.1.3.1 Physical properties

Besides an organic oil fraction, the pyrolysis liquid was also composed of an aqueous fraction that mainly consisted of water and water soluble organic compounds formed by decomposition of rapeseed cake during flash pyrolysis. The properties of these aqueous fractions as a function of pyrolysis temperature are presented in Table 4-5.

Table 4-5: Properties of the aqueous fractions produced by flash pyrolysis of rapeseed cake at different temperatures (SD between brackets).

Properties	Pyrolysis temperature			
	350 °C	400 °C	450 °C	550 °C
Water content (wt%)	65.2 (0.5)	65.4 (0.5)	54.6 (0.4)	46.6 (1.0)
pH (20 °C)	7.1	7.6	6.4	6.4

The water content was, as expected, very high but decreased with a temperature increase from 350 to 550 °C. Since the yield of aqueous fraction was rather independent of the pyrolysis temperature (Table 4-1), the former implicates that the amount of water soluble organic compounds must increase at higher pyrolysis temperatures. The pH-values of the aqueous fractions fluctuated between slightly alkaline and slightly acidic at higher pyrolysis temperatures.

4.1.3.2 Chemical composition

The major organic compounds of the aqueous fractions were identified by GC/MS. An overview of the chromatograms is shown in Figure 4-8. Similar to the organic oil fractions, the aqueous fractions turned out to be a complex mixture of a wide variety of compounds. A limited list of the major compounds, based on peak area, is shown in Table 4-6. To make the results more manageable, all identified compounds (about 100 in total) were classified into 9 categories based on their functional groups (Figure 4-9). The methodology for classification was analogous to the one used for the organic oil fractions (section 4.1.2.2). Sugars and sugar-derived compounds (e.g. levoglucosan) were counted as alcohols, while all other O-containing cyclic structures were classified

as O-heterocyclic compounds. An overview of the classes of compounds present in the aqueous fractions produced by flash pyrolysis of rapeseed cake at different temperatures is shown in Figure 4-9.

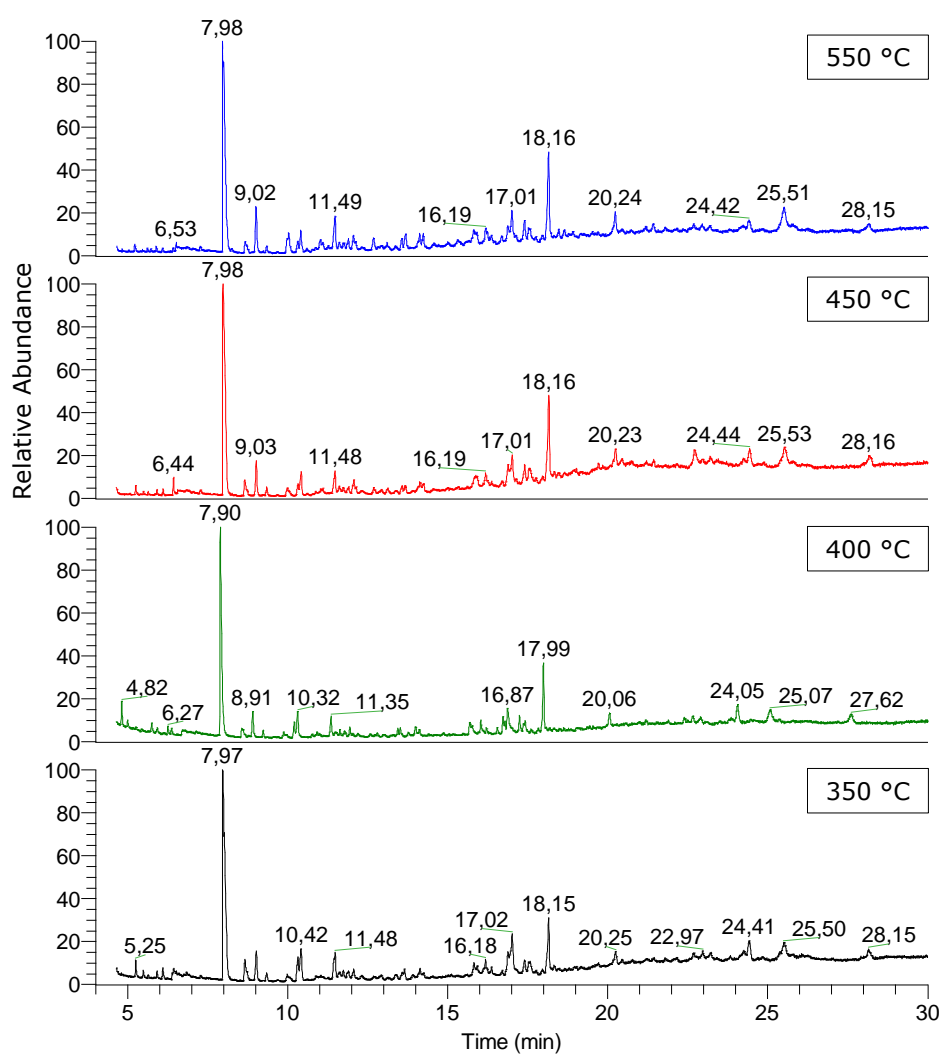


Figure 4-8: GC/MS chromatograms of the aqueous fractions produced by flash pyrolysis of rapeseed cake at different temperatures.

Table 4-6: Major compounds of the aqueous fractions produced by flash pyrolysis of rapeseed cake at different pyrolysis temperatures. Compound abundance is given as peak area (%) in the chromatogram. RT: retention time (min).

RT	Compound	Pyrolysis temperature			
		350 °C	400 °C	450 °C	550 °C
5.23	Pyridine	0.67	0.45	0.36	0.30
5.62	3-methylpyridine	0.17	0.25	0.17	0.13
6.11	Methylpyrazine	0.46	0.44	0.23	0.17
7.27	2-methyl-2-cyclopenten-1-one	-	0.81	0.50	0.57
7.98	Acetic acid	18.19	16.41	16.15	15.64
8.68	Formic acid	1.78	1.09	1.09	0.86
9.02	Propanoic acid	1.86	1.70	1.75	2.39
9.99	Butanoic acid	0.73	0.80	0.78	1.76
10.32	3-furanmethanol	1.39	1.01	0.66	0.61
10.42	3-methylbutanoic acid	2.06	1.95	1.32	1.01
11.49	Acetamide	2.16	1.50	1.93	2.20
11.75	4-methylpentanoic acid	0.68	0.54	0.54	0.66
11.90	Propanamide	0.87	0.60	0.70	0.71
12.06	2-hydroxy-3-methyl-2-cyclopenten-1-one	0.90	1.00	0.86	1.32
12.30	4-methoxyphenol	0.57	0.54	0.64	0.33
13.57	Phenol	0.49	0.59	0.46	0.57
14.24	4-methylphenol	0.56	0.60	0.63	0.92
15.82	2,6-dimethoxyphenol	1.18	1.93	0.79	2.23
16.19	Glycerin	1.84	-	1.46	1.77
16.70	1,2,4-triazine-3,5-dione	-	0.55	0.43	0.61
16.88	1,4,3,6-dianhydro- α -D-glucopyranose	1.52	1.10	1.38	1.29
17.01	3-pyridinol	4.56	3.11	2.78	3.16
17.40	2,5-pyrrolidinedione	1.23	1.43	1.54	1.64
18.16	Xanthosine	-	4.85	5.69	5.80
25.51	Levogluconan	4.41	3.07	3.64	4.39
Cumulative peak area (%):		48.3	46.3	46.5	51.0
Number of compounds:		22	24	25	25

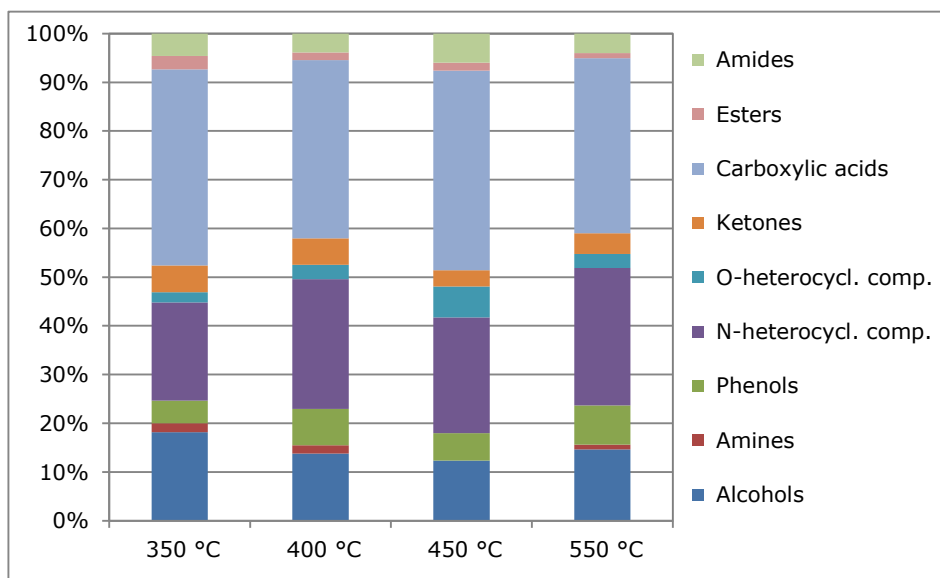


Figure 4-9: Overview of the classes of compounds present in the aqueous fractions produced by flash pyrolysis of rapeseed cake at different temperatures.

No systematic effect of the pyrolysis temperature on the classes of compounds was observed. Carboxylic acids were identified as principal class of compounds for all of the aqueous fractions (Figure 4-9). This result is similar to the one found for the organic oil fractions. However, in contrast to the long-chain fatty acids observed in case of the latter, the acids found in the aqueous fractions were rather short-chain fatty acids, of which acetic acid (RT: 7.98 min) was the most abundant one (Table 4-6). A second major class of compounds was composed of N-heterocyclic compounds that were originating from the thermal degradation of the biomass proteins [14]. Their major representatives were 3-pyridinol (RT: 17.01 min) and 2,5-pyrrolidinedione (RT: 17.40 min). Besides N-heterocyclic compounds, degradation of the proteins also resulted in amines and amides, with acetamide (RT: 11.49 min) as principal compound of the latter. Within the class of alcohols, levoglucosan (RT: 25.51 min) was the most abundant compound and was probably formed during degradation of cellulose by dehydration [15, 16]. Phenols contained the degradation products of lignin components, while the O-heterocyclic compounds were mainly composed of furan-derivatives, mainly originating from hemicellulose degradation [17-19].

4.1.4 Characterization of the solid residue

The solid residue from flash pyrolysis of rapeseed cake was composed of char and ash. Since the flash pyrolysis experiments were performed with sand as a heat transfer medium, considerable amounts of sand were stuck to the surface or were even incorporated within the particles of the solid residue, as is illustrated in Figure 4-10. Therefore, complete separation of the solid residue from the sand was almost impossible.

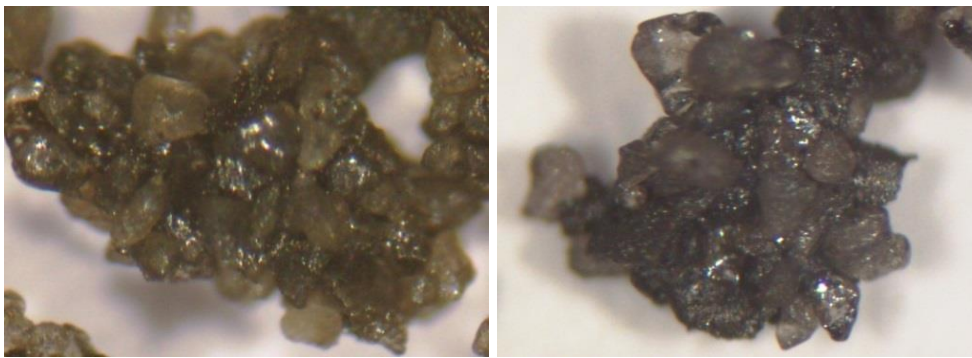


Figure 4-10: Pictures of the sand particles stuck to the surface of the solid residue (550 °C) made by optical microscopy (40x).

Due to its problematic separation from sand, the solid residue produced by flash pyrolysis of rapeseed cake was not a suitable precursor in the production of activated carbon. However, the solid residue still contains a considerable amount of the biomass energy (Table 4-1). In a circulating fluidized bed (CFB) reactor at industrial scale, the solid residue can be valorized by burning it in a secondary reactor (combustor). As a result, heat is provided to the pyrolysis reactor without the need to separate the recirculating sand from the solid residue [20]. In this respect, the higher heating value (HHV) and the ash content of the solid residue are important process design parameters. Therefore, both parameters were estimated as follows. The ash content of the solid residue (ash_{SR}) was calculated from the ash content of the rapeseed cake (ash_{RSC}) and the yield of solid residue using equation 4-2. Hereby, the ash of the rapeseed cake was assumed to remain in the solid residue after the flash pyrolysis experiment [8].

$$\text{Eq. 4-2:} \quad ash_{SR} = ash_{RSC} \times (100/yield_{SR})$$

The HHV of the char fractions (HHV_{char}) was determined using bomb calorimetry and corrected for the amount of sand and ash in the solid residue, as described in section 2.5.3. The standard deviation was found to be less than 1.6 MJ/kg. Finally, the HHV of the solid residues (HHV_{SR}) was calculated using equation 4-3. Results are shown in Table 4-7.

$$\text{Eq. 4-3:} \quad \text{HHV}_{\text{SR}} = \text{HHV}_{\text{char}} \times (\text{char/solid residue})/100$$

Table 4-7: Calculation of the ash content and the HHV of the solid residues from flash pyrolysis of rapeseed cake at different temperatures.

Properties	Pyrolysis temperature			
	350 °C	400 °C	450 °C	550 °C
ash _{SR} (wt%)	12.1	12.4	22.6	28.8
char/solid residue (wt%)	87.9	87.6	77.4	71.2
HHV _{char} (MJ/kg)	30.6	32.1	25.3	23.3
HHV _{SR} (MJ/kg)	26.9	28.1	19.6	16.6

The HHV of the char fractions showed a negative tendency as a function of pyrolysis temperature (Table 4-7). This can be explained by the fact that at lower temperatures, hemicellulose, cellulose and lignin components were predominantly degraded, while the biomass triglycerides mainly remained in the solid residue. At higher pyrolysis temperatures (> 400 °C), flash distillation of the biomass triglycerides was found to be much more pronounced. As a result, the HHV of the char fractions decreased at higher temperatures. Since the ash content of the solid residue increased as a function of pyrolysis temperature, the negative tendency of the HHV of the chars was even more pronounced for the HHV of the solid residues. However, even the solid residue produced at 550 °C still contained a considerable amount of energy (16.6 MJ/kg) that could be used to reheat the circulating sand in an industrial CFB reactor by burning it in a secondary reactor. In this way, the solid residue can be valorized as an internal heat source to provide the process heat requirements with no waste streams other than flue gas and ash [20].

4.2 Flash pyrolysis of rapeseed cake: Reduction of the water content of the pyrolysis liquid – a preliminary study

The water content strongly affects the physicochemical properties of pyrolysis liquids [9]. For instance, a relatively high water content reduces the viscosity and the production of NO_x during combustion of the pyrolysis liquid, but also decreases the HHV [21]. Generally, the positive aspects are outbalanced by the negative consequences of high water contents [10]. Therefore, a (further) reduction in water content of pyrolysis liquids is frequently desirable. In this section, two options are investigated to reduce the water content of pyrolysis liquids produced by flash pyrolysis of rapeseed cake in a preliminary study. Firstly, the potential of a fractionated condensation system to collect the pyrolysis liquid is discussed. Secondly, the opportunities of co-pyrolysis of rapeseed cake with polyethylene glycol (PEG10k) are assessed. In case of the latter, the objective is to obtain a synergetic effect between biomass and polymer resulting in an improved quality of the pyrolysis liquid.

4.2.1 Flash pyrolysis of rapeseed cake with fractionated condensation of the pyrolysis liquid

Flash pyrolysis of rapeseed cake was performed at 450 °C in the lab-scale semi-continuous reactor as described in section 2.2.1. The condensation unit was expanded with a second condensation vessel made of glass (part 3a in Figure 2-2). Hence, two similar condensation vessels were used in series: the first vessel was heated to 105 °C using silicone oil pumped from a heating oil bath, while the second vessel was water cooled. In this way, water and the more volatile organic compounds were expected not to condensate in the first vessel at 105 °C, but to condensate in the second water cooled vessel. As a result, the liquid fraction collected at 105 °C was expected to have a reduced water content. An overview of the yield, properties and energy recovery of both pyrolysis liquid fractions is shown in Table 4-8.

Table 4-8: Yield, properties and energy recovery of the pyrolysis liquid fractions produced by flash pyrolysis of rapeseed cake at 450 °C with fractionated liquid condensation.

Pyrolysis liquid	105 °C vessel	Water cooled vessel
Yield (wt%)	30.8	22.0
Water content (wt%)	10.2	41.9
Mass of water in pyrolysis liquid (g)	3.1	9.2
HHV (MJ/kg)	30.0	24.9
Energy recovery (%)	38.2	22.6

A liquid yield of 30.8 wt% was obtained in the vessel at 105 °C, while the water cooled vessel resulted in a liquid yield of 22.0 wt%. The water content of the liquid fraction collected at 105 °C was significantly lower (- 31.7 wt%) than that of the liquid fraction condensed in the water cooled vessel. As a result, the HHV and the energy recovery were considerably higher for the former liquid fraction compared to the latter fraction, indicating that the fractionated condensation performed well. However, comparison with flash pyrolysis at 450 °C with regular condensation (section 4.1) revealed that fractionated liquid condensation did not improve the properties of the pyrolysis liquid concerning its use as a renewable fuel. Hence, a lower liquid yield (30.8 vs 36.3 wt%), a slightly higher water content (10.2 vs 8.4 wt%) and a slightly lower HHV (30.0 vs 31.7 MJ/kg) were found for the liquid fraction collected at 105 °C compared to the organic oil fraction obtained by regular condensation. This observation can be explained by the polarity of the pyrolysis liquid. The pyrolysis liquid of the regular experiment was a two-phased liquid that spontaneously separated into an organic oil and an aqueous fraction. In this way, most of the water of the pyrolysis liquid (about 75 wt%) was separated into the aqueous fraction, leaving an organic oil fraction with a relatively low water content. In case of fractionated liquid condensation, most of the water (about 75 wt%) was condensed in the water cooled vessel. As a result, the liquid fraction in the vessel at 105 °C did not contain enough water to separate in two phases. In contrast, the liquid fraction collected in the water cooled vessel separated slowly but spontaneously in an organic (50.5 wt%) and an aqueous (49.5 wt%) fraction.

It can be concluded that the spontaneous phase separation of the pyrolysis liquid collected by regular condensation is more effective than fractionated liquid condensation for the production of a pyrolysis liquid with potential as renewable fuel in case of rapeseed cake. However, flash pyrolysis with fractionated liquid condensation is shown to reduce the water content of the pyrolysis liquid fraction collected at 105 °C and therefore this technique has potential to improve the quality of pyrolysis liquids produced from *other* biomass waste streams.

4.2.2 Co-pyrolysis of rapeseed cake with PEG10k polymer

A second option to reduce the water content of pyrolysis liquids is based on a synergetic effect that could occur during co-pyrolysis of the biomass sample with a polymer [22, 23]. In this preliminary study, rapeseed cake was flash co-pyrolyzed with polyethylene glycol (PEG10k; Mw: 10 000 Da) in a mass ratio of 1:1 at 450 °C. Hence, the pyrolysis liquid produced from rapeseed cake is found to contain a relatively high amount of free fatty acids that may be converted into alkyl esters by co-pyrolysis with a suitable polymer according to the following esterification reaction (equation 4-4):



This conversion of fatty acids into less polar ester compounds is expected to assist the separation of the pyrolysis liquid into an organic oil and an aqueous fraction. The higher amount of water resulting from the esterification reaction could favor the separation process as well. As a result, an organic oil fraction with improved properties for renewable fuel use is expected.

PEG10k is chosen as test polymer since its degradation occurs in the same temperature range as the volatilization and/or decomposition of the biomass triglycerides, i.e. around 430 – 435 °C. If any synergetic effect is found in this preliminary study, the possibilities of a waste stream with similar properties as PEG10k can be tested instead of the pure polymer. An overview of the product yield and the energy recovery is given in Table 4-9.

Table 4-9: Product yield and energy recovery from flash co-pyrolysis of rapeseed cake with PEG10k, compared to regular flash pyrolysis of rapeseed cake at 450 °C.

Product yield (wt%)	Co-pyrolysis	Regular pyrolysis
Solid residue	19.3	21.7
<i>Char</i>	16.3	16.8
<i>Ash^a</i>	3.0	4.9
Pyrolysis liquid	54.7	53.4
<i>Organic fraction</i>	24.8	36.3
<i>Aqueous fraction</i>	29.9	17.1
Gas ^b	26.0	24.9
Energy recovery (%)		
Solid residue	21.8	17.5
Organic fraction	28.9	47.6

^a Determined by TGA of the biomass/polymer; ^b Calculated by difference

Co-pyrolysis of rapeseed cake with PEG10k decreased, as expected, the yield of solid residue, while a slightly higher liquid and gas yield was obtained. The lower solid yield can be explained by the low tendency for char formation and the low ash content (1.0 wt%) of the PEG10k polymer, as determined by TGA. The pyrolysis liquid produced by co-pyrolysis spontaneously separated into an organic oil and an aqueous fraction. The yield of the organic oil fraction was considerably reduced (- 11.5 wt%) compared to that of the regular experiment, while that of the aqueous fraction strongly increased (+ 12.8 wt%). As a result, the energy recovery from the initial biomass-polymer mixture in the organic oil fraction was also significantly lower. An overview of the water and energy content of the pyrolysis liquids is shown in Table 4-10.

Table 4-10: Properties of the organic and aqueous fractions produced by flash co-pyrolysis of rapeseed cake with PEG10k at 450 °C, compared to those from regular flash pyrolysis at 450 °C.

Properties	Co-pyrolysis	Regular pyrolysis
Water content (wt%)		
- Organic fraction	7.6 (0.2)	8.4 (0.4)
- Aqueous fraction	26.1 (0.7)	54.6 (0.4)
Absolute mass of water (g)		
- Organic fraction	1.89	3.05
- Aqueous fraction	7.81	9.34
HHV (MJ/kg)		
- Organic fraction	29.7 (0.1)	31.7 (0.1)

The water content of the organic and aqueous fraction was considerably lower than that of both fractions produced by regular flash pyrolysis. However, since only half the amount of rapeseed cake was used in this study and the PEG10k polymer did not contain a considerable amount of residual moisture, it could be better to have a look at the amount of water in the pyrolysis liquid in absolute terms. Co-pyrolysis resulted in a total water amount of 9.70 g, compared to 12.39 g for regular flash pyrolysis. Hence, there was less water in the pyrolysis liquid in case of co-pyrolysis. However, since only half the amount of rapeseed cake was used in co-pyrolysis, it was expected to find only half the amount of water (6.19 g) as well. Since an additional amount of 3.51 g water was found, this had to be originating from PEG10k. This additional amount of water could be produced by esterification of the fatty acids with alcohols formed by decomposition of PEG10k. However, GC/MS analysis of the organic and aqueous fractions revealed that most of the PEG10k was decomposed in medium to long fragments of ether compounds instead of in alcohols needed for esterification. Moreover, long-chain fatty acids were identified as major compounds of the organic oil fraction. Therefore, it is concluded that there is no significant reaction between the free fatty acids and the degradation products of PEG10k. The additional amount of water can be explained by the elimination of water from the PEG10k fragments. Despite the lower water content, the organic oil fraction produced by co-pyrolysis had a slightly lower HHV. The high amount of ether fragments might also explain this observation.

4.3 Slow pyrolysis of rapeseed cake: Collection of the pyrolysis liquid in fractions as a function of pyrolysis temperature

Slow pyrolysis is performed at much lower heating rates and with longer vapor residence times than flash pyrolysis [15, 24]. Moreover, the biomass sample is not almost instantly converted into pyrolysis products, but decomposes gradually over a longer period of time. As a result, the pyrolysis liquid can be collected in fractions as a function of increasing pyrolysis temperature. In this way, valuable information on the pyrolytic behavior of the biomass components as a function of temperature can be obtained.

4.3.1 Experimental setup and observations

Slow pyrolysis of rapeseed cake was performed in a lab-scale reactor setup as described in section 2.2.2. The condensation vessel, equipped with a valve at the bottom, allowed the collection of the pyrolysis liquid in fractions as a function of pyrolysis temperature. During the experiment, the appearance of the collected pyrolysis liquid was visually monitored between 195 and 550 °C. Once a change in color or viscosity was observed, the liquid fraction was removed from the condensation vessel via the valve and the collection of a new fraction could start. In this way, five liquid fractions were obtained. An overview of the visual appearance and the temperature range in which each fraction was collected is shown in Table 4-11.

Table 4-11: Visual appearance of the liquid fractions collected as a function of temperature during slow pyrolysis of rapeseed cake.

Fract.	T (°C)	Visual appearance of the liquid fractions
1	195 – 210	Clear aqueous liquid
2	210 – 265	Yellow-brown aqueous liquid
3	265 – 350	First white to grey fume is condensed into liquid
4	350 - 400	First viscous dark brown drops are collected together with clear liquid resulting in a two-phased liquid
5	400 - 550	Mainly dark brown drops are condensed into pyrolysis liquid (two-phased liquid)

4.3.2 Product yield and properties of the liquid fractions

Slow pyrolysis of rapeseed cake up to 550 °C resulted in a solid yield of 28.0 wt%, a total liquid yield of 48.2 wt% and a gas yield of 23.8 wt% (determined by difference). Compared to flash pyrolysis at 550 °C (section 4.1.1), slow pyrolysis gave rise to a higher solid yield (+ 11.0 wt%), mainly at the expense of the liquid yield (- 10.0 wt%), while the gas yield (- 1.0 wt%) was hardly affected. The yield and some physical properties of each liquid fraction collected as a function of temperature during slow pyrolysis are shown in Table 4-12.

Table 4-12: Yield and properties of the liquid fractions collected as a function of temperature during slow pyrolysis of rapeseed cake up to 550 °C.

Fract.	T (°C)	Type	Yield (wt%)	Water content (wt%)	pH-value (20 °C)
1	195 - 210	Aqueous	2.6	87.3 (1.1)	3.4
2	210 - 265	Aqueous	4.3	72.6 (1.1)	4.2
3	265 - 350	Aqueous	1.9	72.1 (1.1)	6.0
4	350 - 400	Aqueous	8.6	59.7 (1.3)	9.2
		Organic	6.5	18.6 (0.2)	9.0
5	400 - 550	Aqueous	1.4	42.5 (1.3)	9.3
		Organic	22.9	4.9 (0.3)	9.0

Fractions 1, 2 and 3 (195 – 350 °C) were single-phased liquids with a very high water content. Their cumulative yield (8.8 wt% in absolute terms) suggested that pyrolysis of rapeseed cake was rather limited below 350 °C. Fractions 4 and 5 (350 - 550 °C) were two-phased liquids that spontaneously separated into an organic oil and an aqueous fraction. Fraction 4 was considered as a transition fraction since it consisted of both a clear aqueous and a dark brown oily liquid. In contrast, fraction 5 was almost completely composed of dark brown oily liquid that was mainly collected at a pyrolysis temperature below about 480 °C.

4.3.3 Chemical composition of the liquid fractions

Each liquid fraction was characterized by GC/MS for a better understanding of the pyrolytic behavior of rapeseed cake (Figure 4-11). The major compounds (based on peak area) are listed in Table 4-13.

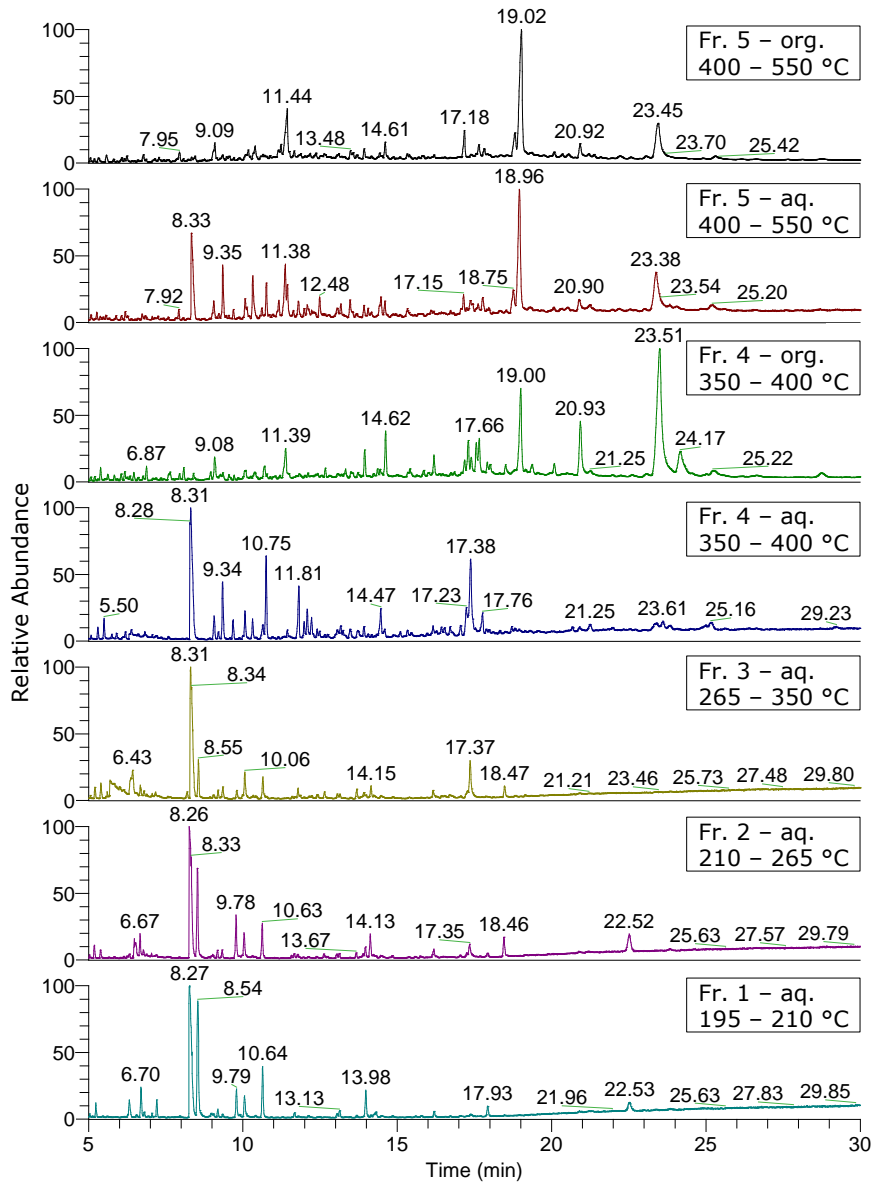


Figure 4-11: GC/MS chromatograms of the aqueous (aq.) and organic (org.) liquid fractions collected as a function of temperature during slow pyrolysis of rapeseed cake up to 550 °C.

Table 4-13: GC/MS analysis of the liquid fractions produced by slow pyrolysis of rapeseed cake with collection of the pyrolysis liquid as a function of temperature. Compound abundance is given as peak area (%) in the chromatogram. RT: retention time (min).

RT	Compound	Pyrolysis liquid fraction						
		1 aq.	2 aq.	3 aq.	4 aq.	5 aq.	5 org.	
5.27	3-penten-2-ol	0.99	0.98	0.95	0.52	-	0.44	-
5.47	Pyridine	0.16	0.75	1.25	1.00	0.57	0.15	-
5.66	Propylbenzene	-	-	-	-	0.38	0.11	-
5.88	4-methylpyridine	-	0.20	-	0.33	0.27	0.30	-
6.14	N,N-dimethylaminoethanol	-	-	3.57	-	-	-	-
6.39	Methylpyrazine	-	-	-	1.42	-	-	-
6.67	1-hydroxy-2-propanone	2.80	2.04	0.80	-	-	-	-
6.82	4-methoxy-1-butanol	-	0.85	-	1.03	-	-	-
6.86	Butylbenzene	-	-	-	-	0.63	0.14	0.15
7.58	2-methyl-2-cyclopenten-1-one	-	-	-	0.14	-	-	-
8.33	Acetic acid	24.21	21.58	22.11	14.52	0.31	7.78	0.14
8.55	3-furaldehyde	14.46	8.59	3.55	-	-	-	-
9.04	1-(2-furanyl)-ethanone	0.53	-	0.50	0.51	-	-	-
9.07	2-methyl-4-hexyne-3-one	-	-	-	1.35	-	-	-
9.21	3-methoxy-1-butanol	0.82	0.69	0.79	-	-	0.25	-
9.35	Propanoic acid	0.39	0.88	1.50	3.17	-	2.84	-
9.78	5-methyl-2-furancarboxaldehyde	3.39	4.18	0.92	-	-	-	-
10.32	Butanoic acid	-	-	-	1.28	0.91	3.07	-

T_{fract. 1}: 195 – 210 °C; T_{fract. 2}: 210 – 265 °C, T_{fract. 3}: 265 – 350 °C; T_{fract. 4}: 350 – 400 °C and T_{fract. 5}: 400 – 550 °C

Table 4-13: Continued.

RT	Compound	Pyrolysis liquid fraction						
		1 aq.	2 aq.	3 aq.	4 aq.	5 aq.	5 org.	
10.65	3-furanmethanol	4.84	3.26	2.19	1.15	-	-	-
10.76	3-methylbutanoic acid	-	-	-	4.85	-	2.20	-
11.38	8-heptadecene	-	-	-	-	2.25	4.11	7.67
11.80	Acetamide	-	-	0.96	3.32	-	1.20	-
12.08	4-methylpentanoic acid	-	-	-	1.80	0.56	0.71	-
12.23	Propanamide	-	-	-	1.55	-	-	-
12.40	2-hydroxy-3-methyl-2-cyclopenten-1-one	-	-	-	0.54	-	-	-
12.64	4-methoxyphenol	-	0.62	0.86	0.24	0.52	-	-
13.47	Heptanoic acid	-	-	-	0.73	0.41	1.16	0.54
13.92	Phenol	-	0.54	0.61	0.74	1.31	-	0.80
14.43	Octanoic acid	-	-	-	-	0.63	0.65	0.38
14.60	4-methylphenol	-	-	-	0.42	2.62	1.25	1.56
15.38	2-ethylphenol	-	-	-	-	0.62	0.27	0.35
15.56	4-hydroxy-2-methylacetophenone	-	0.27	-	-	0.14	-	-
16.16	2,6-dimethoxyphenol	-	-	1.37	0.97	1.35	-	-
16.54	Glycerin	-	-	-	0.73	-	-	-
16.74	1,2,4-triazine-3,5-dione	-	-	-	0.84	-	0.36	-
17.15	Hexadecanenitrile	-	-	-	-	0.93	0.98	2.59

T_{fract. 1}: 195 – 210 °C; T_{fract. 2}: 210 – 265 °C, T_{fract. 3}: 265 – 350 °C; T_{fract. 4}: 350 – 400 °C and T_{fract. 5}: 400 – 550 °C

Table 4-13: Continued.

RT	Compound	Pyrolysis liquid fraction						
		1 aq.	2 aq.	3 aq.	4 aq.	5 org.		
17.27	1,2,3-trimethoxy-5-methylbenzene	-	-	1.14	-	2.28	-	-
17.38	3-piridinol	-	2.63	5.67	8.66	1.25	-	-
17.56	Indole	-	-	-	-	1.98	-	0.20
17.64	Methyl-9-octadecenoate	-	-	-	-	2.62	-	1.52
17.76	2,5-pyrrolidinedione	-	-	-	2.10	-	1.34	-
18.46	3,5-dimethoxyacetophenone	-	2.30	-	-	-	-	-
18.75	Octadecanenitrile	-	-	-	-	-	2.37	3.31
18.96	9-octadecenitrile	-	-	-	-	7.29	13.71	20.91
20.90	Hexadecanoic acid	-	-	-	-	-	1.58	2.63
23.06	Octadecanoic acid	-	-	-	-	0.50	-	0.60
23.38	9-octadecenoic acid	-	-	-	1.74	25.14	6.87	11.13
24.17	9,12-octadecadienoic acid	-	-	-	-	5.59	-	-
25.22	Methyl-9,12,15-octadecatrienoate	-	-	-	-	1.62	-	-
28.73	9-octadecenamide	-	-	-	-	1.09	-	-
Cumulative peak area (%):		52.59	50.36	48.74	55.65	63.77	53.84	54.48
Number of compounds:		10	16	17	27	27	24	16

T_{fract. 1}: 195 – 210 °C; T_{fract. 2}: 210 – 265 °C, T_{fract. 3}: 265 – 350 °C; T_{fract. 4}: 350 – 400 °C and T_{fract. 5}: 400 – 550 °C

Since it was impossible to list all identified compounds, these compounds were categorized into 12 classes of compounds as described in sections 4.1.2.2 and 4.1.3.2. An overview for each liquid fraction is shown in Figure 4-12.

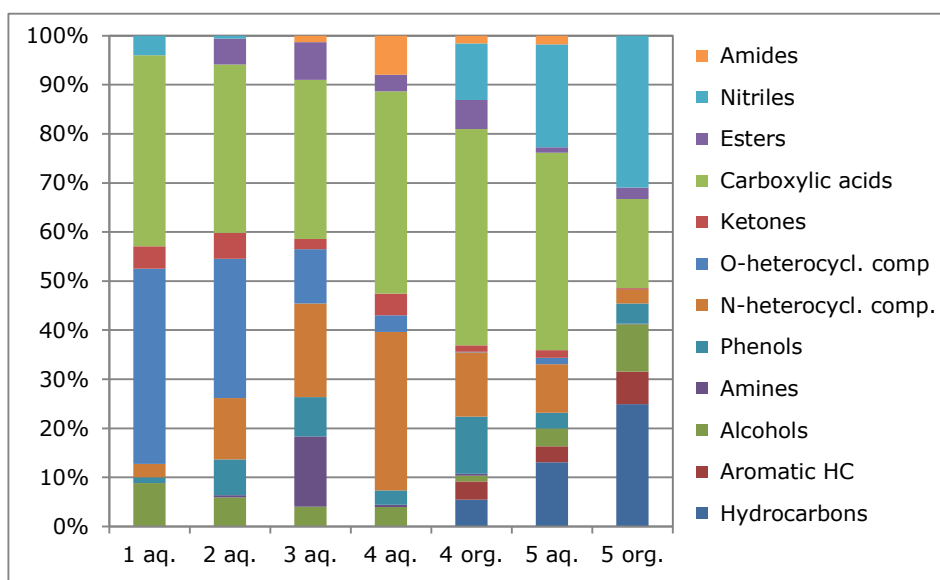


Figure 4-12: Overview of the classes of compounds present in the aqueous (aq.) and organic (org.) liquid fractions collected as a function of temperature during slow pyrolysis of rapeseed cake.

Fraction 1, collected between 195 – 210 °C, had a very high water content (87.3 wt%). As a result, this aqueous fraction contained only a minor amount of water soluble organic compounds. The O-heterocyclic compounds and carboxylic acids were found as principal classes of compounds (Figure 4-12). The former class was mainly composed of furan-derivatives (e.g. 3-furaldehyde (RT: 8.55 min) and 3-furanmethanol (RT: 10.65 min)), while acetic acid (RT: 8.33 min) was the major compound of the latter class (Table 4-13). These compounds were considered as degradation products of hemicellulose [15], indicating that decomposition of this component already occurred at 195 °C. The high amount of short-chain organic acids could also explain the low pH-value of 3.4 found for this fraction.

Fraction 2 (210 – 265 °C) had a significant lower water content (- 14.7 wt%) than fraction 1. Again, carboxylic acids and O-heterocyclic compounds were

found as most abundant classes, while the amount of N-heterocyclic compounds, phenols and esters increased compared to fraction 1.

In case of **fraction 3** (265 – 350 °C), the amount of O-heterocyclic compounds further decreased, while the classes of N-heterocyclic compounds and amines considerably increased. This suggests that hemicellulose degradation was almost complete, while decomposition of the biomass proteins became more and more pronounced. The latter could explain the increase of the pH-value from 4.2 to 6.0. However, carboxylic acids still were the most dominant class of compounds, indicating that acetic acid was not only formed by the deacetylation of hemicellulose components [15], but also by degradation of other biomass components.

Fraction 4 (350 – 400 °C) was a two-phased liquid that spontaneously separated into an aqueous (8.6 wt%) and an organic oil fraction (6.5 wt%). The aqueous fraction was mainly composed of carboxylic acids, N-heterocyclic compounds and amides. In case of the organic oil fraction, carboxylic acids were also the most abundant class of compounds next to the phenols and nitriles, while the amount of N-heterocyclic compounds was less pronounced compared to the aqueous fraction. Table 4-13 shows that the carboxylic acids of the aqueous fraction were mainly short-chain organic acids (e.g. acetic acid), while those of the organic oil fraction predominantly consisted of long fatty acids (e.g. 9-octadecenoic acid (RT: 23.38 min)). This indicates that the degradation of the biomass triglycerides only started at about 350 °C.

The long-chain fatty acids, which are much less polar than short-chain fatty acids, are believed to cause the phase separation of the pyrolysis liquid. Moreover, GPC analysis of the organic oil fraction did not reveal the presence of triglycerides, indicating that these components were completely decomposed under slow pyrolysis conditions (Figure 4-13). This result is different from the observation of flash distillation of the biomass triglycerides during flash pyrolysis of rapeseed cake at temperatures above 400 °C (section 4.1.2.3). A comparison between the GPC chromatograms of the organic oil fractions produced by flash pyrolysis and the organic fractions 4 and 5 from slow pyrolysis is shown in Figure 4-13. The alkaline pH-values of the aqueous and organic oil fraction were assigned to the high amount of N-containing compounds.

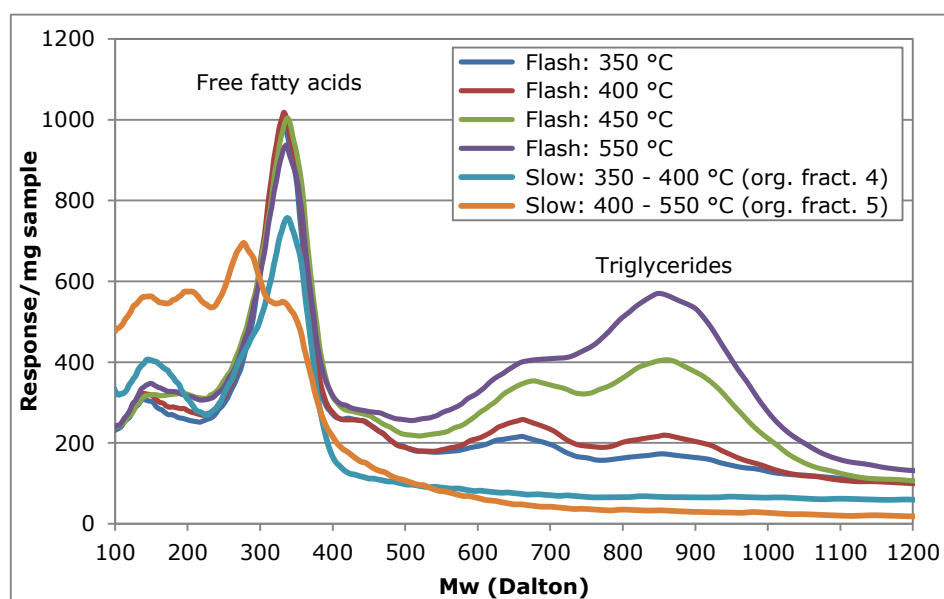


Figure 4-13: GPC chromatograms of the organic oil fractions produced by flash pyrolysis at different temperatures compared to those of the organic fractions 4 and 5 from slow pyrolysis of rapeseed cake.

Fraction 5 (400 – 550 °C) was also a two-phased liquid. However, the yield of the organic oil fraction (22.9 wt%) was much larger than that of the aqueous fraction (1.4 wt%). This shows that triglyceride decomposition mainly occurred above 400 °C. In the organic oil fraction, nitriles and hydrocarbons became the most dominant classes, while the amount of carboxylic acids was strongly reduced. The nitriles were believed to be formed by reaction of the fatty acids with in-situ formed ammonia or amines, followed by a dehydration step with amides as intermediate product (see also section 4.4.3.2, p. 166). The low water content of the organic oil fraction (4.9 wt%) supported this hypothesis. Additionally, no triglycerides were found by GPC analysis (Figure 4-13). In case of the aqueous fraction, carboxylic acids and nitriles were the principal classes, while the N-heterocyclic compounds were less dominant compared to the aqueous fraction 4.

4.4 Slow catalytic pyrolysis of rapeseed cake: Product yield and characterization of the pyrolysis liquid

The observations and conclusions of this section have been orally presented on the IV International Symposium on Energy from Biomass and Waste (2012) in Venice – Italy and submitted for publication in Biomass & Bioenergy:

Slow catalytic pyrolysis of rapeseed cake: Product yield and characterization of the pyrolysis liquid;
K. Smets, A. Roukaerts, J. Czech, S. Schreurs, R. Carleer, J. Yperman;
Biomass and Bioenergy (accepted)

Flash pyrolysis at higher pyrolysis temperatures (450 and 550 °C) has already been demonstrated to be very promising in converting rapeseed cake into an organic oil fraction with potential as renewable fuel (section 4.1). However, upgrading of the pyrolysis liquid turns out to be still necessary to meet the quality standards of conventional petroleum-derived fuels [25, 26].

In essence, upgrading of pyrolysis liquids corresponds to performing a deoxygenation step. Catalytic hydrotreating and catalytic upgrading are two commonly used methods [26, 27]. Catalytic hydrotreating (at high hydrogen pressure) releases oxygen as water and results in a hydrogenation and hydrocracking of high molecular weight compounds [27]. On the other hand, catalytic upgrading (atmospheric pressure) can be carried out both *after* (as post-treatment) or *during* the production of pyrolysis liquid in a special designed reactor (in-situ setup). From an economic point of view, the latter technique is favorable since it eliminates costly condensation and re-evaporation steps [28]. Catalysts used for upgrading of pyrolysis liquid can be categorized into four main classes: activated alumina, molecular sieve catalysts, sodium carbonate and transition metal catalysts [29]. Catalyst acidity, pore size and shape selectivity are important characteristics that strongly affect the yield and composition of the pyrolysis liquids [30, 31].

In this section, the opportunities of slow catalytic pyrolysis to convert rapeseed cake into a renewable liquid fuel are investigated. Despite flash pyrolysis is known to result in higher liquid yields, slow pyrolysis is preferred for three reasons. Firstly, review of literature indicates that triglycerides are too big to enter the pores (0.56 nm) of the HZSM-5 catalyst (a commonly used cracking catalyst) [30, 31]. Since the biomass triglycerides are found to be rather completely decomposed into (mainly) fatty acids by slow pyrolysis (section 4.3)

than flash distilled during flash pyrolysis (section 4.1), slow pyrolysis is more convenient to perform the (preliminary) tests. Secondly, the flash pyrolysis reactor setup used in this study is believed not to be suitable to test in-situ catalytic upgrading in ex-bed mode due to the large amount of pyrolysis vapors that have to be handled. Moreover, extensive modifications are required to mount catalysts as a fixed-bed at the exhaust of the flash pyrolysis reactor without pressure build-up and keeping gas catalytic conditions. Thirdly, the solid residue of slow (catalytic) pyrolysis also has potential as precursor in the production of activated carbon. In this regard, rapeseed cake can be a source of renewable fuel (via the organic oil fraction) and of a precursor of activated carbon (via the solid residue). In case of flash pyrolysis, separation of the solid residue from the sand (used as heat transfer medium) is required, but has already been demonstrated to be problematic for rapeseed cake.

4.4.1 Experimental setup and catalyst characteristics

Slow catalytic pyrolysis of rapeseed cake was performed in a batch slow catalytic reactor setup. For more details on the experimental setup and the design of the horizontal tubular quartz reactor is referred to section 2.2.4. Based on literature [29], three types of catalysts with particular characteristics were selected (Table 4-14). The HZSM-5 zeolite is a crystalline and shape selective catalyst with high strength Brønsted acid sites and some Lewis acid sites [31]. Na_2CO_3 is an amorphous alkaline catalyst, while $\gamma\text{-Al}_2\text{O}_3$ is an amorphous acidic catalyst without shape selectivity. The catalysts were tested in two configuration modes: in-bed and ex-bed mode. In case of in-bed mode, rapeseed cake and catalyst were premixed and placed in the same reactor compartment. On the other hand, there was no direct contact between rapeseed cake and catalyst when tested in ex-bed mode. Hence, the rapeseed cake was loaded in the first reactor compartment, while the catalyst was placed as fixed bed in the second reactor compartment (see Figure 2-3). The HZSM-5 and $\gamma\text{-Al}_2\text{O}_3$ catalysts were tested in both ex-bed and in-bed mode, while Na_2CO_3 was only tested in in-bed mode.

Table 4-14: Catalyst characteristics used in slow catalytic pyrolysis of rapeseed cake up to 550 °C.

Catalyst	Form	Acidity	Configuration mode
HZSM-5	Pellets	Strong acidic	In-bed and ex-bed mode
γ -Al ₂ O ₃	Pellets	Acidic-neutral	In-bed and ex-bed mode
Na ₂ CO ₃	Powder	Alkaline	In-bed mode

Firstly, the influence of catalyst type and configuration on the product yield and energy recovery are discussed. Then, important physicochemical properties of the organic oil fractions are determined to evaluate their potential as renewable fuel. Finally, the chemical composition of both organic oil and aqueous fractions is investigated by complementary analytical techniques to gain a better understanding of the effect of the catalysts on the conversion of rapeseed cake under slow pyrolysis conditions.

4.4.2 Product yield and energy recovery

Slow catalytic pyrolysis of rapeseed cake was performed up to 550 °C in order to evaluate the effect of catalyst type and/or configuration on the product yield and energy recovery. Results are presented in Table 4-15. The non-catalytic test was included as a reference test to determine the effect of thermal cracking without catalyst.

Slow pyrolysis of rapeseed cake without catalyst resulted in a solid residue of 27.9 wt%. Hence, 72.1 wt% of the rapeseed cake was converted into pyrolysis liquid, tar and gas. Ex-bed tested γ -Al₂O₃ and HZSM-5 could not affect the biomass conversion since these catalysts were not in direct contact with the rapeseed cake. Using these catalysts in in-bed mode slightly increased the biomass conversion in case of γ -Al₂O₃, while no significant effect was observed for HZSM-5. In-bed Na₂CO₃ considerably reduced the solid yield (- 4.0 wt%)¹¹, while the gas yield strongly increased (+ 9.5 wt%) compared to the non-catalytic experiment.

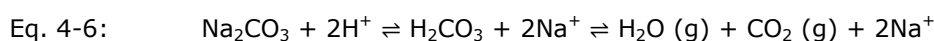
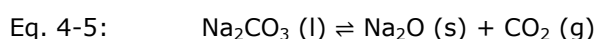
¹¹ In case of in-bed tested catalysts, the solid yield was calculated by subtracting the mass of the catalyst before the experiment from the mass of the solid residue/catalyst mixture after the experiment. Hence, it was assumed that there was no decomposition or loss of the catalyst.

Table 4-15: Product yield and energy recovery obtained by slow catalytic pyrolysis of rapeseed cake up to 550 °C (SD between brackets).

Product yield (wt%)	No catalyst		Y-Al ₂ O ₃		Y-Al ₂ O ₃		HZSM-5		HZSM-5		Na ₂ CO ₃	
			ex-bed	in-bed	ex-bed	in-bed	ex-bed	in-bed	ex-bed	in-bed	ex-bed	in-bed
Solid residue	27.9 (1.0)		27.5 (0.4)	26.2 (0.4)	28.0 (0.3)	27.8 (0.3)	28.0 (0.3)	27.8 (0.5)	23.9 (0.6)			
Char	23.0 (1.0)		22.6 (0.4)	21.3 (0.4)	23.1 (0.3)	22.9 (0.3)	22.9 (0.5)	19.0 (0.6)				
Asph ^a	4.9		4.9	4.9	4.9	4.9	4.9	4.9				
Pyrolysis liquid	47.1 (1.2)		40.8 (0.5)	48.4 (0.6)	44.9 (0.8)	44.6 (5.9)	41.8 (0.9)					
Organic fraction	35.7 (1.1)		21.3 (1.0)	35.3 (2.1)	23.3 (0.9)	27.1 (6.0)	20.8 (0.0)					
Aqueous fraction	11.4 (0.1)		19.5 (1.5)	13.1 (1.5)	21.6 (0.1)	17.5 (0.0)	21.0 (1.0)					
Tar	1.2 (0.4)		2.6 (1.6)	1.1 (0.0)	1.5 (0.7)	2.9 (2.5)	1.0 (0.7)					
Gas ^b	23.8 (0.2)		29.1 (0.7)	24.3 (1.0)	25.6 (0.4)	24.7 (3.9)	33.3 (0.3)					
Biomass conversion ^c	72.1		72.5	73.8	72.0	72.2	76.1					
Energy recovery (%)												
Solid residue	25.2		24.4	23.2	25.0	22.5	21.3					
Organic fraction	43.1		26.9	44.2	34.9	35.5	31.6					

^a Determined by TGA of the biomass; ^b Calculated by difference; ^c Calculated as: 100% - %solid residue

The lower solid yield for in-bed Na_2CO_3 was not in accordance with literature, i.e. the Na_2CO_3 catalyst is reported to increase char formation [32]. On the other hand, Na_2CO_3 is also used as an activation agent to convert solid residue (char) into activated carbon [33]. Since the slow catalytic pyrolysis was performed at a relatively high temperature (550 °C for 30 min), part of the solid residue could be gasified by reaction with Na_2CO_3 , explaining the lower yield of solid residue. Additionally, although thermal decomposition of pure Na_2CO_3 (equation 4-5) is reported not to occur below its melting point at about 850 °C [34], the direct contact between catalyst and solid residue or reaction with protons originating from the degradation of biomass components (equation 4-6) could enhance the decomposition of Na_2CO_3 . As a result, an apparently lower solid yield and a higher gas yield could be obtained compared to the non-catalytic test.



A liquid yield of 47.1 wt% and a gas yield of 23.8 wt% were found for the non-catalytic test. Addition of a catalyst significantly reduced the liquid yields in favor of the gas yields in all cases, except for in-bed $\gamma\text{-Al}_2\text{O}_3$. These observations indicate that (most) catalysts interacted with the pyrolysis vapors and cracked them into smaller compounds. These low molecular weight compounds could not be condensed anymore into pyrolysis liquid and left the reactor setup as pyrolysis gas. This cracking was found to be most dominant for ex-bed tested $\gamma\text{-Al}_2\text{O}_3$ and in-bed tested Na_2CO_3 , while other catalysts increased the gas yield only to a lesser extent.

All pyrolysis liquids spontaneously separated into an organic oil and a water-rich aqueous fraction. Without catalyst, an organic oil fraction of 75.8 wt% and an aqueous fraction of 24.2 wt% were obtained after phase separation. The presence of a catalyst considerably reduced the yield of the organic oil fraction (except for in-bed $\gamma\text{-Al}_2\text{O}_3$) in favor of the yield of the aqueous fraction (Table 4-15). The largest decreases in organic oil yield were found for in-bed Na_2CO_3 (-14.9 wt%), ex-bed $\gamma\text{-Al}_2\text{O}_3$ (-14.4 wt%) and ex-bed HZSM-5 (-12.4 wt%). The increased yield of the aqueous fractions was found to be mainly caused by a higher (absolute) amount of water, regardless the catalyst (see also the remark

in section 4.4.4.2, p. 177). This indicates that the pyrolysis vapors were not only catalytically cracked into smaller compounds (resulting in lower organic oil yields), but also that dehydration reactions were much more pronounced in presence of the catalysts.

Tar yields were low for all experiments. Only in-bed HZSM-5 and ex-bed $\gamma\text{-Al}_2\text{O}_3$ resulted in a slightly higher tar yield compared to the non-catalytic test.

The energy recovery was calculated by equation 4-1 (section 4.1.1). Without catalyst, 25.2 % of the energy of the rapeseed cake was recovered in the solid residue by slow pyrolysis. Similar results (as expected) were found for the ex-bed tested catalysts, while the in-bed tested catalysts slightly reduced the energy recovery in the solid residue compared to the non-catalytic test. About 43.1 % of the initial biomass energy was recovered in the organic oil fraction without catalyst. This energy recovery was significantly reduced for the catalytic experiments, except for in-bed $\gamma\text{-Al}_2\text{O}_3$.

It can be concluded that in-bed $\gamma\text{-Al}_2\text{O}_3$ is the only catalyst that performs slightly better than the non-catalytic test in terms of liquid yield and energy recovery, although HZSM-5 (both in-bed and ex-bed) also performs well. However, besides yield and energy recovery, physicochemical properties are also important to evaluate catalyst use in the production of renewable fuels. Therefore, the organic oil and aqueous fractions of the pyrolysis liquids are investigated by complementary analytical techniques (sections 4.4.3 to 4.4.4).

4.4.3 Characterization of the organic oil fraction

4.4.3.1 Physicochemical properties

The physicochemical properties of the organic oil fractions were investigated in order to determine their potential to be valorized as renewable fuels or fuel additives. Results are shown in Table 4-16.

Table 4-16: Physicochemical properties of the organic oil fractions produced by slow (catalytic) pyrolysis of rapeseed cake up to 550 °C (SD between brackets).

Properties	No catalyst	Y-Al ₂ O ₃		Y-Al ₂ O ₃		HZSM-5		HZSM-5		Na ₂ CO ₃	
		ex-bed	in-bed	ex-bed	in-bed	ex-bed	in-bed	ex-bed	in-bed	ex-bed	in-bed
Elemental analysis (wt%)											
C	61.5 (2.4)	69.9 (2.3)	62.5 (0.9)	73.1 (0.7)	65.4 (0.4)	72.8 (0.6)					
H	9.1 (0.4)	10.2 (0.4)	8.9 (0.2)	10.4 (0.8)	9.2 (0.2)	9.5 (0.7)					
N	5.1 (0.2)	5.1 (0.4)	4.4 (0.2)	5.9 (0.2)	4.4 (0.3)	5.6 (0.1)					
S	0.6 (0.5)	0.8 (0.8)	0.4 (0.1)	0.8 (1.2)	0.5 (0.1)	0.6 (0.3)					
O ^a	23.7	14.0	23.8	9.8	20.5	11.5					
H/C molar ratio	1.76	1.73	1.69	1.70	1.68	1.55					
O/C molar ratio	0.29	0.15	0.29	0.10	0.24	0.12					
Water content (wt%)	14.9 (1.4)	14.6 (2.3)	22.1 (1.7)	6.3 (0.9)	15.5 (2.5)	2.3 (0.3)					
HHV (MJ/kg)	29.2 (1.3)	30.6 (0.8)	30.3 (0.1)	36.2 (0.4)	31.7 (0.2)	36.8 (1.0)					
pH (20 °C)	7.8	8.0	7.3	8.2	6.9	8.6					
Density (g/mL)	0.98	0.97	0.98	0.96	0.98	0.97					
Kinematic viscosity (cSt)	701	156	ND	116	ND	85					

^a Calculated by difference; ND: not determined.

Slow pyrolysis of the rapeseed cake without catalyst resulted in an organic oil fraction with a higher carbon (+ 6.5 wt%) and hydrogen (+ 1.3 wt%) content compared to the initial rapeseed cake, while the oxygen content was significantly lower (- 7.4 wt%). Addition of a catalyst strongly affected the elemental composition of the organic oil fractions. The carbon and hydrogen contents were considerably increased by both ex-bed tested catalysts and in-bed Na_2CO_3 , while the oxygen contents were significantly reduced. The in-bed tested HZSM-5 and $\gamma\text{-Al}_2\text{O}_3$ catalysts turned out to be much less effective in improving the elemental composition of the organic oil fractions. The oxygen removal was found to be most pronounced for ex-bed HZSM-5 (- 13.9 wt%) and in-bed Na_2CO_3 (- 12.2 wt%), resulting in oxygen contents of respectively 9.8 and 11.5 wt%. This catalytic deoxygenation was believed to be mainly achieved by dehydration, decarbonylation and decarboxylation reactions [35]. Despite of these significant reductions, not all oxygenated compounds could be removed from the organic oil fractions by the catalysts mentioned above. The contents of nitrogen and sulfur, both undesirable elements in fuels, were slightly reduced by in-bed HZSM-5 and in-bed $\gamma\text{-Al}_2\text{O}_3$, while the other catalysts resulted in a slightly higher content of these elements. However, the amount of sulfur remained quite low compared to fuel oil nos. 4 and 6 (1.5 – 4.0 wt%) [36]. Moreover, it should be noted that the determination of the sulfur content was not very accurate, as indicated by the high standard deviation.

The non-catalytic organic oil fraction had a water content of 14.9 wt% and a HHV of 29.2 MJ/kg. Ex-bed HZSM-5 and especially in-bed Na_2CO_3 drastically reduced the water content to 6.3 wt% and 2.3 wt%, respectively. These low water contents, together with the relatively low oxygen contents, gave rise to HHVs of 36.2 and 36.8 MJ/kg, respectively. These values were rather high for pyrolysis oils derived from biomass feedstock and came close to these of petroleum-derived fuels (about 43 – 46 MJ/kg) [37]. Ex-bed $\gamma\text{-Al}_2\text{O}_3$ slightly reduced the water content of the organic oil fraction, while in-bed HZSM-5 and in-bed $\gamma\text{-Al}_2\text{O}_3$ even led to higher water contents. As a result, the calorific values were hardly improved by these catalysts compared to the non-catalytic test.

The pH-values of all organic oil fractions varied between neutral to slightly alkaline. These values are beneficial for the quality of the organic oil fractions because a low acidity results in less corrosion and stability problems during

storage and their use as renewable fuels [32]. The viscosity of the organic oil fractions was significantly reduced by the catalysts. The lowest viscosity (85 cSt) was found for in-bed Na_2CO_3 and was only slightly higher than that of fuel oil no. 6 (65 cSt) [36].

It is concluded that catalyst type and/or configuration (strongly) affect the physicochemical properties of the organic oil fractions. These properties are improved the most by ex-bed HZSM-5 and in-bed Na_2CO_3 , making the corresponding organic oil fractions promising as renewable fuels or fuel additives. In contrast, the in-bed tested HZSM-5 and $\gamma\text{-Al}_2\text{O}_3$ catalysts hardly improve the HHV and the oxygen content of the organic oil fractions, while even (slightly) higher water contents are obtained compared to the non-catalytic test. These results indicate that the **acidic catalysts** (HZSM-5 and $\gamma\text{-Al}_2\text{O}_3$) should preferably be used in **ex-bed mode** in case of slow pyrolysis of rapeseed cake. Additionally, Samolada et al. report that acidic catalysts are preferably used in ex-bed mode to prevent acid-catalyzed polymerization and coke formation reactions as much as possible [28].

4.4.3.2 Chemical composition

The organic oil fractions were analyzed by GC/MS. An overview of the chromatograms is shown in Figure 4-14. Butylated hydroxytoluene (BHT; RT about 13.30 min) was used as an internal standard to allow better comparison of the chromatograms. Since about 230 different compounds were identified in all organic oil fractions together, it was impossible to list them all. Therefore, only a (limited) list of the most important individual compounds (based on peak area normalized against BHT) is shown in Table 4-17. The total absolute peak area was included in this table as an indication of the total area of the chromatogram that was represented by the listed compounds. All identified compounds were classified into 9 categories based on their functional groups, analogously as described in section 4.1.2.2. In this way, the effect of catalyst type and/or configuration on the chemical composition of the organic oil fractions could be investigated. However, it should be noticed that this approach only allowed comparison of the organic oil fractions on a relative basis and not on a biomass

feedstock weight basis. An overview of the classes of compounds present in the organic oil fractions is shown in Figure 4-15.

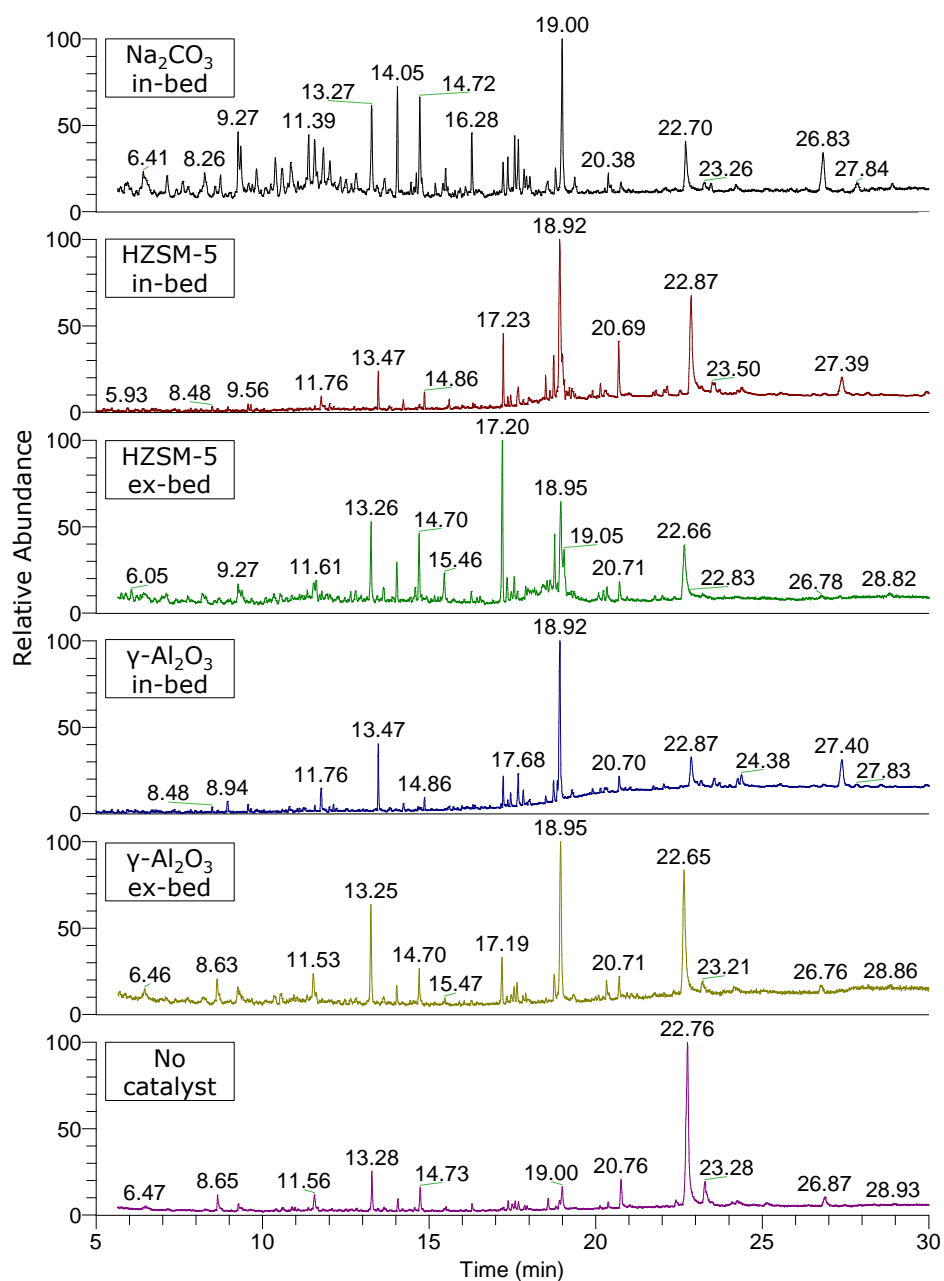


Figure 4-14: GC/MS chromatograms of the organic oil fractions produced by slow (catalytic) pyrolysis of rapeseed cake up to 550 °C.

Table 4-17: Major compounds of the organic oil fractions produced by slow (catalytic) pyrolysis of rapeseed cake up to 550 °C. Compound abundance is given as peak area normalized against BHT (%). RT: retention time (min).

RT	Compound	No catalyst	γ-Al ₂ O ₃		Y-Al ₂ O ₃		HZSM-5		HZSM-5		Na ₂ CO ₃	
			ex-bed	in-bed	ex-bed	in-bed	ex-bed	in-bed	ex-bed	in-bed	ex-bed	in-bed
6.20	4-methylpyridine	-	-	0.03	0.10	0.10	0.08	0.07	0.07			
6.23	Propylbenzene	0.05	-	0.03	0.11	0.11	0.08	0.09	0.09			
6.72	3-dodecene	-	-	0.06	-	-	0.11	-	-			
6.85	Styrene	-	-	0.05	0.10	0.10	0.11	0.21	0.21			
6.93	1-ethyl-2-methylbenzene	-	-	0.04	0.12	0.12	0.08	0.09	0.09			
7.16	1,3,5-trimethylbenzene	-	-	0.01	0.10	0.10	-	0.25	0.25			
7.74	Butylbenzene	-	-	0.03	0.17	0.17	-	0.34	0.34			
8.56	Tetradecane	-	-	0.10	-	-	0.16	0.38	0.38			
8.95	Acetic acid	0.52	0.37	0.26	-	-	-	-	-			
9.27	Pyrrole	0.18	0.22	-	0.23	0.23	0.24	0.56	0.56			
9.64	Pentadecane	-	0.17	0.16	-	-	0.24	0.56	0.56			
9.77	(1,3-dimethylbutyl)-benzene	-	-	-	0.11	0.11	-	0.14	0.14			
9.88	1-pentadecene	-	-	0.07	-	-	-	0.23	0.23			
10.85	3-hexadecene	-	0.23	0.15	-	-	-	-	-			
11.17	3-furanmethanol	0.15	-	0.06	-	-	0.10	-	-			
11.61	Heptadecane	-	-	0.11	-	-	0.13	0.52	0.52			

Table 4-17: Continued.

RT	Compound	No catalyst	Y-Al ₂ O ₃		Y-Al ₂ O ₃ in-bed	HZSM-5		Na ₂ CO ₃ in-bed
			ex-bed	0.59		ex-bed	in-bed	
11.83	8-heptadecene	0.60	0.59	0.56	0.40	0.49	0.66	
13.10	4-methoxyphenol	0.07	-	0.07	-	0.08	0.25	
14.37	Phenol	0.26	0.23	0.17	0.37	0.36	0.79	
14.66	4-ethylphenol	0.03	-	-	-	0.08	0.16	
15.06	4-methylphenol	0.58	0.44	0.23	0.68	0.49	0.88	
15.70	3-ethylphenol	0.09	-	0.05	-	-	0.21	
16.38	2,6-dimethoxyphenol	0.19	0.15	0.07	0.21	0.15	0.57	
17.31	Hexadecanenitrile	0.09	0.47	0.48	1.71	1.94	0.23	
17.45	1,2,3-trimethoxy-5-methylbenzene	0.26	-	0.13	0.26	0.27	0.35	
17.58	Pyridinol	0.20	-	0.27	-	0.31	0.11	
17.68	Indole	0.25	0.18	-	0.27	0.21	0.49	
17.83	Methyl-9-octadecenoate	0.23	0.27	0.74	-	0.58	0.55	
17.87	1,1-dimethoxy-9-octadecene	-	-	0.27	-	0.15	0.22	
18.01	5-methyl-1H-indole	0.11	-	0.05	0.13	0.24	0.14	
18.57	3,4-dimethoxyacetophenone	-	-	0.15	-	0.85	-	
18.91	Octadecanenitrile	0.17	0.31	0.44	0.99	1.72	0.26	
19.11	Octadecanenitrile	0.78	2.61	4.88	3.21	12.21	1.70	
19.29	9-octadecanenitrile	-	-	0.31	-	-	0.22	

Table 4-17: Continued.

RT	Compound	No catalyst	Y-Al ₂ O ₃		HZSM-5		Na ₂ CO ₃	
			ex-bed	in-bed	ex-bed	in-bed	ex-bed	in-bed
20.27	Eicosanenitrile	-	-	0.34	0.17	0.76	0.07	
20.45	2-ethylhexylhexanedioate	0.26	0.30	-	0.26	-	0.24	
20.88	Hexadecanoic acid	0.91	0.35	0.54	0.47	2.32	0.18	
22.87	Octadecanoic acid	0.26	-	-	-	0.36	-	
23.16	9-octadecenoic acid	8.02	3.15	1.96	3.20	10.80	1.43	
23.56	9,12-octadecadienoic acid	1.56	-	-	-	0.58	-	
27.83	9-octadecenamide	0.68	0.22	1.97	0.15	3.89	0.95	
Total absolute peak area (%):		59.0	43.6	50.0	43.8	63.1	47.2	
Number of compounds:		25	17	34	23	32	34	

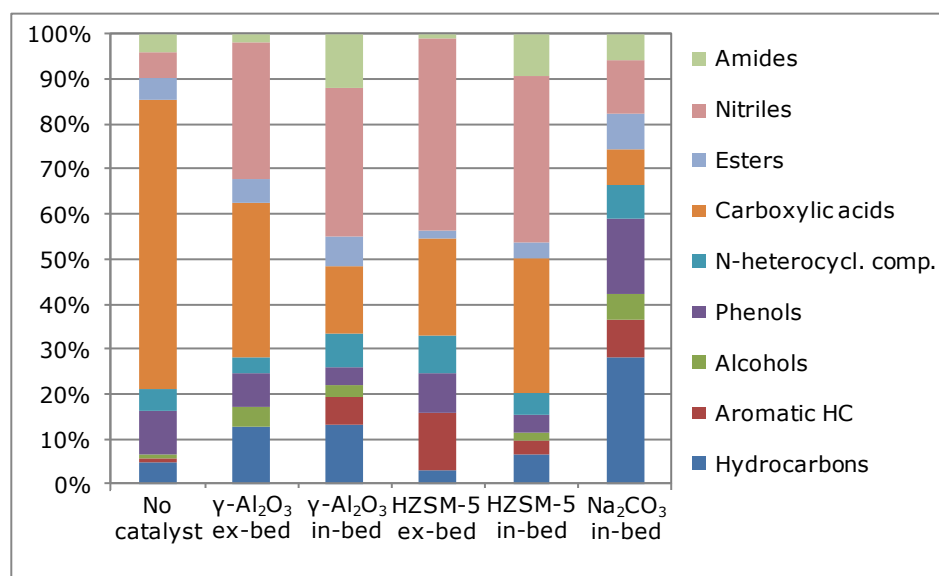


Figure 4-15: Overview of the classes of compounds present in the organic oil fractions produced by slow (catalytic) pyrolysis of rapeseed cake up to 550 °C.

In case of the **non-catalytic oil fraction**, carboxylic acids were found to represent the major class of compounds (Figure 4-15). This class was mainly composed of (unsaturated) fatty acids of which 9-octadecenoic acid (RT: 23.16 min) was the most abundant one (Table 4-17). The fatty acids were assumed to be produced by almost complete thermal degradation of the biomass triglycerides. Thermal conversion of the fatty acids into esters, nitriles or amides was rather limited. The class of phenols consisted of compounds formed by thermal degradation of lignin components present in the rapeseed cake, while the N-heterocyclic compounds originated from the biomass proteins. Esters, nitriles, amides, hydrocarbons, aromatic hydrocarbons and alcohols made up minor classes of compounds and were only formed to a lesser extent by slow pyrolysis without catalyst.

Slow pyrolysis with **ex-bed γ -Al₂O₃** reduced the amount of carboxylic acids (mainly long-chain fatty acids) in favor of nitriles and to a lesser extent of hydrocarbons and alcohols, compared to the non-catalytic test. The nitriles are believed to be formed out of the fatty acids according to a two-step mechanism (Figure 4-16). Firstly, fatty acids are converted into amides by reaction with

ammonia or amines originating from the biomass proteins. Secondly, the formed amides are further converted into nitriles by a dehydration step. Although both reaction steps are reversible, the presence of acidic catalysts (such as $\gamma\text{-Al}_2\text{O}_3$) and the relatively high pyrolysis temperature assist the dehydration step and, as a result, shift the equilibrium towards nitriles [38].

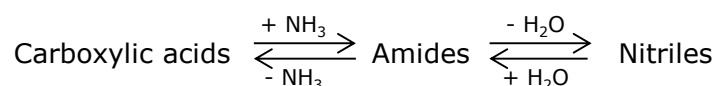


Figure 4-16: Scheme of the acid catalyzed conversion of fatty acids into nitriles in presence of the $\gamma\text{-Al}_2\text{O}_3$ and HZSM-5 catalysts.

The increase in hydrocarbon content is assigned to the decarboxylation of fatty acids, since $\gamma\text{-Al}_2\text{O}_3$ is reported in literature as a very effective decarboxylation catalyst for fatty acids [39]. The formed hydrocarbons, in turn, can be further converted into short-chain hydrocarbons by additional (catalytic) cracking. The amounts of phenols, N-heterocyclic compounds and esters were hardly influenced by *ex-bed* $\gamma\text{-Al}_2\text{O}_3$, while almost no aromatic hydrocarbons were observed.

Testing **$\gamma\text{-Al}_2\text{O}_3$ in *in-bed mode*** strongly affected the chemical composition of the organic oil fraction. The proportion of carboxylic acids and phenols was strongly reduced, while the amount of amides and aromatic hydrocarbons was considerably higher. The larger amide yield may be explained by the higher water content of the organic oil fraction produced in presence of *in-bed* $\gamma\text{-Al}_2\text{O}_3$ (see Table 4-16). As a result, this higher water content slightly opposes the dehydration of amides to form nitriles, explaining the increase of the amide content. The higher amount of aromatic hydrocarbons can be explained by a more pronounced degradation of the phenolic compounds through direct contact between biomass and catalyst.

***Ex-bed* HZSM-5** significantly reduced the amount of carboxylic acids compared to the non-catalytic experiment, whereas nitriles became the major class of compounds. Since HZSM-5 has strong Brønsted acid sites, conversion of fatty acids into nitriles is assumed to occur similarly as described for *ex-bed* $\gamma\text{-Al}_2\text{O}_3$ (Figure 4-16). Giannakopoulou et al. also report this mechanism in their study of HZSM-5, but find a shift of the equilibrium towards fatty acids instead of towards

nitriles [38]. The strong increase in aromatic hydrocarbon content is assigned to the good acid-catalyzed cyclization and aromatization ability of HZSM-5 [35, 40]. The shape selectivity, related to a network of internal pores with well-defined diameters (0.56 nm), is believed to be responsible for these properties [31]. Dupain et al. report that formation of aromatic hydrocarbons is enhanced for triglycerides composed of unsaturated fatty acids [12]. Besides triglycerides, other biomass components such as hemicellulose, cellulose and lignin can also be converted into aromatic hydrocarbons by the HZSM-5 zeolite [35]. The amount of esters and amides was decreased in comparison to the non-catalytic oil fraction, while the amount of N-heterocyclic compounds was slightly increased.

When using **HZSM-5** in **in-bed mode** instead of ex-bed mode, the reduction of the carboxylic acid content was less pronounced. Moreover, lower amounts of nitriles, phenols and aromatic hydrocarbons were found, while the amount of amides strongly increased, compared to ex-bed mode. The higher water content of the organic oil fraction in case of the in-bed tested catalyst (Table 4-16) can explain the latter in a similar way as described for in-bed $\gamma\text{-Al}_2\text{O}_3$.

In-bed Na_2CO_3 reduced the amount of carboxylic acids the most. In contrast to the acidic catalysts, this alkaline catalyst showed a rather small increase of nitriles compared to the non-catalytic test, while the amount of phenols, aromatic hydrocarbons and especially of the non-aromatic hydrocarbons considerably increased. The strong increase of the latter can be explained by following mechanism (Figure 4-17). Firstly, the fatty acids, formed out of biomass triglycerides by thermal cracking, react with Na_2CO_3 to produce salts of fatty acids [41]. Then, these salts further decompose into mainly hydrocarbons and a small amount of aromatic hydrocarbons [42, 43]. The strong increase in phenolic compounds indicated that Na_2CO_3 could favor lignin decomposition compared to the non-catalytic test.

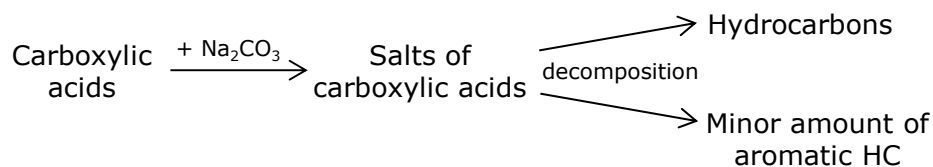


Figure 4-17: Scheme for conversion of fatty acids in presence of the in-bed tested alkaline Na_2CO_3 catalyst.

4.4.3.3 GPC analysis

GPC was performed on the organic oil fractions because compounds with high molecular weights (> 500 Da) such as triglycerides could not be detected by the used GC/MS setup. For the organic oil fraction, produced by slow pyrolysis without catalyst, an intensive peak indicative for fatty acids was observed (around 330 Da), while the triglyceride peak (around 860 Da) was completely absent (Figure 4-18). These observations were different from the results obtained under flash pyrolysis conditions where a prominent triglyceride peak was found (section 4.1.2.3). In case of slow catalytic pyrolysis, the peaks indicative for fatty acids were found to be significantly lower compared to the non-catalytic test, while peaks representing compounds of lower molecular weight were mostly increased. These findings support the hypothesis of thermal decomposition of triglycerides into fatty acids that, in turn, are (partly) converted into lower molecular weight compounds by the tested catalysts.

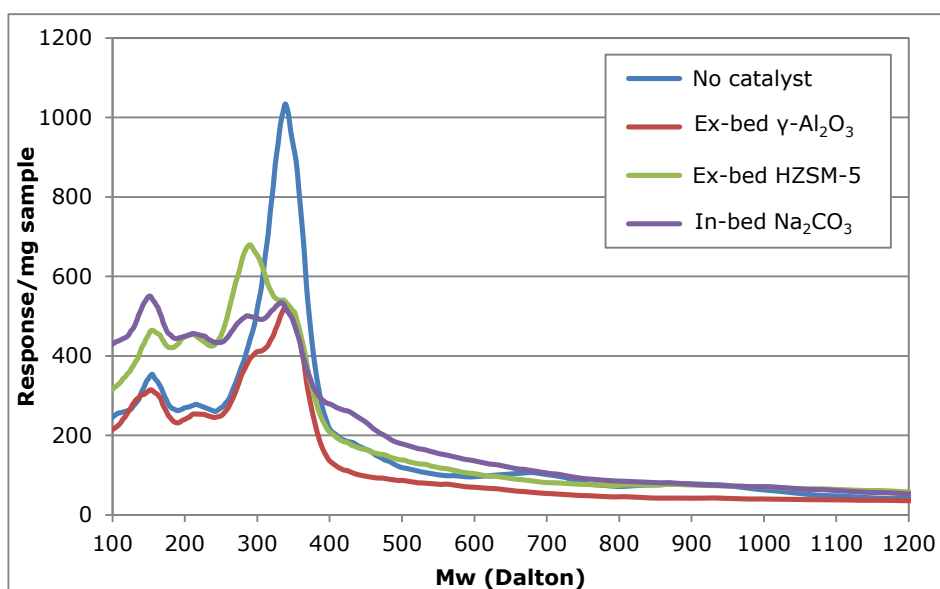


Figure 4-18: GPC chromatograms of the organic oil fractions produced by slow (catalytic) pyrolysis of rapeseed cake up to 550 °C (in-bed $\gamma\text{-Al}_2\text{O}_3$ and in-bed HZSM-5 were not analyzed).

4.4.3.4 FTIR analysis

The functional groups present in the organic oil fractions were also identified by FTIR spectroscopy. An overview is shown in Figure 4-19.

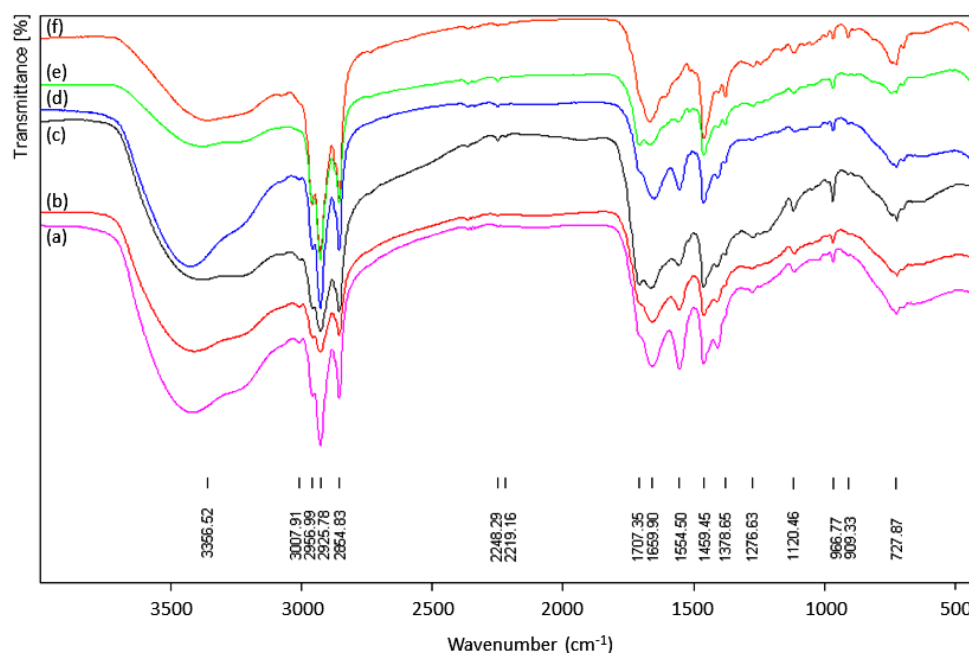


Figure 4-19: FTIR spectra of the organic oil fractions produced by slow (catalytic) pyrolysis of rapeseed cake up to 550 °C: (a) no catalyst, (b) in-bed γ - Al_2O_3 , (c) in-bed HZSM-5, (d) ex-bed γ - Al_2O_3 , (e) ex-bed HZSM-5 and (f) in-bed Na_2CO_3 .

The broad absorption bands between 3600 and 2300 cm^{-1} were assigned to the O-H stretching vibration of water, next to these of carboxylic acid and alcohol functionalities. The intensity of these bands, an indication of the water content of the organic oil fractions, were in accordance with the results found by Karl Fischer titration (Table 4-16). The asymmetric and the symmetric C-H stretching vibrations between 2960 and 2865 cm^{-1} , the C-H deformation vibrations between 1465 and 1375 cm^{-1} and the CH_2 -rocking vibrations around 728 cm^{-1} were indicative of (long) aliphatic chains of fatty acids, their derivatives (esters, amide and nitriles) and hydrocarbons. The C=O stretch band at 1707 cm^{-1} and the C-O stretch band at 1277 cm^{-1} were typical for carboxylic acids and were (mainly) assigned to fatty acids. The absence of bands around 1740 and 1170

cm^{-1} (respectively the C=O and the C-O stretching vibration of esters) confirmed the hypothesis of complete thermal degradation of the biomass triglycerides during slow catalytic pyrolysis of rapeseed cake. The absorption bands between 1675 and 1430 cm^{-1} and the weak bands just above 3000 cm^{-1} , representing the C=C and the Csp²-H stretching vibrations respectively, were indicative of alkenes, aromatic and N-heterocyclic compounds. In this spectral region, some differences in intensity of the bands were observed. However, it was not possible to assign these differences to changes in the proportions of the classes of compounds found by GC/MS (Figure 4-15). The weak absorption bands at 2248 and 2219 cm^{-1} were assigned to the C≡N stretching vibration of nitriles.

4.4.4 Characterization of the aqueous fraction

4.4.4.1 Chemical composition

The aqueous fractions of the pyrolysis liquids were analyzed by GC/MS. An overview of the chromatograms is shown in Figure 4-20. The most important identified compounds (based on peak area normalized against BHT; RT about 13.43 min) are listed in Table 4-18. The total absolute peak area was included in this table as an indication of the area of the chromatogram that was represented by the listed compounds. All identified compounds (about 270 in total) were classified into 9 classes of compounds based on their functional groups, analogously as described in section 4.1.3.2. In this way, the effect of catalyst type and/or configuration on the chemical composition of the aqueous fractions produced by slow catalytic pyrolysis could be studied. An overview is shown in Figure 4-21.

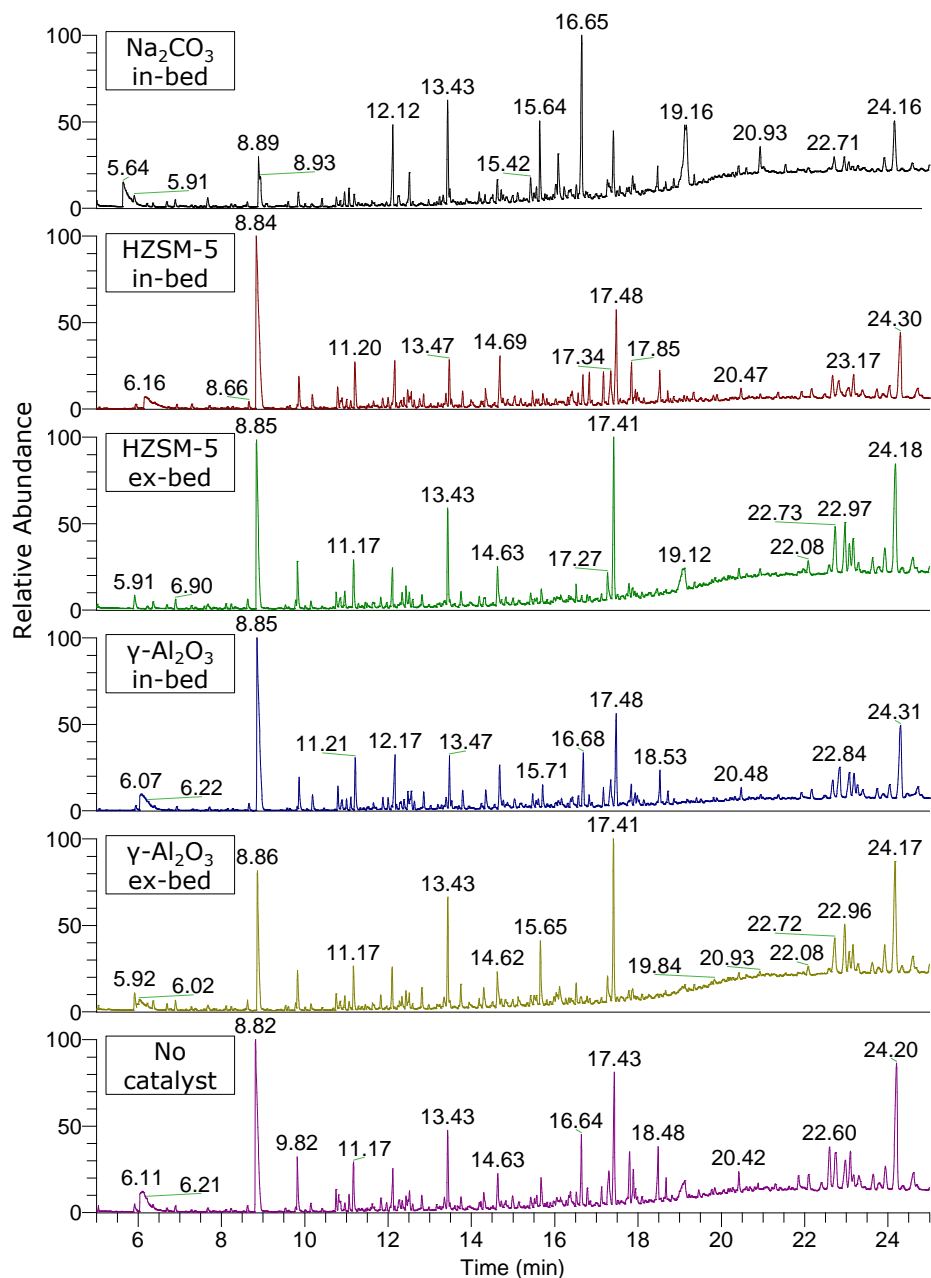


Figure 4-20: GC/MS chromatograms of the aqueous fractions produced by slow (catalytic) pyrolysis of rapeseed cake up to 550 °C.

Table 4-18: Major compounds of the aqueous fractions produced by slow (catalytic) pyrolysis of rapeseed cake up to 550 °C. Compound abundance is given as peak area normalized against BHT (%). RT: retention time (min).

RT	Compound	No catalyst	Y-Al ₂ O ₃		Y-Al ₂ O ₃		HZSM-5		HZSM-5		Na ₂ CO ₃	
			ex-bed	in-bed	ex-bed	in-bed	ex-bed	in-bed	ex-bed	in-bed	ex-bed	in-bed
5.94	Pyridine	0.16	0.23	0.15	0.22	0.16	0.31					
6.07	N,N-dimethylaminoethanol	1.71	0.52	2.17	-	2.19	1.02					
6.39	3-methylpyridine	0.33	0.17	0.30	0.13	-	0.05					
6.92	Methylpyrazine	0.10	0.12	0.10	0.13	0.12	0.10					
8.14	2-methyl-2-cyclopenten-1-one	0.04	0.05	0.04	0.07	0.05	0.01					
8.66	N,N-dimethylacetamide	0.09	0.12	0.16	0.14	0.18	0.07					
8.85	Acetic acid	5.10	2.13	7.92	3.18	9.92	0.94					
9.86	Propanoic acid	0.78	0.43	0.76	0.56	0.79	0.17					
10.79	Butanoic acid	0.27	0.16	0.47	0.17	0.48	0.10					
10.90	4-hydroxybutanoic acid	0.13	0.15	0.32	0.19	-	0.08					
11.00	N-methylacetamide	0.13	0.16	0.26	0.28	-	0.16					
11.11	3-furanmethanol	0.22	0.10	0.27	-	0.19	0.18					
11.21	3-methylbutanoic acid	0.76	0.50	1.19	0.58	1.24	0.16					
11.87	Pentanoic acid	0.23	0.16	0.35	0.13	0.31	0.05					
12.17	Acetamide	0.72	0.44	1.27	0.49	1.35	0.97					
12.48	4-methylpentanoic acid	0.20	0.18	0.36	0.23	0.41	-					
12.56	Propanamide	0.20	0.16	0.32	0.19	0.34	0.38					

Table 4-18: Continued.

RT	Compound	No catalyst	Y-Al ₂ O ₃		Y-Al ₂ O ₃		HZSM-5 ex-bed	HZSM-5 in-bed	Na ₂ CO ₃ in-bed
			ex-bed	in-bed	ex-bed	in-bed			
12.85	Hexanoic acid	0.20	0.28	0.39	0.21	0.36	-		
13.39	5-hexenoic acid	0.25	0.19	0.30	0.14	0.36	-		
13.79	Heptanoic acid	0.21	0.35	0.41	0.24	0.39	-		
14.23	Phenol	0.10	0.12	0.12	0.14	0.14	0.13		
14.34	5-methyl-5-hexenoic acid	0.30	0.31	0.53	0.18	0.35	-		
14.68	2-pyrrolidinone	0.61	0.56	1.07	0.58	1.37	0.29		
14.87	4-methylphenol	0.10	0.11	0.14	0.10	0.35	-		
15.47	2-piperidinone	0.19	0.14	0.35	0.16	0.34	0.28		
16.03	1-methyl-1H-pyrazole	0.23	0.11	0.11	0.07	0.07	0.22		
16.14	3,4,5-trimethylpyrazole	0.28	0.32	0.29	0.18	-	0.60		
16.31	2,6-dimethoxyphenol	0.11	-	0.11	-	0.18	-		
16.56	3-methyl-2(1H)-pyridinone	0.24	0.21	0.27	0.19	0.28	0.16		
16.68	Glycerin	1.04	0.14	1.20	0.03	0.78	2.10		
16.83	Ethosuximide	0.27	0.08	0.28	0.09	0.76	0.07		
17.17	1,2,4-triazine-3,5-dione	0.35	0.07	-	0.11	0.71	0.06		
17.48	3-pyridinol	2.15	1.85	2.19	1.93	2.93	0.79		
17.84	2,5-pyrrolidinedione	0.77	0.15	0.50	0.21	1.00	0.12		
17.93	5-hydroxymethylidihydrofuran-2-one	0.51	0.15	0.35	0.08	0.17	0.27		

Table 4-18: Continued.

RT	Compound	No catalyst	Y-Al ₂ O ₃		Y-Al ₂ O ₃		HZSM-5		HZSM-5		Na ₂ CO ₃	
			ex-bed	in-bed	ex-bed	in-bed	ex-bed	in-bed	ex-bed	in-bed	ex-bed	in-bed
18.71	Isosorbide	0.38	0.05	0.25	0.06	0.25	0.11					
20.42	Pyrrrole-2-carboxamide	0.50	0.19	-	0.26	-	0.25					
22.67	d-allose	1.12	-	0.73	0.27	0.94	-					
22.84	5-methyl-2,4-imidazolidinedione	1.26	0.89	1.52	1.20	1.28	0.53					
22.97	Nimorazole	0.97	0.93	-	1.09	-	0.31					
23.08	3-ethoxy-4-methoxyphenol	0.95	0.40	-	0.57	-	0.16					
23.27	1-methylimidazolidin-2-one	0.64	0.52	0.44	0.68	0.07	0.12					
23.39	7-methyl-7H-purin-6-amine	0.64	0.22	0.44	0.28	0.59	0.14					
23.87	N-4-diethyl-4-heptanamide	0.26	0.26	0.22	0.26	0.27	0.10					
24.31	5,10-dithoxy-2,3,7,8-tetrahydro-1H,6H-dipyrrolo(1,2-a;1',2'-a)pyrazine	3.59	2.58	3.30	2.66	3.17	1.19					
24.73	Uric acid	0.65	0.73	0.58	0.51	0.81	0.37					
Total absolute peak area (%):		63.7	59.4	54.3	62.3	52.4	43.4					
Number of compounds:		46	44	42	43	39	38					

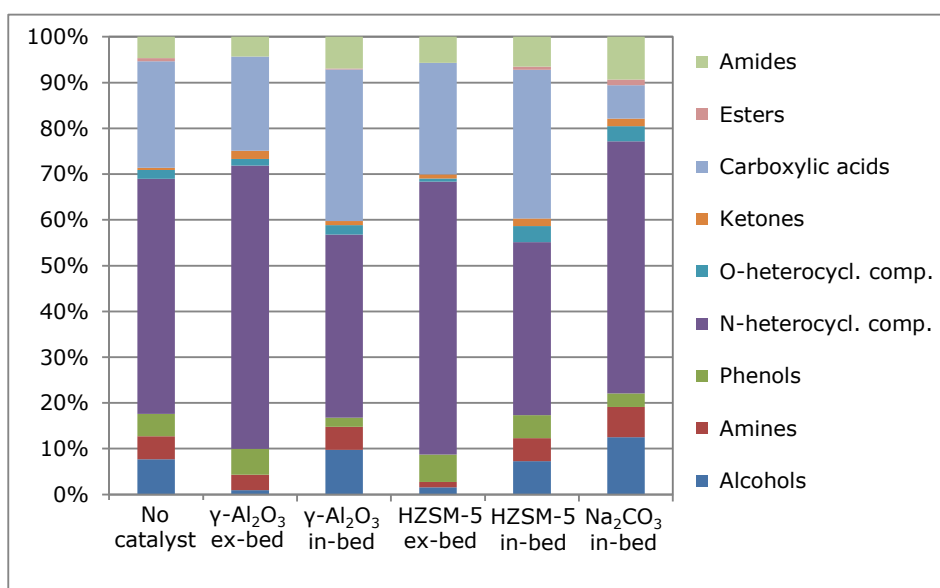


Figure 4-21: Overview of the classes of compounds present in the aqueous fractions produced by slow (catalytic) pyrolysis of rapeseed cake at 550 °C.

The N-heterocyclic compounds represented the major class of compounds in all aqueous fractions. This class mainly consisted of pyridine, pyrazine, imidazole and pyrazole derivatives that were formed by thermal degradation of the biomass proteins or by reaction between ammonia (a degradation product of proteins) and O-heterocyclic compounds. The amount of N-heterocyclic compounds was increased by in-bed Na₂CO₃ and by both ex-bed tested catalysts, while in-bed γ-Al₂O₃ and in-bed HZSM-5 resulted in a slightly smaller yield compared to the non-catalytic test. Carboxylic acids formed the second major class of compounds and consisted of short-chain organic acids, originating from the degradation of fatty acids and O-containing compounds (mainly hemicellulose). Acidic catalysts hardly affected the amount of carboxylic acids when tested in ex-bed mode, while a considerable increase was found when these catalysts were tested in in-bed mode. On the other hand, the alkaline Na₂CO₃ catalyst led to a significant decrease in amount of carboxylic acids. The class of alcohols was strongly dependent on catalyst type and configuration. Acidic catalysts led to a large reduction when used in ex-bed mode, while the amount of alcohols slightly increased in case of Na₂CO₃. The yield of the phenolic

compounds, formed by degradation of lignin, was slightly decreased by in-bed $\gamma\text{-Al}_2\text{O}_3$ and in-bed Na_2CO_3 . The O-heterocyclic compounds were produced by (thermal) degradation of cellulose and hemicellulose present in the rapeseed cake. Since these compounds could easily be converted into other compounds such as N-heterocyclic compounds or ketones, their yield was rather limited. Esters, ketones, amines and amides represented minor classes of compounds.

4.4.4.2 Physical properties

The physical properties of the aqueous fractions are shown in Table 4-19.

Table 4-19: Physical properties of the aqueous fractions produced by slow (catalytic) pyrolysis of rapeseed cake up to 550 °C.

Aqueous fraction	Water content (wt%)	pH (20°C)
No catalyst	67.7 (4.0)	7.2
$\gamma\text{-Al}_2\text{O}_3$ ex-bed	82.3 (4.2)	8.9
$\gamma\text{-Al}_2\text{O}_3$ in-bed	79.7 (6.1)	7.2
HZSM-5 ex-bed	78.7 (3.2)	8.2
HZSM-5 in-bed	74.1 (3.7)	6.4
Na_2CO_3 in-bed	67.7 (5.5)	9.3

The aqueous fraction of the pyrolysis liquid produced without catalyst had a water content of 67.7 wt%. Most of this water was believed to be pyrolytic water. This water content was hardly affected by in-bed Na_2CO_3 , while it was significantly increased by the acidic catalysts (both in-bed and ex-bed). The rather neutral pH-value of the aqueous fraction produced by the non-catalytic test was converted into slightly to strongly alkaline values by catalyst use.

Due to their high water contents, none of the aqueous fractions are suitable for renewable fuel use. However, they may be a source of added-value chemicals if the separation/extraction of these chemicals is economically feasible. The N-heterocyclic compounds have opportunities for valorization in plastic, food and pharmaceutical industries, while the O-containing compounds might be used in the production of chemicals such as bio-polymers [27].

Remark on the absolute amount of water in the organic and aqueous fractions

Since the yield of the organic oil and aqueous fractions was considerably affected by catalyst use and/or configuration (see Table 4-15), comparison in absolute amounts of water (instead of water content) might be more appropriate. Therefore, the yield of each liquid fraction was multiplied by its water content to calculate the absolute amount of water in each fraction originating from 100 g of rapeseed cake. Results are presented in Table 4-20.

It can be seen that the total absolute amount of water was strongly increased by catalyst use. This indicated that the catalysts strongly favored dehydration reactions during slow pyrolysis of rapeseed cake and that the production of pyrolytic water, in absolute terms, was considerably increased. In case of the ex-bed tested catalysts and in-bed Na_2CO_3 , most of the pyrolytic water ended up in the aqueous fraction, resulting in an organic oil fraction with a very low (absolute) amount of water (especially in case of ex-bed HZSM-5 and in-bed Na_2CO_3). In contrast, the total amount of organic compounds was significantly reduced by the used catalysts. However, most of the organic compounds ended up in the organic oil fraction that showed (strongly) enhanced physical properties compared to the non-catalytic oil fraction concerning their use as renewable fuels or fuel additives (Table 4-16).

Table 4-20: Absolute amount of water and organic compounds in the organic oil and aqueous fractions produced by slow catalytic pyrolysis of rapeseed cake up to 550 °C.

Yield/property	No catalyst	$\gamma\text{-Al}_2\text{O}_3$ ex-bed	$\gamma\text{-Al}_2\text{O}_3$ in-bed	HZSM-5 ex-bed	HZSM-5 in-bed	Na_2CO_3 in-bed
Pyrolysis liquid yield (wt%) ^a	47.1	40.8	48.4	44.9	44.6	41.8
Organic fraction	35.7	21.3	35.3	23.3	27.1	20.8
Aqueous fraction	11.4	19.5	13.1	21.6	17.5	21.0
Water content (wt%)						
Organic fraction ^b	14.9	14.6	22.1	6.3	15.5	2.3
Aqueous fraction ^c	67.7	82.3	79.7	78.7	74.1	67.7
Absolute water (g) ^d						
Organic fraction	5.32	3.11	7.80	1.47	4.20	0.48
Aqueous fraction	7.72	16.05	10.44	17.00	12.97	14.22
Total amount of water	13.04	19.16	18.24	18.47	17.17	14.70
Absolute organic compounds (g) ^d						
Organic fraction	30.38	18.19	27.50	21.83	22.90	20.32
Aqueous fraction	3.68	3.45	2.66	4.60	4.53	6.78
Total amount of organic compounds	34.06	21.64	30.16	26.43	27.43	27.10

^a Pyrolysis liquid yield from Table 4-15; ^b Water content determined by Karl Fischer titration from Table 4-16;

^c Water content determined by Karl Fischer titration from Table 4-19; ^d expressed for 100 g of rapeseed cake.

4.4.5 Characterization of the solid residue

Besides the pyrolysis liquid, the solid residue obtained by slow (catalytic) pyrolysis also has potential as valorization pathway for rapeseed cake. Frequently, solid residue is converted into activated carbon that is used to remove pollutants from water or gas streams (see Chapter 6).

Another option is to burn the solid residue to provide process heat to maintain the temperature during slow pyrolysis at industrial scale. In this respect, the HHV and the ash content of the solid residue are important process design parameters. Results are shown in Table 4-21. The ash contents were calculated by equation 4-2 (section 4.1.4). Since the in-bed tested HZSM-5 catalyst could not be completely separated from the solid residue, the HHV of this solid residue was calculated by equation 4-3. The HHVs turned out to be hardly affected by catalyst use (except for in-bed HZSM-5) and still contained a considerable amount of energy.

Table 4-21: HHV and ash content of the solid residues produced by slow (catalytic) pyrolysis of rapeseed cake up to 550 °C (SD between brackets).

Solid residue	HHV (MJ/kg)	Ash (wt%)
No catalyst	21.9 (0.1)	17.6
γ -Al ₂ O ₃ ex-bed	21.5 (0.2)	17.9
γ -Al ₂ O ₃ in-bed	21.4 (0.1)	18.7
HZSM-5 ex-bed	21.6 (0.1)	17.5
HZSM-5 in-bed	19.6 (0.2)	17.6
Na ₂ CO ₃ in-bed	21.6 (0.2)	20.5

4.5 Conclusion

The product yield from **flash pyrolysis** of rapeseed cake is strongly dependent on the **pyrolysis temperature**. A significant decrease in solid yield (- 23.6 wt%) and a minor decrease in gas yield (- 6.3 wt%) in favor of the liquid yield (+ 29.9 wt%) is found for a temperature increase from 350 to 550 °C. The pyrolysis liquid spontaneously separates into an organic oil and aqueous fraction, regardless the pyrolysis temperature. The larger liquid yield at higher pyrolysis temperatures is caused by an increase in organic oil fraction. Hence, at higher pyrolysis temperatures (450 and 550 °C), flash distillation (rather than flash pyrolysis) of the biomass triglycerides is found to be much more dominant than at lower temperatures. This hypothesis is supported by GPC, HPLC, FTIR and ¹H-NMR analyses. GC/MS identifies fatty acids (related to triglycerides) as principal compounds in the organic oil fractions, together with compounds originating from the degradation of hemicellulose, cellulose, lignin and proteins. The aqueous fractions are composed of a wide variety of polar compounds mainly originating from protein, hemicellulose and cellulose components. However, the yield and composition of the aqueous fraction turn out to be hardly affected by the pyrolysis temperature.

Concerning the valorization of rapeseed cake as source of renewable fuel, flash pyrolysis at 550 °C turns out to have the highest potential. A liquid yield of 58.2 wt% is obtained. This pyrolysis liquid spontaneously separates into an aqueous (16.1 wt%) and an organic oil fraction (42.1 wt%). The latter represents 57 % of the initial biomass energy and is characterized by a low water content (6.7 wt%), a high calorific value (32.8 MJ/kg) and a neutral pH-value (6.9). At industrial scale, the solid residue can be valorized as solid fuel to provide process heat to a CFB reactor setup.

Flash pyrolysis at 450 °C with fractionated liquid condensation (using two condensation vessels in series: one water cooled vessel and one at 105 °C) cannot improve the water content of the pyrolysis liquid compared to regular flash pyrolysis of rapeseed cake. Hence, the liquid fraction collected at 105 °C turns out to be single-phased and has a slightly higher water content (+ 1.8 wt%) than the organic oil fraction produced by regular flash pyrolysis followed by spontaneous phase separation. Moreover, the yield of the liquid fraction

collected at 105 °C is significantly lower (- 5.5 wt%) than that of the organic oil fraction obtained by regular condensation and subsequent phase separation. However, since the liquid fraction collected at 105 °C has a lower water content than the liquid fraction in the water cooled vessel, it can be concluded that flash pyrolysis with fractionated liquid condensation has potential to reduce the water content of (single-phased) pyrolysis liquids produced from *other* biomass waste streams.

Co-pyrolysis of rapeseed cake with PEG10k at 450 °C results in a slightly lower water content (- 0.8 wt%) of the organic oil fraction. However, co-pyrolysis also considerably reduces the yield (- 11.5 wt%) of this fraction compared to regular flash pyrolysis. Moreover, the desired synergetic effect between rapeseed cake and PEG10k (i.e. the esterification of the biomass fatty acids with the degradation products of PEG10k) that is expected to assist the spontaneous phase separation of the pyrolysis liquid is not achieved, as determined by GC/MS.

Slow pyrolysis with fractionated collection of the pyrolysis liquid as a function of temperature provides a better understanding of the pyrolytic behavior of rapeseed cake and the composition of the pyrolysis liquid. Fractions collected between 195 and 350 °C are single-phased liquids with a high water content, while fractions obtained between 350 and 550 °C are two-phased liquids. At lower temperatures (< 350 °C), O-heterocyclic compounds (mainly originating from hemicellulose) and carboxylic acids (mainly composed of short-chain acids) are the major classes of compounds present in aqueous fractions. At higher temperatures (> 350 °C), long-chain fatty acids become predominant and result in a phase separation of the pyrolysis liquid. As a result, an organic oil fraction is formed with a much lower polarity and water content than the aqueous fractions. At temperatures above 400 °C, this phase separation is more pronounced and the organic oil fraction becomes the most abundant fraction. Moreover, fatty acids are partly converted into nitriles due to the presence of N-containing compounds and dehydration reactions. N-heterocyclic compounds, degradation products of the biomass proteins, are mainly observed in the aqueous fractions collected between 265 and 400 °C.

Catalyst type and/or configuration (strongly) affect the product yield and energy recovery in **slow catalytic pyrolysis** of rapeseed cake up to 550 °C. In general, lower liquid and higher gas yields are obtained compared to the non-catalytic test, except for in-bed $\gamma\text{-Al}_2\text{O}_3$. Hence, the latter is the only catalyst that results in a slightly higher liquid yield and energy recovery compared to the non-catalytic test, although HZSM-5 (both in-bed and ex-bed) is also performing well. All pyrolysis liquids spontaneously separate into an organic oil and an aqueous fraction. Catalyst addition reduces the yield of the organic oil fraction in favor of the aqueous fraction in all cases.

Physicochemical properties of the organic oil fractions are strongly affected by catalyst use. Especially in-bed Na_2CO_3 and ex-bed HZSM-5 improve the properties of the organic oil fraction, making it promising for renewable fuel use. Hence, ex-bed HZSM-5 performs the most effective deoxygenation (- 13.9 wt%), while in-bed Na_2CO_3 results in the highest calorific value (36.8 MJ/kg). The physicochemical properties are hardly improved by in-bed $\gamma\text{-Al}_2\text{O}_3$ and in-bed HZSM-5, indicating that these acidic catalysts should preferably be used in ex-bed mode in case of slow catalytic pyrolysis of rapeseed cake.

The chemical composition of the organic oil fraction strongly depends on catalyst type and/or configuration. An overall trend is the reduction in amount of fatty acids, formed by thermal decomposition of the biomass triglycerides. In case of the acidic catalysts, these fatty acids are mainly converted into nitriles by an acid catalyzed two-step mechanism with amides as an intermediate product. The formation of nitriles is favored when these catalysts are used in ex-bed mode, while the equilibrium is shifted a little bit more towards amides when testing them in in-bed mode. The alkaline Na_2CO_3 catalyst converts fatty acids mainly into aliphatic hydrocarbons by decarboxylation reactions. It is concluded that the use of a suitable catalyst can enhance the quality of the organic oil fraction produced by slow pyrolysis of rapeseed cake. The aqueous fractions have a very high water content, but contained considerable amounts of polar organic compounds as well. N-heterocyclic compounds and carboxylic acids are determined as major classes of compounds. The solid residue has a HHV of about 21.5 MJ/kg and can be used as a precursor in the production of activated carbon.

4.6 References

- [1] Smets, K., Adriaensens, P., Reggers, G., Schreurs, S., Carleer, R. and Yperman, J. Flash pyrolysis of rapeseed cake: Influence of temperature on the yield and the characteristics of the pyrolysis liquid. *Journal of Analytical and Applied Pyrolysis*, 2011. **90**(2): 118-125.
- [2] Onay, O. and Kockar, O.M. Slow, fast and flash pyrolysis of rapeseed. *Renewable Energy*, 2003. **28**(15): 2417-2433.
- [3] Ucar, S. and Ozkan, A.R. Characterization of products from the pyrolysis of rapeseed oil cake. *Bioresource Technology*, 2008. **99**(18): 8771-8776.
- [4] Zabaniotou, A., Ioannidou, O. and Skoulou, V., Rapeseed residues utilization for energy and 2nd generation biofuels, *Fuel*. 2008, p. 1492-1502
- [5] Yorgun, S., Sensoz, S. and Kockar, O.M. Flash pyrolysis of sunflower oil cake for production of liquid fuels. *Journal of Analytical and Applied Pyrolysis*, 2001. **60**(1): 1-12.
- [6] Özbay, N., Pütün, A.E., Uzun, B.B., and Pütün, E. Biocrude from biomass: pyrolysis of cottonseed cake. *Renewable Energy*, 2001. **24**(3-4): 615-625.
- [7] Özbay, N., Pütün, A.E. and Pütün, E. Structural analysis of bio-oils from pyrolysis and steam pyrolysis of cottonseed cake. *Journal of Analytical and Applied Pyrolysis*, 2001. **60**(1): 89-101.
- [8] Oasmaa, A. and Peacocke, C. A guide to physical property characterisation of biomass-derived fast pyrolysis liquids, ed. Finland, T.r.c.o. Vol. 450. 2001, Technical research centre of Finland, Espoo, Finland: VTT Publications.
- [9] Mortensen, P.M., Grunwaldt, J.D., Jensen, P.A., Knudsen, K.G. and Jensen, A.D. A review of catalytic upgrading of bio-oil to engine fuels. *Applied Catalysis A: General*, 2011. **407**(1-2): 1-19.
- [10] Czernik, S. and Bridgwater, A.V. Overview of applications of biomass fast pyrolysis oil. *Energy & Fuels*, 2004. **18**(2): 590-598.
- [11] Meier, D., Oasmaa, A. and Peacocke, G.V.C. Properties of fast pyrolysis liquids: status of test methods. In: *Fast pyrolysis of biomass: a handbook*, Bridgwater, A., et al., Editors. CPL Press: Newbury, UK. 1999.
- [12] Dupain, X., Costa, D.J., Schaverien, C.J., Makkee, M. and Moulijn, J.A. Cracking of a rapeseed vegetable oil under realistic FCC conditions. *Applied Catalysis B: Environmental*, 2007. **72**(1-2): 44-61.

- [13] Pouchert, C.J. The Aldrich library of infrared spectra. 2nd ed. 1975, Milwaukee: Aldrich Chem Co Library.
- [14] Du, Z.Y., Hu, B., Ma, X.C., Cheng, Y.L., Liu, Y.H., Lin, X.Y., Wan, Y.Q., Lei, H.W., Chen, P. and Ruan, R. Catalytic pyrolysis of microalgae and their three major components: Carbohydrates, proteins, and lipids. *Bioresource Technology*, 2013. **130**: 777-782.
- [15] Mohan, D., Pittman, C.U. and Steele, P.H. Pyrolysis of wood/biomass for bio-oil: A critical review. *Energy & Fuels*, 2006. **20**(3): 848-889.
- [16] Shen, D.K. and Gu, S. The mechanism for thermal decomposition of cellulose and its main products. *Bioresource Technology*, 2009. **100**(24): 6496-6504.
- [17] Shen, D.K., Gu, S., Luo, K.H., Wang, S.R. and Fang, M.X. The pyrolytic degradation of wood-derived lignin from pulping process. *Bioresource Technology*, 2010. **101**(15): 6136-6146.
- [18] Radlein, D. The production of chemicals from fast pyrolysis bio-oils. In: *Fast pyrolysis of biomass: a handbook*, Bridgwater, A.V., et al., Editors. CPL Press: Newbury, UK. 1999. 164 - 188.
- [19] Shen, D.K., Gu, S. and Bridgwater, A.V. Study on the pyrolytic behaviour of xylan-based hemicellulose using TG-FTIR and Py-GC-FTIR. *Journal of Analytical and Applied Pyrolysis*, 2010. **87**(2): 199-206.
- [20] Bridgwater, A.V. Review of fast pyrolysis of biomass and product upgrading. *Biomass and Bioenergy*, 2012. **38**(0): 68-94.
- [21] Stals, M., Pyrolysis of heavy metal contaminated biomass: characterization of obtained pyrolysis oils and study of derived activated carbon, PhD thesis - Research Group: Analytical and Applied Chemistry. 2011, Hasselt University: Diepenbeek. p. 201
- [22] Cornelissen, T., Jans, M., Yperman, J., Reggers, G., Schreurs, S. and Carleer, R. Flash co-pyrolysis of biomass with polyhydroxybutyrate: Part 1. Influence on bio-oil yield, water content, heating value and the production of chemicals. *Fuel*, 2008. **87**(12): 2523-2532.
- [23] Cornelissen, T., Flash pyrolysis of biomass and co-pyrolysis with biopolymers, PhD thesis - Research Group: Applied and Analytical Chemistry. 2009, Hasselt University: Diepenbeek. p. 202
- [24] Goyal, H.B., Seal, D., and Saxena, R.C. Bio-fuels from thermochemical conversion of renewable resources: A review. *Renewable & Sustainable Energy Reviews*, 2008. **12**(2): 504-517.
- [25] Pütün, E. Catalytic pyrolysis of biomass: Effects of pyrolysis temperature, sweeping gas flow rate and MgO catalyst. *Energy*, 2010. **35**(7): 2761-2766.

- [26] Vitolo, S., Seggiani, M., Frediani, P., Ambrosini, G. and Politi, L. Catalytic upgrading of pyrolytic oils to fuel over different zeolites. *Fuel*, 1999. **78**(10): 1147-1159.
- [27] Bridgwater, A.V. Catalysis in thermal biomass conversion. *Applied Catalysis A: General*, 1994. **116**(1-2): 5-47.
- [28] Samolada, M.C., Papafotica, A. and Vasalos, I.A. Catalyst evaluation for catalytic biomass pyrolysis. *Energy & Fuels*, 2000. **14**: 1161 - 1167.
- [29] Maher, K.D. and Bressler, D.C. Pyrolysis of triglyceride materials for the production of renewable fuels and chemicals. *Bioresource Technology*, 2007. **98**(12): 2351-2368.
- [30] Katikaneni, S.P.R., Adjaye, J.D. and Bakhshi, N.N. Catalytic conversion of canola oil to fuels and chemicals over various cracking catalysts. *The Canadian Journal of Chemical Engineering*, 1995. **73**: 484-497.
- [31] Idem, R.O., Katikaneni, S.P.R. and Bakhshi, N.N. Catalytic conversion of canola oil to fuels and chemicals: Roles of catalyst acidity, basicity and shape selectivity on product distribution. *Fuel Processing Technology*, 1997. **51**(1-2): 101-125.
- [32] Wang, J., Zhang, M., Chen, M., Min, F., Zhang, S., Ren, Z. and Yan, Y. Catalytic effects of six inorganic compounds on pyrolysis of three kinds of biomass. *Thermochimica Acta*, 2006. **444**(1): 110-114.
- [33] Tay, T., Ucar, S. and Karagöz, S. Preparation and characterization of activated carbon from waste biomass. *Journal of Hazardous Materials*, 2009. **165**(1-3): 481-485.
- [34] Kim, J.W. and Lee, H.G. Thermal and carbothermic decomposition of Na_2CO_3 and Li_2CO_3 . *Metallurgical and Materials Transactions B*, 2001. **32**(1): 17-24.
- [35] Mihalcik, D.J., Mullen, C.A. and Boateng, A.A. Screening acidic zeolites for catalytic fast pyrolysis of biomass and its components. *Journal of Analytical and Applied Pyrolysis*, 2011. **92**(1): 224-232.
- [36] Özçimen, D. and Karaosmanoglu, F. Production and characterization of bio-oil and biochar from rapeseed cake. *Renewable Energy*, 2004. **29**(5): 779-787.
- [37] Diebold, J.P., Milne, T.A., Czernik, S., Oasmaa, A., Bridgwater, A.V., Cuevas, A., Gust, S., Huffman, D. and Piskorz, J. Proposed specifications for various grades of pyrolysis oils. In: *Fast pyrolysis of biomass: a handbook*, Bridgwater, A.V., et al., Editors. CPL Press: Newbury, UK. 1999. 102 - 114.

- [38] Giannakopoulou, K., Lukas, M., Vasiliev, A., Brunner, C. and Schnitzer, H. Conversion of rapeseed cake into bio-fuel in a batch reactor: Effect of catalytic vapor upgrading. *Microporous and Mesoporous Materials*, 2010. **128**(1-3): 126-135.
- [39] Vonghia, E., Boocock, D.G.B., Konar, S.K. and Leung, A. Pathways for the deoxygenation of triglycerides to aliphatic-hydrocarbons over activated alumina. *Energy & Fuels*, 1995. **9**(6): 1090-1096.
- [40] Prasad, Y.S., Bakhshi, N.N., Mathews, J.F. and Eager, R.L. Catalytic conversion of canola oil to fuels and chemical feedstocks part 1. Effect of process conditions on the performance of HZSM-5 catalyst. *The Canadian Journal Of Chemical Engineering*, 1986. **64**(2): 278-284.
- [41] Dandik, L. and Aksoy, H.A. Pyrolysis of used sunflower oil in the presence of sodium carbonate by using fractionating pyrolysis reactor. *Fuel Processing Technology*, 1998. **57**(2): 81-92.
- [42] Konwer, D., Taylor, S.E., Gordon, B.E., Otvos, J.W. and Calvin, M. Liquid fuels from *Mesua ferrea* L. seed oil. *Journal Of The American Oil Chemists Society*, 1989. **66**(2): 223-226.
- [43] Lappi, H. and Alén, R. Production of vegetable oil-based biofuels - Thermochemical behavior of fatty acid sodium salts during pyrolysis. *Journal of Analytical and Applied Pyrolysis*, 2009. **86**(2): 274-280.

5 Valorization of raspberry seed cake

5.1 Flash pyrolysis of raspberry seed cake: Influence of pyrolysis temperature on the product yield and the characteristics of the pyrolysis liquid

5.1.1 Product yield and energy recovery

Flash pyrolysis of raspberry seed cake was performed in the semi-continuous lab-scale reactor setup (section 2.2.1) at three pyrolysis temperatures: 350, 450 and 550 °C. These temperatures were selected based on TGA (section 3.1.2). Hence, the highest rate of biomass decomposition was observed just above 350 °C, while pyrolysis was found to be almost complete at 450 °C. The experiment at 550 °C was included to investigate the effect of a further temperature increase and to have a similar temperature range as for the flash pyrolysis experiments of rapeseed cake (see section 4.1). The product yield and energy recovery from flash pyrolysis of raspberry seed cake are presented in Table 5-1.

Table 5-1: Product yield and energy recovery from flash pyrolysis of raspberry seed cake at three different temperatures.

Product yield (wt%)	Pyrolysis temperature		
	350 °C	450 °C	550 °C
Solid residue	52.1	25.6	18.8
<i>Char</i>	49.5	23.0	16.2
<i>Ash^a</i>	2.6	2.6	2.6
Pyrolysis liquid	27.0	53.6	45.0
Gas ^b	20.9	20.8	36.2
Energy recovery (%)			
Solid residue	63.6	30.9	-
Pyrolysis liquid	14.5	49.2	41.2
Gas ^b	21.9	19.9	-

^a Determined by TGA of the biomass; ^b Calculated by difference

The yield of solid residue was significantly reduced (- 26.5 wt%) by a temperature increase from 350 to 450 °C. Since the gas yield was hardly

affected in this temperature range, the decrease in solid yield was completely in favor of the liquid yield (+ 26.6 wt%). A further temperature increase to 550 °C resulted in a lower solid (- 6.8 wt%) and a lower liquid (- 8.6 wt%) yield, while the gas yield was considerably increased (+ 15.4 wt%) compared to 450 °C. This indicates that 450 °C was the optimum temperature for the production of pyrolysis liquid by flash pyrolysis, while gasification reactions turned out to become dominant at higher temperatures. In contrast, the temperature of 350 °C might be too low for complete conversion of raspberry seed cake by flash pyrolysis, as suggested by the high yield of solid residue.

The energy recovery was calculated by equation 4.1 (section 4.1.1). Most of the biomass energy was recovered in the solid residue at low pyrolysis temperature, while about 49.2 % was converted to the pyrolysis liquid at 450 °C. The HHV of the solid residue produced at 550 °C could not be determined due to the high amount of sand that could not be removed completely.

It can be concluded that the pyrolysis temperature significantly affected the product yield in flash pyrolysis of raspberry seed cake. Concerning the production of pyrolysis liquid, flash pyrolysis at 450 °C turned out to be most favorable in terms of both liquid yield and energy recovery. In contrast to flash pyrolysis of rapeseed cake (section 4.1), a further increase in pyrolysis temperature to 550 °C did not result in a higher liquid yield.

5.1.2 Characterization of the pyrolysis liquid

To determine the best valorization pathway, the pyrolysis liquid was investigated by complementary analytical techniques. Firstly, physicochemical properties were determined to assess the opportunities for use as renewable fuel (additive). Secondly, the chemical composition was determined to gain a better understanding of the effect of pyrolysis temperature on the pyrolytic behavior of raspberry seed cake and to screen for possible added-value chemicals.

5.1.2.1 Physical properties

The pyrolysis liquid obtained by flash pyrolysis of raspberry seed cake was a single-phased dark brown liquid, regardless the pyrolysis temperature. The most important physical properties of the liquids are presented in Table 5-2.

Table 5-2: Physical properties of pyrolysis liquids produced by flash pyrolysis of raspberry seed cake at different temperatures (SD between brackets).

Properties	Pyrolysis temperature		
	350 °C	450 °C	550 °C
Water content (wt%)	52.5 (1.4)	26.2 (1.2)	24.0 (0.1)
HHV (MJ/kg)	10.9 (0.2)	18.6 (0.2)	18.6 (0.1)
pH (20 °C)	2.7	3.2	3.4

The water content of the pyrolysis liquid was drastically reduced (- 26.3 wt%) between 350 to 450 °C, while a further temperature increase to 550 °C only led to a minor decrease (- 2.2 wt%). Since raspberry seed cake was dried prior to the experiments (residual moisture: 1.5 wt%, Table 3-2), most of the water had to be pyrolytic water. The high water content of the liquid produced at 350 °C suggested that dehydration reactions (probably of hemicellulose) were very prominent at this low temperature and that only limited degradation (pyrolysis) of other biomass components (such as cellulose and lignin) occurred. The HHV considerably increased between 350 and 450 °C (+ 7.7 MJ/kg), while it was hardly affected by a further temperature increase to 550 °C. These observations were in accordance with the water contents. The pH-values indicated that the pyrolysis liquids were quite acidic. Elemental analysis was only performed on the pyrolysis liquid produced at 450 °C and resulted in the following composition: 51.9 wt% C, 6.5 wt% H, 2.1 wt% N, 0.1 wt% S and 39.4 wt% O. The high oxygen content was in accordance with the low HHV and the relatively high water content.

These results show that flash pyrolysis of raspberry seed cake give rise to pyrolysis liquids with physicochemical properties that are comparable to those of pyrolysis liquids derived from lignocellulosic biomass [1, 2]. In contrast to pyrolysis liquids produced by flash pyrolysis of rapeseed cake (section 4.1), no spontaneous phase separation in an (water-poor) organic oil and (water-rich) aqueous fraction was achieved, making pyrolysis liquids derived from raspberry seed cake less suitable for renewable fuel use than those of rapeseed cake.

5.1.2.2 Chemical composition

The chemical composition of the pyrolysis liquids was investigated by GC/MS. An overview of the chromatograms as a function of pyrolysis temperature is shown in Figure 5-1. The major compounds of these chromatograms are listed in Table 5-3. The compound abundance was calculated by dividing the peak area of the compound by that of the internal standard (BHT) and corrected for weight differences during sample preparation. The total absolute peak area is included in the table as an indication of the percentage of the total chromatogram area that is represented by the listed compounds. It should be noted that two compounds with similar peak area were not necessarily present in the same amount due to different response factors [3].

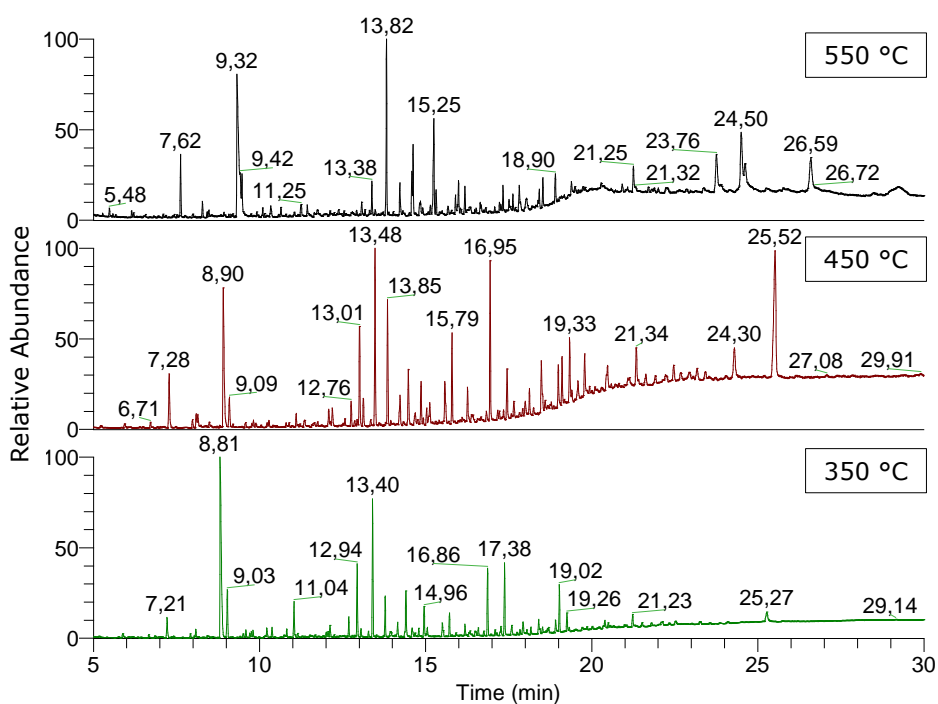


Figure 5-1: GC/MS chromatograms of the pyrolysis liquids produced by flash pyrolysis of raspberry seed cake at different temperatures. The internal standard (BHT) had a signal at a RT of 13.40, 13.48 and 13.82 min for samples produced at 350, 450 and 550 °C, respectively.

Table 5-3: Major compounds of pyrolysis liquids produced by flash pyrolysis of raspberry seed cake at different temperatures. Compound abundance is given as peak area normalized against BHT (%). RT: retention time (min).

RT	Compound	Pyrolysis temperature		
		350 °C	450 °C	550 °C
5.22	3-penten-2-one	-	0.018	0.030
5.88	Pyridine	0.033	0.031	0.021
7.21	1-hydroxy-2-propanone	0.138	0.328	0.194
7.91	2-cyclopenten-1-one	0.026	0.045	0.054
8.08	1-hydroxy-2-butanone	0.052	0.080	0.025
8.81	Acetic acid	1.638	0.935	1.101
9.03	Furfural	0.315	0.187	0.135
9.80	Propanoic acid	0.042	0.033	0.043
10.74	Butanoic acid	0.016	0.021	0.060
11.04	3-furanmethanol	0.200	0.066	0.036
11.14	3-methylbutanoic acid	0.029	0.021	-
12.01	2(5H)-furanone	0.033	0.098	0.012
12.06	Acetamide	0.038	0.025	0.029
12.12	1,5-cyclopentanedione	0.078	0.109	0.017
12.94	2-methoxyphenol	0.375	0.498	0.100
13.78	2-methoxy-4-methylphenol	0.230	0.591	0.147
14.16	Phenol	0.084	0.127	0.201
14.40	4-ethyl-2-methoxyphenol	0.274	0.299	0.036
14.59	2-pyrrolidinone	0.082	-	0.024
14.79	4-methylphenol	0.051	0.230	0.396
15.05	2-methoxy-4-propylphenol	0.057	0.119	0.063
15.50	Eugenol	0.080	0.168	0.027
15.53	4-ethylphenol	0.021	0.074	0.093
15.72	2-methoxy-4-vinylphenol	0.125	0.400	0.032
16.19	2-methoxy-6-(1-propenyl)-phenol	0.067	0.213	0.087
16.58	Glycerin	0.044	0.062	-
16.86	2-methoxy-4-(1-propenyl)-phenol	0.378	0.749	-
17.38	3-pyridinol	0.415	0.263	0.094
17.75	2,5-pyrrolidinedione	0.024	0.041	-
18.05	4-(2-propenyl)-phenol	0.043	0.154	0.056

Table 5-3: Continued.

RT	Compound	Pyrolysis temperature		
		350 °C	450 °C	550 °C
18.40	3-hydroxy-4-methoxybenzaldehyde	0.084	0.242	-
19.02	1-(4-hydroxy-3-methoxyphenol)- 2-propanone	0.261	0.256	-
19.26	1,2-benzenediol	0.118	0.400	-
19.71	4-methyl-1,2-benzenediol	0.039	0.320	-
20.50	4-butylphenol	0.046	0.084	-
21.23	4-hydroxy-3-methoxybenzeneacetic acid	0.102	0.295	0.027
21.29	3,5-dihydroxytoluene	0.011	0.060	0.027
21.52	Hydroquinone	0.047	0.144	-
23.76	9-octadecenoic acid	-	-	0.465
24.50	9,12-octadecadienoic acid	-	-	1.088
25.27	Levoglucofan	0.228	1.727	0.594
Total absolute peak area:		55.1	48.7	44.6
Number of compounds:		38	38	31

The pyrolysis liquids turned out to be complex mixtures of compounds with a wide variety of chemical functionalities (Table 5-3). To make the results more manageable, all identified compounds were classified into 11 categories based on their functional groups. If a compound had more than one functional group, the functional group with the highest number of bonds with a hetero-atom was given priority. For instance, a compound with an alcohol and a ketone functionality was classified as ketone. The hydrocarbons included saturated, unsaturated as well as cyclic hydrocarbons, while aromatic hydrocarbons were classified in a separate class. Compounds with a phenol structure, an O-heterocyclic or a N-containing cyclic structure were classified as phenols, O-heterocyclic or N-heterocyclic compounds respectively, no matter what other functional group was present in their chemical structure. Sugar derivatives were classified as alcohols. Finally, the sum of the peak areas of all classes was normalized to 100% since not all compounds present in the pyrolysis liquid could

be identified. Figure 5-2 shows an overview of the classes of compounds present in the pyrolysis liquids produced by flash pyrolysis of raspberry seed cake.

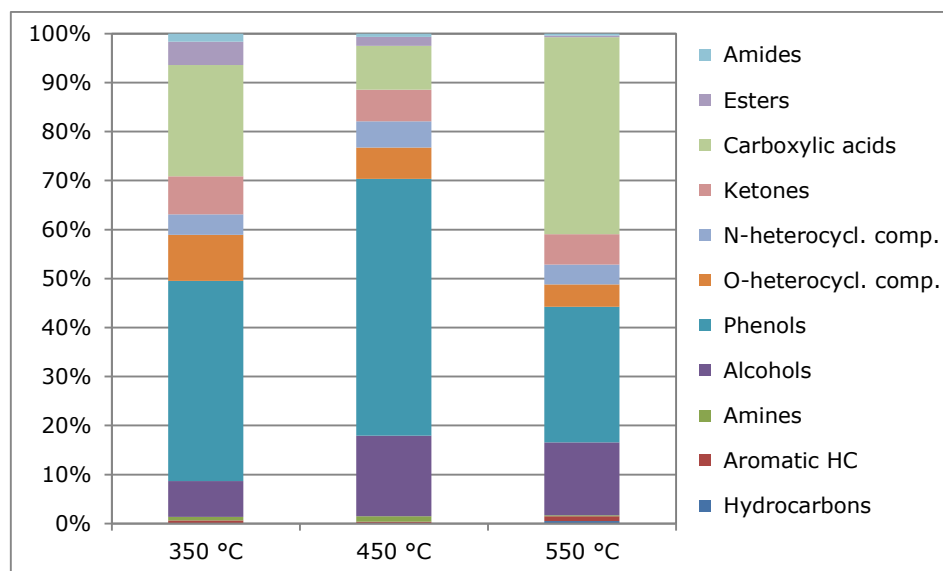


Figure 5-2: Overview of the classes of compounds present in the pyrolysis liquids produced by flash pyrolysis of raspberry seed cake at different temperatures.

Phenols, carboxylic acids and alcohols (including sugar derivatives) were found as major classes of compounds (Figure 5-2). Phenols represented the principal class of compounds for pyrolysis liquids produced at 350 and 450 °C, while carboxylic acids were predominant at 550 °C. The high amount of phenols was in accordance with the high lignin content of raspberry seed cake as found by component analysis (Table 3-1). Some major representatives were 2-methoxy-4-(1-propenyl)-phenol (RT: 16.86 min), 2-methoxyphenol (RT: 12.94 min), 2-methoxy-4-methylphenol (RT: 13.78 min) and 4-methylphenol (RT: 14.79 min). Acetic acid (RT: 8.81 min), a short-chain fatty acid, was the main compound of the carboxylic acids at all pyrolysis temperatures and was considered as a degradation product of hemicellulose [4]. In contrast, 9-octadecenoic acid (RT: 23.76 min) and 9,12-octadecadienoic acid (RT: 24.50 min), both long-chain fatty acids, were only identified at 550 °C. This indicated that triglycerides present in the raspberry seed cake (5.2 wt%, Table 3-1) were only decomposed

at pyrolysis temperatures above 450 °C. A third class of compounds was formed by alcohols with levoglucosan (RT: 25.27 min) as major representative. This compound, also known as 1,6-anhydroglucopyranose, was believed to be formed by degradation of cellulose components [4-6]. The O-heterocyclic compounds were mainly composed of furan-derivatives, originating from the degradation of hemicellulose, while N-heterocyclic compounds were formed by decomposition of the biomass proteins [7]. Hydrocarbons, aromatic hydrocarbons, amines, esters and amides were only detected in minor amounts.

From economic point of view, levoglucosan and some derivatives of phenol (such as 1-(4-hydroxy-3-methoxyphenol)-2-propanone, 2-methoxy-4-methylphenol and 2-methoxy-4-vinylphenol) were the most interesting compounds because of their relatively high value. However, it must be verified if these compounds can be separated from the pyrolysis liquid in an economically favorable way.

5.1.3 Characterization of the solid residue

Flash pyrolysis of raspberry seed cake required sand as heat transfer medium. As a result, considerable amounts of sand were stuck to the surfaces or even incorporated within the particles of the solid residue, making complete separation of sand and solid residue very problematic. Hence, valorization of the solid residue as precursor in the production of activated carbon was not an option. However, the solid residue still contained a considerable amount of energy that could be recovered as process heat at industrial scale [8]. In this view, the HHV and the ash content of the solid residue are important process design parameters [9]. Therefore, both parameters were estimated analogously as described in section 4.1.4. The HHV_{char} was measured as described in section 2.5.3. Results are shown in Table 5-4.

The solid residue turned out to contain a considerable amount of energy, which seemed to decrease slightly with increasing pyrolysis temperature due to build-up of ashes. This indicates that solid residue produced by flash pyrolysis of raspberry seed cake has potential as solid energy carrier with ash as only waste product. The HHV of the solid residue produced at 550 °C, as already mentioned, could not be determined due to the large amount of sand that could not be removed readily from the solid residue.

Table 5-4: Ash content and HHV of the solid residues produced by flash pyrolysis of raspberry seed cake at different temperatures.

Properties	Pyrolysis temperature		
	350 °C	450 °C	550 °C
ash _{SR} (wt%)	5.0	10.1	13.9
char/solid residue (wt%)	95.0	89.9	86.1
HHV _{char} (MJ/kg)	26.1	27.2	-
HHV _{SR} (MJ/kg)	24.8	24.5	-

5.2 Slow pyrolysis of raspberry seed cake: Collection of the pyrolysis liquid in fractions as a function of pyrolysis temperature

The potential of slow pyrolysis to valorize raspberry seed cake is investigated in this section. Since slow pyrolysis involves a much lower heating rate than flash pyrolysis, sand is no longer required as heat transfer medium, avoiding the problematic separation of solid residue from sand. By collecting the pyrolysis liquid in fractions as a function of temperature during slow pyrolysis, valuable information on the pyrolytic behavior of raspberry seed cake can be obtained.

5.2.1 Product yield and properties of the liquid fractions.

Slow pyrolysis up to 450 °C was performed using the lab-scale reactor setup as described in section 2.2.2, but without sand as heat transfer medium. This resulted in a solid yield of 36.2 wt%, a total liquid yield of 44.4 wt% and a gas yield of 19.4 wt% (by difference). Compared to flash pyrolysis (Table 5-1), a considerable higher solid yield (+ 10.6 wt%), a significantly lower liquid yield (- 9.2 wt%) and a slightly lower gas yield (- 1.4 wt%) were obtained, as expected. The condensation vessel with valve allowed to collect the pyrolysis liquid in separate fractions, based on a change in color and/or viscosity, as a function of pyrolysis temperature. The yield of each fraction and the corresponding pyrolysis temperature interval are shown in Table 5-5.

Table 5-5: Yield and properties of the liquid fractions collected as a function of temperature during slow pyrolysis of raspberry seed cake up to 450 °C.

Fract.	T (°C)	Type	Yield (wt%)^a	Water content (wt%)	HHV (MJ/kg)
1	220 - 320	Aqueous	11.8	60.4 (2.0)	-
2	320 - 350	Aqueous	10.3	45.9 (0.8)	14.5 (0.4)
3	350 - 450	Aqueous	10.2	67.4 (1.5)	-
3	350 - 450	Organic	12.1	9.3 (1.2)	27.0 (0.7)

^a Expressed as wt% to the initial biomass

Fraction 1 (220 – 320 °C) was an aqueous liquid with a very high water content (60.4 w%) and a light brown color. **Fraction 2** (320 – 350 °C) had a relatively high water content (45.9 wt%) and could be considered as a transition fraction between fraction 1 and 3. **Fraction 3** (350 – 450 °C) had a dark brown color and was more viscous than fraction 1 and 2. Moreover, this fraction spontaneously separated in two fractions: an aqueous fraction with a very high water content (67.4 wt%) and an organic oil fraction. The latter was found to have a relatively low water content (9.3 wt%) and a relative high energy content (27.0 MJ/kg). Elemental analysis revealed the following composition of this organic fraction: 63.4 wt% C, 7.5 wt% H, 2.3 wt% N and 26.8 wt% O. These characteristics suggest that the organic oil fraction has potential for use as renewable fuel or fuel additive. However, it should be investigated if the rather low yield (12.1 wt% with respect to the initial raspberry seed cake) does not compromise the economics of the process at an industrial scale.

5.2.2 Chemical composition of the liquid fraction

The pyrolysis liquid fractions were investigated by GC/MS in order to gain a better understanding of the pyrolytic behavior of raspberry seed cake and to screen for added-value chemicals. The chromatograms are shown in Figure 5-3. More than 300 different compounds were identified in all fractions together. Since it was impossible to list all compounds, a limited list of the major compounds (based on peak area vs the internal standard BHT) is presented in Table 5-6. To make the results more manageable, all identified compounds were classified into 11 classes of compounds, using the same methodology as described in section 5.1.2.2. A graphical overview for each liquid fraction is shown in Figure 5-4.

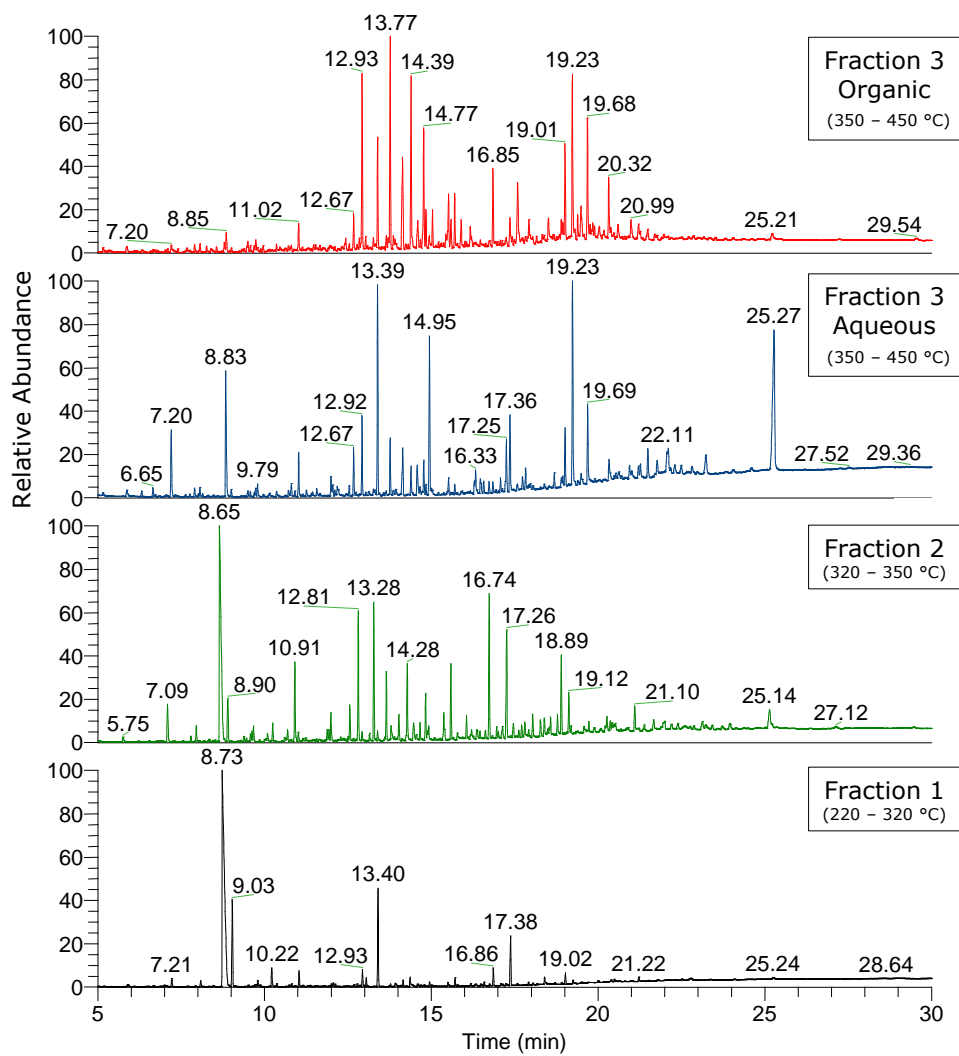


Figure 5-3: GC/MS chromatograms of the liquid fractions collected as a function of temperature during slow pyrolysis of raspberry seed cake up to 450 °C. The internal standard (BHT) had a signal at a RT of 13.40, 13.28, 13.39 and 13.77 min for respectively fraction 1, 2, 3 aq. and 3 org.

Table 5-6: GC/MS analysis of the liquid fractions from slow pyrolysis of raspberry seed cake with separate liquid collection. Compound abundance is given as peak area normalized against BHT (%). RT: retention time.

RT	Compound	Fraction			
		1 aq.	2 aq.	3 aq.	3 org.
5.86	Pyridine	0.020	0.034	0.034	-
7.20	1-hydroxy-2-propanone	0.058	0.204	0.231	-
7.90	2-cyclopenten-1-one	0.005	0.029	0.029	0.071
7.95	1-hydroxy-2-butanone	0.043	0.079	-	-
8.85	Acetic acid	3.465	2.006	0.444	0.188
8.90	Furfural	0.533	0.233	-	-
9.50	1-(2-furanyl)-ethanone	0.013	0.030	0.024	0.114
9.79	Propanoic acid	0.036	0.064	0.040	0.044
10.36	3-methoxypyridine	0.017	0.071	0.014	0.071
10.71	Butanoic acid	-	0.020	0.022	0.081
10.80	Butyrolactone	0.022	0.067	0.046	0.054
11.02	3-furanmethanol	0.086	0.329	0.127	0.256
11.13	3-methylbutanoic acid	0.011	0.052	-	0.050
11.99	2(5H)-furanone	0.015	0.045	-	0.037
12.04	Acetamide	0.022	0.050	0.040	-
12.10	2-hydroxy-2-cyclopenten-1-one	0.017	0.129	0.024	0.040
12.67	2-hydroxy-3-methyl-2-cyclopenten-1-one	0.014	0.141	0.147	0.327
12.93	2-methoxyphenol	0.009	0.505	0.222	1.501
13.77	2-methoxy-4-methylphenol	0.020	0.280	0.170	1.696
13.91	Maltol	0.039	0.088	0.035	0.071
14.14	Phenol	0.040	0.111	0.136	0.771
14.39	4-ethyl-2-methoxyphenol	0.006	0.301	0.079	1.451
14.57	2-pyrrolidinone	0.023	0.110	0.122	-
14.77	4-methylphenol	0.009	0.068	0.107	1.064
15.03	2-methoxy-4-propylphenol	-	0.054	0.009	0.350
15.49	Eugenol	0.031	0.117	-	0.114
15.52	4-ethylphenol	-	0.037	0.049	0.394
15.70	2-methoxy-4-vinylphenol	0.050	0.310	0.038	0.468
15.90	Methyl hexadecanoate	-	0.037	0.017	0.320

T_{fract.1}: 220 – 320 °C; T_{fract.2}: 320 – 350 °C; T_{fract.3}: 350 – 450 °C.

Table 5-6: Continued.

RT	Compound	Fraction			
		1 aq.	2 aq.	3 aq.	3 org.
16.17	2-methoxy-6-(1-propenyl)-phenol	0.019	0.103	0.017	0.188
16.57	Glycerin	0.026	0.046	0.037	-
16.85	2-methoxy-4-(1-propenyl)-phenol	0.098	0.592	0.034	0.663
17.36	3-pyridinol	0.305	0.515	0.241	0.303
17.59	Methyl-9-octadecenoate	-	0.073	0.037	0.966
17.74	2,5-pyrrolidinedione	0.005	0.043	0.068	-
18.04	4-(2-propenyl)-phenol	0.017	0.043	-	0.145
18.38	3-hydroxy-4-methoxy-benzaldehyde	0.085	0.102	-	0.104
18.51	1-octadecanol	-	0.106	-	0.364
19.01	1-(4-hydroxy-3-methoxyphenol)-2-propanone	0.063	0.360	0.174	-
19.23	1,2-benzenediol	0.034	0.205	0.657	1.491
19.68	4-methyl-1,2-benzenediol	-	0.035	0.301	1.178
20.32	4-ethylcatechol	-	-	0.089	0.582
21.21	4-hydroxy-3-methoxy-benzeneacetic acid	0.037	0.155	0.047	0.175
21.27	3,5-dihydroxytoluene	-	-	0.054	0.101
21.49	Hydroquinone	-	0.050	0.126	0.205
22.60	9-octadecenoic acid	-	0.107	-	-
25.21	Levogluconan	-	0.267	1.210	0.229
Total absolute peak area:		70.0	61.9	51.5	48.2
Number of compounds:		35	45	38	37

$T_{\text{fract.1}}$: 220 – 320 °C; $T_{\text{fract.2}}$: 320 – 350 °C; $T_{\text{fract.3}}$: 350 – 450 °C.

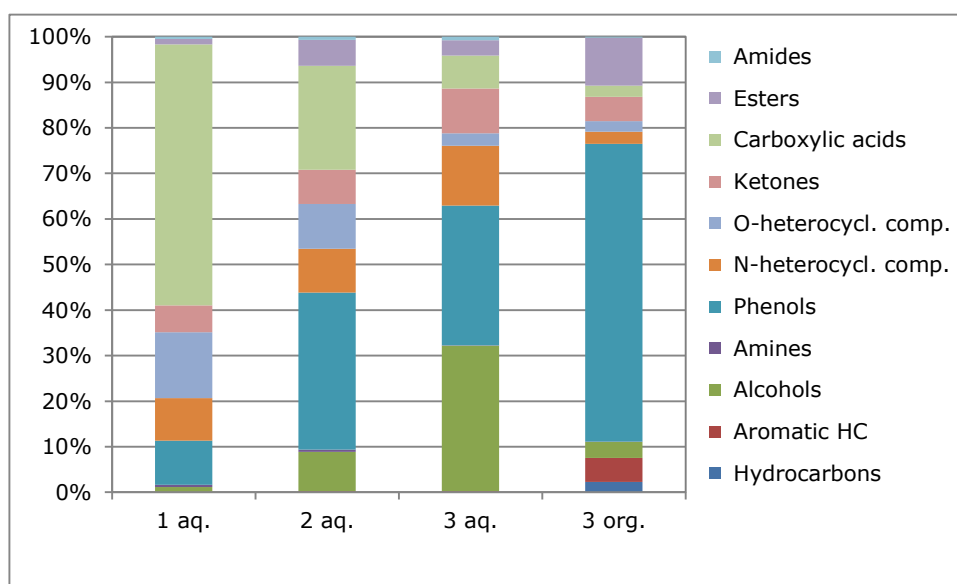


Figure 5-4: Overview of the classes of compounds present in the aqueous (aq.) and organic (org.) fractions collected as a function of temperature during slow pyrolysis of raspberry seed cake up to 450 °C.

Figure 5-4 reveals that **fraction 1** (220 – 320 °C) was mainly composed of carboxylic acids, of which acetic acid (RT: 8.85 min) was the major compound (Table 5-6). Other major classes of compounds were the O-heterocyclic and the N-heterocyclic compounds. The former consisted mainly of furan derivatives originating from degradation of hemicellulose, while the latter were formed by degradation of biomass proteins [7]. Phenols were only detected as a minor class, indicating that phenol degradation was rather limited at these relatively low temperatures.

Fraction 2 (320 – 350 °C), considered as a transition fraction, mainly consisted of phenols and carboxylic acids.

Fraction 3 spontaneously separated in two fractions. The aqueous fraction was mainly composed of alcohols, phenols and N-heterocyclic compounds. Within the class of alcohols, levoglucosan was an interesting compound from an economic point of view. This anhydrosugar has a relatively high value and was the most dominant compound of the aqueous fraction, enhancing its recovery possibilities. The organic oil fraction was almost completely composed of phenols, all derivatives of lignin components. These compounds were believed to be

responsible for the rather good properties of this fraction for use as renewable fuel (additive). Moreover, phenolic compounds also have potential to be valorized as added-value chemicals in the production of phenol-formaldehyde resins [2, 4] or as synthetic raw materials, flavor chemicals (e.g. vanillin), plant grow inhibitors, plant pathogen control agents and pharmaceutical precursors [10].

5.2.3 Solid residue

Ultimate analysis of the solid residue revealed the following composition: 77.9 wt% C, 3.1 wt% H, 3.1 wt% N, 12.1 wt% O and an ash content of 3.8 wt%. No significant amount of sulfur was detected. A HHV of 30.9 ± 0.1 MJ/kg was found by bomb calorimetry, indicating its relatively high energy content. These properties made the solid residue promising for valorization in stationary fuel applications. Other valorization pathways are the use in soil amelioration or as adsorbent. The potential of the solid residue produced by slow pyrolysis of raspberry seed cake without sand as heat transfer medium to be valorized in the production of AC is discussed in Chapter 6.

5.3 Conclusion

The pyrolysis temperature has a significant effect on the yield and properties of the products obtained by **flash pyrolysis** of raspberry seed cake. A temperature of 450 °C turned out to be optimal in terms of liquid yield (53.6 wt%). Hence, flash pyrolysis is found to be incomplete at 350 °C, while gasification reactions are more pronounced at 550 °C. The pyrolysis liquid produced at 450 °C is single-phased with a water content of 26.2 wt%, a HHV of 18.6 MJ/kg and a pH of 3.2. These physicochemical properties are comparable with those of pyrolysis liquids produced by flash pyrolysis of lignocellulosic biomass (e.g. wood). GC/MS analysis reveals phenols, carboxylic acids and alcohols as major classes of compounds. Regarding the production of added-value chemicals, levoglucosan and some phenolic compounds are interesting because of their high economic value. This high value is also necessary to make their recuperation from the pyrolysis liquid economically feasible. Separation of the solid residue from sand is problematic, making its valorization as precursor in the production of activated carbon unfavorable. However, its high energy content allows valorization as solid energy carrier at an industrial scale.

The pyrolysis liquid produced by **slow pyrolysis** of raspberry seed cake up to 450 °C is collected in three fractions. Fraction 1 (220 – 320 °C) is an aqueous liquid with a very high water content and carboxylic acids and O-heterocyclic compounds as major classes of compounds. Fraction 2 (320 - 350 °C) is considered as a transition fraction and is mainly composed of phenols and carboxylic acids. Fraction 3 (350 – 450 °C) spontaneously separates in an aqueous and organic oil fraction. The organic oil fraction is almost completely composed of phenolic compounds. Moreover, this fraction has a relatively low water content (9.3 wt%) and a relatively high calorific value (27.0 MJ/kg), making it promising for use as renewable fuel. Nevertheless, it should be investigated if the rather low yield of 12.1 wt% does not compromise the economics of the process. The aqueous fraction has a very high water content (67.4 w%), but contained a high amount of levoglucosan, an added-value chemical with high potential. The solid residue can be valorized as solid energy carrier because of its high calorific value (30.9 MJ/kg). In addition, the solid residue is also a possible precursor in the production of activated carbon since no separation from sand is required.

5.4 References

- [1] Mortensen, P.M., Grunwaldt, J.D., Jensen, P.A., Knudsen, K.G. and Jensen, A.D. A review of catalytic upgrading of bio-oil to engine fuels. *Applied Catalysis A: General*, 2011. **407**(1–2): 1-19.
- [2] Czernik, S. and Bridgwater, A.V. Overview of applications of biomass fast pyrolysis oil. *Energy & Fuels*, 2004. **18**(2): 590-598.
- [3] Meier, D., Oasmaa, A. and Peacocke, G.V.C. Properties of fast pyrolysis liquids: status of test methods. In: *Fast pyrolysis of biomass: a handbook*, Bridgwater, A., et al., Editors. CPL Press: Newbury, UK. 1999.
- [4] Mohan, D., Pittman, C.U. and Steele, P.H. Pyrolysis of wood/biomass for bio-oil: A critical review. *Energy & Fuels*, 2006. **20**(3): 848-889.
- [5] Radlein, D. Study of levoglucosan production - a review. In: *Fast pyrolysis of biomass: a handbook*, Vol. 2, Bridgwater, A.V., Editor. CPL Press: Newbury, UK. 2002. 205 - 241.
- [6] Shen, D.K. and Gu, S. The mechanism for thermal decomposition of cellulose and its main products. *Bioresource Technology*, 2009. **100**(24): 6496-6504.
- [7] Du, Z.Y., Hu, B., Ma, X.C., Cheng, Y.L., Liu, Y.H., Lin, X.Y., Wan, Y.Q., Lei, H.W., Chen, P. and Ruan, R. Catalytic pyrolysis of microalgae and their three major components: Carbohydrates, proteins and lipids. *Bioresource Technology*, 2013. **130**: 777-782.
- [8] Bridgwater, A.V. Review of fast pyrolysis of biomass and product upgrading. *Biomass and Bioenergy*, 2012. **38**(0): 68-94.
- [9] Basu, P. *Biomass gasification and pyrolysis - Practical design and theory*. 2010: Elsevier Inc.
- [10] Radlein, D. The production of chemicals from fast pyrolysis bio-oils. In: *Fast pyrolysis of biomass: a handbook*, Bridgwater, A.V., et al., Editors. CPL Press: Newbury, UK. 1999. 164 - 188.

6 Production and characterization of AC from agricultural waste cake

6.1 Introduction

Pyrolysis of agricultural waste cake results, besides pyrolysis liquid, also in a valuable solid residue. This solid residue can be valorized as energy source, as already discussed in Chapters 4 and 5. However, since a considerable amount of volatile organic compounds is removed during pyrolysis (carbonization), the solid residue shows a certain degree of raw porosity. Therefore, use of the solid residue as precursor in the production of activated carbon (AC) can be a promising valorization pathway as well.

Regular AC production is very costly due to the use of non-renewable and relatively expensive raw materials (e.g. coal, lignite or wood) [1, 2]. Recently, there has been a growing interest in the production of ACs from cheap precursor materials such as agricultural by-products [3-6]. To convert the raw porosity of solid residues into the well-developed porosity typical of ACs, physical or chemical activation at higher temperatures is required. Hence, carbonization (pyrolysis) up to 600 °C is generally not enough to remove all tars and volatile matter from the pores that are therefore partially blocked. Chemical activation involves mixing (impregnation) of the solid residue with a chemical reagent (such as $ZnCl_2$, H_2SO_4 , H_3PO_4 , KOH , $NaOH$, K_2CO_3 , Na_2CO_3 , etc.) prior to activation [7]. In case of physical activation, (mild) oxidizing gases (such as steam or CO_2) are used for controlled gasification of the solid residue avoiding the use of costly and/or environmentally harmful chemicals [3]. However, physical activation typically requires higher activation temperatures and longer activation times compared to chemical activation [7, 8].

In this chapter, the solid residue produced by slow pyrolysis of agricultural waste cake (i.e. rapeseed cake and raspberry seed cake) was used as precursor for the production of AC. The effect of the activation conditions (temperature, time and activation agent) on the yield and characteristics of the ACs was investigated. The ACs were characterized texturally by N_2 adsorption and morphologically by SEM. Additionally, their performance in liquid adsorption was assessed by batch phenol adsorption tests.

6.2 Production of activated carbon

6.2.1 Production of solid residue – AC precursor

Two agricultural waste cakes (rapeseed cake and raspberry seed cake) were carbonized at 450 °C for 1 h during slow pyrolysis (heating rate: 10 °C/min) in the semi-continuous reactor setup (section 2.2.3). Slow pyrolysis is preferred over flash pyrolysis because it generally leads to higher yields of solid residue and it does not require sand as heat transfer medium. Especially the latter is a considerable advantage since the separation of solid residue from sand is found to be problematic for both waste cakes (sections 4.1.4 and 5.1.3). An overview of the product yield is shown in Table 6-1. Results indicate that raspberry seed cake is a better precursor for AC production than rapeseed cake in terms of solid yield and ash content. The higher solid yield for raspberry seed cake can be explained by its high lignin content [9] (see Table 3-1).

Table 6-1: Product yield from slow pyrolysis of two agricultural waste cakes up to 450 °C for 1 h (SD between brackets).

Product yield (wt%)	Rapeseed cake	Raspberry seed cake
Solid residue	27.3 (0.5)	34.9 (1.3)
Char	22.4 (0.5)	32.3 (1.3)
Ash ^a	4.9	2.6
Pyrolysis liquid	52.1 (0.3)	44.8 (0.4)
Gas ^b	20.6 (0.8)	20.3 (1.0)

^a Determined by TGA of the biomass; ^b Calculated by difference

6.2.2 Production of activated carbon by physical activation

6.2.2.1 Yield of activated carbon

The solid residue, obtained as described in section 6.2.1, was physically activated under various experimental conditions using the horizontal tubular reactor setup (section 2.6). Two activation agents were used: steam (0.1 mL/min H₂O in 70 mL/min N₂) and CO₂ (70 mL/min). The influence of the activation temperature (T_{act}) was investigated at 850, 900 and 950 °C for a fixed activation time of 30 min, while the effect of activation time (t_{act}) was studied by four experiments (30, 60, 90 and 120 min) at a fixed temperature of 900 °C. The AC yield as a function of activation conditions is shown in Table 6-2.

Table 6-2: Yields of activated carbon produced from agricultural waste cake by physical activation (steam or CO₂) using various conditions of activation temperature (T_{act}) and activation time (t_{act}).

Activation	AC from rapeseed cake				AC from raspberry seed cake			
	T _{act} (°C)	t _{act} (min)	Burn-off ^a (wt%)	AC yield ^b (wt%)	Total yield ^c (wt%)	Burn-off ^a (wt%)	AC yield ^b (wt%)	Total yield ^c (wt%)
Steam	850	30	26.3	73.7	20.1	21.7	78.3	27.3
	900	30	35.1	64.9	17.7	35.0	65.0	22.7
	950	30	36.5	63.5	17.3	49.4	50.6	17.7
	900	30	35.1	64.9	17.7	35.0	65.0	22.7
	900	60	43.9	56.1	15.3	46.6	53.4	18.6
CO ₂	900	90	59.2	40.8	11.1	55.8	44.2	15.4
	900	120	69.6	30.4	8.3	63.4	36.6	12.8
	850	30	23.2	76.8	21.0	16.2	83.8	29.3
	900	30	23.1	76.9	21.0	19.3	80.7	28.2
	950	30	34.1	65.9	18.0	22.0	78.0	27.2
CO ₂	900	30	23.1	76.9	21.0	19.3	80.7	28.2
	900	60	30.4	69.6	19.0	22.7	77.3	27.0
	900	90	41.3	58.7	16.0	27.0	73.0	25.5
	900	120	49.6	50.4	13.8	31.2	68.8	24.0

^a Burn-off (wt%) = $(m_{\text{solid residue}} - m_{\text{activated carbon}}) / m_{\text{solid residue}} \times 100$

^b AC yield (wt%) = 100% - burn-off

^c Total yield = AC yield x yield of solid residue (Table 6-1)

The degree of burn-off represents the amount of solid residue that is removed (gasified) during activation and is generally strongly related to the development of pores in ACs.

Table 6-2 shows that burn-off values were increased by higher temperatures for both activation agents, regardless the precursor material. This indicated that the reaction of steam or CO₂ with carbon was endothermic and that high temperatures were required. Longer activation times (and so larger amounts of activation agent) considerably increased the degree of burn-off. The increase in burn-off with higher activation temperatures and longer activation times was generally more pronounced for steam than for CO₂ under analogous conditions. Moreover, CO₂ activation was found to be much more effective for rapeseed cake than for raspberry seed cake. Therefore, it was concluded that steam was more reactive than CO₂ and that the reactivity of the activation agent was also affected by the precursor material. In literature, the higher reactivity of steam is assigned to its more advantageous kinetics. Hence, steam has a lower molecular size than CO₂ that allows faster diffusion through the porous network and, as a consequence, an easier access to the micropores [10, 11].

In view of commercial AC production, the "total yield" is an important parameter. It represents the amount of AC that is produced per 100 g of agricultural waste cake and was calculated by multiplying the yield of solid residue (carbonization yield; Table 6-1) by the AC yield (activation yield). The total yield varied between 8.3 and 21.0 wt% for rapeseed cake and between 12.8 and 29.3 wt% for raspberry seed cake, depending on the activation conditions. These values are quite satisfactory since total yields between 10 and 20 wt% are reported for AC production to be economically viable [12].

6.2.2.2 *Ash content of activated carbon and HCl-washing*

A large amount of solid residue was gasified during physical activation as indicated by the burn-off. As a result, the inorganic ash was expected to concentrate progressively in the sample with higher degrees of burn-off. Therefore, the ash content of the solid residue was determined by calculation (ash_{calc}) and by TGA at 850 °C under oxygen atmosphere (ash_{TGA}). Results are shown in Table 6-3.

Table 6-3 Ash content (wt%) of the solid residue (no activation) and ACs derived from two agricultural waste cakes using various activation conditions.

Activation	T _{act} (°C)	t _{act} (min)	Rapeseed cake			Raspb. seed cake	
			ash _{calc} ^a	ash _{TGA}	ash _{HCl}	ash _{calc} ^a	ash _{TGA}
No activation	-	-	17.9	21.3	-	7.5	3.8
Steam	850	30	24.4	28.6	17.0	9.5	7.5
	900	30	27.7	28.4	13.4	11.5	6.2
	950	30	28.3	30.4	12.8	14.7	8.2
	900	30	27.7	28.4	13.4	11.5	6.2
	900	60	32.0	33.9	7.1	14.0	6.3
	900	90	44.1	45.4	14.6	16.9	8.3
	900	120	59.0	57.7	21.3	20.3	13.0
CO ₂	850	30	23.3	25.4	18.7	8.9	5.7
	900	30	23.3	26.5	18.6	9.2	6.7
	950	30	27.2	27.6	18.2	9.6	5.8
	900	30	23.3	26.5	18.6	9.2	6.7
	900	60	25.8	27.7	13.7	9.6	5.9
	900	90	30.6	31.5	12.2	10.2	8.0
	900	120	35.5	37.0	17.8	10.8	10.0

$$^a \text{ash}_{\text{calc}} = \text{ash}_{\text{biomass}} \times (100/\text{total AC yield})$$

In case of ACs derived from **rapeseed cake**, an ash content between 25.4 and 57.7 wt% was found by TGA. These results were in good agreement with the ash contents determined by calculation. This indicates that the inorganic ash of the rapeseed cake precursor (4.9 wt%) remains (almost) completely inside the AC after the carbonization and activation process. However, high ash contents are undesirable since they (almost) have no contribution to the adsorption process. Therefore, the ACs produced from rapeseed cake were boiled under reflux with HCl (0.1 M) for 1 h in order to remove as much ashes as possible. After this **HCl-washing** step, the ACs were subsequently washed with hot and cold distilled water to remove the remaining HCl, before being dried at 105 °C. Although complete ash removal could not be achieved, HCl-washing considerably reduced the ash content of the ACs (ash_{HCl}), as shown in Table 6-3. Moreover, the amount of ash removed from the AC (= ash_{TGA} - ash_{HCl}) increased for more

severe activation conditions and varied between 6.7 and 36.4 wt%. However, it should be noted that this ash removal is at the cost of the total yield of AC.

Figure 6-1 shows the FTIR spectra of a representative sample of AC produced from rapeseed cake (steam activation at 900 °C for 120 min; S-900-120) before and after HCl washing. The intense absorption bands at 1076 and 1039 cm^{-1} and at 592 and 564 cm^{-1} were assigned to the symmetric and asymmetric stretch vibrations of P-O bonds and to bending vibrations of O-P-O, respectively. The intensity of these bands was considerably reduced by HCl-washing, indicating that the compounds removed from the AC were mainly composed of salts of phosphates. This result was supported by ICP-AES analysis which revealed P together with Ca, K and Mg as major elements in the HCl-solution after HCl-washing of the AC.

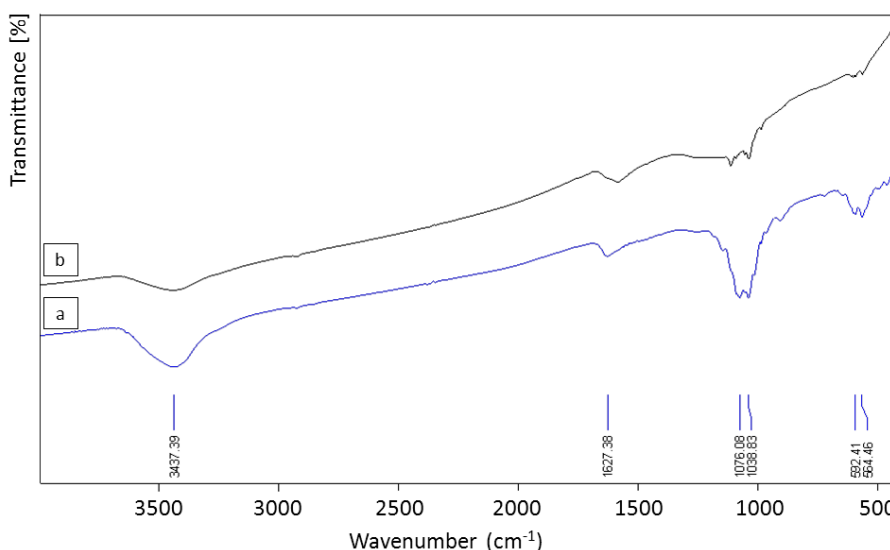


Figure 6-1: FTIR spectra of an AC produced from rapeseed cake (S-900-120) before (a) and after (b) HCl-washing (1 mg AC in 250 mg KBr).

The ACs derived from **raspberry seed cake** had a much lower ash content (5.7 - 13.0 wt%) than those produced from rapeseed cake (Table 6-3). It was remarkable that the calculated ash contents were (considerably) higher than those determined by TGA. This suggested that part of ashes was “lost” during carbonization and activation. Because of their relatively low ash content, the ACs from raspberry seed cake were not treated by an additional HCl-washing step.

6.3 Characterization of activated carbon

6.3.1 Nitrogen adsorption isotherms and pore size distributions

Physical activation of the solid residues was performed in order to obtain ACs with a well-developed porosity. The effects of the activation temperature, time and agent on the porosity of the ACs were investigated by N₂ adsorption at 77 K. For further information on the experimental work and the classification of adsorption isotherms is referred to section 2.7.1.

6.3.1.1 Rapeseed cake

The first step in interpreting N₂ adsorption isotherms is to identify the type of isotherm, as indicated by IUPAC [13]. In this way, preliminary information on the adsorption mechanism and the porous structure of the ACs is obtained. An overview is shown in Figure 6-2. In this figure, the ACs were designated X-T-t, where X is the activation agent (S and C for steam and CO₂, respectively), T the activation temperature and t the activation time.

The N₂ adsorption isotherms of the ACs derived from rapeseed cake (HCl-washed) were classified as type IV isotherms [14]. This type of isotherm is commonly found for mesoporous industrial adsorbents [13]. The very steep initial part of the isotherm ($p/p_0 < 0.05$) was assigned to micropore filling, indicating that the ACs had a considerable degree of microporosity (pore widths < 2 nm) as well. The second part of the isotherm ($p/p_0 > 0.4$) consisted of two separated branches: one branch for adsorption and one for desorption. This phenomenon is called hysteresis and is associated with capillary condensation in mesopores (2 – 50 nm). For all samples, the hysteresis loop was classified as type H4 (according to the IUPAC classification), resembling those of microporous adsorbents with narrow slit-shaped pores [13]. The hysteresis loops were found to become more pronounced for samples activated at higher temperatures and for longer activation times.

Figure 6-3 gives an overview of the pore size distribution (PSD) of the ACs in the micro- and mesopore range. In case of steam activation, both micro- and mesopores increased between 850 and 900 °C, while a further temperature increase to 950 °C hardly improved the porosity (Figure 6-3a). An extension of the activation time from 30 to 60 min increased both the micro- and mesopore volume for steam activated samples (Figure 6-3b). However, a further increase

in activation time (90 and 120 min) did not result in an enhanced microporosity, but rather in a considerable widening of the mesopores. In case of CO₂ activation, almost no mesopores were observed for the AC produced at 850 °C, while the increase in mesopore volume from 900 to 950 °C occurred at the expense of the micropore volume (Figure 6-3c). Longer activation times increased both the micro- and mesopore volume of the CO₂ activated samples (Figure 6-3d). This increase in mesopore volume was rather limited up to an activation time of 90 min, while a considerable increase, together with a significant widening of the mesopores, was observed for 120 min.

6.3.1.2 Raspberry seed cake

Figure 6-4 shows the N₂ adsorption isotherms of the ACs produced from raspberry seed cake. In case of steam activation, type IV adsorption isotherms with type H4 hysteresis loops were found for all samples, except for the one activated at the lowest temperature (850 °C). In contrast, the adsorption isotherms of the CO₂ activated samples behaved rather like type I isotherms, except for the ones with longer activation times (90 and 120 min). These observations suggest that the activation agent played an important role in the pore development in case of raspberry seed cake. This becomes more clear when looking at the PSDs (Figure 6-5). In case of steam activation, no mesopores were observed for the sample activated at 850 °C, while (limited) mesopore development was found at 900 and 950 °C (Figure 6-5a). Longer activation times turned out to increase both micro- and mesopore volumes simultaneously up to 90 min, while a further extension to 120 min seemed mainly to increase the mesopore volume (Figure 6-5b). In contrast, the PSDs of CO₂ activated samples did not show mesopores up to activation times of 90 and 120 min, while the micropore volume was considerably increased by higher activation temperatures and longer activation times (Figure 6-5c-d). Therefore, it is concluded that CO₂ results in microporous ACs at the early stage of activation and that mesopore development starts at a later stage (more severe activation conditions) leading to ACs with a mixed micro- and mesoporous structure. In contrast, micro- and mesopores are formed simultaneously from the early stage of activation in case of steam activation.

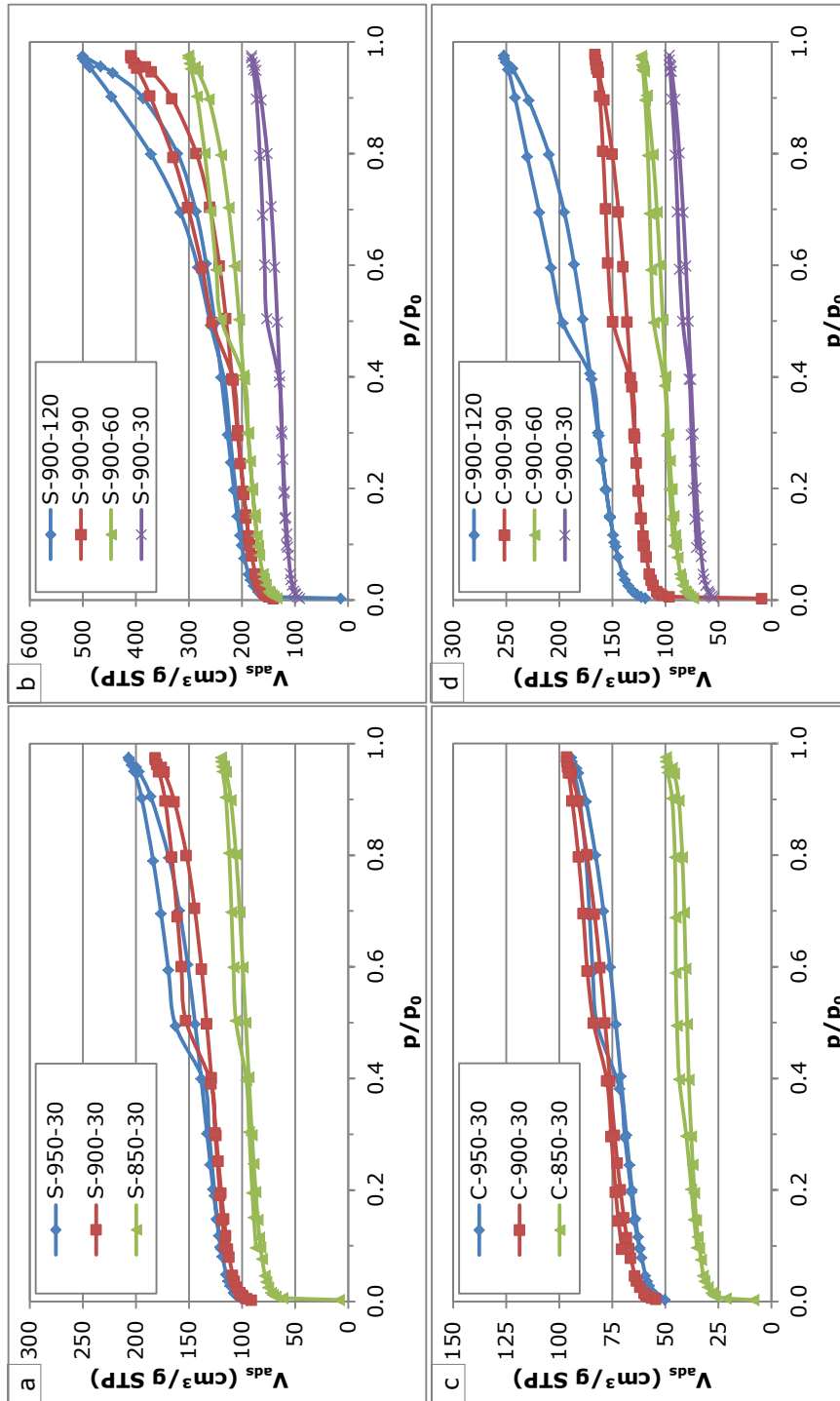


Figure 6-2: N_2 adsorption isotherms of ACs (HCl-washed) produced from rapeseed cake by steam activation as a function of temperature (a) and activation time (b); and by CO_2 activation as a function of temperature (c) and time (d). (Sample code: X-T-t).

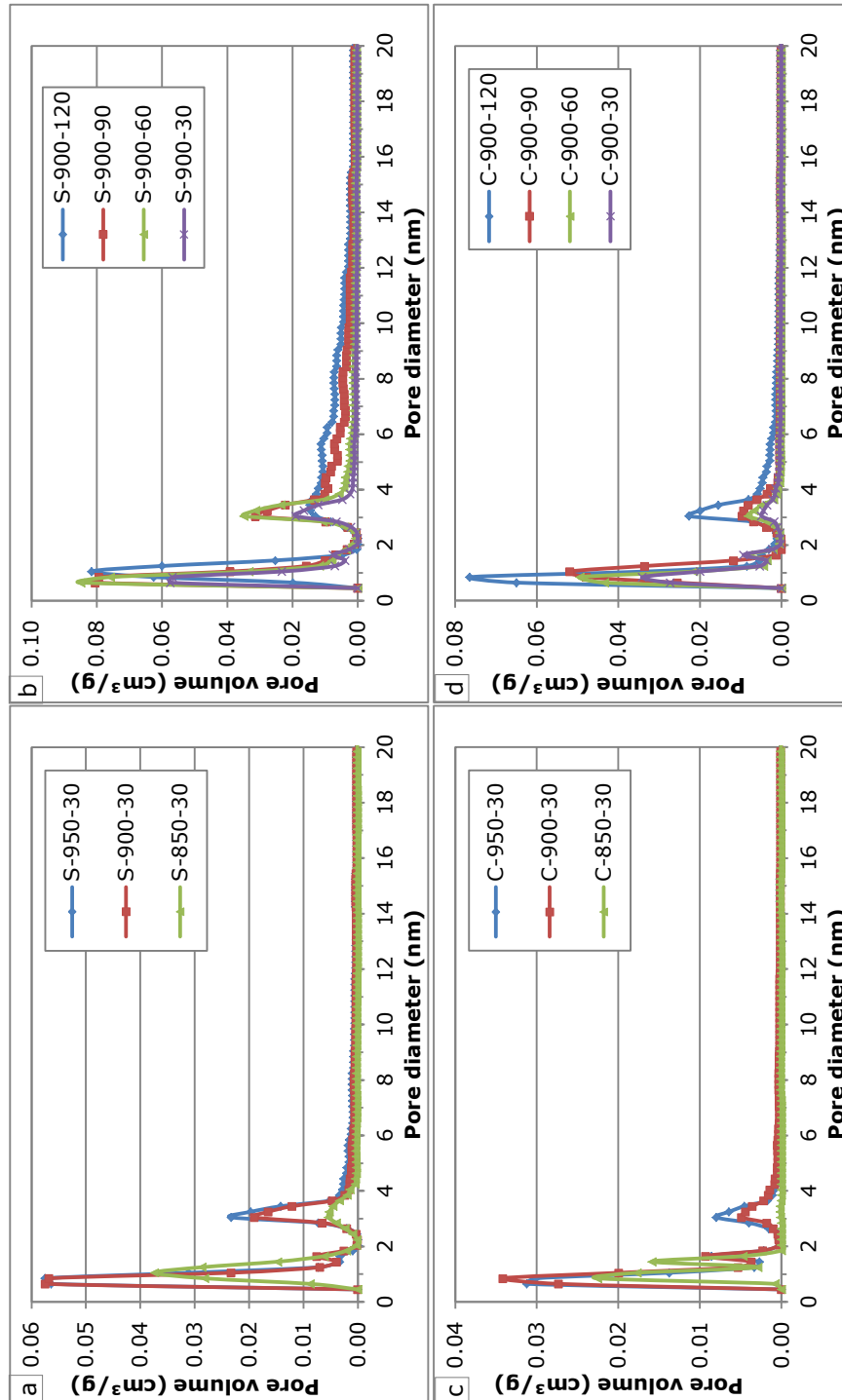


Figure 6-3: Pore size distribution by the QSDFT method of ACs (HCl-washed) produced from rapeseed cake by steam activation as a function of temperature (a) and activation time (b); and by CO₂ activation as a function of temperature (c) and time (d). (Sample code: X-T-t).

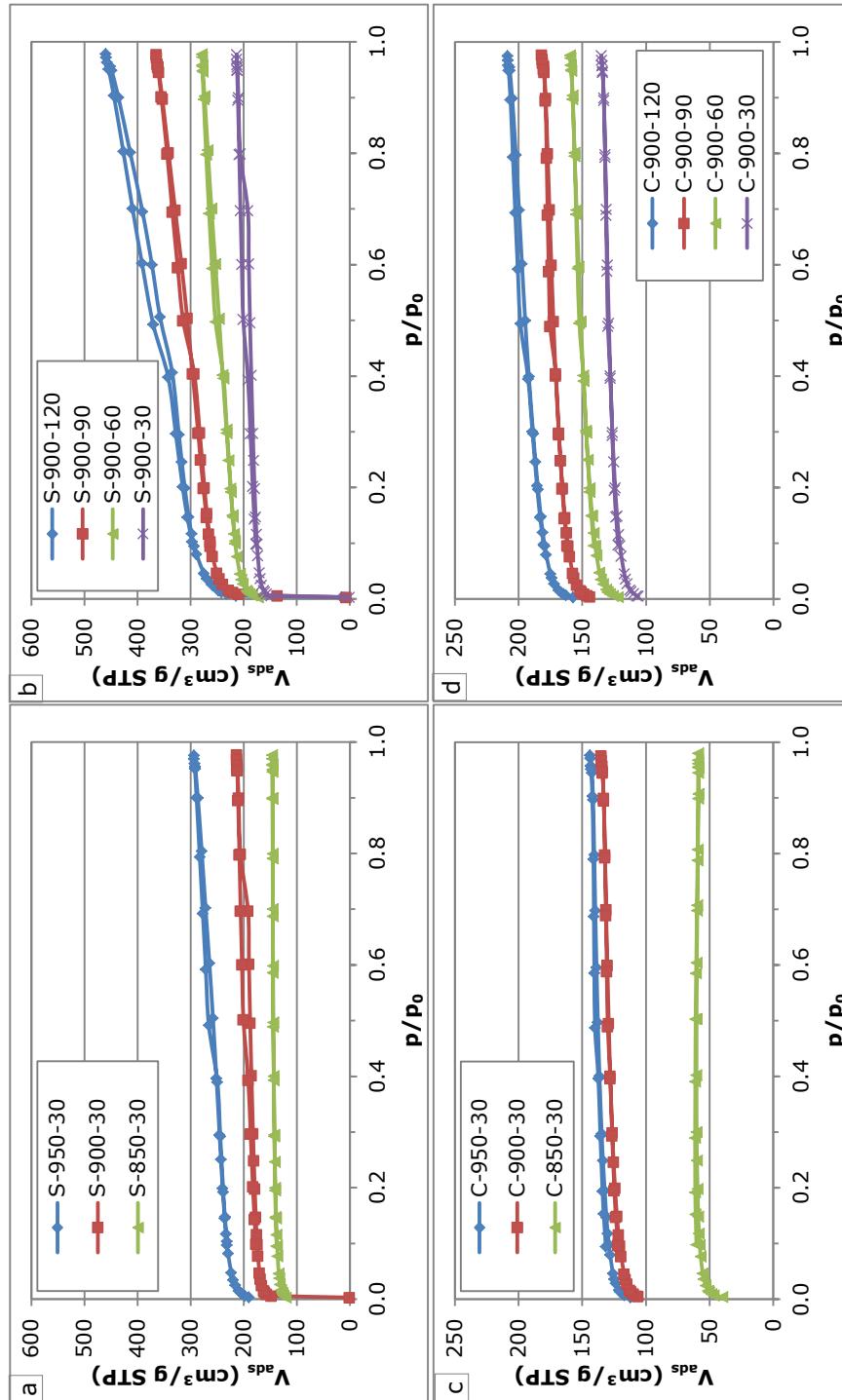


Figure 6-4: N₂ adsorption isotherms of ACs produced from raspberry seed cake by steam as a function of temperature (a) and activation time (b); and by CO₂ activation as a function of temperature (c) and time (d). (Sample code: X-T-t).

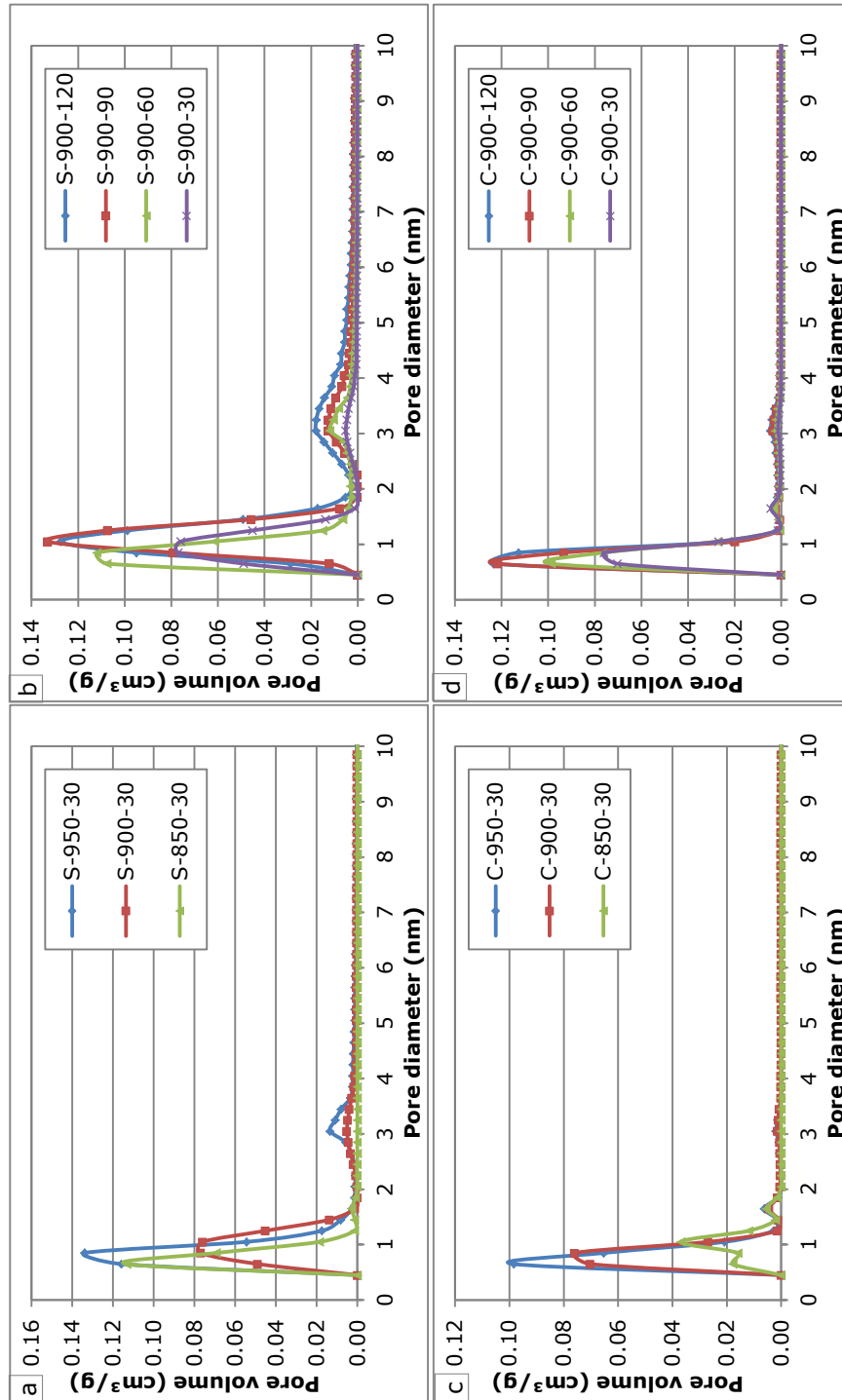


Figure 6-5: Pore size distribution by the QSDFT method of ACs produced from raspberry seed cake by steam activation as a function of temperature (a) and activation time (b); and by CO_2 activation as a function of temperature (c) and time (d). (Sample code: X-T-t).

6.3.2 Textural characteristics of ACs

Several important textural characteristics of the ACs were inferred from the N₂ adsorption isotherms. The BET specific surface area (s_{BET}), the total pore volume (V_{t}), the mesopore volume (V_{me}), the micropore volume by the Dubinin-Radushkevich method (V_{DR}) and the average micropore width (L_0) were obtained as described in sections 2.7.1.3 to 2.7.1.5. The contribution of the micropore volume to the total pore volume was assessed by the $V_{\text{DR}}/V_{\text{t}}$ ratio.

6.3.2.1 Rapeseed cake

The textural characteristics of the ACs produced from rapeseed cake (after HCl-washing) are summarized in Table 6-4.

The **solid residue** had a very low BET specific surface area (0.5 m²/g), making characterization of its porosity impossible. This strongly indicated that activation was absolutely necessary to obtain a well-performing AC.

Higher **activation temperatures** increased the BET specific surface area and the pore volumes (V_{t} , V_{me} , and V_{DR}) of all samples, except for the one activated by CO₂ at 950 °C. In case of the latter, s_{BET} , V_{t} and V_{DR} decreased between 900 and 950 °C, while V_{me} slightly increased. Therefore, a part of the microporosity was believed to be destructed and converted into mesoporosity. In general, the $V_{\text{DR}}/V_{\text{t}}$ ratio decreased as a function of activation temperature, indicating that the contribution of the micropore volume to the total pore volume decreased in favor of the mesopore volume, although micro- and mesopore volumes both increased in absolute terms (except for CO₂ activation at 950 °C).

An extension of the **activation time** from 30 to 120 min considerably increased the BET specific surface area and the porosity of all ACs, regardless the activation agent. In case of steam activation, the $V_{\text{DR}}/V_{\text{t}}$ ratio was considerably decreased by longer activation times, while the average micropore diameter (L_0) significantly increased. This indicated that micropores became wider and that mesopores had a larger contribution to the total pore volume when longer activation times were used. In contrast, CO₂ activation resulted in a $V_{\text{DR}}/V_{\text{t}}$ ratio that first (slightly) increased between 30 and 60 min, remained constant (60 – 90 min) and then significantly decreased between 90 and 120 min. This suggested that the contribution of micropores to the total pore volume reached an optimum before decreasing considerably as a function of activation time.

Table 6-4: Textural characteristics of ACs (HCl-washed) produced from rapeseed cake under various activation conditions as determined by N₂ adsorption at 77 K.

Activation	T _{act} (°C)	t _{act} (min)	Burn-off (wt%)	S _{BET} (m ² /g)	V _t (cm ³ /g)	V _{me} (cm ³ /g)	V _{DR} (cm ³ /g)	L ₀ (nm)	V _{DR} /V _t
Steam	850	30	26.3	336	0.181	0.047	0.134	1.44	0.74
	900	30	35.1	458	0.272	0.092	0.180	1.02	0.66
	950	30	36.5	483	0.309	0.118	0.191	1.04	0.62
	900	30	35.1	458	0.272	0.092	0.180	1.02	0.66
	900	60	43.9	678	0.446	0.178	0.268	1.11	0.60
	900	90	59.2	737	0.589	0.294	0.295	1.32	0.50
	900	120	69.6	804	0.720	0.392	0.328	1.94	0.46
	850	30	23.2	141	0.073	0.015	0.058	2.57	0.79
	900	30	23.1	272	0.147	0.039	0.108	1.12	0.73
	950	30	34.1	250	0.142	0.043	0.099	1.01	0.69
CO ₂	900	30	23.1	272	0.147	0.039	0.108	1.12	0.73
	900	60	30.4	362	0.187	0.045	0.142	0.94	0.76
	900	90	41.3	487	0.253	0.061	0.192	1.08	0.76
	900	120	49.6	591	0.379	0.145	0.234	1.09	0.62
Commercial AC	-	-	-	1115	0.581	0.124	0.457	2.63	0.79

Comparison of the **activation agents** revealed that steam was more effective (reactive) than CO₂ in terms of burn-off, BET specific surface area and porosity under analogous activation conditions. However, comparison of both activation agents for samples with similar degrees of burn-off can provide valuable information on the activation mechanism (Figure 6-6). In case of steam, the increase in total pore volume was caused by a simultaneous increase in micro- and mesopore volume from the early stage of activation up to a burn-off of 43.9 wt%. At higher burn-off values, the rate of micropore development decreased while that of the mesopores remained unchanged. As a result, the mesopore volume became even predominant over the micropore volume at burn-off values higher than 60.0 wt% (Figure 6-6a). In case of CO₂ activation, the rate of micropore development was rather constant over the complete range of burn-off (23.2 – 49.6 wt%). In contrast, the mesopore volume remained small during the early stages of activation, before increasing considerably for burn-off values higher than 41.3 wt% (Figure 6-6b). In all cases, steam resulted in larger pore volumes (V_{tr} , V_{me} , and V_{DR}) than CO₂ at similar degrees of burn-off (compare Figure 6-6a with Figure 6-6b). Therefore, it is concluded that steam is more reactive than CO₂ in terms of pore development when similar degrees of burn-off are considered. This higher reactivity of steam may be related to its smaller molecular size compared to CO₂, which facilitates its diffusion within the porous structure of the AC during activation [15]. Moreover, it is reported in literature that steam simultaneously attacks active sites at the pore center and on the pore walls, whereas CO₂ primarily reacts with active sites at the pore center before attacking the pore walls. Therefore, CO₂ activation requires longer activation times to develop new microporosity and to broaden the existing micropores [3, 10, 16].

The characteristics of a **commercial grade AC** (Norit GAC 1240)¹² were included in Table 6-4. In general, ACs produced from rapeseed cake had a considerably lower BET specific surface area and lower micropore volumes than the commercial AC. However, steam activation at 900 °C for 90 or 120 min turned out to be the best performing activation conditions, but resulted in ACs with a considerably higher degree of mesoporosity than the commercial AC.

¹² Norit GAC 1240 is an acid washed granular AC that is produced by steam activation of coal.

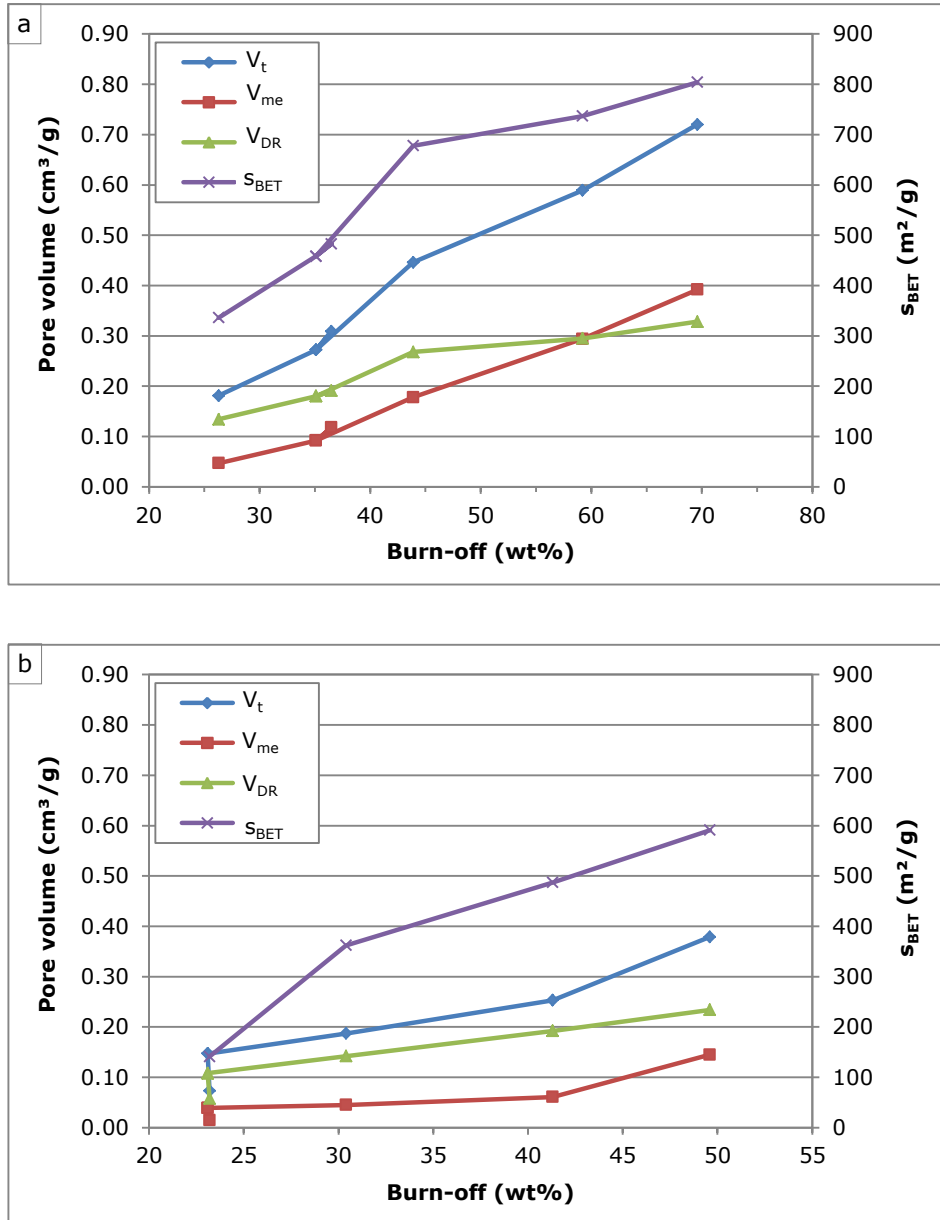


Figure 6-6: BET specific surface area (s_{BET}) and pore volumes (V_t , V_{me} and V_{DR}) as a function of burn-off for ACs (HCl-washed) produced from rapeseed cake by steam (a) and CO₂ activation (b). (Sample C-950-30 and the s_{BET} of C-900-30 were omitted from Figure 6-6b).

6.3.2.2 Raspberry seed cake

The **solid residue** of raspberry seed cake was found to have a BET specific surface area of 20 m²/g. This was higher than that of rapeseed cake, but still not comparable to normal values of ACs (500 to 2000 m²/g [7]).

Higher **activation temperatures** gave rise to higher BET specific surface areas and larger pore volumes (V_t , V_{me} and V_{DR}), regardless the activation agent (Table 6-5). However, both activation agents acted differently. In case of steam, both parameters showed a linear increase between 850 and 950 °C. In contrast, CO₂ activation led to a strong increase up to 900 °C followed by a slight increase between 900 and 950 °C. This indicated that temperatures above 850 °C were required for effective pore development in case of CO₂ activation.

Longer **activation times** increased the BET specific surface area and the porosity of all ACs. In case of steam, the V_{DR}/V_t ratio decreased with longer activation times, indicating that the contribution of the micropore volume to the total pore volume decreased in favor of the mesopore volume. The increase in average micropore diameter (L_0) with the activation time suggested that the micropores were enlarged and partly converted into mesopores. In contrast, the V_{DR}/V_t ratio and the L_0 value were hardly affected by the activation time in case of CO₂ activation.

Comparison of both **activation agents** showed that steam was much more effective than CO₂ in terms of burn-off, BET specific surface area and pore development under analogous conditions. For a better understanding of the pore development, samples with similar degrees of burn-off were compared (Figure 6-7). In case of steam, the micro- and mesopore volume simultaneously increased from the early stage of activation up to a burn-off value of 49.4 wt%. At higher burn-off values, the increase in mesopore volume became more pronounced than that of the micropore volume, although the latter remained predominant in absolute terms (Figure 6-7a). In case of CO₂ activation, the micropore volume steadily increased with the degree of burn-off, while almost no mesopores were found (Figure 6-7b). This indicated that CO₂ activation led to ACs with a very high degree of microporosity in case of raspberry seed cake. Therefore, it is concluded that steam is a more effective activation agent than CO₂ when samples with a similar degree of burn-off are considered.

Table 6-5: Textural characteristics of the ACs prepared from raspberry seed cake under different activation conditions as determined by N_2 adsorption at 77 K.

Activation	T_{act} (°C)	t_{act} (min)	Burn-off (wt%)	S_{BET} (m^2/g)	V_t (cm^3/g)	V_{me} (cm^3/g)	V_{DR} (cm^3/g)	L_0 (nm)	V_{DR}/V_t
	850	30	21.7	563	0.226	0.009	0.217	0.62	0.96
	900	30	35.0	721	0.328	0.048	0.280	0.82	0.85
	950	30	49.4	941	0.451	0.081	0.370	0.98	0.82
Steam	900	30	35.0	721	0.328	0.048	0.280	0.82	0.85
	900	60	46.6	873	0.429	0.086	0.343	0.95	0.80
	900	90	55.8	1081	0.559	0.117	0.442	2.02	0.79
	900	120	63.4	1179	0.698	0.209	0.489	2.24	0.70
	850	30	16.2	236	0.091	0.000	0.091	1.51	1.00
	900	30	19.3	492	0.208	0.018	0.190	0.69	0.92
	950	30	22.0	529	0.221	0.017	0.204	0.68	0.93
CO ₂	900	30	19.3	492	0.208	0.018	0.190	0.69	0.92
	900	60	22.7	572	0.246	0.026	0.220	0.64	0.90
	900	90	27.0	660	0.279	0.025	0.254	0.63	0.91
	900	120	31.2	735	0.320	0.036	0.284	0.66	0.89
Commercial AC	-	-	-	1115	0.581	0.124	0.457	2.63	0.79

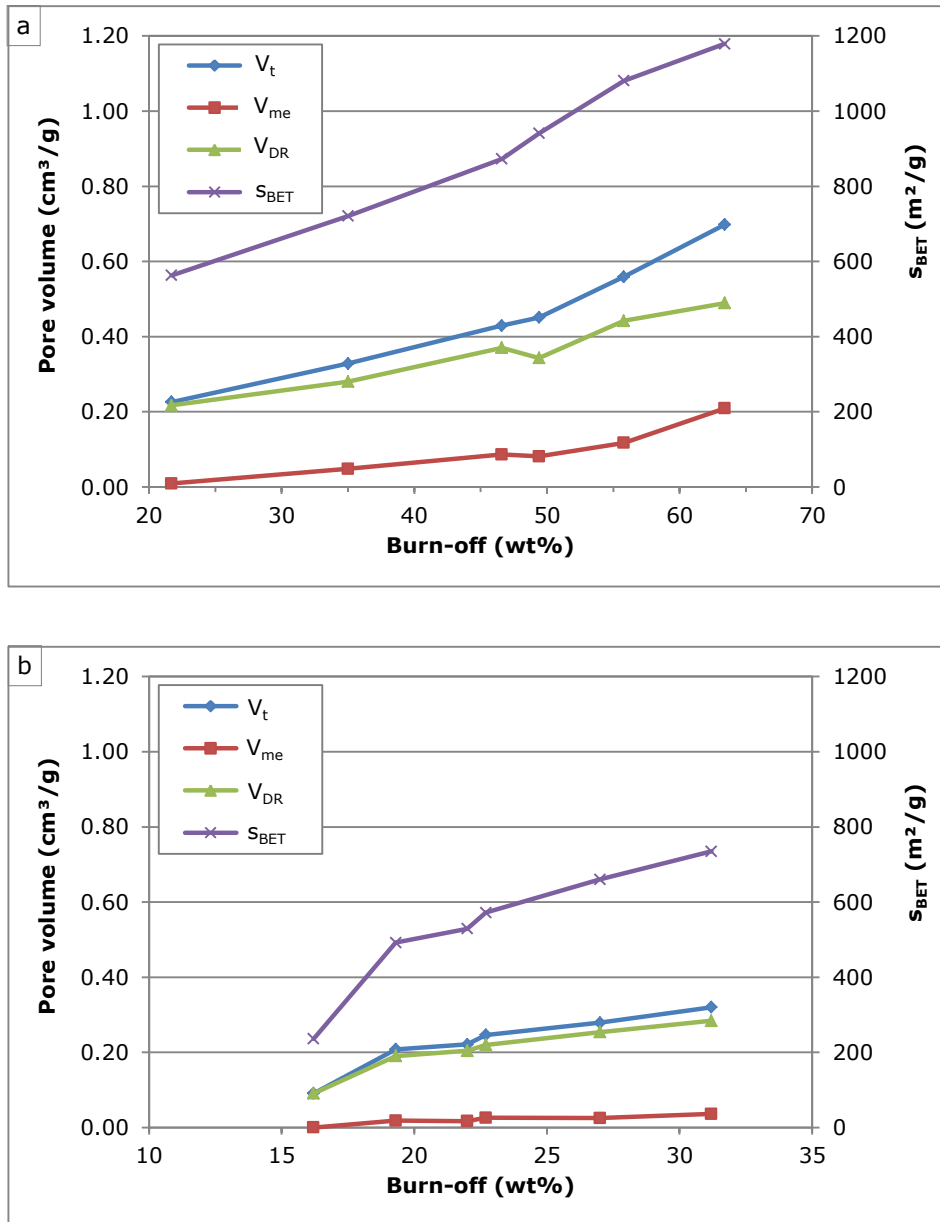


Figure 6-7: BET specific surface area (s_{BET}) and pore volume (V_t , V_{me} , V_{DR}) as a function of burn-off for ACs produced from raspberry seed cake by steam (a) and CO₂ activation (b).

The conclusion made above is in accordance with literature [10, 16] and the conclusions made for rapeseed cake. However, the development of mesopores could not be observed in case of the CO₂ activated samples due to the rather limited range of burn-off (16.2 – 31.2 wt%) that was obtained under the applied activation conditions.

The AC produced by steam activation at 900 °C for 90 min showed a BET specific surface area and a pore volume distribution (V_{tr} , V_{me} and V_{DR}) that was very similar to that of the **commercial grade AC**, while even better textural characteristics were observed for an activation time of 120 min (Table 6-5). Therefore, it is concluded that the solid residue of raspberry seed cake has a very high potential to be valorized in the production of AC by steam activation. Activation by CO₂ is less effective, but results in ACs that have potential to be valorized in adsorption processes requiring microporous adsorbents.

6.3.3 Elemental composition of activated carbons

The elemental composition of solid residues and ACs were determined as described in section 2.7.2. Results are shown in Table 6-6. The ACs derived from rapeseed cake were HCl-washed prior to analysis.

The ACs had a higher carbon content and a lower content of hydrogen and nitrogen than the corresponding solid residue, regardless the precursor material. In case of rapeseed cake, physical activation did not reduce the oxygen content of the ACs, while the oxygen content of ACs derived from raspberry seed cake was significantly lower than that of the solid residue. Comparison of both waste cakes revealed that ACs produced from raspberry seed cake had a higher carbon content and a lower content of hydrogen, nitrogen, sulfur and oxygen than those derived from rapeseed cake.

In literature, the sulfur content of ACs is reported as an important parameter for the use of ACs as an adsorbent, i.e. sulfur contents below 1 wt% are desirable [17]. This requirement was easily met for ACs produced from raspberry seed cake since only minor amounts of sulfur were detected in both solid residue and ACs. In contrast, the ACs derived from rapeseed cake still contained a considerable amount of sulfur. However, longer activation times seemed to favor sulfur removal, leading to values less than 1 wt%.

Table 6-6: Elemental analysis (wt%) of the solid residues (no activation) and ACs produced from rapeseed cake (HCl-washed) and raspberry seed cake under various activation conditions.

Activation	T _{act} (°C)	t _{act} (min)	Rapeseed cake (HCl-washed)						Raspberry seed cake					
			C	H	N	S	O ^a	Ash ^b	C	H	N	S	O ^a	Ash ^b
No activation ^c	-	-	64.5	2.5	5.8	0.3	5.5	21.3	77.9	3.1	3.1	<0.1	12.1	3.8
	850	30	68.8	1.6	3.9	1.2	7.6	17.0	89.1	1.1	2.1	<0.1	0.2	7.5
	900	30	77.0	1.3	3.5	1.0	3.8	13.4	89.1	0.9	1.5	<0.1	2.4	6.2
	950	30	77.1	1.1	3.0	1.4	4.6	12.8	88.7	0.9	1.5	<0.1	0.7	8.2
Steam	900	30	77.0	1.3	3.5	1.0	3.8	13.4	89.1	0.9	1.5	<0.1	2.4	6.2
	900	60	82.6	1.2	3.4	0.5	5.3	7.1	88.9	0.8	1.3	<0.1	2.7	6.3
	900	90	75.8	1.1	2.7	0.6	5.2	14.6	88.7	0.9	1.3	<0.1	0.9	8.3
	900	120	69.8	1.2	1.5	0.4	5.8	21.3	86.7	1.0	1.1	<0.1	-	13.0
	850	30	69.4	1.2	4.9	1.4	4.4	18.7	87.7	0.8	2.1	<0.1	3.6	5.7
	900	30	73.9	1.2	4.6	1.5	0.1	18.6	89.5	0.9	2.2	<0.1	0.7	6.7
	950	30	72.9	1.1	4.2	1.3	2.4	18.2	88.9	0.8	2.2	<0.1	2.3	5.8
CO ₂	900	30	73.9	1.2	4.6	1.5	0.1	18.6	89.5	0.9	2.2	<0.1	0.7	6.7
	900	60	73.3	1.0	4.6	0.2	7.2	13.7	88.6	0.8	2.3	<0.1	2.4	5.9
	900	90	77.1	1.1	4.7	0.3	4.5	12.2	88.3	0.8	2.2	<0.1	0.7	8.0
	900	120	72.1	1.6	3.9	0.6	4.1	17.8	88.6	0.8	2.2	<0.1	-	10.0

^a Calculated by difference; ^b Determined by TGA; ^c The solid residue of rapeseed cake was not HCl-washed.

6.3.4 Functional groups of activated carbons

In general, heteroatoms (such as oxygen and nitrogen) are important elements concerning the surface chemistry of ACs since they are mostly part of organic functional groups at the edge of carbon crystallites. In this view, oxygen typically occurs in carboxyl, carbonyl, phenol, ether or lactone functionalities, while nitrogen is mainly found as a part of amines or nitro-groups [18]. Because surface functional groups can play an important role in adsorption processes, the solid residues and ACs were investigated by ATR-FTIR spectroscopy as described in section 2.7.3. Figure 6-8 shows the spectra of the solid residues and of four representative ACs produced from both agricultural waste cakes.

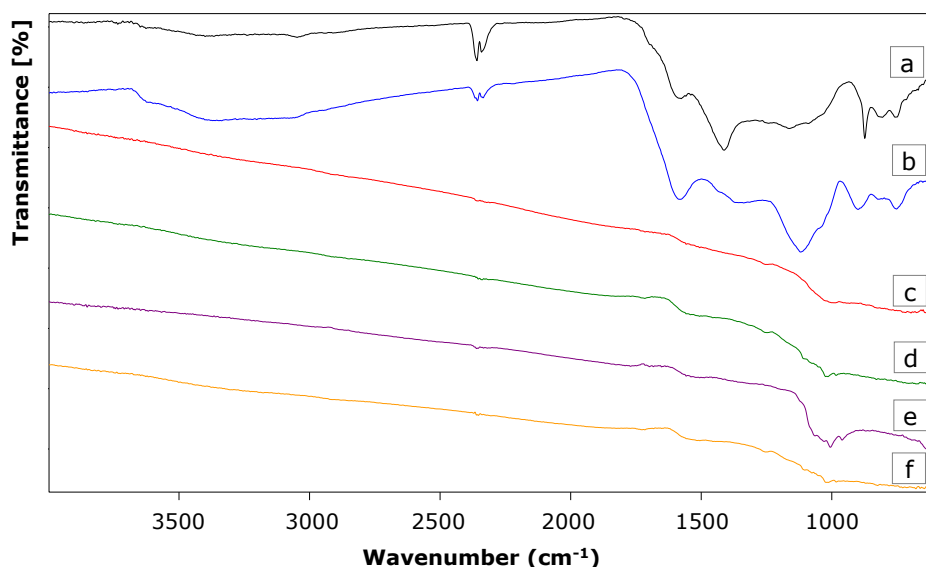


Figure 6-8: ATR-FTIR spectra of the solid residue from raspberry seed cake (a) and from rapeseed cake (b); of ACs produced from raspberry seed cake (c) and rapeseed cake (d) by CO₂ activation (C-900-120); and ACs derived from raspberry seed cake (e) and rapeseed cake (f) by steam activation (S-900-90, HCl-washed in case of rapeseed cake).

Several broad overlapping bands were observed in the ATR-FTIR spectra of the **solid residues** (Figure 6-8a-b). Approximate band assignment suggested the presence of carboxyls, carbonyls, lactones, phenols, olefinic and aromatic structures. Hence, the spectral region of 1750 – 1550 cm⁻¹ is associated with C=O stretching vibrations of carbonyls, carboxylic acids and lactones, and with

C=C bonds in olefinic and aromatic structures. The bands between 1460 and 1000 cm^{-1} could represent C-O and O-H bending vibrations [4]. However, assignment of a specific wavenumber to a given functional group was not possible due to overlap and shifts of the absorption bands of various functional groups [4].

The surface chemistry of **activated carbons** differed significantly from that of solid residues. Hence, almost no absorption bands were found in case of the representative ACs (Figure 6-8c-f). This indicated that almost all surface functional groups were removed by the applied activation conditions.

6.3.5 Surface morphology of activated carbons

The ACs of both waste cakes were investigated by SEM. No systematic effect of the activation conditions (temperature, time and activation agent) on the morphology of the ACs could be observed from the SEM images. However, the morphology of the ACs did significantly depend on the precursor material. An overview of two representative samples is shown in Figure 6-9.

In case of rapeseed cake (Figure 6-9a-c), a lot of AC particles had a sponge-like porous structure (Figure 6-9b) which consisted of long parallel nearly cylindrical shaped pores with quite uniform pore widths (Figure 6-9c). For the ACs derived from raspberry seed cake (Figure 6-9d-f), many particles showed a layered surface with porous edges (Figure 6-9e). A closer look at the edges (Figure 6-9f) revealed pores with nonuniform widths and quite irregular shapes.

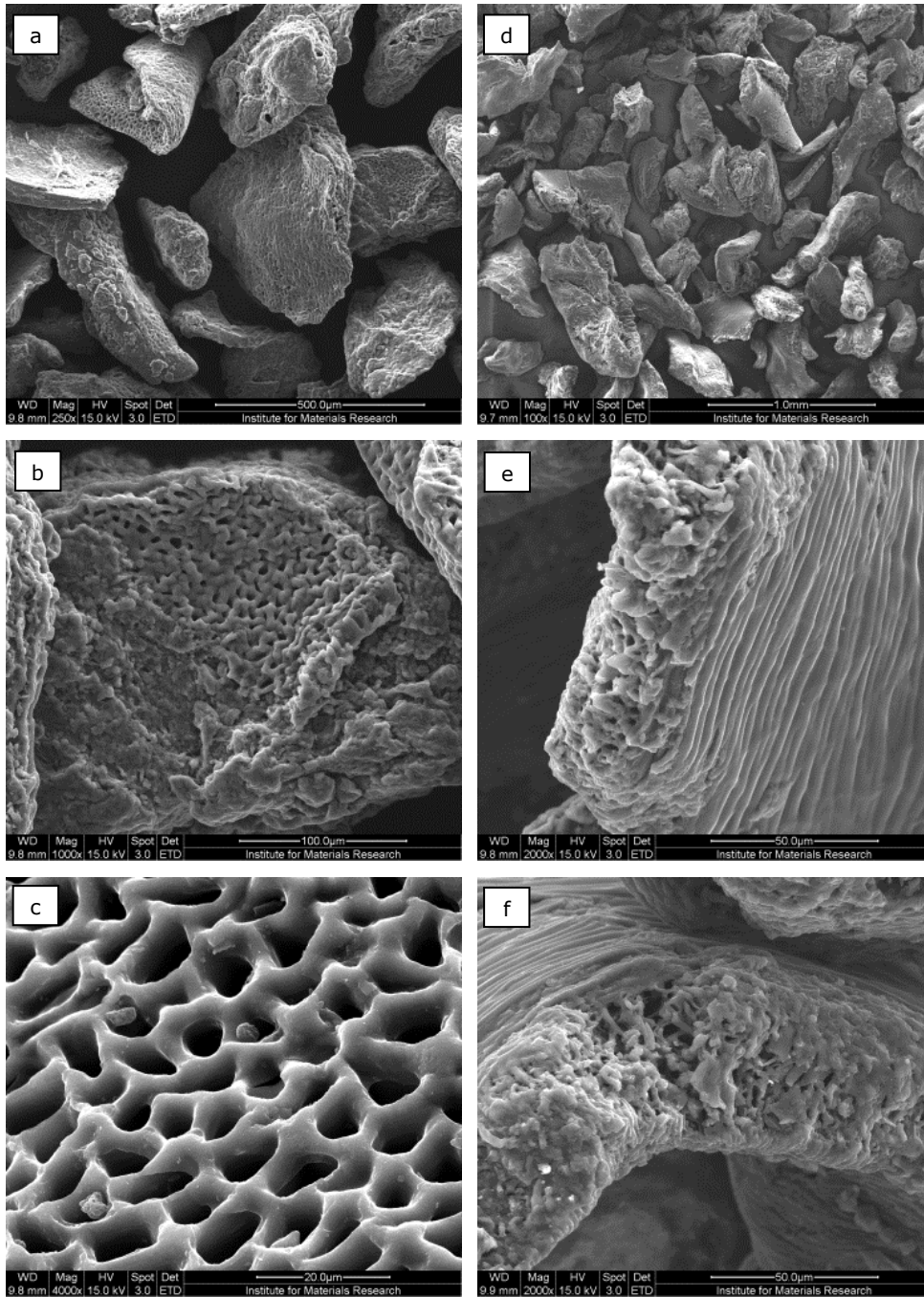


Figure 6-9: SEM images of ACs produced from rapeseed cake (C-900-60) with a magnification factor of 250 (a), 1000 (b) and 4000 (c); and ACs produced from raspberry seed cake (C-950-30) with a magnification factor of 100 (d), 2000 (e) and (f).

6.4 Phenol adsorption study

The performance of the ACs in liquid adsorption is investigated by adsorption of phenol from aqueous solutions. Phenol is chosen as target compound because it is found as persistent pollutant in many wastewaters such as those of petroleum refining, pharmaceutical and plastic industries [19]. Moreover, phenol has detrimental effects on human health and aquatic life and therefore must be removed from wastewaters [20]. Among several methods (such as oxidation, precipitation and ion exchange), adsorption of phenol on AC is one of the most effective and widely used treatment techniques for phenolic wastewaters [20, 21]. In this regard, a high adsorption capacity, a large surface area and a high degree of microporosity are important AC characteristics [22].

6.4.1 Phenol adsorption isotherms

Phenol adsorption experiments were carried out at 25 °C for 48 h by loading the AC (about 25 mg) into aqueous solutions (25 mL) with at least six different initial concentrations of phenol (5 - 400 mg/L). For additional information on the experimental work is referred to section 2.8.

6.4.1.1 Rapeseed cake

The phenol adsorption isotherms of ACs derived from rapeseed cake are shown in Figure 6-10. The solid residue showed almost no phenol adsorption, indicating that activation was absolutely necessary for a significant uptake of phenol.

Higher **activation temperatures** gave rise to better adsorption characteristics, regardless the activation agent. Steam activated samples performed much better than CO₂ activated samples under similar conditions. Moreover, phenol adsorption was hardly improved by CO₂ activation at 850 °C compared to the solid residue, suggesting that activation temperatures higher than 850 °C were required to obtain a well-performing AC in case of CO₂ activation.

Longer **activation times** significantly improved the phenol adsorption. Again, steam led to better performing ACs than CO₂ under similar conditions. The biggest increase in phenol uptake was observed between 30 and 60 min for steam activation and between 60 and 90 min for CO₂ activation. A further increase of the activation time up to 120 min hardly improved the phenol adsorption, regardless the activation agent.

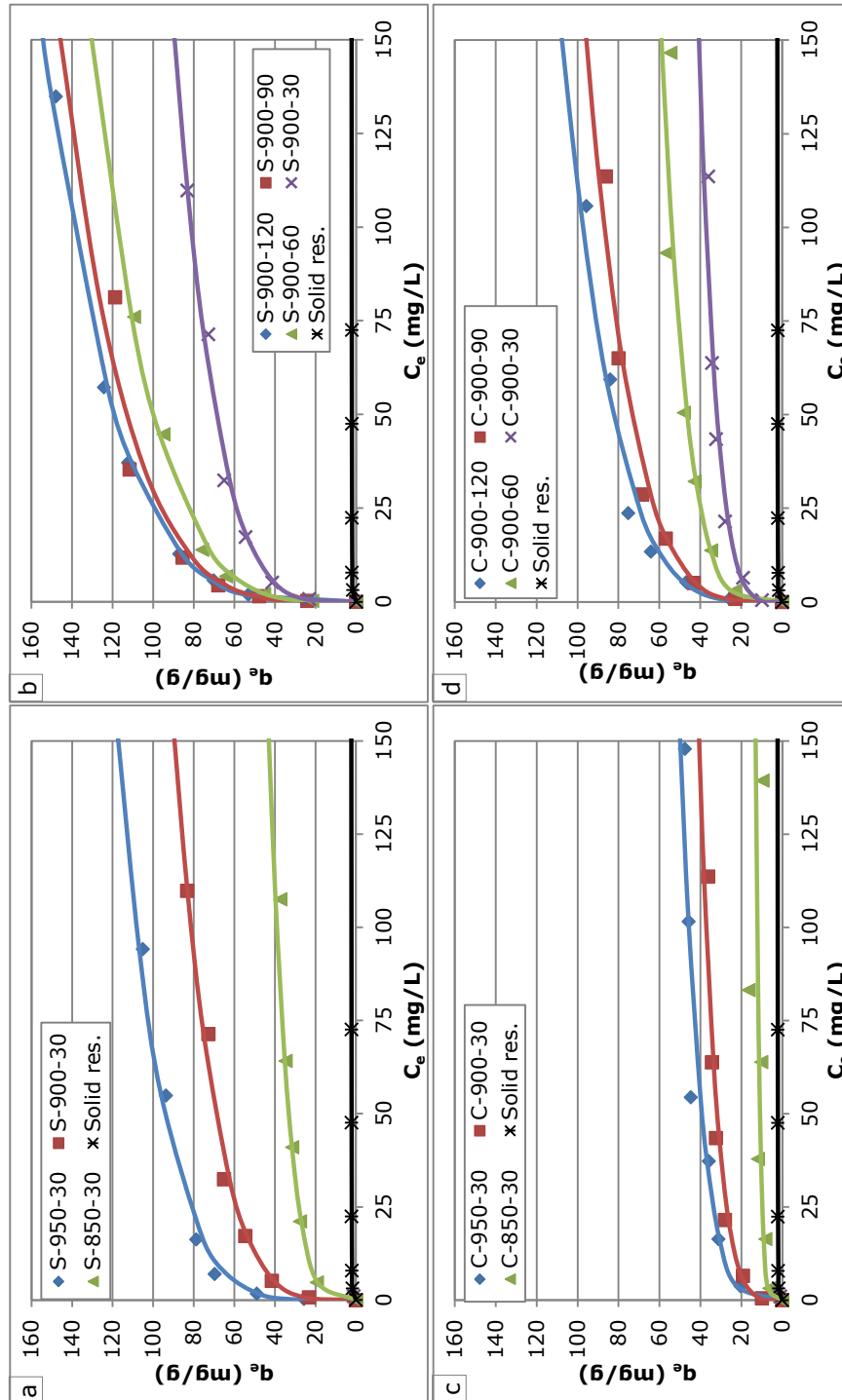


Figure 6-10: Phenol adsorption isotherms (dots: experimental data; curves: fit of the Freundlich model) of ACs (HCl-washed) from rapeseed cake by steam activation as a function of temperature (a) and time (b); and by CO₂ activation as a function of temperature (c) and activation time (d). (Sample code: X-T-t).

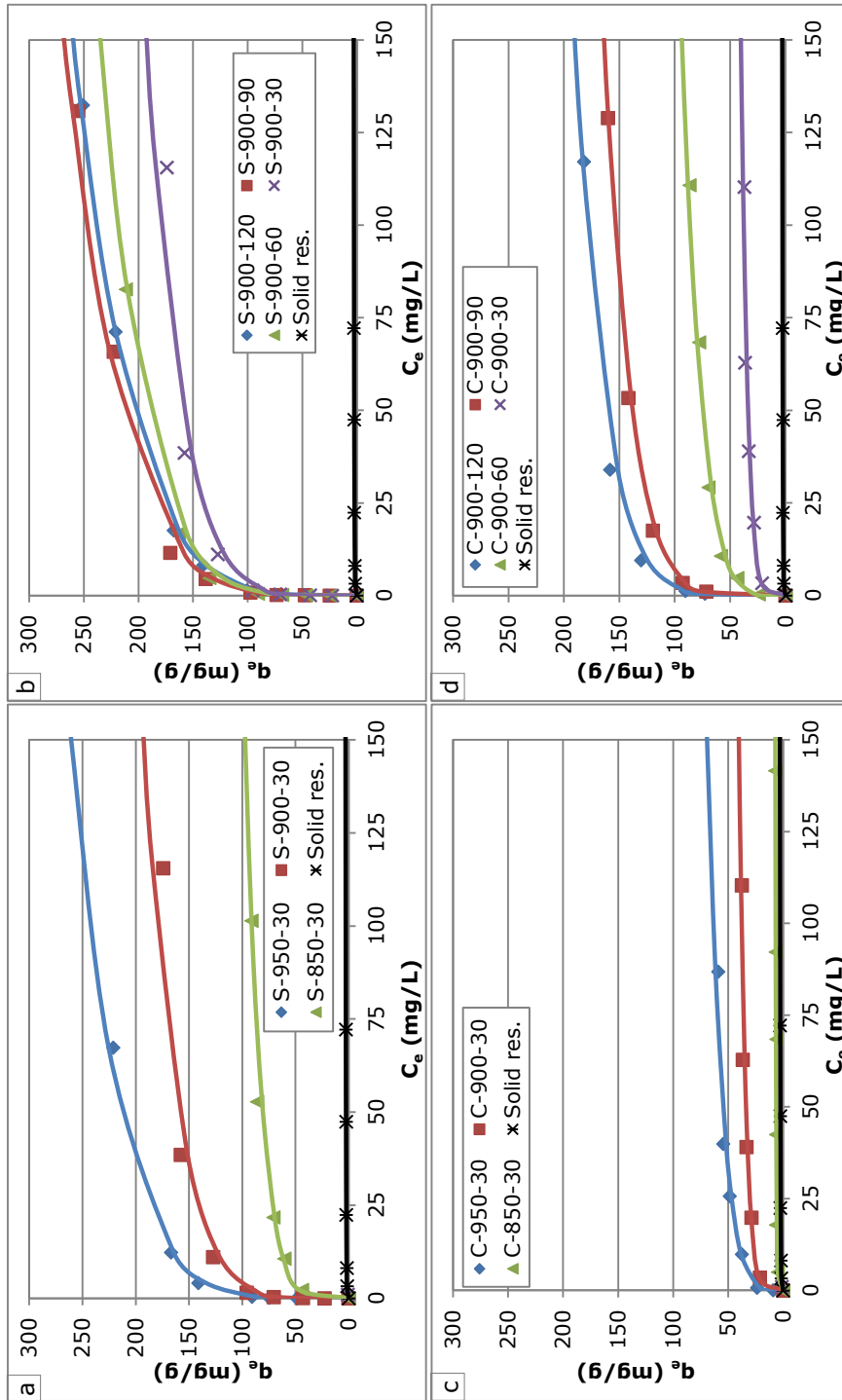


Figure 6-11: Phenol adsorption isotherms (dots: experimental data; curves: fit of the Freundlich model) of ACs produced from raspberry seed cake by steam activation as a function of temperature (a) and time (b); and by CO₂ activation as a function of temperature (c) and activation time (d). (Sample code: X-T-t).

6.4.1.2 *Raspberry seed cake*

The phenol adsorption isotherms of the ACs produced from raspberry seed cake are shown in Figure 6-11. Without activation, the solid residue showed a very low uptake of phenol.

Higher **activation temperatures** considerably increased the phenol adsorption. Steam activated samples were much more effective than CO₂ activated samples. Moreover, the AC produced by CO₂ activation at 850 °C showed almost no improvement compared to the solid residue. This observation was similar but more pronounced than the one made for the AC produced from rapeseed cake under similar conditions.

Longer **activation times** resulted in a higher uptake of phenol. Again, steam activation was found to give rise to better performing ACs than CO₂ activation. However, the influence of activation time was much more pronounced for CO₂ than for steam (compare Figure 6-11b with Figure 6-11d). Hence, the difference between the best and the worst performing AC was much smaller for steam than for CO₂ activation. As a result, CO₂ activation at 900 °C for 120 min resulted in an AC with a phenol adsorption that was comparable to that of the steam activated samples. Moreover, steam activation at 900 °C for 90 min led to a better performing AC than steam activation for 120 min. This suggested that too long activation times became counterproductive for the phenol adsorption capacity. Additionally, steam activation at 950 °C for 30 min was almost as effective as activation at 900 °C for 90 min. Therefore, it is believed that not only the amount of activation agent (3 mL water for 30 min vs 9 mL for 90 min) is important to produce well performing ACs, but also the activation temperature. In this respect, an activation temperature of 850 °C appears to be too low for CO₂ activation.

6.4.2 **Adsorption models of Freundlich and Langmuir**

To gain a better understanding of the adsorption mechanism and to optimize the design of the adsorption system, the experimental data (C_e , q_e) were analyzed by two isotherm models i.e. the Freundlich model and the Langmuir model. The model parameters were calculated using **non-linear regression** according to the least squares method, as described in section 2.8.2. The model that fitted the experimental data best is already shown in Figures 6-10 and 6-11.

6.4.2.1 Rapeseed cake

The parameters of the Freundlich and Langmuir model for ACs (HCl-washed) from rapeseed cake using different activation conditions are shown in Table 6-7.

Table 6-7: Adsorption parameters of the Freundlich and Langmuir model for ACs (HCl-washed) produced from rapeseed cake using different activation conditions.

Activation	T _{act} (°C)	t _{act} (min)	Freundlich			Langmuir		
			K _F ^a	1/n _F	R ²	q _m ^b	K _L ^c	R ²
No activation	-	-	1.7	0.06	0.990	2.2	1.23	0.998
Steam	850	30	13	0.24	0.991	41	0.13	0.944
	900	30	27	0.24	0.996	78	0.23	0.944
	950	30	43	0.20	0.987	96	0.60	0.952
	900	30	27	0.24	0.996	78	0.23	0.944
	900	60	38	0.25	0.993	104	0.30	0.955
	900	90	45	0.23	0.980	116	0.39	0.966
	900	120	47	0.24	0.999	139	0.19	0.955
CO ₂	850	30	6	0.16	0.765	12	0.25	0.785
	900	30	13	0.23	0.989	36	0.20	0.954
	950	30	17	0.22	0.982	48	0.14	0.973
	900	30	13	0.23	0.989	36	0.20	0.954
	900	60	20	0.22	0.985	56	0.16	0.970
	900	90	28	0.24	0.991	84	0.20	0.960
	900	120	32	0.24	0.986	93	0.20	0.970

^a K_F in mg/g(L/mg)^{1/n}; ^b q_m in mg/g and ^c K_L in L/mg.

The adsorption equilibrium data were best represented by the **Freundlich model**, as indicated by the R² values. Therefore, the ACs were believed to contain some heterogeneity on the surfaces and/or pores that participated in the adsorption of phenol. The Freundlich constant (K_F) was an indication for the relative adsorption capacity of the ACs [23]. In general, higher activation temperatures and longer activation times led to higher values of K_F. The 1/n_F parameter had values less than one for all samples, suggesting that phenol adsorption was a favorable process [23]. However, no systematic trend as a function of the activation conditions was found for the 1/n_F parameter.

Although the **Langmuir model** did not fit the experimental data as well as the Freundlich model, it could still provide valuable information. In general, higher activation temperatures and longer activation times significantly increased the monolayer adsorption capacity (q_m). The separation factor (R_L)¹³ was always less than one and decreased for higher initial concentrations of phenol solution (data not shown). This indicated that phenol adsorption was a favorable process for all ACs and that it became more favorable for higher initial concentrations of phenol.

6.4.2.2 *Raspberry seed cake*

The parameters of the Freundlich and Langmuir model for the ACs produced from raspberry seed cake are shown in Table 6-8.

The experimental data were best represented by the **Freundlich model**, as indicated by the R^2 values. Therefore, the ACs were believed to contain also some surface heterogeneity. The Freundlich constant (K_F), an indication of the relative adsorption capacity, increased with higher activation temperatures and longer activation times, except for steam activation between 90 and 120 min. For steam, the K_F value was found to be most affected by the activation temperature, while the activation time turned out to be the most effective parameter in case of CO_2 activation. The values of the $1/n_F$ parameter were less than one for all samples, suggesting that phenol adsorption was favorable. The $1/n_F$ values were found to increase as a function of activation time for the steam activated samples and as a function of activation temperature for the CO_2 activated samples, indicating a decrease of the surface heterogeneity in both cases [24].

The **Langmuir model** was less suitable to fit the experimental data. The monolayer adsorption capacity (q_m) considerably increased for higher activation temperatures and longer activation times. The separation factor (R_L) was always less than one and decreased with increasing initial phenol concentration (data not shown). This indicated that phenol adsorption became more favorable at higher initial phenol concentrations.

¹³ For more information on the separation factor is referred to equation 2-11 (section 2.8.2).

Table 6-8: Adsorption parameters of the Freundlich and Langmuir model for ACs produced from raspberry seed cake using various activation conditions.

Activation	T _{act} (°C)	t _{act} (min)	Freundlich			Langmuir		
			K _F ^a	1/n _F	R ²	q _m ^b	K _L ^c	R ²
No act.	-	-	1.4	0.16	0.983	2.6	0.41	0.982
steam	850	30	40	0.18	0.994	94	0.25	0.960
	900	30	79	0.18	0.978	153	2.05	0.931
	950	30	103	0.18	0.995	184	2.88	0.898
	900	30	79	0.18	0.978	153	2.05	0.931
	900	60	91	0.19	0.985	195	1.69	0.914
	900	90	96	0.21	0.988	216	1.04	0.891
	900	120	88	0.22	0.999	223	0.40	0.911
	CO ₂	850	30	4	0.11	0.980	7	0.41
900		30	18	0.16	0.996	38	0.30	0.974
950		30	23	0.22	0.990	53	0.94	0.933
900		30	18	0.16	0.996	38	0.30	0.974
900		60	33	0.21	0.993	84	0.25	0.936
900		90	75	0.16	0.998	155	0.51	0.951
900		120	88	0.15	0.994	174	0.93	0.946

^a K_F in mg/g(L/mg)^{1/n}; ^b q_m in mg/g and ^c K_L in L/mg.

6.4.3 Phenol adsorption vs textural characteristics of ACs

In this paragraph, the relationship between the textural characteristics of the ACs (section 6.3.2) and their performance during phenol adsorption (section 6.4.2) is investigated. Therefore, the adsorption capacity (q) for an equilibrium phenol concentration of 150 mg/L was calculated using the Freundlich model. In this way, a good estimation of the maximum adsorption capacity of the ACs was obtained (see Figures 6-10 and 6-11). A plot of this adsorption capacity together with the micro- and mesopore volume as a function of the burn-off is shown in Figure 6-12. Results show that the adsorption capacity generally increased with the degree of burn-off. Moreover, the adsorption capacity seemed to be more related to the micropore volume (V_{DR}) than to mesopore volume (V_{me}). These results are in accordance with literature data reporting that phenol adsorption mainly occurs in micropores of the ACs [18].

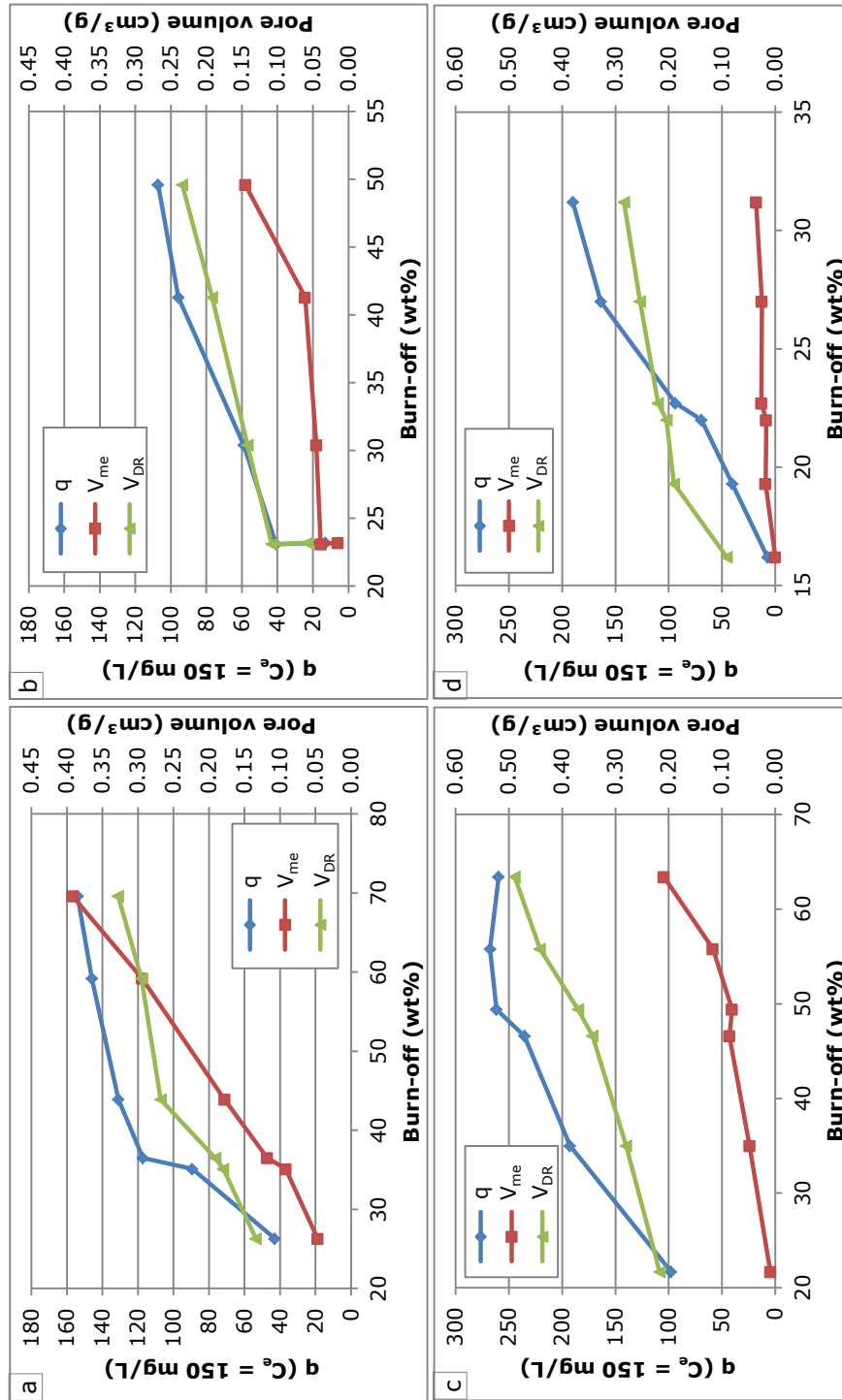


Figure 6-12: Comparison of the phenol adsorption capacity (q) calculated by the Freundlich model, with the micro- (V_{DR}) and mesopore (V_{me}) volume determined by N₂ adsorption for ACs from rapeseed cake (HCl-washed) by steam (a) and CO₂ (without C-950-30) (b); from raspberry seed cake by steam (c) and CO₂ (d).

6.4.4 AC from agricultural waste cake vs commercial grade AC

Based on the results of the phenol adsorption study, a selection of the most suitable activation conditions in terms of phenol uptake was made for ACs originating from both agricultural waste cakes. In this view, the AC produced at 900 °C for 90 min was selected for steam activation, while 900 °C and 120 min was chosen for the CO₂ activation. Both ACs were compared to commercial grade AC (Norit GAC 1240). Results are shown in Figure 6-13.

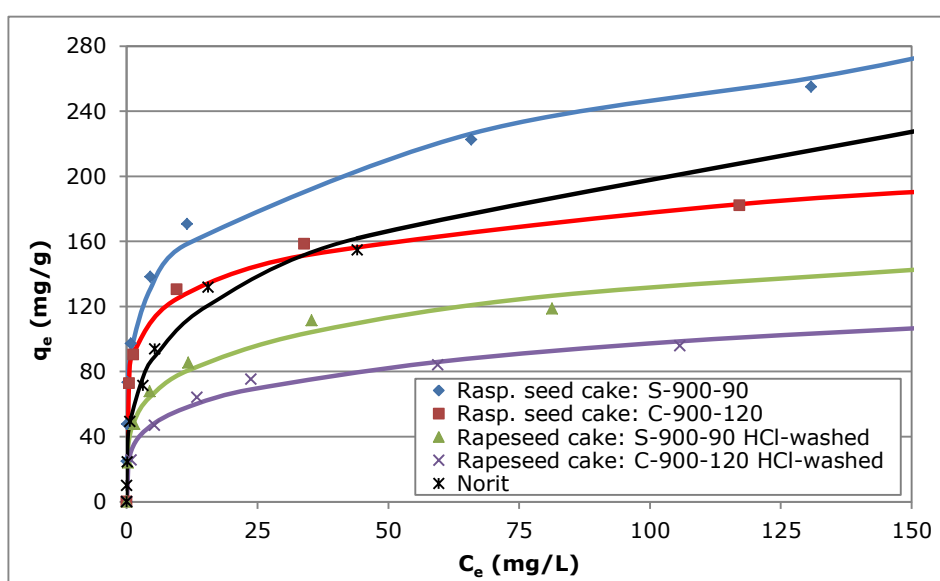


Figure 6-13: Phenol adsorption isotherms of selected ACs produced from agricultural waste cake compared to commercial grade AC (Norit) (dots: experimental data; curves: fit of the Freundlich model).

The ACs derived from **raspberry seed cake** performed quite well compared to the commercial AC. Both steam and CO₂ activated samples resulted in a higher phenol uptake at low residual equilibrium phenol concentrations (beginning of the isotherm). However, only the steam activated sample (S-900-90) resulted in a higher phenol adsorption capacity at the end of the isotherm, while the CO₂ activated sample (C-900-120) led to a slightly lower phenol uptake. The ACs derived from **rapeseed cake** had significant lower phenol uptakes compared to Norit. It can be concluded that the solid residue produced by slow pyrolysis of

agricultural waste cake can be valorized as AC, especially the ones produced from raspberry seed cake.

6.4.5 Effect of solution's initial pH on phenol removal

The effect of the solution's initial pH on the phenol removal was investigated for selected ACs from both waste cakes. For more information on the experimental setup is referred to section 2.8.3. Results are shown in Figure 6-14.

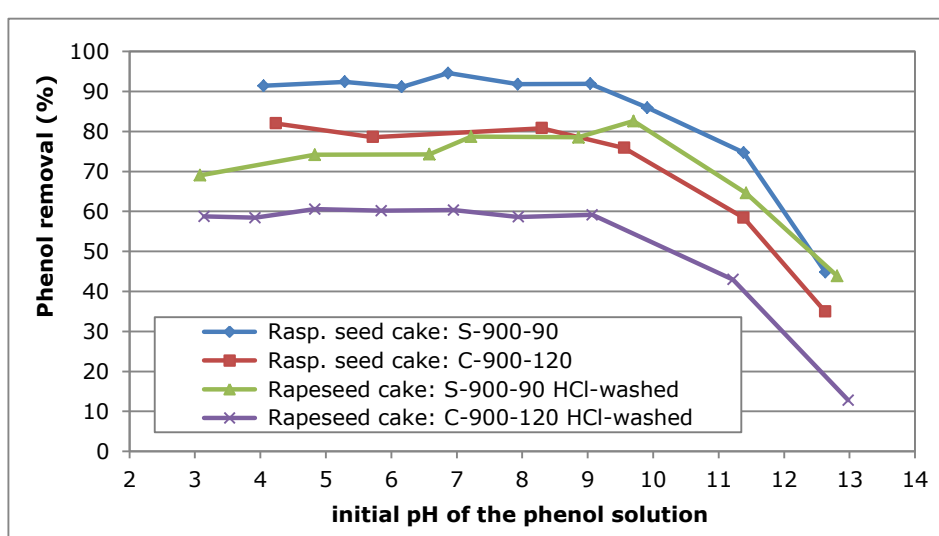


Figure 6-14: Influence of the initial pH on the phenol removal by ACs produced from rapeseed cake (C_0 : 150 mg/L) and raspberry seed cake (C_0 : 200 mg/L) by physical activation with steam or CO_2 . (Sample code: X-T-t).

The initial pH of the solution affects the phenol removal by a combination of two factors: the acid-base behavior of phenol and the surface charge of the AC. Hence, phenol is a weak acid with a pK_a of about 9.89 (25 °C) [4]. Therefore, the uncharged molecular form dominates at pH-values less than 9.89, while at higher pH-values the phenolate anion is the predominant form. On the other hand, the surface functional groups of the ACs might be either neutral or negatively charged at higher pH-values [4]. Figure 6-14 shows that the phenol removal was rather independent on the initial pH of the solution in the range from 4 to 9, while it was significantly reduced at more alkaline pH-values. Therefore, dispersive interactions between the aromatic ring of phenol and the

basal planes of the AC with a high π -electron density were believed to be responsible for phenol adsorption at pH-values between 4 and 9. In contrast, electrostatic repulsion between the negative surface charge of the AC and the phenolate anions could explain the lower phenol removal at more alkaline pH-values. The leak of significant amounts of functional groups, as observed in the FTIR spectra (section 6.3.4), supported this hypothesis. However, the small amount of functional groups could still affect indirectly the dispersive interactions between phenol and the ACs by influencing the π -electron density at the surface of the latter. For instance, electron withdrawing groups (such as carbonyls or carboxylic acids) could reduce the π -electron density and thus led to weaker dispersive interactions [25]. Similar observations are reported in literature [18, 26]. Hence, it can be concluded that besides porosity, phenol adsorption on AC also depends on the solution's initial pH and the surface chemistry of the AC.

6.4.6 Phenol adsorption: kinetic study

Kinetic parameters provide important information on designing and modeling of the adsorption process [23]. Therefore, phenol adsorption of selected ACs of both agricultural waste cakes was investigated by a kinetic study. The experimental data were modeled using the pseudo-first-order (PFO) and the pseudo-second-order (PSO) model, as described in section 2.8.4. The model parameters are summarized in Table 6-9.

Table 6-9: Parameters of the pseudo-first-order (PFO) and the pseudo-second-order (PSO) model of ACs produced from two agricultural waste cakes compared to commercial grade AC (Norit).

Activated carbon	PFO			PSO		
	q_1 (mg/g)	k_1 (1/min)	R^2	q_2 (mg/g)	k_2 (g/mg min)	R^2
Rapeseed cake: S-900-90 ^a	83	0.11	0.927	88	0.0018	0.978
Rapeseed cake: C-900-120 ^a	64	0.064	0.930	68	0.0014	0.973
Rasp. seed cake: S-900-90	87	0.098	0.947	92	0.0017	0.989
Rasp. seed cake: C-900-120	84	0.039	0.968	91	0.00060	0.990
Norit	90	0.013	0.991	97	0.00019	0.997

^a HCl-washed

For all samples, the adsorption process was best described by the PSO kinetic model, as indicated by the R^2 values. An overview of the experimental data, together with the fit of the PSO model is presented in Figure 6-15.

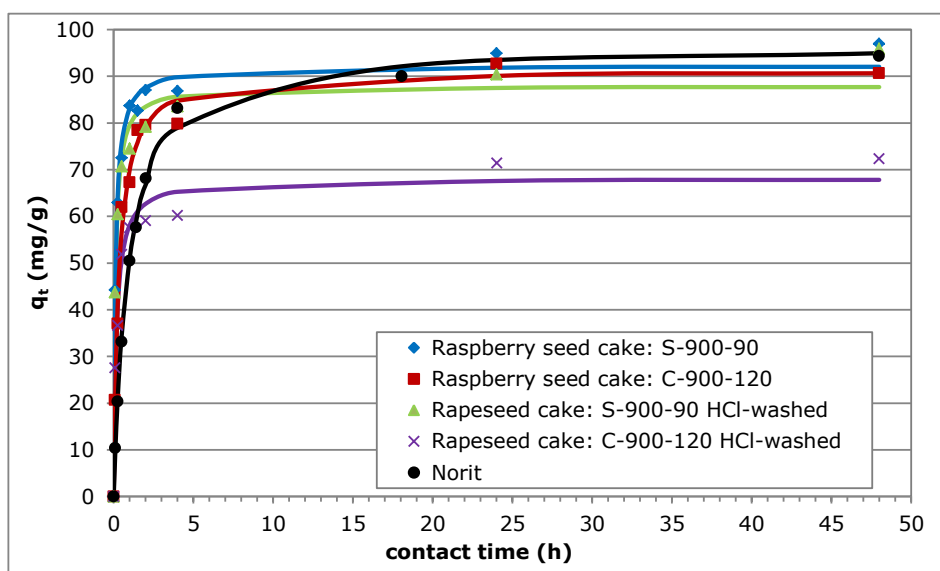


Figure 6-15: Phenol adsorption kinetic study (dots: experimental data; curves: fit of the PSO model) of the ACs produced from raspberry seed cake and rapeseed cake (HCl-washed), compared to Norit ($C_0 = 100$ mg/L).

The results reveals that the phenol adsorption was fast at the initial stage of adsorption and became slower near the equilibrium. Hence, a large number of vacant surface sites were available for adsorption during the initial stage, while for longer contact times the remaining vacant surface sites were more difficult to be occupied due to the small number of vacancies available and the repulsive force between the phenol molecules on the AC and the ones in the bulk liquid phase [27].

Steam activated samples reached the equilibrium faster than the corresponding CO_2 activated samples. The higher porosity of the former might explain this observation since four consecutive mass transport steps can be distinguished during adsorption on a porous adsorbent [22, 27]. Firstly, the phenol molecules have to migrate through the bulk solution to the film surrounding the adsorbing

particle. Then, the solute has to diffuse from the film to the surface of the particle (film diffusion) and subsequently from the particle surface into the interior site of the adsorbent (pore diffusion). Finally, phenol molecules are adsorbed on the active sites of the adsorbent [22, 28]. The last step is considered to be very fast and thus it cannot be the rate limiting step [27]. For liquid-solid adsorption, either external mass transfer or intraparticle diffusion or both usually characterize the solute transfer process. However, the overall rate of adsorption will be controlled by the slowest step, which would be either film diffusion or pore diffusion [29].

6.4.7 Intraparticle diffusion model

The intraparticle diffusion (IPD) model, presented by Weber and Morris [30], was applied on the results of the kinetic study (section 6.4.6) to gain a better understanding of the diffusion mechanism. This empirically found model assumes that the phenol uptake varies almost proportionally with the square root of time ($t^{1/2}$), as shown by equation 6-1:

$$\text{Eq. 6-1:} \quad q_t = k_{pi}t^{1/2} + C_i$$

where q_t (mg/g) is the amount of phenol adsorbed at time t (min), k_{pi} (mg/(g min^{1/2})) is the IPD rate constant of stage i and C_i (mg/g) gives an idea about the thickness of the boundary layer, i.e. the larger C_i the greater the boundary layer effect [27, 31]. If intraparticle diffusion occurs, the plot of q_t against $t^{1/2}$ yields a straight line with k_{pi} as slope and C_i as intercept. If the plot passes through the origin, then intraparticle diffusion is the only rate limiting process. Otherwise, the plot may present multi-linearity indicating that some other mechanism, together with intraparticle diffusion, is involved as well. In general, the rate of uptake might be limited by the size of adsorbate molecule, the concentration of the adsorbate, its affinity for the adsorbent, the diffusion coefficient of the adsorbate in the bulk phase, the pore size distribution of the AC and the degree of mixing [32].

Figure 6-16 shows the plots of the IPD model for selected ACs produced from rapeseed cake and raspberry seed cake, and for the commercial AC (Norit). It

can be observed that the plots are not linear over the whole time range, implying that more than one process affects the phenol adsorption.

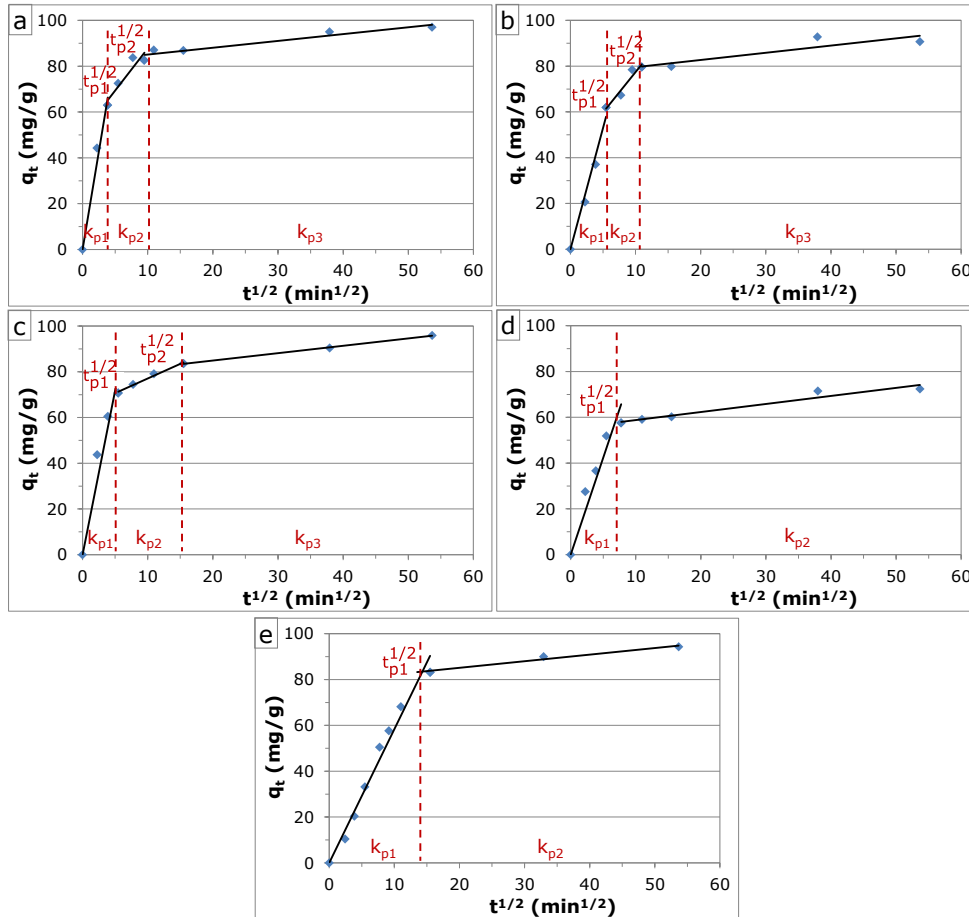


Figure 6-16: Plots of the IPD model for phenol adsorption on ACs produced from raspberry seed cake by (a) steam activation [S-900-90] or (b) CO₂ activation [C-900-120], and ACs from rapeseed cake by (c) steam activation [S-900-90 HCl-washed] or (d) CO₂ activation [C-900-120 HCl-washed] compared to commercial AC (e).

Up to three stages were distinguished in the IPD plots (Figure 6-16). The first stage represented instantaneous adsorption or adsorption on the external surface of the AC (boundary layer diffusion). This step was completed within 60 min for the ACs produced from rapeseed cake and raspberry seed cake, while the commercial AC required about 205 min. The second stage was assigned to

gradual adsorption with rate limiting intraparticle diffusion. The third region was the final equilibrium stage where intraparticle diffusion started to slow down due to the extremely low adsorbate concentrations left in the solutions [32-34]. This stage was only observed for ACs derived from raspberry seed cake and from rapeseed cake by steam activation (Figure 6-16a-c), while it was absent for the AC produced from rapeseed cake by CO₂ activation and the commercial AC (Figure 6-16d-e). The multistage character of the IPD plots and the fact that the linear lines of the second and/or third stage did not pass through the origin, indicated that intraparticle diffusion was not the only rate limiting mechanism and that boundary layer diffusion also affected the adsorption to some extent [29, 32].

The values of k_{pi} , C_i and R^2 were inferred from the IPD plots and listed in Table 6-10. For all ACs, the values of k_{pi} were found to decrease between stage 1 and 3 while that of C_i increased. This indicated that respectively the adsorption rate was slowed down and that the boundary layer effect became greater when the contact time increased. In case of the ACs derived from **raspberry seed cake**, the steam activated sample had a considerably higher k_{p1} and a slightly higher k_{p2} rate constant than the corresponding CO₂ activated sample, while almost no difference was found for k_{p3} . The values of C_2 and C_3 were also considerably higher for the steam activated than for the CO₂ activated sample. This indicated that steam activation resulted in ACs with a faster adsorption on the external surface, a higher intraparticle diffusion and a greater boundary layer effect compared to CO₂ activation. In case of **rapeseed cake**, the k_{p1} and k_{p2} rate constants were (considerably) higher for the steam activated sample than for the CO₂ activated sample, while no k_{p3} rate constant was found in case of CO₂ activation. These observations might be explained by the higher porosity (both micro- and mesopores) of the steam activated sample compared to the CO₂ activated sample for both waste cakes (see Tables 6-4 and 6-5). Comparison of the ACs from the waste cakes with each other and with the commercial AC revealed that the precursor material also had a strong effect on the adsorption and diffusion mechanism. The AC derived from raspberry seed cake by steam activation (S-900-90) and the commercial AC, for instance, had very similar textural characteristics (see Table 6-5) but showed a very different behavior in the IPD plots.

Table 6-10: Intraparticle diffusion model constants and correlation coefficients for adsorption of phenol on selected ACs derived from rapeseed cake and raspberry seed cake compared to commercial AC (Norit).

Activated carbon	k_{p1} (mg/(g min ^{1/2}))			C_i (mg/g)			Corr. coefficient			$t_{p1}^{1/2}$	$t_{p2}^{1/2}$
	k_{p1}	k_{p2}	k_{p3}	C_1	C_2	C_3	$(R^2)_1$	$(R^2)_2$	$(R^2)_3$	(min ^{1/2})	(min ^{1/2})
Rasp. seed cake: S-900-90	17.14	3.68	0.30	0	50.99	82.09	0.978	0.875	0.920	3.79	9.20
Rasp. seed cake: C-900-120	10.60	3.53	0.31	0	42.10	76.42	0.980	0.935	0.807	5.95	10.66
Rapeseed cake: S-900-90 (HCl-washed)	14.38	1.28	0.32	0	64.31	78.46	0.924	0.985	0.999	4.91	14.74
Rapeseed cake: C-900-120 (HCl-washed)	8.49	0.35	-	0	55.28	-	0.911	0.943	-	7.79	-
Commercial AC (Norit)	5.83	0.29	-	0	79.32	-	0.978	0.969	-	14.32	-

6.5 Conclusion

The valorization of solid residue produced by (slow) pyrolysis (without sand as heat transfer medium) of agricultural waste cake as precursor for the production of AC is assessed. Therefore, the solid residue is converted into AC by physical activation using steam or CO₂. The effects of activation temperature (850 – 950 °C) and activation time (30 – 120 min) on the textural characteristics (BET specific surface area and porosity) and the adsorption capacity in phenol adsorption are studied.

The N₂ adsorption isotherms of ACs derived from **rapeseed cake** are classified as type IV isotherms with type H4 hysteresis loops. The latter become more pronounced for longer activation times and at higher temperatures. Micro- and mesopores turn out to be formed simultaneously regardless of the activation agent, although mesopore development is less pronounced at the early stage of activation in case of CO₂.

In case of **raspberry seed cake**, type IV isotherms with type H4 hysteresis loops are also found for ACs produced by steam (except 850 °C) and by CO₂ for longer activation times (90 and 120 min). In contrast, CO₂ activation (except 90 and 120 min) and steam activation at 850 °C result in type I isotherms, indicating that there is (almost) no mesoporosity. Therefore, it is concluded that CO₂ results in microporous ACs at the early stage of activation and that mesopore development will start at a later stage (more severe activation conditions) leading to ACs with a mixed micro- and mesoporous structure. In contrast, micro- and mesopores are formed simultaneously from the early stage of activation in case of steam.

In general, steam is found to be more reactive than CO₂ in terms of specific surface area and both micro- and mesopore development. Moreover, the reactivity of the activation agent is dependent on precursor material, since CO₂ is found to be much more effective in activating the solid residue of rapeseed cake than that of raspberry seed cake under analogous conditions.

The ACs produced from rapeseed cake have a very high ash content. These ash contents are considerably decreased by performing an additional HCl-washing step. In contrast, no additional HCl-washing is necessary for ACs derived from raspberry seed cake because of their relatively low ash content.

Elemental analysis shows that ACs derived from raspberry seed cake have a higher carbon content than those of rapeseed cake, while the content of hydrogen, nitrogen, sulfur and oxygen are lower. However, the total content of heteroatoms is relatively low for both ACs. No significant amounts of surface functional groups are observed in the ATR-FTIR spectra.

In general, phenol adsorption increases for ACs produced at higher temperatures and for longer activation times. Steam is more effective than CO₂ under similar conditions. The experimental data are best fitted by the Freundlich isotherm model in all cases. Moreover, a strong correlation between the adsorption capacity and the micropore volume is found.

Based on the phenol adsorption study and the total yield, steam activation at 900 °C for 90 min and CO₂ activation at 900 °C for 120 min are selected as best activation conditions for both waste cakes. Comparison to a commercial grade AC reveals that these ACs have potential for treating phenol polluted wastewaters. Especially, the AC produced from raspberry seed cake by steam activation at 900 °C for 90 min is very effective with a phenol uptake of 260 mg/L for an initial phenol concentration of 400 mg/L.

The initial pH of the phenol solution influences the phenol removal of the ACs. The phenol removal is independent on the initial pH of the solution between 4 and 9, indicating that (mainly) dispersive interactions between the aromatic ring of phenol and the basal planes with a high π -electron density of the AC are responsible for adsorption. In contrast, the decrease in phenol removal at pH-values higher than 9 is explained by electrostatic repulsion between the negative surface charge of the AC and the phenolate anions.

A kinetic study shows that phenol adsorption is better described by the PSO than by the PFO kinetic model in case of the best performing ACs derived from each agricultural waste cake. Moreover, phenol adsorption at the initial stage of adsorption is found to be quicker for ACs derived from both agricultural waste cakes compared to the commercial AC. Application of the intraparticle diffusion model of Weber and Morris indicates that both boundary layer and intraparticle diffusion controlled the rate of phenol adsorption on the AC.

6.6 References

- [1] Stavropoulos, G.G. and Zabaniotou, A.A. Production and characterization of activated carbons from olive-seed waste residue. *Microporous and Mesoporous Materials*, 2005. **82**(1-2): 79-85.
- [2] Izquierdo, M.T., Martínez de Yuso, A., Rubio, B. and Pino, M.R. Conversion of almond shell to activated carbons: Methodical study of the chemical activation based on an experimental design and relationship with their characteristics. *Biomass and Bioenergy*, 2011. **35**(3): 1235-1244.
- [3] Román, S., González, J.F., González-García, C.M. and Zamora, F. Control of pore development during CO₂ and steam activation of olive stones. *Fuel Processing Technology*, 2008. **89**(8): 715-720.
- [4] Singh, K.P., Malik, A., Sinha, S. and Ojha, P. Liquid-phase adsorption of phenols using activated carbons derived from agricultural waste material. *Journal of Hazardous Materials*, 2008. **150**(3): 626-641.
- [5] Dias, J.M., Alvim-Ferraz, M.C.M., Almeida, M.F., Rivera-Utrilla, J. and Sanchez-Polo, M. Waste materials for activated carbon preparation and its use in aqueous-phase treatment: A review. *Journal of Environmental Management*, 2007. **85**(4): 833-846.
- [6] Stavropoulos, G.G. and Zabaniotou, A.A. Minimizing activated carbons production cost. *Fuel Processing Technology*, 2009. **90**(7-8): 952-957.
- [7] Tay, T., Ucar, S. and Karagöz, S. Preparation and characterization of activated carbon from waste biomass. *Journal of Hazardous Materials*, 2009. **165**(1-3): 481-485.
- [8] Xin-hui, D., Srinivasakannan, C., Jin-hui, P., Li-bo, Z. and Zheng-yong, Z. Comparison of activated carbon prepared from *Jatropha* hull by conventional heating and microwave heating. *Biomass and Bioenergy*, 2011. **35**(9): 3920-3926.
- [9] Raveendran, K., Ganesh, A. and Khilar, K.C. Pyrolysis characteristics of biomass and biomass components. *Fuel*, 1996. **75**(8): 987-998.
- [10] Gonzalez, J.F., Roman, S., Gonzalez-Garcia, C.M., Nabais, J.M.V. and Ortiz, A.L. Porosity Development in Activated Carbons Prepared from Walnut Shells by Carbon Dioxide or Steam Activation. *Industrial & Engineering Chemistry Research*, 2009. **48**(16): 7474-7481.
- [11] Wigmans, T. Industrial aspects of production and use of activated carbons. *Carbon*, 1989. **27**(1): 13-22.

- [12] Bacaoui, A., Yaacoubi, A., Dahbi, A., Bennouna, C., Luu, R.P.T., Maldonado-Hodar, F.J., Rivera-Utrilla, J. and Moreno-Castilla, C. Optimization of conditions for the preparation of activated carbons from olive-waste cakes. *Carbon*, 2001. **39**(3): 425-432.
- [13] Sing, K.S.W., Everett, D.H., Haul, R.A.W., Moscou, L., Pierotti, R.A., Rouquerol, J. and Siemieniewska, T. Reporting physisorption data for gas solid systems with special reference to the determination of surface-area and porosity (recommendations 1984). *Pure and Applied Chemistry*, 1985. **57**(4): 603-619.
- [14] Marsh, H. and Rodríguez-Reinoso, F. *Activated carbon*. 2006: Elsevier Science & Technology Books. 536.
- [15] López, G., Olazar, M., Artetxe, M., Amutio, M., Elordi, G. and Bilbao, J. Steam activation of pyrolytic tyre char at different temperatures. *Journal of Analytical and Applied Pyrolysis*, 2009. **85**(1-2): 539-543.
- [16] Rodríguez-Reinoso, F., Molina-Sabio, M. and González, M.T. The use of steam and CO₂ as activating agents in the preparation of activated carbons. *Carbon*, 1995. **33**(1): 15-23.
- [17] Carrasco-Marín, F., Domingo-García, M., Fernández-Morales, I. and López-Garzón, F.J. Dynamic adsorption of methyl iodide on activated carbons. *Carbon*, 1991. **29**(4-5): 629-634.
- [18] Salame, I.I. and Bandosz, T.J. Role of surface chemistry in adsorption of phenol on activated carbons. *Journal of Colloid and Interface Science*, 2003. **264**(2): 307-312.
- [19] Özkaya, B. Adsorption and desorption of phenol on activated carbon and a comparison of isotherm models. *Journal of Hazardous Materials*, 2006. **129**(1-3): 158-163.
- [20] Jia, Q. and Lua, A.C. Effects of pyrolysis conditions on the physical characteristics of oil-palm-shell activated carbons used in aqueous phase phenol adsorption. *Journal of Analytical and Applied Pyrolysis*, 2008. **83**(2): 175-179.
- [21] Radhika, M. and Palanivelu, K. Adsorptive removal of chlorophenols from aqueous solution by low cost adsorbent—Kinetics and isotherm analysis. *Journal of Hazardous Materials*, 2006. **138**(1): 116-124.
- [22] Hameed, B.H. and Rahman, A.A. Removal of phenol from aqueous solutions by adsorption onto activated carbon prepared from biomass material. *Journal of Hazardous Materials*, 2008. **160**(2-3): 576-581.
- [23] Vargas, A.M.M., Cazetta, A.L., Kunita, M.H., Silva, T.L. and Almeida, V.C. Adsorption of methylene blue on activated carbon produced from flamboyant pods (*Delonix regia*): Study of adsorption isotherms and kinetic models. *Chemical Engineering Journal*, 2011. **168**(2): 722-730.

- [24] Haghseresht, F. and Lu, G.Q. Adsorption characteristics of phenolic compounds onto coal-reject-derived adsorbents. *Energy & Fuels*, 1998. **12**(6): 1100-1107.
- [25] Radovic, L.R., Silva, I.F., Ume, J.I., Menendez, J.A., Leon, C. and Scaroni, A.W. An experimental and theoretical study of the adsorption of aromatics possessing electron-withdrawing and electron-donating functional groups by chemically modified activated carbons. *Carbon*, 1997. **35**(9): 1339-1348.
- [26] Tessmer, C.H., Vidic, R.D. and Uranowski, L.J. Impact of oxygen-containing surface functional groups on activated carbon adsorption of phenols. *Environmental Science & Technology*, 1997. **31**(7): 1872-1878.
- [27] Tan, I.A.W., Ahmad, A.L. and Hameed, B.H. Adsorption isotherms, kinetics, thermodynamics and desorption studies of 2,4,6-trichlorophenol on oil palm empty fruit bunch-based activated carbon. *Journal of Hazardous Materials*, 2009. **164**(2-3): 473-482.
- [28] El-Sheikh, A.H., Newman, A.P., Said, A.J., Alzawahreh, A.M. and Abu-Helal, M.M. Improving the adsorption efficiency of phenolic compounds into olive wood biosorbents by pre-washing with organic solvents: Equilibrium, kinetic and thermodynamic aspects. *Journal of Environmental Management*, 2013. **118**(0): 1-10.
- [29] Aravindhan, R., Rao, J.R. and Nair, B.U. Application of a chemically modified green macro alga as a biosorbent for phenol removal. *Journal of Environmental Management*, 2009. **90**(5): 1877-1883.
- [30] Weber, W.J. and Morris, J.C. Advances in water pollution research: Removal of biologically resistant pollutant from waste water by adsorption, in *International Conference on Water Pollution Symposium*. vol. 2. 1962: Pergamon, Oxford. 231 - 266.
- [31] McKay, G., Otterburn, M.S., and Sweeney, A.G. The removal of colour from effluent using various adsorbents—III. Silica: Rate processes. *Water Research*, 1980. **14**(1): 15-20.
- [32] Lorenc-Grabowska, E. and Gryglewicz, G. Adsorption characteristics of Congo Red on coal-based mesoporous activated carbon. *Dyes and Pigments*, 2007. **74**(1): 34-40.
- [33] Sun, Q. and Yang, L. The adsorption of basic dyes from aqueous solution on modified peat-resin particle. *Water Research*, 2003. **37**(7): 1535-1544.
- [34] Wu, F.-C., Tseng, R.-L. and Juang, R.-S. Initial behavior of intraparticle diffusion model used in the description of adsorption kinetics. *Chemical Engineering Journal*, 2009. **153**(1-3): 1-8.

7 Water content of pyrolysis liquids: Comparison between Karl Fischer titration, GC/MS-corrected azeotropic distillation and $^1\text{H-NMR}$ spectroscopy

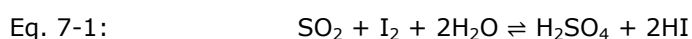
The observations and conclusions of this chapter have already been published:
Water content of pyrolysis oil: Comparison between Karl Fischer titration, GC/MS-corrected azeotropic distillation and $^1\text{H-NMR}$ spectroscopy;
K. Smets, P. Adriaensens, J. Vandewijngaarden, M. Stals, T. Cornelissen, S. Schreurs, R. Carleer, J. Yperman;
Journal of Analytical and Applied Pyrolysis, 2011. 90(2): 100 – 105.

7.1 Introduction

Generally, pyrolysis liquids are dark brown organic liquids that mainly consist of complex mixtures of oxygenated compounds and water [1]. Their composition is affected by the biomass feedstock and important pyrolysis process parameters such as temperature, heating rate and vapor residence time [2]. Therefore, a thorough characterization of a given pyrolysis liquid is absolutely necessary to determine its most appropriate application. Hereby, the water content is one of the key parameters. Hence, it influences the calorific value, the flow properties (viscosity) and the stability of pyrolysis liquids, all important characteristics concerning their use in fuel applications [3-5]. Therefore, an accurate and precise analytical method to determine the water content of pyrolysis liquids is indispensable.

Karl Fischer (KF) titration and azeotropic distillation by the Dean-Stark method are both methods commonly mentioned in literature. In this work, $^1\text{H-NMR}$ spectroscopy is proposed as an alternative water determination technique for pyrolysis liquids.

Volumetric **KF titration** is a fast, precise and accurate water determination technique that is highly selective and has a wide measuring range (ppm to pure water) [6]. It is based on the following redox reaction (equation 7-1):



In this reaction, sulfur dioxide is oxidized by iodine with the consumption of water in presence of an organic base (e.g. imidazole) and anhydrous methanol as a solvent [7]. The reaction mechanism, although been studied by many researchers, has not been fully understood yet [8]. Nevertheless, KF titration is used as standard technique for water determination in many products [9], including petroleum products [10]. Concerning water determination of pyrolysis liquids, some authors [1, 11, 12] highly recommend this technique. However, pyrolysis liquids contain several compounds including aldehydes, ketones, amines and organic acids that might cause interference according to the ASTM E203 method [9]. Therefore, the use of a suitable buffer solution is recommended to prevent positive interference from aldehydes and ketones due to acetal or ketal formation with methanol yielding water as a reaction product [6, 13].

Azeotropic distillation by the Dean-Stark method is an analytical technique used to determine the water content of various types of samples: herbs, spices and petroleum products [14]. It is based on the formation of an azeotropic mixture between water and a co-solvent (e.g. xylene or toluene) during distillation. Some authors use azeotropic distillation for water determination of pyrolysis liquids [15-19]. In contrast, other authors specifically mention that this technique is not suitable for pyrolysis liquids due to interference from water soluble volatile organic compounds (VOCs) that would be distilled away with the co-solvent as well [6, 11].

¹H-NMR spectroscopy is a technique normally applied for chemical analysis and structural research. However, it can also be used to detect or study water in different kinds of applications including the determination of the water and fat content in foods [20], to study adsorbed water layers on the surface of adsorbents [21] or to determine the amount of condensation water in the study of chemical reactions [22]. However, the application of ¹H-NMR spectroscopy for water determination of pyrolysis liquids has not been mentioned in literature.

In this chapter, KF titration is assessed for interference from compounds commonly present in pyrolysis liquids. Then, the water content of several pyrolysis liquids is determined by the conventional analytical techniques (KF titration and azeotropic distillation). Samples are selected to cover a wide range of water contents and are originating from different types of biomass. The

results of the azeotropic distillation are corrected for interference from water soluble VOCs by GC/MS data (if necessary). Moreover, the potential of $^1\text{H-NMR}$ spectroscopy as a new analytical technique for water determination of pyrolysis liquids is investigated [23].

7.2 Experimental setup

7.2.1 Pyrolysis liquids

An overview of the pyrolysis liquids investigated in this chapter is given in Table 7-1. Flash pyrolysis of rapeseed cake at four different temperatures resulted in a first set of samples (nos. 1 to 4). A second set (nos. 5 and 6) consisted of two samples with a very high water content, obtained by spontaneous phase separation of pyrolysis liquids produced by flash pyrolysis of rapeseed cake at 350 and 450 °C. The third set (nos. 7 to 10) was produced by pyrolysis of different types of biomass. In this way, a broad range of water contents and types of biomass was covered.

Table 7-1: Overview of the investigated pyrolysis liquids.

No.	Sample	Biomass (waste)	Temperature	Water content
1	RSC-550	Rapeseed cake	550 °C	Low
2	RSC-450	Rapeseed cake	450 °C	Low
3	RSC-400	Rapeseed cake	400 °C	Low/intermediate
4	RSC-350	Rapeseed cake	350 °C	Low/intermediate
5	RSC-W1	Rapeseed cake	450 °C	High
6	RSC-W2	Rapeseed cake	350 °C	High
7	Sludge	Sludge of industrial waste	450 °C	Low
8	RSC-PEG	Rapeseed cake/PEG10k	450 °C	Intermediate
9	Willow	Willow	350 °C	Intermediate
10	Cellulose	Pure cellulose	450 °C	Intermediate

7.2.2 Water determination of pyrolysis liquids

7.2.2.1 Volumetric Karl Fischer titration

The volumetric KF titration was performed with an apparatus of Schott Geräte (Titrator TR85). An one-component solution (Combititrant 5, Merck) was used as

a titrating agent medium and methanol (Normapur AR1, VWR) as a working medium. A double platinum electrode (type Pt1400) was used to detect the endpoint of titration (+ 100 mV).

The KF apparatus was calibrated by titrating six amounts of pure water in triplicate. The calibration curve was made according to the method of the least squares [7]. Pyrolysis liquid samples were loaded on a plastic container and weighed with an analytical balance (Mettler Toledo AG245). Sample size (about 50 mg) was set to produce results within the calibration curve. After weighing, the sample was charged (on the plastic container) into the titration vessel of the KF apparatus. Once the sample was properly dissolved, the titration was started. Each sample was measured in triplicate to allow the calculation of a 99% confidence interval.

7.2.2.2 Azeotropic distillation by the Dean-Stark method

Azeotropic distillation was performed on the pyrolysis liquid samples (about 7 g) in a 500 mL flask using 80 mL of toluene (Normapur AR1, VWR). The water-toluene mixture was boiled azeotropically into a graduated Dean-Stark reservoir and spontaneously separated in two fractions during cooling (Figure 7-1). As a result, the amount of water could be read allowing the calculation of the water content of the pyrolysis liquid. Due to the rather large sample size required for analysis and the limited amount of pyrolysis liquid available, only one azeotropic distillation per sample could be performed.

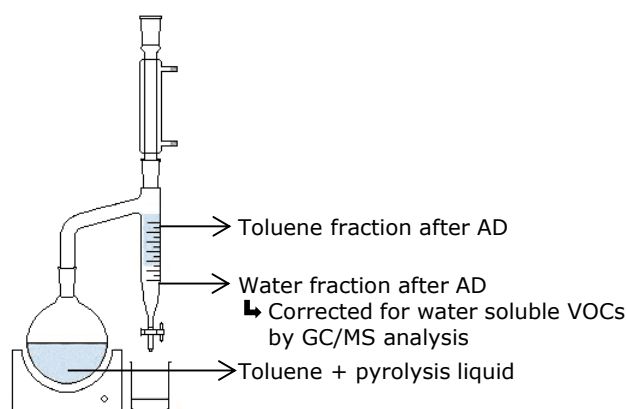


Figure 7-1: Experimental setup of the azeotropic distillation (AD) by the Dean-Stark method.

7.2.2.3 GC/MS-correction for azeotropic distillation by the Dean-Stark method

Based on literature and experience, azeotropic distillation was found to be sensitive for interference from water soluble VOCs. GC/MS was used to identify and to quantify these interfering compounds in the water fraction after azeotropic distillation (see also Figure 7-1). In this way, the water content of the pyrolysis liquid determined by azeotropic distillation could be corrected for interfering compounds.

GC/MS analysis was performed with a Varian 3400 gas chromatograph equipped with a DB-WAX capillary fused silica column (30 m x 0.25 mm; $d_f = 0.25 \mu\text{m}$; Agilent Technologies) and a Finnigan TSQ 700 mass detector. The column temperature was programmed from 35 to 220 °C at 12 °C/min after an isothermal period of 1 min at 35 °C. The samples (i.e. the water fractions after azeotropic distillation) were dissolved in a mixture of 40 V/V% methanol (< 0.1% H₂O, Merck Suprasolv) and 60 V/V% dichloromethane (< 0.01% H₂O, Merck Suprasolv) to obtain a concentration between 1 and 10 m/V%. Deuterated acetic acid (D 99.5%; Acros Organics) was used as an internal standard for GC/MS analysis. Calibration curves were made for the most important interfering compounds (acetic and formic acid) by setting out the ratio of the peak area of the interfering compound and the peak area of the internal standard as a function of the concentration of the interfering compound. A typical chromatogram of the water fraction after azeotropic distillation is shown in Figure 7-2. The peaks at 7.73 min and 8.26 min were assigned to acetic acid and formic acid, respectively, while the internal standard (deuterated acetic acid) was found at 7.68 min. The chromatogram shows that other compounds (e.g. propanoic acid (RT: 8.68 min) and acetamide (RT: 11.82 min)) were rather negligible. Therefore, the correction for interfering compounds in the water fraction after azeotropic distillation was only focused on acetic and formic acid. With the aid of the calibration curves, the amount of these compounds in the water fraction after azeotropic distillation could be calculated. Finally, the water content of the pyrolysis liquid could be "GC/MS-corrected" for these interfering compounds.

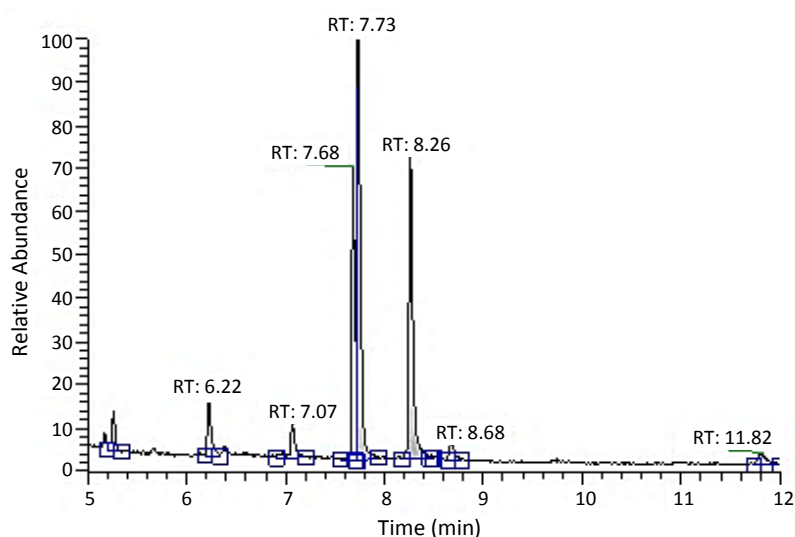


Figure 7-2: Typical chromatogram of the water fraction after azeotropic distillation.

7.2.2.4 $^1\text{H-NMR}$ spectroscopy

A Varian Inova 300 spectrometer was used for water determination of the pyrolysis liquids by $^1\text{H-NMR}$ spectroscopy. The analyses were performed in a 5 mm four-nucleus PFG probe with a spectral width of 4.2 kHz, a 90° pulse of 4 μs , an acquisition time of 4 s and a preparation delay of 60 or 90 s.

The pyrolysis liquid (about 10.0 mg) was dissolved in 800 μL deuterated acetone ($\text{D} 99.9\%$, < 84 ppm H_2O , Cambridge Isotope Laboratories Inc). This concentration (about 1.25 m/V%) was experimentally determined as being the best to reduce the occurrence of other resonance signals superimposed on the water resonance signal. Hence, the position of the latter was found to be a function of the water content of the sample. Therefore, the concentration of a sample with an unknown amount of water could need some fine-tuning to reduce the interference of signals superimposed on this water signal. Experiments indicated that an increase in concentration of the pyrolysis liquid sample resulted in a shift of the water signal to higher ppm values. Figure 7-3, for example, shows two concentrations of the same pyrolysis liquid sample. In this case, the low sample concentration (1.7 m/V%) is preferable because the sharp peak at 3.3 ppm is not superimposed on the water signal (2.9 to 3.3 ppm) as is the case for the high sample concentration (3.2 m/V%).

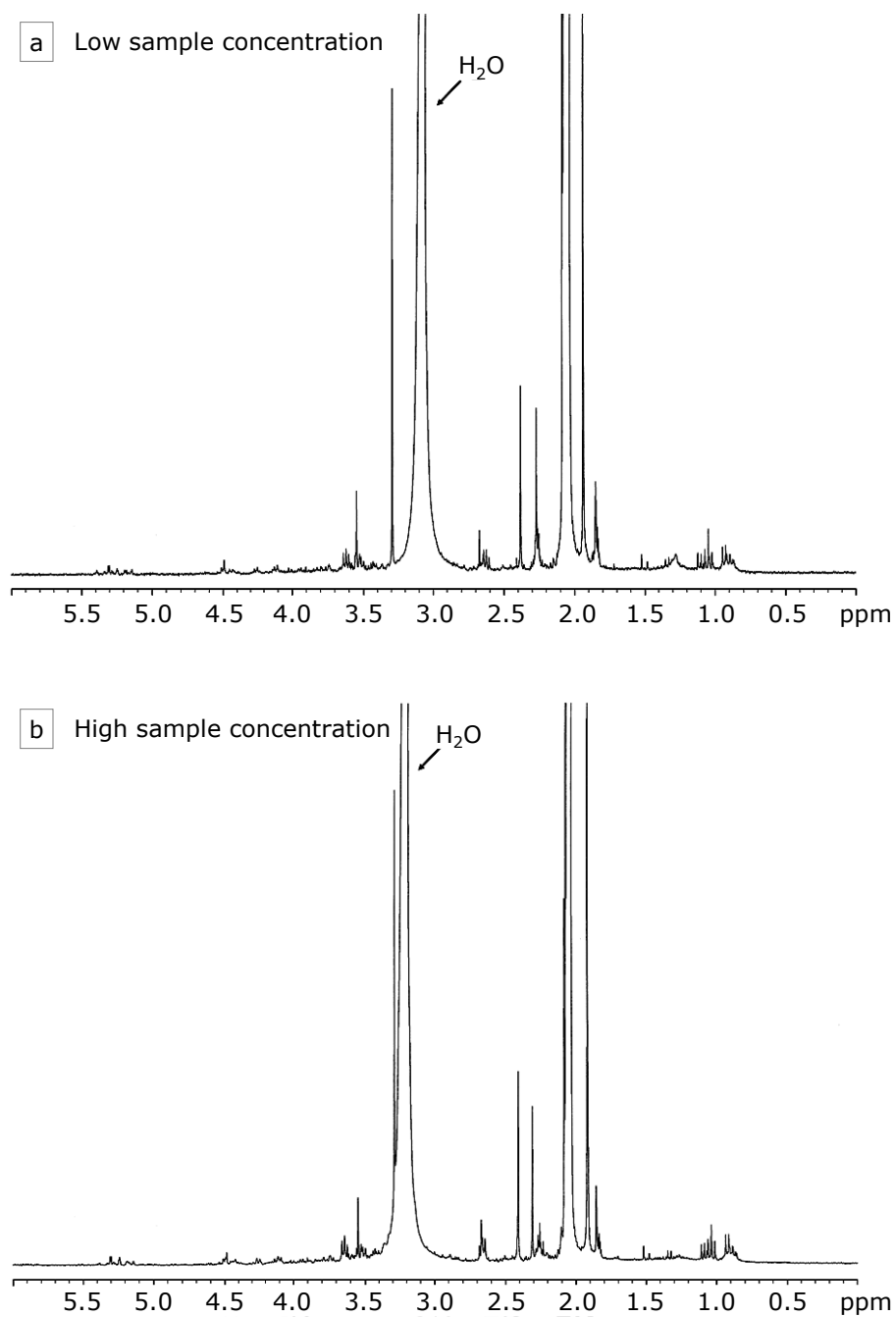


Figure 7-3: Change of the position of the water signal in the $^1\text{H-NMR}$ spectrum: (a) Low sample concentration (1.7 m/V%); (b) High sample concentration (3.2 m/V%).

7.3 Results and discussion

7.3.1 Karl Fischer titration: sensitivity for interferences

Before determining the water content of the pyrolysis liquids, the KF titration was assessed for interfering compounds present in the pyrolysis liquids. Therefore, a series of pure model compounds (pro analysis quality) were titrated in amounts (about 250 μL) that were at least five times higher than the total amount of a typical sample of pyrolysis liquid (about 50 mg). Before starting the titration, a waiting time longer than the maximum titration time used for a pyrolysis liquid with a high water content (5 min) was applied. The tested compounds and their water contents are presented in Table 7-2.

Table 7-2: Model compounds used to assess the KF titration for interference from compounds present in the pyrolysis liquids (SD between brackets).

Compound	Class	Water content (m/V%)
Acetic acid	Organic acid	0.30 (0.04)
Formic acid	Organic acid	1.66 (0.12)
Diethylamine	Amine	1.63 (0.11)
Acetaldehyde	Aldehyde	1.37 (0.09)
Benzaldehyde	Aldehyde	1.27 (0.08)
Aceton	Ketone	0.14 (0.11)
2-furaldehyde	O-heterocyclic compound	<0.1
Pyridine	N-heterocyclic compound	<0.1
Phenol	Phenolic compound	<0.1
Decanonitrile	Nitrile	<0.1
Acetamide	Amide	<0.1

Table 7-2 shows that low water contents were found for all model compounds. Only in case of formic acid, diethylamine, acetaldehyde and benzaldehyde, a water content slightly higher than indicated by the supplier (i.e. < 1 m/V%) was found. Since these compounds were tested in amounts much higher than they could be present in the pyrolysis liquids, it is believed that they do not significantly affect the water content determined by KF titration within the investigated period of time. However, other untested compounds present in the pyrolysis liquid could still affect the water content determined by KF titration.

7.3.2 Water content of pyrolysis liquids

7.3.2.1 Pyrolysis liquids with a low water content

A first set of pyrolysis liquids was produced by flash pyrolysis of rapeseed cake at different temperatures (Table 7-1). As a result, samples with a different water content but with a similar matrix (consisting of triglycerides, free fatty acids and oxygenated compounds) were obtained. These samples were very suitable to study and to compare KF titration, azeotropic distillation (AD) and $^1\text{H-NMR}$ spectroscopy as water determination techniques. The results are shown in Table 7-3.

Table 7-3: Water content of the pyrolysis liquids determined by different water determination techniques.

No. Sample	KF titration (wt%)		AD (wt%)		$^1\text{H-NMR}$ (wt%)
	Value	99% CI ^a	Uncorr.	GC/MS corr.	
1 RSC-550	6.7	5.4 – 8.0	8.5	-	8.6
2 RSC-450	8.4	7.1 – 9.6	9.4	-	9.6
3 RSC-400	14.9	14.6 – 15.2	15.1	-	14.9
4 RSC-350	17.9	16.7 – 19.1	18.9	-	18.1
5 RSC-W1	62.3	60.6 – 64.0	72.0	61.0	47.1
6 RSC-W2	65.2	64.6 – 65.8	70.2	65.7	51.5
7 Sludge	12.0	9.8 – 14.1	11.4	10.3	11.5
8 RSC-PEG	26.6	24.6 – 28.6	31.0	28.6	25.5
9 Willow	38.0	35.5 – 40.6	47.7	36.9	38.9
10 Cellulose	20.7	19.9 – 21.5	25.2	18.2	24.3

^a 99% confidence interval

In case of samples nos. 1 to 4, the water content determined by KF titration was rather low and in accordance with expectations of lower water amounts at higher pyrolysis temperatures. Measurements in triplicate allowed the calculation of a 99% confidence interval. The borders of this confidence interval were rather broad, but still acceptable bearing in mind the small sample size (about 50 mg). The results of the azeotropic distillation were systematically higher than those of the KF titration. An explanation could be the presence of water soluble volatile organic compounds that form azeotropic mixtures with water or toluene during azeotropic distillation (see also section 7.3.2.2). However, the results of the

azeotropic distillation were situated within the 99% confidence interval of the KF titration, except for sample no. 1.

The water content by the new proposed $^1\text{H-NMR}$ technique was determined by the water addition method. Firstly, a spectrum of the pyrolysis liquid dissolved in acetone- d_6 was recorded. Then, 1 μL of pure water was added to the same sample using a syringe (Hamilton Microliter 701N; absolute error = 0.05 μL) and a second spectrum was taken. In this way, the signal corresponding to water in the pyrolysis liquid could be identified. As illustration, the two spectra of the RSC-350 sample are shown in Figure 7-4. The signal corresponding to water in the pyrolysis liquid was situated approximately between 3 and 4 ppm (Figure 7-4a). In this range, the broad signal was increased by the addition of pure water (Figure 7-4b), while the rest of the spectrum remained unchanged. Integration of the water signal *before* and *after* the addition of 1 μL of pure water resulted in an area of 42.72 and 65.69, respectively. The difference between the two areas (22.97) corresponded to 1 mg (or 1 μL) water. The amount of water in the original sample was calculated by dividing 42.72 by 22.97 and equaled to 1.86 mg H_2O . This amount of water was present in 10.3 mg of pyrolysis liquid, resulting in a water content of 18.1 wt%. The water content of the other pyrolysis liquids was calculated in a similar way.

Table 7-3 shows that the water content determined by KF titration and by $^1\text{H-NMR}$ spectroscopy was almost identical for sample nos. 3 and 4. For sample nos. 1 and 2, however, $^1\text{H-NMR}$ resulted in a small overestimation compared to KF titration. The increasing relative influence of resonance signals superimposed on the water signal in the $^1\text{H-NMR}$ spectrum for samples with a low water content could explain this small overestimation.

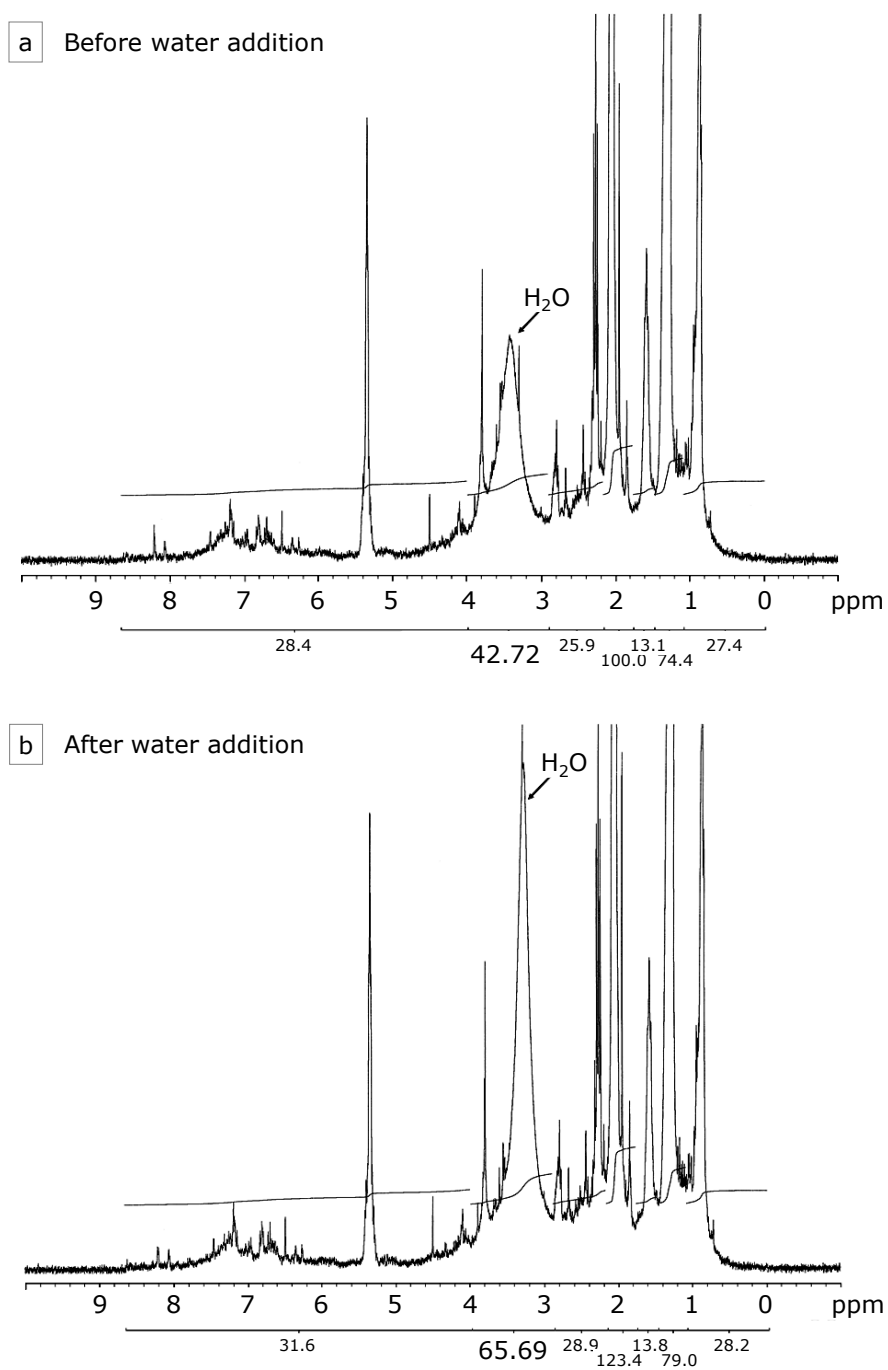


Figure 7-4: $^1\text{H-NMR}$ spectrum of RSC-350, dissolved in acetone- d_6 , before (a) and after (b) the addition of pure water ($1\ \mu\text{L}$). The peak area of the water signal (3.0 to 4.0 ppm) is shown at the bottom line.

7.3.2.2 *Pyrolysis liquids with a high water content*

Samples nos. 5 and 6 were expected to have a very high water content. Frequently, pyrolysis liquids with a high water content contain a considerable amount of water soluble volatile organic compounds as well. Therefore, this set of samples was very suitable to test the sensitivity of the three investigated water determination techniques for (possible) interference from these compounds. Results are shown in Table 7-3 (p. 259).

The data of the KF titration were in accordance with the expected high water content of the samples. Uncorrected azeotropic distillation resulted in a water content that was significantly and systematically higher than the upper limit of the 99% confidence interval of the KF titration. To explain this overestimation, each water fraction after azeotropic distillation was investigated by GC/MS (see also Figure 7-1). Besides water, also water soluble volatile organic compounds were found to be boiled over during azeotropic distillation. The most important interfering compounds were formic acid and especially acetic acid, while propanoic acid and acetamide caused minor interferences. Therefore, it was decided to correct the water content obtained by azeotropic distillation only for interference from acetic and formic acid by means of quantitative GC/MS (Table 7-3). The water contents by azeotropic distillation after GC/MS correction were in good agreement with those of the KF titration and were situated within the 99% confidence interval. In contrast, the $^1\text{H-NMR}$ results were significantly lower than these of the KF titration and azeotropic distillation after GC/MS correction. In the $^1\text{H-NMR}$ spectra, not only one but two water peaks were observed. In other words, water occurred in two different chemical environments. The additional water resonance peak was situated in the (crowded) spectral region at about 2 ppm and could be assigned to "unbounded" water, next to the peak of "bounded" water at about 3 – 3.5 ppm. The water molecules in the two environments were in slow exchange on the NMR time scale and both signals increased upon standard addition of water. This made an accurate water determination by $^1\text{H-NMR}$ spectroscopy very difficult for pyrolysis liquids with a very high water content, since the initial amount of unbounded water could not be determined in the crowded region at about 2 ppm.

7.3.2.3 *Pyrolysis liquids originating from different types of biomass*

A third set consisted of pyrolysis liquids formed by pyrolysis of different types of biomass. In this way, a broad range of biomass types was covered, preventing narrowing down the study to one type of biomass. Results are shown in Table 7-3 (p. 259). Uncorrected azeotropic distillation systematically led to a higher water content than KF titration, except for sample no. 7. As stated earlier, this overestimation is believed to be related to the presence of water soluble volatile organic compounds. After GC/MS-correction (analogous as in section 7.3.2.2), the water contents determined by azeotropic distillation were within the 99% confidence interval of the KF titration, except for sample no. 10. The $^1\text{H-NMR}$ results again were comparable with these of the KF titration and the azeotropic distillation after GC/MS correction, except for sample 10. Here, $^1\text{H-NMR}$ led to an overestimation compared to the two conventional techniques.

7.3.2.4 *Overview of the different water determination methods*

An overview of the water content determined by azeotropic distillation (corrected and uncorrected) and by $^1\text{H-NMR}$ spectroscopy as a function of the water content by KF titration is shown in Figure 7-5 for all investigated pyrolysis liquids.

The results of the azeotropic distillation were comparable with these of the KF titration in case of pyrolysis liquids with a low water content. At higher water contents, however, uncorrected azeotropic distillation resulted in a significant overestimation. Correcting the results of the azeotropic distillation with GC/MS data for the interference from water soluble volatile organic compounds led to a linear fit that was in good agreement with the KF results (dashed line; Figure 7-5). This confirms the hypothesis that water soluble volatile organic compounds are responsible for the overestimation of the water content determined by azeotropic distillation compared to KF titration. Moreover, it is also an indication that KF titration and GC/MS-corrected azeotropic distillation are free of interferences, since almost similar results are obtained by these two independent water determination techniques for the investigated pyrolysis liquids. However, for other types of pyrolysis liquids, one should always investigate the samples for possible interfering compounds. The $^1\text{H-NMR}$ results for the samples with a low and intermediate water content are also included in

Figure 7-5. It is clear that the results are in accordance with those of the two conventional techniques. Only at very high water contents (> 50 wt%), which normally do not appear in pyrolysis liquids that are interesting for further use, one should be careful for underestimation of the water content by $^1\text{H-NMR}$ spectroscopy, as illustrated by the inset of Figure 7-5. However, if the samples with a high water content are omitted (Figure 7-5), the linear fit of the $^1\text{H-NMR}$ results is in very good agreement with the fit of the KF titration and the GC/MS corrected azeotropic distillation.

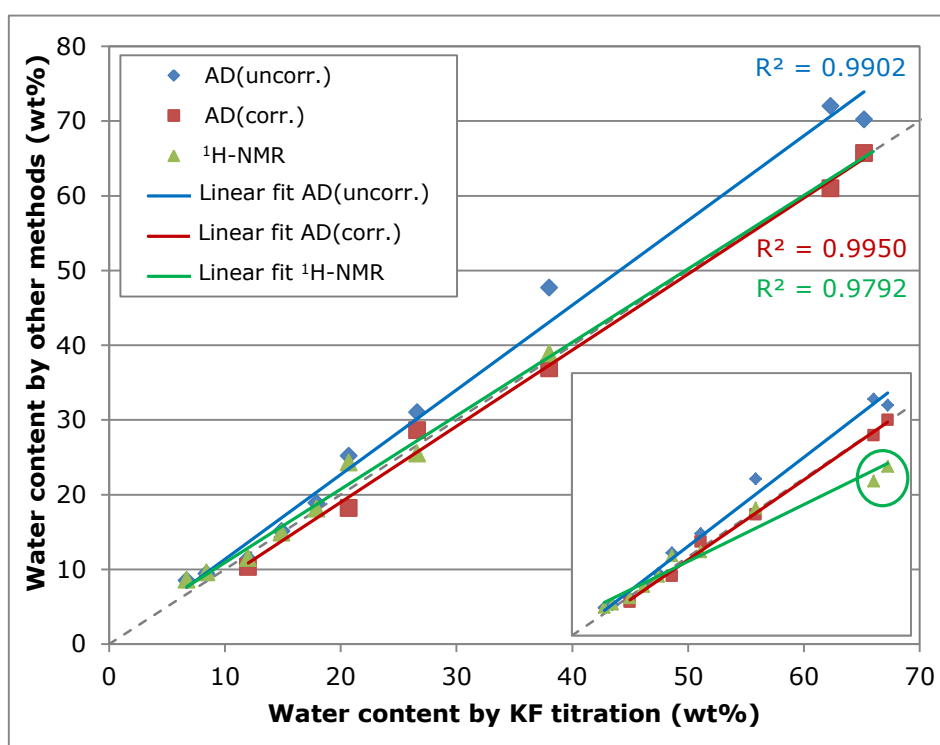


Figure 7-5: Overview of the water contents determined by azeotropic distillation (AD), both uncorrected and GC/MS corrected, and $^1\text{H-NMR}$ spectroscopy as a function of the water content by KF titration. The inset shows the result for $^1\text{H-NMR}$ spectroscopy including the samples with a high water content (nos. 5 and 6).

7.4 Conclusion

In case of pyrolysis liquids with a low water content, the results obtained by KF titration and by azeotropic distillation are almost the same. For samples with a higher water content, azeotropic distillation systematically overestimates the water content due to water soluble volatile organic compounds. GC/MS analysis of the water fraction after azeotropic distillation identifies formic acid and especially acetic acid as main source of this positive interference. Azeotropic distillation with quantitative GC/MS correction results in water contents that are situated within the 99% confidence interval of the KF titration. The results of the new proposed $^1\text{H-NMR}$ technique are in good agreement with KF titration and GC/MS-corrected azeotropic distillation for pyrolysis liquids with a low to intermediate water content. Only at very high water contents (> 50 wt%), $^1\text{H-NMR}$ spectroscopy underestimates the water content because water then appears in a "bounded" and an "unbounded" state. The 99% confidence interval of the KF titration demonstrates that all methods are very comparable if performed on correct base. Hence, besides KF, also other techniques such as azeotropic distillation with GC/MS correction and $^1\text{H-NMR}$ spectroscopy can be used for water determination of most pyrolysis liquids if performed according to well-defined procedures.

7.5 References

- [1] Mohan, D., Pittman, C.U. and Steele, P.H. Pyrolysis of wood/biomass for bio-oil: A critical review. *Energy & Fuels*, 2006. **20**(3): 848-889.
- [2] Akhtar, J. and Amin, N.S. A review on operating parameters for optimum liquid oil yield in biomass pyrolysis. *Renewable & Sustainable Energy Reviews*, 2012. **16**(7): 5101-5109.
- [3] Czernik, S. and Bridgwater, A.V. Overview of applications of biomass fast pyrolysis oil. *Energy & Fuels*, 2004. **18**(2): 590-598.
- [4] Bridgwater, A.V. Review of fast pyrolysis of biomass and product upgrading. *Biomass and Bioenergy*, 2012. **38**(0): 68-94.
- [5] Fahmi, R., Bridgwater, A., Donnison, I., Yates, N. and Jones, J.M. The effect of lignin and inorganic species in biomass on pyrolysis oil yields, quality and stability. *Fuel*, 2008. **87**(7): 1230-1240.
- [6] Oasmaa, A. and Peacocke, C. A guide to physical property characterisation of biomass-derived fast pyrolysis liquids, ed. Finland, T.r.c.o. Vol. 450. 2001, Technical research centre of Finland, Espoo, Finland: VTT Publications.
- [7] Skoog, D.A., West, D.M., Holler, S.R., Crouch, S.R. *Analytical Chemistry: An introduction*. 7th ed. 2000: Brooks/Cole and Thomson Learning.
- [8] Grünke, S. Main and side reactions in the Karl Fischer solution. *Food Control*, 2001. **12**(7): 419-426.
- [9] ASTM E203 "Standard Test Method for Water Using Volumetric Karl Fischer Titration" 2004. Annual Book of ASTM standards.
- [10] ASTM D1744 "Standard Test Method for Determination of Water in Liquid Petroleum Products by Karl Fischer Reagent" 2004. Annual Book of ASTM standards.
- [11] Bridgwater, A., Czernik, S., Diebold, U., Meier, D., Oasmaa, A., Pajares, C., Piskorz, J. and Radlein, D. *Fast pyrolysis of biomass: a handbook*. 1999, Newbury, UK: CPL Press.
- [12] Oasmaa, A. and Meier, D. Norms and standards for fast pyrolysis liquids 1. Round robin test. *Journal of Analytical and Applied Pyrolysis*, 2005. **73**(2): 323-334.
- [13] Meier, D., Oasmaa, A. and Peacocke, G.V.C. Properties of fast pyrolysis liquids: status of test methods. In: *Fast pyrolysis of biomass: a handbook*, Bridgwater, A., et al., Editors. CPL Press: Newbury, UK. 1999.

- [14] ASTM D95 "Standard Test Method for Water in Petroleum Products and Bituminous Materials by Distillation" 2004. Annual Book of ASTM standards.
- [15] Özbay, N., Pütün, A.E. and Pütün, E. Structural analysis of bio-oils from pyrolysis and steam pyrolysis of cottonseed cake. *Journal of Analytical and Applied Pyrolysis*, 2001. **60**(1): 89-101.
- [16] Ates, F., Pütün, A.E. and Pütün, E. Pyrolysis of two different biomass samples in a fixed-bed reactor combined with two different catalysts. *Fuel*, 2006. **85**(12-13): 1851-1859.
- [17] Acikgoz, C. and Kockar, O.M. Flash pyrolysis of linseed (*Linum usitatissimum* L.) for production of liquid fuels. *Journal of Analytical and Applied Pyrolysis*, 2007. **78**(2): 406-412.
- [18] Onay, O. Fast and catalytic pyrolysis of pistacia khinjuk seed in a well-swept fixed bed reactor. *Fuel*, 2007. **86**(10-11): 1452-1460.
- [19] Cornelissen, T., Yperman, J., Reggers, G., Schreurs, S. and Carleer, R. Flash co-pyrolysis of biomass with polylactic acid. Part 1: Influence on bio-oil yield and heating value. *Fuel*, 2008. **87**(7): 1031-1041.
- [20] Todt, H., Guthausen, G., Burk, W., Schmalbein, D. and Kamlowksi, A. Water/moisture and fat analysis by time-domain NMR. *Food Chemistry*, 2006. **96**(3): 436-440.
- [21] Turov, V.V. and Leboda, R. Application of H-1 NMR spectroscopy method for determination of characteristics of thin layers of water adsorbed on the surface of dispersed and porous adsorbents. *Advances in Colloid and Interface Science*, 1999. **79**(2-3): 173-211.
- [22] Scheepers, M.L., Adriaensens, P.J., Gelan, J.M., Carleer, R.A., Vanderzande, D.J., Devries, N.K. and Brandts, P.M. Demonstration of methylene-ether bridge formation in melamine-formaldehyde resins. *Journal of Polymer Science: Part A: Polymer Chemistry*, 1995. **33**(6): 915-920.
- [23] Smets, K., Adriaensens, P., Vandewijngaarden, J., Stals, M., Cornelissen, T., Schreurs, S., Carleer, R. and Yperman, J. Water content of pyrolysis oil: Comparison between Karl Fischer titration, GC/MS-corrected azeotropic distillation and ¹H NMR spectroscopy. *Journal of Analytical and Applied Pyrolysis*, 2011. **90**(2): 100-105.

Summary and general conclusion

The demand for energy and its sources is increasing every day due to the rapid growth of world's population and developing technologies. Nowadays, the largest part of world's energy demand is still mainly fulfilled from conventional fossil fuels while biofuels and waste only have minor contributions. However, growing environmental concern, predictions of scarcity, supply oscillations, rising prices and the need for a more secure and diversified energy supply strongly stimulate the search for sustainable and renewable energy sources. Among various renewable sources (e.g. solar, water, tidal, wind and geothermal power), biomass is considered as the energy source with the highest potential to contribute to the energy needs of modern society. Nonetheless, conversion of (solid) biomass into a more useful and valuable (usually liquid) form is required. Within a wide range of conversion techniques, pyrolysis is very promising because it is the only technique that converts biomass into three fractions: solid, liquid and gas. Pyrolysis is defined as the thermochemical decomposition of material, including biomass waste, at moderate temperatures (350 - 700 °C) and in an oxygen deficient atmosphere. The yield of each product fraction depends on the applied pyrolysis conditions (temperature, heating rate, vapor residence time, etc.) and the properties of the biomass feedstock.

In this thesis, the valorization of three agricultural waste cakes, i.e. rapeseed cake, raspberry seed cake and olive waste cake, using pyrolysis as conversion technique is the main objective. Firstly, the **agricultural waste cakes are characterized** to determine their **major constituents** (component analysis), their **thermochemical behavior** under pyrolysis conditions (TGA) and their **physicochemical characteristics** (elemental analysis and HHV). Rapeseed cake is found to have the highest content of triglycerides and proteins, while the highest content of lignin (an important precursor of char) is observed for raspberry seed cake. Elemental analysis reveals that rapeseed cake has a slightly higher C- and H-content and a significantly lower O-content than both other waste cakes, explaining its relatively high calorific value (24.2 MJ/kg). Secondly, the product yield and the quality of the pyrolysis liquid is evaluated for each waste cake by **preliminary flash pyrolysis** experiments at 450 °C. Based on these results, rapeseed cake is found to have a high potential as source of

renewable fuel since it is converted, after spontaneous phase separation of the pyrolysis liquid, into the organic fraction (36.3 wt%) with the highest calorific value (31.7 MJ/kg) and the lowest water content (8.4 wt%) of all tested samples. The organic fraction from olive waste cake is less promising due to its low yield (13.1 wt%) and very viscous appearance, while raspberry seed cake is converted into a single-phased pyrolysis liquid (53.7 wt%) with properties comparable to those of pyrolysis liquids from lignocellulosic biomass. Additionally, raspberry seed cake is a promising precursor in the production of activated carbon primarily based on its high solid yield (25.6 wt%). Therefore, it is decided to focus the research on valorization of rapeseed cake and raspberry seed cake as source of renewable fuels and as precursor of activated carbon. Olive waste cake is not further investigated due to the lower quality of the pyrolysis liquid compared to that of rapeseed cake and the fact that, in contrast to raspberry seed cake, it has already been studied extensively in literature as precursor in the production of activated carbon.

The effects of several pyrolysis conditions on the product yield and the physicochemical characteristics of the pyrolysis products produced from **rapeseed cake** are investigated. Hereby, the main focus lies on the valorization of the pyrolysis liquid as renewable fuel.

Firstly, the effect of **temperature** on the yield and properties of the pyrolysis products produced by **flash pyrolysis** is investigated. A significant decrease in solid yield (- 23.6 wt%) and a minor decrease in gas yield (- 6.3 wt%) in favor of the liquid yield (+ 29.9 wt%) is found for a temperature increase from 350 to 550 °C. The pyrolysis liquid spontaneously separates into an organic oil and aqueous fraction for all pyrolysis temperatures. The larger liquid yield at higher temperatures is caused by an increase in organic oil fraction. Hence, flash distillation (rather than flash pyrolysis) of the biomass triglycerides is found to be much more dominant at higher (450 and 550 °C) than at lower (350 and 400 °C) pyrolysis temperatures. This hypothesis is supported by GPC, HPLC, FTIR and ¹H-NMR data of the organic oil fractions of the pyrolysis liquids. GC/MS identifies fatty acids, related to triglycerides, as principal compounds in the organic oil fractions, together with compounds originating from the degradation of hemicellulose, cellulose, lignin and proteins. The aqueous fractions of the

pyrolysis liquids are composed of a wide variety of polar compounds mainly originating from protein, hemicellulose and cellulose components. Nonetheless, the yield and composition of the aqueous fraction are hardly affected by the pyrolysis temperature. Concerning the valorization of rapeseed cake as source of renewable fuel, flash pyrolysis at 550 °C has the highest potential. Hence, it results in the highest yield (58.2 wt%) of pyrolysis liquid that spontaneously separates into an aqueous (16.1 wt%) and an organic oil fraction (42.1 wt%). The latter is characterized by a low water content (6.7 wt%), a high calorific value (32.8 MJ/kg) and a neutral pH-value (6.9). Separation of the solid residue from the sand (used as heat transfer medium) is problematic regardless the pyrolysis temperature. However, at industrial scale, the solid residue can be valorized as solid fuel to provide process heat to a CFB reactor setup.

Secondly, **flash pyrolysis with fractionated liquid condensation** and **flash co-pyrolysis with polyethylene glycol (PEG10k)** are assessed on their abilities to reduce the water content of the pyrolysis liquid. Flash pyrolysis at 450 °C with fractionated liquid condensation (one vessel at 105 °C and one water cooled vessel) cannot reduce the water content of the pyrolysis liquid compared to that produced by regular flash pyrolysis of rapeseed cake followed by spontaneous phase separation. However, since the liquid fraction collected at 105 °C has a lower water content (10.2 wt%) than the liquid fraction collected in the water cooled vessel (41.9 wt%), flash pyrolysis with fractionated liquid condensation turns out to have potential to reduce the water content of (single-phased) pyrolysis liquids produced from *other* biomass waste streams. Co-pyrolysis of rapeseed cake with PEG10k slightly reduces the water content (- 0.8 wt%) of the organic oil fraction, but also results in a significantly lower yield (- 11.5 wt%) of this fraction compared to regular flash pyrolysis. Moreover, the desired synergetic effect between rapeseed cake and PEG10k, i.e. the esterification of the fatty acids with the degradation products of PEG10k, that is expected to assist the spontaneous phase separation of the pyrolysis liquid is not achieved, as determined by GC/MS.

Thirdly, **slow pyrolysis with collection of the pyrolysis liquid in fractions as a function of temperature** is studied to gain a better understanding of the pyrolytic behavior of rapeseed cake and the composition of the pyrolysis liquid. At lower temperatures (195 - 350 °C), the liquid fractions are single-phased and

mainly composed of water, O-heterocyclic compounds and carboxylic acids (mainly short-chain acids). At higher temperatures (350 – 550 °C), long-chain fatty acids become predominant and result in a phase separation of the pyrolysis liquid. As a result, an organic oil fraction with a lower polarity and water content than the aqueous fractions is formed. At temperatures above 400 °C, this phase separation is more pronounced and the organic oil fraction becomes dominant. Moreover, fatty acids are partly converted into nitriles by reaction with N-containing compounds and dehydration reactions. The N-heterocyclic compounds, degradation products of biomass proteins, are mainly observed in the aqueous fractions collected between 265 and 400 °C.

Fourthly, **slow catalytic pyrolysis** of rapeseed cake up to 550 °C is studied to improve the organic oil fraction concerning its use as renewable fuel. Three catalyst types (γ -Al₂O₃, HZSM-5 and Na₂CO₃) and two configurations (ex-bed and in-bed mode) are considered. The chemical composition of the pyrolysis liquids is characterized in detail for better understanding of the catalyst activity and the (improved) physicochemical properties of the liquids. The product yield and energy recovery are found to be considerably affected by catalyst type and/or configuration. In general, lower liquid and higher gas yields are obtained compared to the non-catalytic test, except for in-bed γ -Al₂O₃. Hence, the latter is the only catalyst that results in a slightly higher liquid yield (48.4 wt%) and energy recovery (44.2 %) compared to the non-catalytic test (47.1 wt% and 43.1 %, respectively), although HZSM-5 (both in-bed and ex-bed) also performs well. All pyrolysis liquids spontaneously separate into an organic oil and an aqueous fraction. Catalyst addition reduces the yield of the organic oil fraction in favor of the aqueous fraction in all cases. Physicochemical properties of the organic oil fractions are strongly affected by the catalysts used in this study. Especially in-bed Na₂CO₃ and ex-bed HZSM-5 improve the properties of the organic oil fraction, making it promising for renewable fuel use. Hence, in-bed Na₂CO₃ results in the highest calorific value (36.8 MJ/kg), while ex-bed HZSM-5 performs the most effective deoxygenation (- 13.9 wt% compared to the non-catalytic organic oil fraction) resulting in a relatively low oxygen content of 9.8 wt%. In contrast, the physicochemical properties of the organic oil fractions are hardly improved by in-bed γ -Al₂O₃ and in-bed HZSM-5, indicating that these acidic catalysts should preferably be used in ex-bed mode in case of slow

catalytic pyrolysis of rapeseed cake. It is concluded that the use of a suitable catalyst can enhance the quality of the organic oil fraction produced by slow pyrolysis of rapeseed cake up to 550 °C. The chemical composition of the organic oil fractions strongly depends on catalyst type and/or configuration. An overall trend is the reduced amount of fatty acids (formed by thermal decomposition of triglycerides). In case of the acidic catalysts (HZSM-5 and γ -Al₂O₃), the fatty acids are mainly converted into nitriles by an acid catalyzed two-step mechanism with amides as intermediate products. The formation of nitriles is favored when these catalysts are used in ex-bed mode, while the equilibrium is shifted a little bit more towards amides when testing these catalysts in in-bed mode. The alkaline Na₂CO₃ catalyst converts fatty acids mainly into aliphatic hydrocarbons by decarboxylation reactions. The aqueous fractions have a very high water content, but contained a considerable amount of polar organic compounds as well. N-heterocyclic compounds and carboxylic acids are determined as major classes of compounds. The solid residue has a relatively high calorific value (about 21.5 MJ/kg) and has potential as precursor in the production of activated carbon.

The valorization of **raspberry seed cake** by flash and slow pyrolysis is investigated as well. During **flash pyrolysis**, the temperature has a significant effect on the yield and properties of the pyrolysis products. The liquid yield (53.6 wt%) reaches an optimum at 450 °C. The pyrolysis liquid is single-phased with a high water content (26.2 wt%), a low HHV (18.6 MJ/kg) and an acidic pH (3.2). These properties are comparable to those of pyrolysis liquids produced from lignocellulosic biomass (e.g. wood). GC/MS analysis reveals phenols, carboxylic acids and alcohols as major classes of compounds. Regarding the production of added-value chemicals, levoglucosan and some phenolic compounds are interesting because of their high economic value. This high value is necessary to make their recuperation from the pyrolysis liquid economically valuable. Separation of the solid residue from sand is problematic, making its valorization as precursor in the production of activated carbon unfavorable. However, the high energy content of the solid residue (about 24.5 MJ/kg) allows its valorization as solid energy carrier to provide process heat at industrial scale.

The pyrolysis liquid produced by **slow pyrolysis** of raspberry seed cake up to 450 °C is collected in three fractions. Fraction 1 (220 – 320 °C) is an aqueous liquid with water, O-heterocyclic compounds and carboxylic acids as major compounds. Fraction 2 (320 - 350 °C) is considered as a transition fraction and is mainly composed of phenols and carboxylic acids. Fraction 3 (350 – 450 °C) spontaneously separates in an aqueous and organic oil fraction. The organic oil fraction (12.1 wt%), mainly composed of phenolic compounds, has a relatively low water content (9.3 wt%) and a relatively high calorific value (27.0 MJ/kg), making it promising for use as renewable fuel. The aqueous fraction (10.2 wt%) has a very high water content (67.4 wt%), but also contains a high amount of levoglucosan, an added-value chemical with high potential. The solid residue can be valorized as solid energy carrier because of its high calorific value (30.9 MJ/kg), as fertilizer or as precursor in the production of activated carbon.

The production of **activated carbon** using the solid residue from slow pyrolysis up to 450 °C (without sand as heat transfer medium) of **rapeseed cake** and **raspberry seed cake** is performed by physical activation using steam or CO₂. The effect of the activation temperature (850, 900 and 950 °C) is studied for a fixed activation time of 30 min, while the effect of the activation time (30, 60, 90 and 120 min) is investigated at a fixed temperature of 900 °C. After activation, the textural characteristics (BET specific surface area and porosity) and the performance of the AC in phenol adsorption are studied.

The ACs derived from rapeseed cake are characterized by type IV **N₂ adsorption isotherms** with type H4 hysteresis loops. The latter, related to mesopores, become more pronounced for longer activation times and at higher temperatures. Micro- and mesopores turn out to be formed simultaneously regardless the activation agent, although mesopore development is less pronounced at the early stage of activation in case of CO₂. In case of raspberry seed cake, type IV isotherms with type H4 hysteresis loops are found for ACs produced by steam (except 850 °C) and by CO₂ for longer activation times (90 and 120 min). In contrast, CO₂ activation (except 90 and 120 min) and steam activation at 850 °C result in type I isotherms, indicating that there is (almost) no mesoporosity. This indicates that CO₂ results in microporous ACs at the early stage of activation and that mesopore development will start at a later stage

(more severe activation conditions) leading to ACs with a mixed micro- and mesoporous structure. In contrast, steam is found to create micro- and mesopores simultaneously from the early stage of activation. For both waste cakes, steam is more reactive than CO₂ in terms of specific surface area and both micro- and mesopore development. Moreover, the reactivity of the activation agent is dependent on the precursor material, since CO₂ is found to be a much more effective activation agent for ACs from rapeseed cake than for those produced from raspberry seed cake under analogous conditions.

The ACs produced from rapeseed cake have a very high **ash content** that is considerably decreased by performing an additional HCl-washing step. This extra step is not necessary for ACs derived from raspberry seed cake because of their relatively low ash content. No significant amounts of **surface functional groups** are found by ATR-FTIR analysis of the ACs from both waste cakes.

The **phenol adsorption study** reveals that higher activation temperatures and longer activation times generally increase the phenol uptake for the investigated ACs. Again, steam activated samples perform better than samples activated by CO₂ under similar conditions. The experimental adsorption data are best fitted by the Freundlich isotherm model in all cases. Moreover, the adsorption capacity seems to be more related to the micropore volume (V_{DR}) than to the mesopore volume (V_{me}).

Based on textural characteristics, phenol uptake and total AC yield, steam activation at 900 °C for 90 min and CO₂ activation at 900 °C for 120 min are selected as best activation conditions for both waste cakes. Comparison to commercial grade AC (Norit) reveals that the ACs from both agricultural waste cakes have potential for treating phenol polluted wastewaters. Especially the AC from raspberry seed cake activated by steam at 900 °C for 90 min is very effective with a phenol uptake of 260 mg/L for an initial phenol concentration of 400 mg/L.

The phenol removal is found to be independent on **the initial pH of the solution** between 4 and 9, indicating that (mainly) dispersive interactions between the basal planes with a high π -electron density of the AC and the aromatic ring of phenol are responsible for adsorption. At pH-values higher than 9, in contrast, the phenol removal is considerably lower due to electrostatic

repulsion between the negative surface charge of the AC and the phenolate anions.

Phenol adsorption is best described by the **pseudo-second-order kinetic model** for the selected ACs of both waste cakes. Moreover, phenol uptake of ACs derived from both waste cakes is found to be faster than that of the commercial AC at the initial stage of adsorption. Application of the **intraparticle diffusion model** of Weber and Morris indicates that both boundary layer and intraparticle diffusion control the rate of phenol adsorption on the ACs.

Two conventional techniques for **determination of the water content of pyrolysis liquids** (i.e. Karl Fischer titration and azeotropic distillation) and a new proposed technique based on $^1\text{H-NMR}$ spectroscopy are compared in a final chapter. Samples are selected to cover a wide range of water contents and are originating from different types of biomass. Similar results are found by **Karl Fischer titration** and **azeotropic distillation** for pyrolysis liquids with a low water content, while azeotropic distillation systematically overestimates the water content for pyrolysis liquids with a high water content. GC/MS analysis of the water fraction after azeotropic distillation identifies formic acid and especially acetic acid as main source of this positive interference. Hence, the water contents determined by azeotropic distillation are situated within the 99% confidence interval of the Karl Fischer titration after performing a quantitative **GC/MS correction** for these interfering compounds. The results of the new proposed **$^1\text{H-NMR}$ technique** are in good agreement with the Karl Fischer titration and the GC/MS-corrected azeotropic distillation for pyrolysis liquids with a low to intermediate water content. Only at very high water contents (> 50 wt%), $^1\text{H-NMR}$ spectroscopy underestimates the water content because water then appears in a "bounded" and an "unbounded" state.

This research shows that agricultural waste cake (i.e. rapeseed cake and raspberry seed cake) can successfully be valorized by pyrolysis. However, further research is required to investigate the **economic feasibility** of the processes described in this thesis. The pyrolysis liquids with potential for **renewable fuel** use should be further characterized for important fuel properties and tested in a **bench-scale engine setup**. Moreover, further

research is required concerning the **recuperation** (technically as well as economically) of promising **added-value chemicals** (such as levoglucosan and phenolic compounds) from the pyrolysis liquids. Finally, the **regeneration of the activated carbons** needs also to be studied into more detail since it is an important factor in the determination of the economic value of activated carbons.

Samenvatting en algemeen besluit

De snelle groei van de wereldbevolking en de snelle ontwikkeling van allerhande technologieën doet de vraag naar energie en energiebronnen zienderogen stijgen. Het grootste gedeelte van deze vraag wordt momenteel beantwoord met het gebruik van conventionele fossiele brandstoffen terwijl biobrandstoffen en energie uit afval eerder een beperkte bijdrage leveren. Gelukkig wordt de zoektocht naar duurzame en hernieuwbare energiebronnen steeds meer gestimuleerd door een toenemend milieubewustzijn, voorspellingen van schaarste en bijhorende stijgende brandstofprijzen en door de nood aan een veiligere en meer gediversifieerde energievoorziening. Binnen een uitgebreide waaier aan hernieuwbare energiebronnen (zoals zonne-energie, windenergie, energie uit water en geothermische energie) wordt biomassa beschouwd als de energiebron met het hoogste potentieel om aan de energiebehoeften van de moderne samenleving bij te dragen. Desondanks is vaak een omzetting van de (vaste) biomassa in een meer bruikbare en waardevolle (meestal vloeibare) vorm een vereiste. Binnen een uitgebreid gamma aan conversietechnieken is pyrolyse veelbelovend omdat het als enige techniek de biomassa omvormt in drie fracties: vast, vloeibaar en gas. Pyrolyse kan gedefinieerd worden als de thermochemische afbraak van een materiaal, zoals bijvoorbeeld biomassa-afval, op een gematigde temperatuur (350 – 700 °C) en in een zuurstofarme atmosfeer. De opbrengst aan elke fractie hangt af van de gebruikte pyrolyseparameters (zoals pyrolysetemperatuur, opwarmingsnelheid en verblijftijd van de gassen in de warme reactor) alsook van de eigenschappen van de biomassa.

De belangrijkste doelstelling van dit proefschrift is het potentieel van pyrolyse te onderzoeken voor de valorisatie van drie agrarische afvalkoeken, nl. koolzaadperskoek, framboospittenkoek en afvalkoek van olijven. In eerste instantie zijn de **belangrijkste componenten** (component analyse), het **thermochemisch gedrag** onder pyrolyseomstandigheden (TGA) en de **fysicochemische eigenschappen** (elementsamenstelling en energiewaarde) **van de agrarische afvalkoeken** bepaald. Koolzaadperskoek blijkt hierbij het hoogste gehalte aan triglyceriden en eiwitten te bevatten, terwijl de framboospittenkoek het hoogste ligninegehalte (een belangrijke precursor voor koolrest) vertoont. Elementanalyse toont aan dat koolzaadperskoek een iets hoger C- en H-gehalte en een

beduidend lager O-gehalte heeft dan beide andere afvalkoeken, wat meteen ook een verklaring is voor de relatief hoge calorische waarde (24,2 MJ/kg) van koolzaadperskoek. Vervolgens wordt de productopbrengst en de kwaliteit van de pyrolysevloeistof voor elke afvalkoek beoordeeld met behulp van **verkennende flash pyrolyse experimenten** op 450 °C. Gesteund door deze resultaten is geoordeeld dat koolzaadperskoek een hoog potentieel bezit als bron van hernieuwbare brandstof omdat het aanleiding geeft tot een organische fractie (36,3 gew%), gevormd na spontane fasescheiding van de pyrolysevloeistof, met de hoogste calorische waarde (31,7 MJ/kg) en het laagste watergehalte (8,4 gew%) van alle geteste stalen. De organische fractie afkomstig van afvalkoek van olijven is minder veelbelovend vanwege zijn lage opbrengst (13,1 gew%) en hoge viscositeit, terwijl framboospittenkoek wordt omgezet in een eenfasige pyrolysevloeistof (53,7 gew%) met eigenschappen vergelijkbaar met die van pyrolysevloeistoffen gevormd uit lignocellulose biomassa. Daarnaast is framboospittenkoek ook een veelbelovende precursor in de productie van actieve kool voornamelijk omwille van zijn relatief hoge opbrengst aan vast residu (25,6 gew%). Daarom is besloten het onderzoek toe te spitsen op de valorisatie van koolzaadperskoek en framboospittenkoek als bron van duurzame brandstof en als precursor van actieve kool. Afvalkoek van olijven wordt niet verder onderzocht omwille van de lagere kwaliteit van de pyrolysevloeistof ten opzichte van die van koolzaadperskoek en het feit dat, in tegenstelling tot framboospittenkoek, afvalkoek van olijven reeds uitvoerig bestudeerd is in de literatuur als precursor in de productie van actieve kool.

Het effect van belangrijke pyrolyseparameters op de productopbrengst en de fysicochemische eigenschappen van de pyrolyseproducten afkomstig van **koolzaadperskoek** is onderzocht. Hierbij ligt de nadruk hoofdzakelijk op de valorisatie van de pyrolysevloeistof als hernieuwbare brandstof.

Ten eerste is het effect van de **pyrolysetemperatuur** op de opbrengst en de eigenschappen van de pyrolyseproducten tijdens **flash pyrolyse** onderzocht. Een sterke afname van de opbrengst aan vast residu (- 23,6 gew%) samen met een kleine afname in gasopbrengst (- 6,3 gew%) ten gunste van de vloeistofopbrengst (+ 29,9 gew%) is vastgesteld voor een temperatuursverhoging van 350 tot 550 °C. De pyrolysevloeistof scheidt spontaan in een

organische en waterige fractie, ongeacht de pyrolysetemperatuur. De hogere vloeistofopbrengst op hogere temperatuur wordt hoofdzakelijk veroorzaakt door een verhoogde opbrengst aan organische fractie. Immers, "flash destillatie" (eerder dan flash pyrolyse) van de biomassa triglyceriden blijkt op hogere pyrolysetemperatuur (450 en 550 °C) veel meer uitgesproken dan op lagere pyrolysetemperatuur (350 en 400 °C). Deze hypothese wordt ondersteund door GPC, HPLC, FTIR en ¹H-NMR analyses van de organische fracties van de pyrolysevloeistoffen. Vetzuren, afkomstig van triglyceriden, en verbindingen gevormd uit de afbraak van hemicellulose, cellulose, lignine en eiwitten zijn door middel van GC/MS geïdentificeerd als belangrijkste verbindingen in de organische fractie. De waterige fractie van de pyrolysevloeistof bevat een grote hoeveelheid polaire verbindingen die voornamelijk afkomstig zijn van eiwitten, hemicellulose en cellulose. Desondanks is de opbrengst en de samenstelling van de waterige fractie nauwelijks afhankelijk van de pyrolysetemperatuur. Betreffende de valorisatie van koolzaadperskoek als bron van hernieuwbare brandstoffen heeft flash pyrolyse bij 550 °C het hoogste potentieel. Immers de hoogste opbrengst aan pyrolysevloeistof (58,2 gew%) die spontaan scheidt in een waterige (16,1 gew%) en een organische fractie (42,1 gew%) wordt verkregen bij deze temperatuur. Bovendien wordt de organische fractie gekenmerkt door een zeer laag watergehalte (6,7 gew%), een relatief hoge calorische waarde (32,8 MJ/kg) en een neutrale pH-waarde (6,9). Scheiding van het vast residu uit het zand (gebruikt als warmteoverdracht medium) is problematisch ongeacht de pyrolysetemperatuur. Desondanks kan het vast residu gevaloriseerd worden als vaste energiedrager om proceswarmte te leveren aan een CFB reactor op industriële schaal.

Ten tweede zijn **flash pyrolyse met gefractioneerde condensatie van de pyrolysevloeistof** en **flash co-pyrolyse met polyethyleenglycol (PEG10k)** beoordeeld op hun vermogen om het watergehalte van de pyrolysevloeistof verder te verminderen. Flash pyrolyse bij 450 °C met gefractioneerde condensatie van de pyrolysevloeistof (gebruikmakend van een condensatievat op 105 °C en een condensatievat gekoeld met stromend water) kan het watergehalte van de pyrolysevloeistof niet verminderen ten opzichte van deze geproduceerd door gewone flash pyrolyse van koolzaadperskoek gevolgd door een spontane fasescheiding van de pyrolysevloeistof. Desalniettemin heeft de

pyrolysevloeistof gecondenseerd bij 105 °C toch een aanzienlijk lager watergehalte (10,2 gew%) dan deze opgevangen in het watergekoeld condensatievat (41,9 gew%), wat aangeeft dat flash pyrolyse met gefractioneerde condensatie van de pyrolysevloeistof toch een aanzienlijk potentieel heeft voor het verminderen van het watergehalte van (eenfasige) pyrolysevloeistoffen geproduceerd uit *andere* biomassa-afvalstromen. Copyrolyse van koolzaadperskoek met PEG10k vermindert lichtjes het watergehalte (- 0,8 gew%) van de organische fractie, maar resulteert ook in een aanzienlijk lagere opbrengst (- 11,5 gew%) van deze fractie in vergelijking met gewone flash pyrolyse. Bovendien kan het gewenste synergetische effect tussen de koolzaadperskoek en PEG10k, nl. de verestering van de vetzuren met de afbraakproducten van PEG10k, dat de spontane fasescheiding van de pyrolysevloeistof zou moeten bevorderen niet vastgesteld worden met behulp van GC/MS.

Ten derde is **trage pyrolyse met condensatie van de pyrolysevloeistof in fracties in functie van de temperatuur** uitgevoerd om een beter inzicht te krijgen in het pyrolytisch gedrag van de koolzaadperskoek en de samenstelling van de pyrolysevloeistof. De vloeibare fracties opgevangen bij lage temperatuur (195 - 350 °C) zijn eenfasig en hoofdzakelijk samengesteld uit water, O-heterocyclische verbindingen en carbonzuren (voornamelijk korte-keten zuren). Bij hogere temperatuur (350 - 550 °C) worden de lange-keten vetzuren overheersend, wat leidt tot een spontane fasescheiding van de pyrolysevloeistof. Hierdoor wordt een organische fractie gevormd met een lagere polariteit en een lager watergehalte dan de waterige fracties. Bij temperaturen boven 400 °C is deze fasescheiding meer uitgesproken en neemt de organische fractie de bovenhand. Bovendien worden de vetzuren gedeeltelijk omgezet in nitrillen door reactie met N-houdende verbindingen en door dehydratiereacties. De N-heterocyclische verbindingen, afbraakproducten van eiwitten, worden hoofdzakelijk waargenomen in de waterige fracties opgevangen tussen 265 en 400 °C.

Ten vierde is **trage katalytische pyrolyse van koolzaadperskoek** tot 550 °C bestudeerd met het oog op verbeterde eigenschappen van de organische fractie betreffende zijn gebruik als hernieuwbare brandstof. Drie types katalysatoren (γ -Al₂O₃, HZSM-5 en Na₂CO₃) en twee configuraties (ex-bed en in-bed) worden

hierbij beschouwd. De chemische samenstelling van de pyrolysevloeistoffen is in detail onderzocht om een beter inzicht te krijgen in de katalysatoractiviteit en de (verbeterde) fysicochemische eigenschappen van de pyrolysevloeistof. De productopbrengst en energierecuperatie blijken sterk afhankelijk van het type katalysator en/of de gebruikte configuratie. Algemeen worden lagere vloeistof- en hogere gasopbrengsten verkregen vergeleken met de niet-katalytische test, behalve voor in-bed $\gamma\text{-Al}_2\text{O}_3$. Immers, laatstgenoemde is de enige katalysator die leidt tot een iets hogere vloeistofopbrengst (48,4 gew%) en energierecuperatie (44,2%) in vergelijking met de niet-katalytische test (respectievelijk 47,1 gew% en 43,1%), hoewel HZSM-5 (zowel in-bed als ex-bed) ook goed presteert. Alle pyrolysevloeistoffen scheiden spontaan in een organische en een waterige fractie. Het gebruik van een katalysator vermindert de opbrengst aan organische fractie ten gunste van de waterige fractie voor alle katalysatoren. De fysicochemische eigenschappen van de organische fracties zijn sterk afhankelijk van het gebruik van een katalysator. Vooral in-bed Na_2CO_3 en ex-bed HZSM-5 verbeteren deze eigenschappen waardoor deze organische fracties veelbelovend worden voor gebruik als hernieuwbare brandstof. Immers, in-bed Na_2CO_3 resulteert in de hoogste calorische waarde (36,8 MJ/kg), terwijl ex-bed HZSM-5 leidt tot de meest effectieve deoxygenatie (- 13,9 gew% ten opzichte van de niet-katalytisch geproduceerde organische fractie) met een relatief laag zuurstofgehalte (9,8 gew%) als gevolg. Anderzijds worden de fysicochemische eigenschappen van de organische fracties nauwelijks verbeterd door in-bed $\gamma\text{-Al}_2\text{O}_3$ en in-bed HZSM-5, wat aangeeft dat deze zure katalysatoren bij voorkeur gebruikt worden in ex-bed mode in het geval van trage katalytische pyrolyse van koolzaadperskoek. Er wordt geconcludeerd dat het gebruik van een geschikte katalysator de kwaliteit van de organische fractie geproduceerd door trage pyrolyse van koolzaadperskoek aanzienlijk kan verbeteren. De chemische samenstelling van de organische fracties is sterk afhankelijk van het type katalysator en/of de gebruikte configuratie. Een algemene trend is het verminderd gehalte aan vetzuren (gevormd door thermische ontbinding van triglyceriden). Bij de zure katalysatoren (HZSM-5 en $\gamma\text{-Al}_2\text{O}_3$) worden de vetzuren gedeeltelijk omgezet in nitrillen volgens een zuurgekatalyseerd tweestaps mechanisme met amiden als tussenproduct. De vorming van nitrillen wordt begunstigd wanneer deze katalysatoren in ex-bed

mode worden gebruikt, terwijl het evenwicht iets meer naar de kant van de amiden wordt verschoven wanneer deze katalysatoren in in-bed mode worden getest. De alkalische katalysator Na_2CO_3 zet de vetzuren voornamelijk om in alifatische koolwaterstoffen via decarboxyleringsreacties. De waterige fracties hebben een zeer hoog watergehalte maar bevatten eveneens een aanzienlijke hoeveelheid polaire organische verbindingen. De N-heterocyclische verbindingen en carbonzuren worden als belangrijkste bindingsklassen teruggevonden. Het vast residu heeft een relatief hoge calorische waarde (ongeveer 21,5 MJ/kg) en heeft ook potentieel als precursor in de productie van actieve kool.

De valorisatie van **framboospittenkoek** met behulp van flash en trage pyrolyse is eveneens onderzocht. Tijdens **flash pyrolyse** blijkt de temperatuur een grote invloed te hebben op de opbrengst en de eigenschappen van de pyrolyseproducten. De vloeistofopbrengst (53,6 gew%) bereikt een optimum bij 450 °C. Deze pyrolysevloeistof is eenfasig en heeft een hoog watergehalte (26,2 gew%), een lage calorische waarde (18,6 MJ/kg) en een zure pH (3,2). Deze eigenschappen zijn vergelijkbaar met die van pyrolysevloeistoffen afkomstig van lignocellulosische biomassa (bijv. hout). Fenolen, carbonzuren en alcoholen worden als belangrijkste bindingsklassen gedetecteerd met behulp van GC/MS. Betreffende de productie van chemicaliën met toegevoegde waarde zijn levoglucosan en sommige fenolische verbindingen interessant vanwege hun hoge economische waarde. Deze hoge waarde is noodzakelijk om hun winning uit de pyrolysevloeistof economisch rendabel te maken. De afscheiding van het vast residu uit het zand (warmteoverdracht medium) is problematisch waardoor de valorisatie als precursor in de productie van actieve kool zeer ongunstig lijkt. Niettemin maakt de hoge energie-inhoud van het vast residu (ongeveer 24,5 MJ/kg) het mogelijk om het, althans op industriële schaal, als vaste energiedrager voor proceswarmte te gebruiken.

De pyrolysevloeistof geproduceerd door **trage pyrolyse** van framboospittenkoek tot 450 °C is opgevangen in drie fracties. Fractie 1 (220 - 320 °C) is een waterige vloeistof met water, O-heterocyclische verbindingen en carbonzuren als belangrijkste componenten. Fractie 2 (320 - 350 °C) wordt beschouwd als een overgangsfractie en bestaat voornamelijk uit fenolen en carbonzuren. Fractie 3 (350 - 450 °C) scheidt spontaan in een waterige en organische fractie. De

organische fractie (12,1 gew%), hoofdzakelijk bestaande uit fenolische verbindingen, heeft een relatief laag watergehalte (9,3 gew%) en een relatief hoge calorische waarde (27,0 MJ/kg), waardoor deze fractie veelbelovend is voor gebruik als hernieuwbare brandstof. De waterige fractie (10,2 gew%) heeft een hoog watergehalte (67,4 gew%), maar bevat eveneens een grote hoeveelheid levoglucosan, een chemische verbinding met een hoge toegevoegde waarde. Het vast residu kan gevaloriseerd worden als vaste energiedrager vanwege de hoge calorische waarde (30,9 MJ/kg), als meststof of als precursor in de productie van actieve kool.

De productie van **actieve kool** uit het vast residu van trage pyrolyse tot 450 °C (zonder zand als warmteoverdracht medium) van **koolzaadperskoek** en **frambozenpittenkoek** is uitgevoerd met behulp van fysische activatie met stoom of CO₂. Het effect van de activeringstemperatuur (850, 900 en 950 °C) is onderzocht voor een vaste activeringstijd van 30 min, terwijl het effect van de activeringstijd (30, 60, 90 en 120 min) bestudeerd is bij een vaste temperatuur van 900 °C. Na activatie zijn de textuureigenschappen (het BET specifieke oppervlak en de porositeit) en de prestaties van de actieve kool in fenoladsorptie onderzocht.

De actieve kool afkomstig van koolzaadperskoek wordt gekenmerkt door type IV **N₂ adsorptie-isothermen** met type H4 hysteresislussen. Deze laatste, gerelateerd aan mesoporiën, zijn meer uitgesproken voor langere activeringstijden en bij hogere temperatuur. Micro- en mesoporiën blijken gelijktijdig gevormd te worden ongeacht het activeringsgas, hoewel de ontwikkeling van mesoporiën minder uitgesproken is in het beginstadium van de activatie in geval van CO₂. Bij framboospittenkoek worden type IV isothermen met type H4 hysteresislussen teruggevonden voor actieve kool geactiveerd met stoom (behalve 850 °C) en met CO₂ voor een langere activeringstijd (90 en 120 min). Activatie met CO₂ (behalve 90 en 120 min) en stoomactivatie bij 850 °C daarentegen resulteren in type I isothermen, wat aangeeft dat er (bijna) geen mesoporiën gevormd zijn. Dit toont aan dat CO₂ leidt tot microporeuze actieve kool in het beginstadium van activatie en dat de ontwikkeling van mesoporiën pas in een later activatiestadium start (na strengere activatiecondities), resulterend in een gecombineerde micro- en mesoporeuze structuur. Stoom

blijkt daarentegen gelijktijdig micro- en mesoporiën te vormen vanaf het beginstadium van activatie. Voor beide afvalkoeken is stoom reactiever dan CO₂ in termen van specifiek oppervlak en de ontwikkeling van micro- en mesoporiën. Bovendien is de reactiviteit van het activeringsgas afhankelijk van de biomassa precursor, aangezien CO₂ veel effectiever blijkt te zijn tijdens de productie van actieve kool uit koolzaadperskoek dan tijdens de productie van actieve kool uit framboospittenkoek onder analoge omstandigheden.

De actieve kool bekomen uit koolzaadperskoek heeft een zeer hoog **asgehalte** dat aanzienlijk verminderd wordt door een extra wasstap met HCl uit te voeren. Deze extra stap is niet nodig voor actieve kool afkomstig van framboospittenkoek omwille van het relatief laag asgehalte. Bovendien zijn er nauwelijks **oppervlakte-functionele groepen** vastgesteld na ATR-FTIR analyse van de actieve kool stalen afkomstig van beide afvalkoeken.

De **fenoladsorptie studie** toont aan dat een hogere activeringstemperatuur en een langere activeringstijd de fenoladsorptie verhogen voor de onderzochte actieve koolstalen. Stoomgeactiveerde actieve kool presteert beter dan deze geactiveerd door CO₂ onder vergelijkbare omstandigheden. De experimentele adsorptiedata worden het best gefit door het adsorptiemodel van Freundlich en dit in alle gevallen. Bovendien lijkt de fenol adsorptiecapaciteit een sterker verband te hebben met het microporiënvolume dan met het mesoporiënvolume van een actieve kool.

Gebaseerd op de textuureigenschappen, de fenoladsorptie en de totale opbrengst aan actieve kool worden stoomactivatie bij 900 °C gedurende 90 min en CO₂ activatie bij 900 °C gedurende 120 min als beste activatiecondities beschouwd voor beide afvalkoeken. Uit vergelijking met commerciële actieve kool (Norit) blijkt dat actieve kool afkomstig van agrarische afvalkoek potentieel heeft om fenol-verontreinigd afvalwater te zuiveren. Vooral actieve kool afkomstig van framboospittenkoek geactiveerd met stoom bij 900 °C voor 90 min is zeer effectief met een fenoladsorptie van 260 mg/L voor een beginconcentratie aan fenol van 400 mg/L.

Fenoladsorptie is onafhankelijk van de **begin-pH van de oplossing** tussen 4 en 9, wat aangeeft dat (voornamelijk) dispersieve interacties tussen de basale vlakken met een hoge π -elektronendichtheid van de actieve kool en de aromatische ring van fenol verantwoordelijk zijn voor adsorptie. Bij pH-waarden

hoger dan 9 daarentegen blijkt de fenoladsorptie aanzienlijk lager te zijn voornamelijk door de elektrostatische afstoting tussen de negatieve oppervlaktelading van de actieve kool en de fenolaat-anionen.

Fenoladsorptie wordt het best beschreven door het **pseudo-tweede-orde kinetisch model** in geval van de geselecteerde actieve koolstalen en dit voor beide agrarische afvalkoeken. Bovendien gebeurt de fenoladsorptie sneller in het begin van het adoptieproces voor de actieve koolstalen afkomstig van agrarische afvalkoek dan voor de commerciële actieve kool. Het "intraparticle diffusion model" van Weber en Morris geeft aan dat zowel "boundary layer" als "intraparticle" diffusie de snelheid van fenoladsorptie controleren.

Twee technieken frequent gebruikt voor de **bepaling van het watergehalte van pyrolysevloeistoffen** (nl. Karl Fischer titratie en azeotrope destillatie) en een nieuwe techniek gebaseerd op $^1\text{H-NMR}$ spectroscopie worden met elkaar vergeleken in een laatste hoofdstuk. De onderzochte pyrolysevloeistoffen zijn afkomstig van verschillende biomassatypes en dekken een brede waaier aan watergehaltes. **Karl Fischer titratie** en **azeotrope destillatie** geven vergelijkbare resultaten voor pyrolysevloeistoffen met een laag watergehalte, terwijl azeotrope destillatie systematisch het watergehalte overschat voor pyrolysevloeistoffen met een hoog watergehalte. GC/MS analyse van de waterfractie na azeotrope destillatie identificeert mierenzuur en vooral azijnzuur als belangrijkste bron van deze positieve interferentie. Immers, het watergehalte bepaald door azeotrope destillatie ligt binnen het 99% betrouwbaarheidsinterval van de Karl Fischer titratie na een kwantitatieve **GC/MS correctie** voor deze interfererende stoffen. De resultaten van de **$^1\text{H-NMR}$ techniek** zijn in overeenstemming met de resultaten van de Karl Fischer titratie en de GC/MS-gecorrigeerde azeotrope destillatie voor pyrolysevloeistoffen met een laag tot gemiddeld watergehalte. Enkel bij zeer hoge watergehaltes (> 50 gew%) blijkt $^1\text{H-NMR}$ spectroscopie het watergehalte te onderschatten omdat water dan zowel in een "gebonden" als in een "ongebonden" vorm wordt gedetecteerd.

Dit proefschrift toont aan dat agrarische afvalkoek (nl. koolzaadperskoek en framboospittenkoek) met succes kan gevaloriseerd worden door middel van pyrolyse. Verder onderzoek is echter nodig om de **economische haalbaarheid** van de in dit proefschrift beschreven processen te onderzoeken. De pyrolysevloeistoffen met potentieel als **hernieuwbare brandstof** kunnen best verder gekarakteriseerd worden met bijkomende analyses voor brandstofgebruik en met behulp van een "**bench-scale**" **motoropstelling**. Bovendien is verder onderzoek nodig betreffende de **recuperatie** (zowel technisch als economisch) van **interessante chemicaliën** met een hoge toegevoegde waarde (zoals levoglucosan en fenolische verbindingen) uit de pyrolysevloeistof. Tenslotte, de **regeneratie van actieve kool** vereist verder onderzoek omdat dit een zeer belangrijke factor is bij het bepalen van de uiteindelijke kostprijs van de actieve kool.

Publications and conference participation

Publications

First author

Flash pyrolysis of rapeseed cake: Influence of temperature on the yield and the characteristics of the pyrolysis liquid; K. Smets, P. Adriaensens, G. Reggers, S. Schreurs, R. Carleer, J. Yperman; *Journal of Analytical and Applied Pyrolysis* **90**(2) 2011, p. 118-125.

Water content of pyrolysis oil: Comparison between Karl Fischer titration, GC/MS-corrected azeotropic distillation and ¹H NMR spectroscopy; K. Smets, P. Adriaensens, J. Vandewijngaarden, M. Stals, T. Cornelissen, S. Schreurs, R. Carleer, J. Yperman; *Journal of Analytical and Applied Pyrolysis* **90**(2) 2011, p. 100-105.

Slow catalytic pyrolysis of rapeseed cake: Product yield and characterization of the pyrolysis liquid; K. Smets, A. Roukaerts, J. Czech, S. Schreurs, R. Carleer, J. Yperman; *Biomass and Bioenergy* (accepted).

Co-author

Evaluation of flash and slow pyrolysis applied on heavy metal contaminated Sorghum bicolor shoots resulted from phytoremediation; Z. Al Chami, N. Amer, K. Smets, J. Yperman, R. Carleer, S. Dumontet, J. Vangronsveld; *Biomass and Bioenergy* (submitted).

Conference participation

Oral presentation

1st Symposium of the 'Cluster Milieu', 2011, Diepenbeek – Belgium. Flash Pyrolysis of Agricultural Waste Cakes.

6th Annual International Symposium on Environment, 2011, Athens – Greece; Flash Pyrolysis of Several Agricultural Waste Cakes: Influence of Temperature on the Yield and the Characteristics of the Pyrolysis Liquid.

WasteEng12, 4th International Conference on Engineering for Waste and Biomass Valorisation, 2012, Porto – Portugal; Activated Carbon from Agricultural Waste Cake: Production and Phenol Adsorption.

Venice2012, IV International Symposium on Energy from Biomass and Waste, 2012, San Servolo, Venice - Italy. Slow Catalytic Pyrolysis of Rapeseed Cake: Product Yield and Characterisation of the Pyrolysis Liquid.

Poster

Knowledge for Growth, 2009, Ghent – Belgium. Pyrolysis of Biomass: Conversion of Biomass to Energy and Chemicals.

I-SUP2010, 2nd International Conference on Innovation for Sustainable Production, 2010, Bruges – Belgium. Flash Pyrolysis of Rapeseed Cake: Influence of Temperature and Characterization of Pyrolysis Liquid.

